Modelling global pyrogeography using data derived from satellite imagery

Tese elaborada para obtenção do Grau de Doutor em Engenharia Florestal e dos Recursos Naturais

Orientador: Doutor José Miguel Cardoso Pereira

Co-Orientadores: Doutor Max Alan Moritz

Doutor João Manuel de Brito Carreiras

Duarte Pedro Jácome Félix Oom

2016

Modelling global pyrogeography using data derived from satellite imagery

Duarte Pedro Jácome Félix Oom

Orientador: Doutor José Miguel Cardoso Pereira

Co-Orientadores: Doutor Max Alan Moritz

Doutor João Manuel de Brito Carreiras

Tese elaborada para obtenção do Grau de Doutor em Engenharia Florestal e dos Recursos Naturais

JÚRI:

Presidente: Doutora Maria Margarida Branco de Brito Tavares Tomé
Professora Catedrática
Instituto Superior de Agronomia da Universidade de Lisboa.

Vogais: Doutor José Miguel Oliveira Cardoso Pereira, Professor Catedrático
Instituto Superior de Agronomia da Universidade de Lisboa;

Doutor Francisco Manuel Cardoso de Castro Rego
Professor Associado com agregação
Instituto Superior de Agronomia da Universidade de Lisboa;

Doutor Paulo Alexandre Martins Fernandes, Professor Associado
Escola de Ciências Agrárias e Veterinárias
Universidade de Trás-os-Montes e Alto Douro;

Doutor Mário Jorge Modesto Gonzalez Pereira, Professor Auxiliar
Escola de Ciências e Tecnologia
Universidade de Trás-os-Montes e Alto Douro;

Doutor João Manuel das Neves Silva, Bolseiro de Investigação
Instituto Superior de Agronomia da Universidade de Lisboa.

2016

Para o Tomás

Resumo

O fogo em vegetação tem um importante impacto na emissão e libertação de gases com efeito de estufa para atmosfera, alterando o forçamento radiativo e afetando a qualidade ambiental e o clima à escala local, regional e global. O reconhecimento do fogo como uma variável crucial na caracterização do clima terrestre e sua influência no funcionamento dos ecossistemas, levou à sua designação como uma variável essencial na definição e caracterização do clima terrestre ("Essential Climate Variable",(ECV)). O tema central desta tese foi o desenvolvimento de uma nova classificação de regimes de fogo à escala global, usando Análise de Correspondência Múltipla (ACM) e uma clusterização hierárquica, usando dados de fogos ativos do sensor MODIS (Moderate Resolution Imaging Spectroradiometer). Esse trabalho, foi precedido por um procedimento de filtragem dos dados, com o intuito de obter um conjunto de dados livre de erros, e que eliminassem fogos gerados por um processo de combustão mas que não constituissem fogos de vegetação. Seguiu-se uma análise espacial dos dados obtidos, que levou ao desenvolvimento de um algoritmo inovador de identificação de clusters de fogos ativos e de uma análise global da desigualdade das distribuições dos tamanhos dos fogos. Complementando este objetivo principal, outros estudos à escala continental e global foram desenvolvidos e são apresentados no âmbito desta tese. Estes estudos lidam i) com o desfazamento temporal entre o período onde as condições meteorológicas são propícias à ocorrência do fogo e o pico da época de fogos, indo desta forma aferir a influência da atividade humana na queima da biomassa, ii) com a variabilidade espacial dos parâmetros extraídos da relação entre a densidade populacional e área queimada e iii) com a influência de práticas religiosas na modelação dos ciclos semanais da queima de vegetação ocorridas em Africa. Esperamos que os resultados provenientes dos diversos estudos efetuados nesta tese sejam uma contribuição útil para o estudo global da geografia do fogo-pirogeografia.

Palavras-chave: fogo de vegetação,pirogeografia, regime do fogo, global, MODIS

Abstract

Vegetation burning has an important impact on the global atmosphere and vegetated land surface. Deforestation fires, peatland fires, and ecosystems with shortening fire return interval contribute substantially to the build-up of atmospheric greenhouse gases affecting environmental quality and the climate system at local and regional scales. Recognition of the role of fire in the Earth system led to its designation as an Essential Climate Variable (ECV), a physical, chemical, or biological variable that has a crucial contribution towards characterization of Earth's climate. The central task of this thesis was the development of a new global classification and map of fire regimes, using multiple correspondence analysis and hierarchical clustering, and relying on active fire data from the Moderate Resolution Imaging Spectroradiometer (MODIS) MCD14ML product. That work was preceded by study dedicated to a thorough screening and exploratory spatial analysis of the dataset, and led to the development of an improved algorithm for identifying individual active fire clusters, and to global analysis of size inequality in their statistical distributions. In addition to this core research, other continental-global pyrogeography studies were developed, and are presented, dealing with: the time lag between the timing of optimal fire weather conditions and peak fire season dates as a diagnostic of anthropogenic vegetation burning; the spatial non-stationarity in the parameters of the relationship between population density and area burned; and the modulation of weekly cycles of vegetation burning in African croplands by regionally dominant religious affiliation. We hope that this set of studies may constitute a useful contribution to the burgeoning topic of global pyrogeography

Keywords: vegetation fires; pyrogeography; fire regime; global scale; MODIS

ACKNOWLEDGMENTS

On behalf of this thesis I have to thank people and institutions, without which it would not be possible to complete this research work. They are:

Institutions

Forest Research Centre, University of Lisbon, Tropical Research Institute at Lisbon and Environmental Science, Policy and Management Department at University of California, Berkeley, USA for being my host institutions where I acquired experience, inspiration, scientific stimulation and all the support and condition to develop research activities.

People

First and foremost I thank my advisor Prof. José Miguel Cardoso Pereira for his unlimited knowledge, intuition, ability to be one step ahead in research but most important for his friendship and for encouraging me to pursue a doctorate study. Without him probably would have been much harder.

My co-advisor Prof. Max Alan Moritz for being part of the genesis of my PhD and for give me the opportunity and conditions to work in one of the most important research centre in the world.

My co-advisor Dr João Manuel de Brito Carreiras for sharing his knowledge, experience and help in my research work.

Some amazing people whom I had the privilege to share some helpful ideas and work : Prof Henrique Garcia Pereira, D^{ra} Maria José Vasconcelos, Meg Krawchuk, Marc Parisien, Nicolas Venet, Tadashi Moody, Prof. Carlos da Camara, Prof. Ricardo Trigo, Per Johsson, Prof. Jorge L. Cadima, Prof. Kamil Feridun Turkman, Prof. Maria Antónia Amaral Turkman and last but not least Pedro Silva, an amazing person and researcher, who I had the privilege to share the long phone calls, meetings and brainstormings.

To my friends and colleagues from LDRAG lab and Tropical Research Institute, that were part of this journey with their singular and amazing friendship and responsible of creating a wonderful and inspiring environments to develop my research. To the "gang" Ana Barros, Yannick Le Page, Sofia Oliveira, João Silva and Ana Sá. A special mention to my two amazing mates Ioannis Bistinas and Gerado Saldaña (Sma&d&n).BFF.

To my big family and specially my parents for the total support, love and for making me what I am today.

To my wife and Tomás, my all world.

In the shadow:
Foundation for Science and Technology, for giving me a grant to help me on my studies (SFRH/BD/47452/2008).

To Matlab, C/C++, Pyhton and computer cores for being my crutches..please keep the pace, because I'll need you again for sure.

To Sporting Lisbon for give me time for research, not having many celebrations to make!!Hopefully this year would be different for sure!!

CONTENTS

CHAPTER 1

Research goal and objectives

The overarching research goal of this thesis is to develop a new global classification map of fire regimes, and contribute towards understanding biophysical and social processes underlying those regimes. This goal is pursued through the characterization of spatial and temporal distributions of global fire activity, using fire data derived from MODIS instruments on board NASA's Terra and Aqua satellites. Creating a global map of pyrogeographic units defined by patterns of coherent relations between key fire regime descriptors, with sufficient thematic resolution to accurately reflect the complex distribution of the Earth's current fire regimes is useful for characterizing major pyrogeographical patterns, monitoring changes in disturbance regimes through time, identifying knowledge gaps, and learning how climate, topography, vegetation, and land use influence fire regimes (Morgan *et al.*, 2001). Such a map may help to focus strategic action concerning global scale fire issues, including those under the scope of the United Nations Framework Convention on Climate Change, Convention to Combat Desertification, and Convention on Biological Diversity.

To achieve its aims, this thesis was divided into two separate parts. The first part focused on building a screened global active fire derived from the MODIS Collection 5 global MCD14ML active fire product (Justice *et al.*, 2002) for the period between 2001 to 2012 based on the work initially developed in Mota et *al.,* (2006). This active fire dataset was the support for all the following analysis performed under this thesis. The second part, global and continental analysis were performed towards improving the understanding of global distribution pattern of wildfire and contributing to enhance the knowledge of the role of key environmental drivers to fire occurrence.

Characterizing global pyrogeography will unfold some underlying questions such as:

i. *Can satellite data be used to quantify global pyrogeography?*
ii. *What are the most relevant set of fire descriptors that could explained the global distribution of fire regimes?*

iii. How humans can be determinant in the relation with fires?

Due the requirements defined in each step, research within this thesis was organized in main research objectives that were followed by collaborative research analysis to complement and enhance the overall goal of this thesis. Chronologically they reflect the progressive orientation of new findings and new hypothesis achieved throughout the investigation, not necessarily the chronological order of paper submission. The state of art and the data available and used were constrained at the time this thesis was undertaken.

Main research

a) To assess and improve the quality the MODIS active fire product (MCD14ML), screening the data for false alarms and non-vegetation fires.
b) To understand the structure of the data, namely its autocorrelation patterns and outliers, through an exploratory spatial data analysis.
c) To develop a new global classification and map of *sensu strictu* fire regimes.
d) To improve the methodology for individualization of fire events using MODIS active fire data, in order to develop more reliable estimates of global scale fire size distributions.

Collaborative research

Additional research was developed for the present thesis, in co-authorship, on topics closely related to those of the main research: Global analysis of time lags between peak fire weather and peak fire season; global analysis of spatial heterogeneity of the relationship between population density and area burned; and demonstration of the role of religious affiliation as a modulator of the weekly cycle of vegetation burning in sub-Saharan Africa.

Thesis structure

This thesis is organized in three chapters. Chapter 1 includes the Introduction, with focus on the importance of fire as a global ecological disturbance, and on the need for reliable, comprehensive and long global fire data record. and the concept of fire regime is presented, in the context of the studies performed within the thesis. Chapter 2 includes six

original contributions, published or submitted to peer-reviewed scientific journals, three as a first author and other three as a second. Chapter 3 includes final conclusions and references.

Context

Global fire activity - the "need" for data

As a global ecological factor, affecting atmospheric and terrestrial systems over multiple temporal and spatial scales (Bowman *et al.*, 2009; Moritz *et al.*, 2012), fire disturbance has been recognized as one of the Essential Climate Variables (ECV) defined by the Global Climate Observing System (GCOS) (Gcos, 2011). In the context of global change, fire plays an important role in regional and global climate change through interactions with the global carbon cycle, Earth surface albedo, and atmospheric chemistry, influenced by greenhouse gases and aerosols emissions derived from biomass burning (Van Der Werf *et al.*, 2010). Fire also affects several ecosystems in their global distribution and ecological properties (Bond *et al.*, 2005). For thousands of years, fire has been used as a tool for, land clearance for agriculture, shifting agriculture practices, fuel reduction, cooking, hunting, pest control or burning crop residues (Giglio *et al.*, 2006). Fire also plays a major role in deforestation in tropical and sub tropical regions (Krawchuk *et al.*, 2009). Nevertheless natural fires are dominant in sparsely populated areas, such as boreal forest in North America and Russia, where 80% of area burned is caused by lightning (Stocks, 1992).
Monitoring and performing a reliable classification and characterization of global fire geography is important to focus strategic action concerning global scale fire issues.

Satellite data

Developing a comprehensive characterization of global fire distribution only is possible through space-borne satellites that monitor the Earth continuously, collecting global fire information, even in remote areas, in accessible by other means (Arino *et al.*, 2012). Satellite sensors can monitor global fire spatial patterns (Dwyer *et al.*, 2000; Csiszar *et al.*, 2005) and increased our understanding of biomass burning emissions (Kaufman *et al.*, 1998; Van Der Werf *et al.*, 2010), land-use/land-cover change (Eva & Lambin, 2000), and fire risk (Chuvieco & Congalton, 1989).

Two types of fire data have been developed and currently are available at global scale: hotspots (HS) and burned area (BA). HS are positive thermal anomalies detected in the emission of energy in the middle and thermal infrared spectral domains, while BA detection is based on fire-indices surface reflectance changes (mainly decrease in near-infrared and short-wave infrared wavelengths,(Pereira *et al.*, 1999). Hotspots detection maps active flame fronts, when the radiometric contrast between fire and the cool surrounding area is high enough (Giglio *et al.*, 2003a). It depends on simultaneity in the timing of fire occurrence and satellite overpass, and clouds and thick smoke that can obscure fire detection. Burned area maps, based on a more persistent fire effects signal, display the full spatial extent of the areas affected by fires. It is consensual that active fire products underestimate area burned (Roy *et al.*, 2008). Weak correlation between both were found by Roy *et al.,* (2008), Hantson *et al.,* (2013), and Korontzi *et al.,* (2006). They concluded that satellite overpass time, cloud cover, or the temperature of the flaming front (Hawbaker *et al.*, 2008) affect correlation between active fires and burned area data. Acknowledging that active fires and burned area data refer to different aspects of fire occurrence, active fire products display lower error levels, namely commission errors than burned area products, because the thermal signal is a more specific diagnostic of burning than the surface darkening observed with burned area detection. Active fire data sets have been found useful by atmospheric chemistry community to assess characterization of the interannual variability and seasonality of emissions (Van Der Werf *et al.*, 2010; Kaiser *et al.*, 2012).

To date, different space-borne sensors were used to derive long-term active fire time series. These include the global Advanced Very High Resolution Radiometer (AVHRR) on board the polar orbiting National Oceanic and Atmospheric Administration (NOAA) (Stroppiana *et al.*, 2000; Dwyer *et al.*, 2000; Carmona-Moreno *et al.*, 2005); nighttime data with the Operational Linescan System (OLS) onboard the Defense Meteorological Satellite Program (DMSP) (Elvidge *et al.*, 1997); the European Space Agency (ESA) Along Track Scanning Radiometer (ATSR) World Fire Atlas (WFA), with 1 km global nighttime data described in Arino & Rosaz (1999) and used by Arino *et al.,* (2005). The regional Geostationary Operations Environmental Satellite (GOES) to study fire activity in the western hemisphere (Prins & Menzel, 1992) or the Tropical Rainfall Measuring Mission (TRMM) Visible and Infrared Scanner (VIRS) aimed at monitoring tropical fires (38ºS-38ºN) (Giglio *et al.*, 2003b) are also some examples of a growing history of fire detection from space. Recently, the Moderate Resolution Imaging Spectroradiometer (MODIS) on the Terra and

Aqua satellites, due their optical and radiometric specifications, has been used to systematically generate a suite of global fire products (Justice *et al.*, 2002). Four daily overpasses (with a constant equatorial overpass) and the use of a sophisticated and accurate fire detection algorithm, allowed the study of global to regional fire interannual variability. Built on the current MODIS algorithm, a new 750m global active product from the two daily overpasses of Visible Infrared Imaging Radiometer Suite (VIIRS) aboard the Suomi-National Polar-orbiting Partnership (S-NPP) satellite (Csiszar *et al.*, 2014) and recently, an improve version with a 375m global product (Schroeder *et al.*, 2014), has been developed, and despite the dataset is still short, a short will provide continuity to MODIS active fire products, taking full advantages of the finer spatial resolution improving detection of smaller fires and refining mapping of larger fires (Schroeder *et al.*, 2014).

Due to the long time series available, improvements achieved with higher sensitivity of the thermal channels and the use of a contextual algorithm (Giglio *et al.,* 2003), MODIS provided a better accurate depiction of global fire activity, lower false alarms (mainly sun glint, deserts and coastlines) and detection of smaller and/or cooler fires, enhancing the inclusion of smaller fires in the quantification of spatial and temporal distribution of fire at global scale (Randerson *et al.*, 2012). Several fire-related global studies used MODIS fire data to analyze long term fire trends and characterize spatial and temporal patterns of the global fire activity (Giglio *et al.*, 2006; Chuvieco *et al.*, 2008; Giglio *et al.*, 2009; Archibald *et al.*, 2013; Oom & Pereira, 2013; Hantson *et al.*, 2014,2015). Despite of more than 14 years of data provided by MODIS and the generalized use to study fire occurrence at global scale, the fire product is not error-free. Several local and regional validations of the product were made (Morisette *et al.*, 2005; Giglio *et al.*, 2006; Schroeder *et al.*, 2008a; Schroeder *et al.*, 2008b), reporting commission errors in the range of 2-3% (Boschetti *et al.*, 2010).

Global Pyrogeography

The concept of pyrogeography borrows from ecology biogeographical concepts like "resource availability", "climate zone" or "reproduction or dispersal", which explain the distribution and abundance of the organisms (Krawchuk *et al.*, 2009). It is possible to establish an analogy with the factors used to explain the distribution and abundance of the organisms with the biophysical factors that control the distribution of global fire activity:

resources availability, environmental conditions suitable for its dispersion and the capacity of disperse (Bowman *et al.*, 2013). The availability of satellite imagery led to a better understanding of the biogeography of fire, revealing the ubiquity of fire on Earth (Bowman *et al.*, 2009). Excluding deserts and some sparsely vegetated lands, fires are present in almost all biomes (Mouillot & Field, 2005). Estimates of annual area burned range between 300 and 450 Mha (Van Der Werf *et al.*, 2010) an area equivalent to the size of India. Around 80-90% of the total global burned area occurs in grasslands and savannas, mainly in Africa sub-Saharan savannas and Miombo woodlands, but also in South America (Brazilian *cerrado*), Southeast Asia, and savannas and woodlands of northern Australia (Figure 1). Africa, "the fire continent" (Goldammer *et al.*, 1993), is responsible for 30 to 50% of the total amount of biomass burned globally each year (Roberts *et al.*, 2009) and for 57% of all tropical burning. Additionally, Africa is the single largest source of biomass burning emissions (Kaiser *et al.*, 2012). Temperate and boreal region fires are less frequent but they also consume large quantities of biomass (Loboda *et al.*, 2011; Barrett & Kasischke, 2013). In regions with high levels of moisture as in boreal regions, where fuel is not a limiting factor, vegetation productivity and moisture levels are high and consequently, fire activity is constrained by dry weather conditions and only burns when flammable conditions are achieved (Pausas & Paula, 2012) leading to extreme events with high intensity.

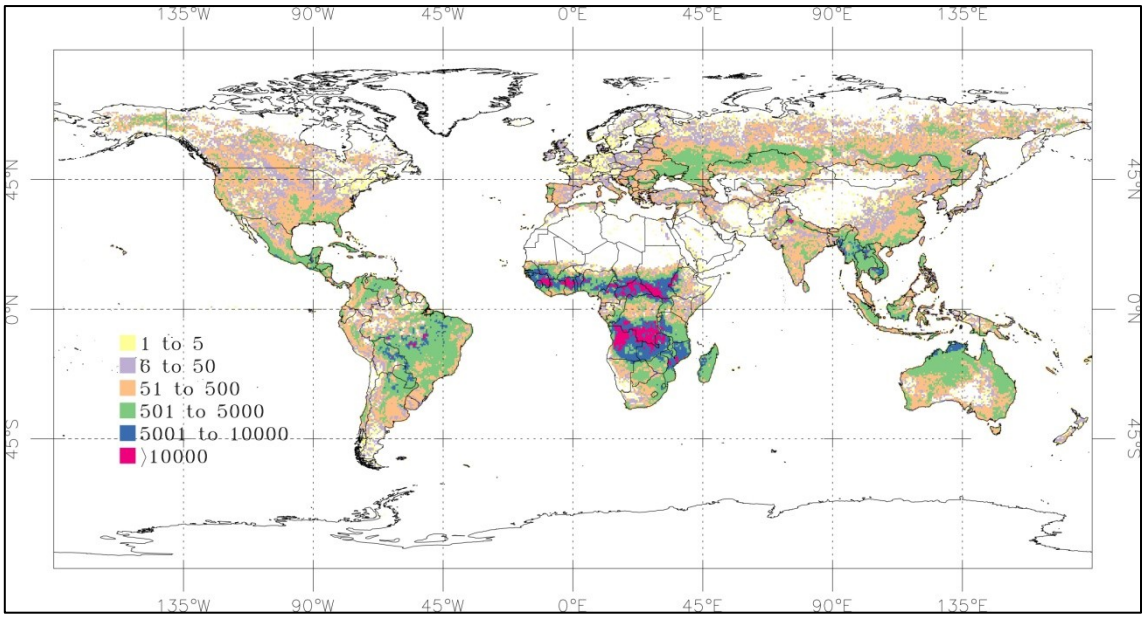

Figure 1 Global map of the number of screened MODIS active fire dataset for the period 2000–2009 in a 0.5º degree cell (Oom & Pereira, 2013).

Fire triangle

Information concerning resources available to burn (fuel), environmental conditions suitable for combustion and fire spread, and ignition sources, whether natural (lightning) or derived from human activities are required to understand fire as an ecological process (Pechony & Shindell, 2010). Although fire needs biotic, abiotic and human factors to coincide in space and time, their importance and interaction changes across scales (Whitlock *et al.*, 2010; Krawchuk & Moritz, 2011), and can be represented schematically by the fire triangle concept (Figure 2).

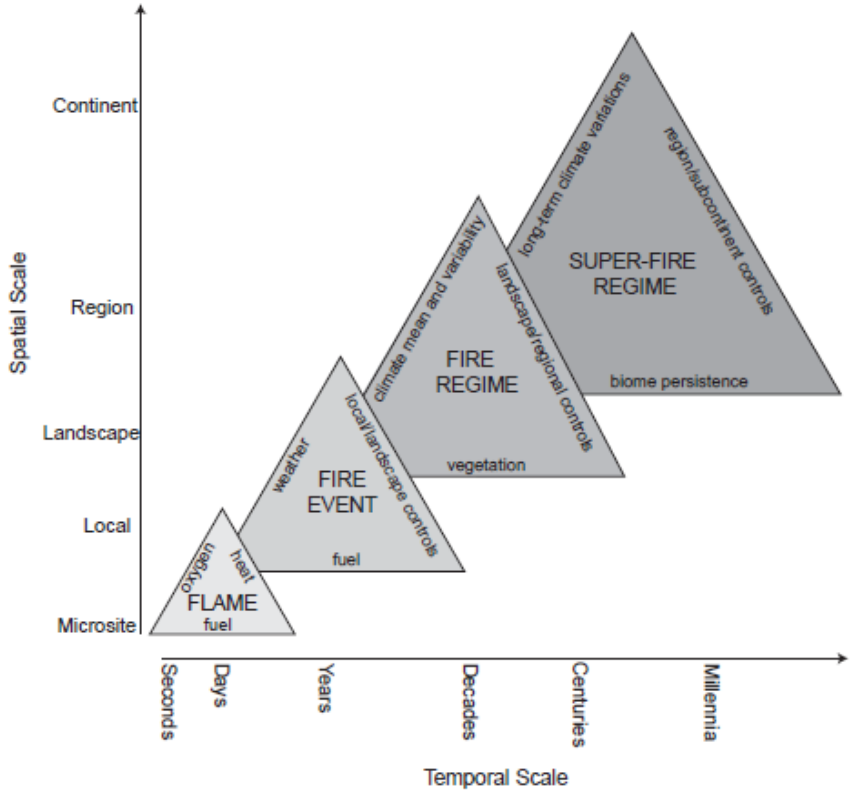

Figure 2 "Fire triangle" reflecting the three key fire determinants in fire distribution (climate, vegetation and ignition agents) at different temporal and spatial scales (Whitlock *et al.*, 2010).

The three key fire determinants in fire distribution are:

- ***Vegetation***

  Vegetation supplies the fuel for fires. The amount, type, structure, productivity, moisture, continuity all are important for defining the type and spread of fires (Flannigan *et al.*, 2013). The different patterns of fuel composition, distribution and moisture, which are greatly influenced by climate, influence fire spread rates, fire

severity and fire extent (Harrison *et al.*, 2010). Bradstock *et al.,* (2010) and Pausas & Paula (2012) showed that there exists a relationship between vegetation productivity, moisture availability and fire. Fire activity changes along a productivity/aridity gradient in a unimodal fashion, with a peak in fire incidence peaks at intermediate levels of the environmental gradient (Figure 3).

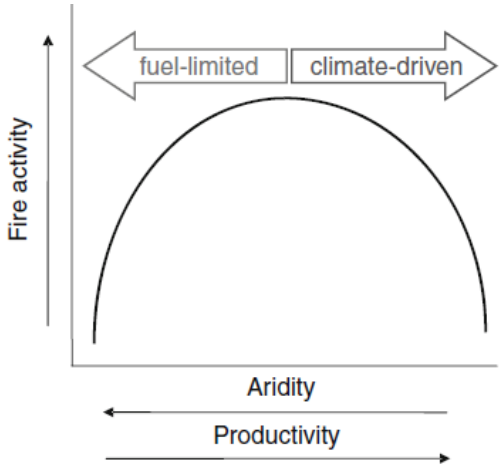

Figure 3 Hypothesized Fire-productivity relationship, showing the influence of fuel and aridity as fire drivers (adapted from Duguy *et al.*, 2013).

Extreme conditions of moisture influence vegetation productivity and consequently the ability to burn. Low/high values of moisture tend to produce insufficient fuel (high aridity, in deserts) or fuels too wet to burn (tropical rainforests). The highest fire frequency tends to occur under intermediate values of climatic conditions and seasonal variations (Parisien & Moritz, 2009; Marlon *et al.*, 2013). Intermediate levels of productivity and aridity provide suitable conditions to sustain fires. These conditions are ideally met in tropical savannas, the most widespread flammable environments on Earth.

- ***Climate***

  Globally, climate affects fire in all its aspects, influencing both the resources as the conditions for fire to occur over multiple scales. Temperature, precipitation and wind are the most important factor determining fuel productivity, continuity, structure and moisture content. Continental and global scale ocean-atmosphere interactions generate

large scale patterns in climate conditions that affect fire regimes, especially in the southern Pacific regions, like Southeast Asia, Australia or South America.

- ***Anthropogenic activities***

  At global scale, most of the fires are caused by human activities (except in remote areas of Canada and Russian Federation boreal forests), whether intentionally as a tool to land management, or even by accident (Archibald *et al.*, 2012). FAO (2007) estimated that an average of 80 % of all fires in Mediterranean, South Asia, South America and Northeast Asia are caused by humans for land management and maintenance of agricultural and pasture lands. All those practices have a profound impact on the fire regimes, changing frequency, intensity or even seasonality of fire at different scales. Although most authors have assumed the existence of a globally valid non-monotonic relationship between population density and fire incidence (Archibald *et al.*, 2008; Aldersley *et al.*, 2011; Barbosa *et al.*, 1999), Bistinas *et al.,* (2013) showed that the parameters of such a relationship vary substantially throughout the globe, mostly as a function of land-use.

The nested fire triangles shown in Figure 2, represent drivers for fire occurrence at scales ranging from the flame in microsites, for a few seconds to days, to super fire regimes within the same biome (Parisien & Moritz, 2009). The importance and limitation of all the fire drivers, the relationships between them and how they shift in the future, were the subject of several studies (Mckenzie *et al.*, 2004; Parisien & Moritz, 2009; Krawchuk *et al.*, 2009; Westerling *et al.*, 2011). Other early studies also show how pyrogeography can lead us to more accurate understanding of the global macro scales fire patterns (Dwyer *et al.*, 2000; Le Page *et al.*, 2010; Krawchuk *et al.*, 2009).

Global pyrogeography highlights spatial and temporal patterns of global fire activity and shows that fire is controlled by a few key environmental variables that, as drivers or as constraints, interact and define suitable regions for the occurrence of distinct fire regimes. Taking into account the importance of the interactions found along the different temporal and spatial combinations in the fire triangle, different scenarios and scales can determine different fire regimes (Archibald *et al.*, 2008). In the next section the fire regime concept, as a key principle of pyrogeography, is briefly described.

Fire regime

The geography of fire is always related with the definition of fire regimes. The concept of fire regime was first advanced by Gill (1975), who proposed that fire activity in a landscape could be characterized by the type, frequency, intensity and season (Murphy *et al.*, 2012). After that, several definitions have been proposed, and the concept of fire regime has evolved , including other parameters related with fire, using different time and spatial scales and applied to different purposes, according to the needs of users (Krebs *et al.*, 2010). For a detail and interesting discussion and evolution of the fire regime concept see Krebs *et al.* (2010) and Whitlock *et al.,* (2010).

Conedera *et al.,* (2009) and Krebs *et al.,* (2010) summarized *sensu strictu* and *sensu lato* fire regimes definitions . While the former represents a sort of a core definition of fire regime, including temporal aspects (frequency, seasonality, duration), spatial aspects (extent, size, shape) and fire type (crown, surface, smoldering, intensity, etc), the latter considers these parameters as part of a wider fire regime definition, including also the conditions controlling fire (fire weather, fuel flammability) and ecological and economic impacts of fire (Figure 4). Understanding the development and diversification of global fire regimes and what determines each one of them by the relationship among its components and their effects on the ecological systems (Bowman *et al.*, 2011) is an important issue to the scientific community. Moreover, assessing the importance of fire in ecosystems and projecting the degree of potential effects of management activities or climate on fire regime responses are also important goals (Liu & Wimberly, 2015).

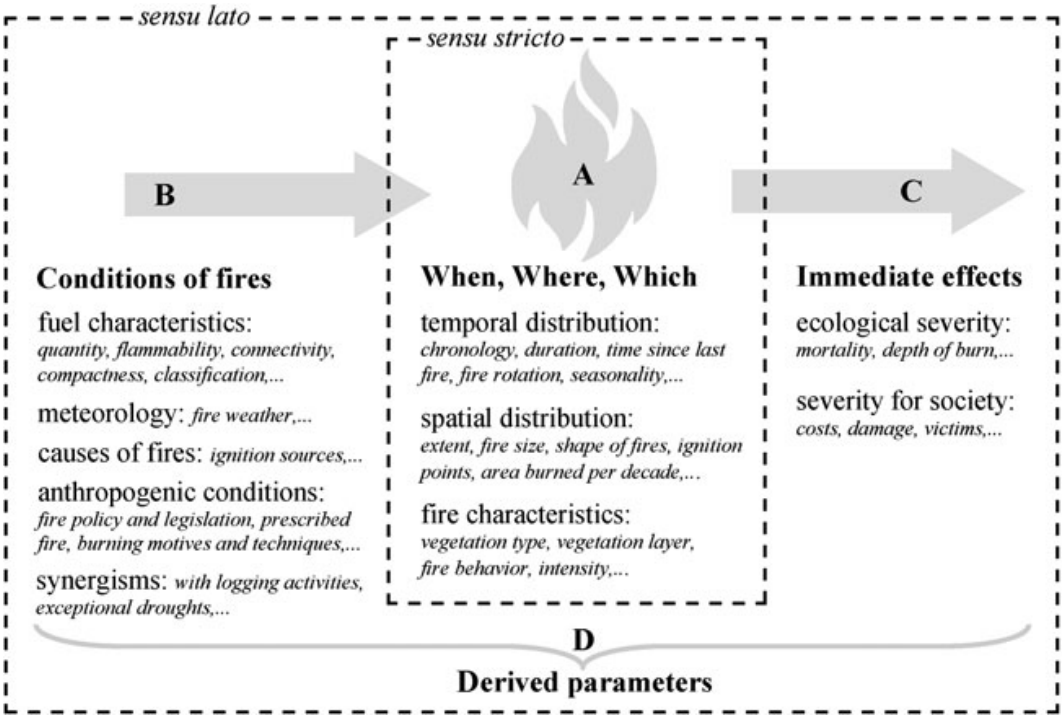

Figure 4 Components of the overall fire regime structure proposed by Krebs *et al.,* (2010). (B) Conditions of fires describe the factors that influence fire occurrence, (A) regime *sensu stricto* assembles the core components of fire regime (frequency, seasonality, extent, fire size, etc) and (C) impacts on the ecosystem measures the direct impact of the fire on the ecosystems (severity). A, B and C together described the fire regime in a wider suite of characteristics (D) in a *sensu lato* perspective.

Key fire regime variables are described below:

- ***Intensity***

  It quantifies the rate of energy release by the vegetation combustion process. Among several broad measures of fire intensity (e.g. heat per unit area, reaction intensity or fire line intensity), the Fire Radiative Power (FRP), available as a product in several satellite sensors, is an usual proxy for the aerosol emission rate (Ichoku & Kaufman, 2005) and for fireline intensity (Smith & Wooster, 2005), quantifying fire intensity at the time of observation (Wooster & Zhang, 2004). The FRP distribution is highly skewed towards low values, with a heavy tail of high values. Since very intense fires are not observed in all land cover types (Wooster & Zhang, 2004), a high FRP quantile is effective to discriminate between fire regimes.

Severity

It measures the direct impact, destruction of biomass by fires on the ecosystems. It is related with the way fire intensity can affect an ecosystem. Several post-fire indicators are used to measure fire severity by organic matter loss indicators. Keeley (2009) described the terminology associated to fire intensity and fire severity.

- ***Frequency***

  It quantifies the occurrence of fire per unit time and space. Several related concepts like fire return interval', 'fire cycle' or 'mean fire return interval' are used to quantify fire frequency.

- ***Fuel consumption and spread***

  Different types of fuel structure, moisture content and chemical compounds will determine different types of fire and fire spread. Crown fires, surface or ground fires will have different behaviors and ecological impacts.

- ***Seasonality***

  Vegetation fires mostly occur during the dry season, when ignition, fuels and fire weather coincide in same space and time. However, humans have greatly altered fire season and the patterns of fire seasonality (Le Page *et al.*, 2010)

The increased human activity, like fire management policies or agricultural expansion (Le Page *et al.*, 2010; Bowman *et al.*, 2011) and climate change through global warming (Moritz *et al.*, 2012) are some of the possible causes that can shift fire regimes at different spatial and temporal scales. Understanding how fire regimes vary across different space and time scales and how are they related to environmental conditions is mandatory to anticipate their responses to future climate change and future impacts at local, regional or global scales (Barrett & Kasischke, 2013). Given the strong effect that climate has on fire weather and fuel availability, future dramatic shifts in fire regimes have been predicted, although the magnitude and even direction of the predicted changes remain highly uncertain.

CHAPTER 2

Original contributions

Some of the research in this dissertation has been previously published, or has been accepted for publication, as peer-reviewed journal articles, or are at various stage of the reviewing process. The order of the different articles is not necessarily the chronological order of paper submission. Even if they are independent studies, they share a common basis of using the MODIS global fire database compiled at the beginning of the doctoral period study, always dependent of the data available at the moment of the study. The thesis is a summary of the following articles, which are referred to in the text by their Roman numerals.

I. **Oom, D**. & Pereira, J. (2013) Exploratory spatial data analysis of global MODIS active fire data. *International Journal of Applied Earth Observation and Geoinformation*, **21**, 326-340.

II. Le Page, Y., **Oom, D**., Silva, J., Jõnsson, P. & Pereira, J. M. (2010) Seasonality of vegetation fires as modified by human action: observing the deviation from eco-climatic fire regimes. *Global Ecology and Biogeography*, **19**, 575-588.

III. Bistinas, I., **Oom, D**., Sá, A. C., Harrison, S. P., Prentice, I. C. & Pereira, J. M. (2013) Relationships between human population density and burned area at continental and global scales. *PloS one*, **8**, e81188.

IV. Pereira, J. M. C., **Oom, D**., Pereira, P., Turkman, A. A. & Turkman, K. F. (2015) Religious Affiliation Modulates Weekly Cycles of Cropland Burning in Sub-Saharan Africa. *PloS one*, **10**, e0139189.

V. **Oom, D**., Silva, C. P., Bistinas, I and Pereira, J. M.C. (2016) Highlighting biome-specific sensitivity of fire size distributions to time-gap parameter using a new algorithm for fire event individuation, submitted to *Remote Sensing*.

VI. **Oom, D.**, Silva, C. P., Bistinas, I., Benali, A., and Pereira, J.M.C. (2016) Global mapping of sensu strictu pyrogeographic regimes using MODIS active fire data, submitted to *Remote Sensing of Environment.*

Other studies were performed during doctoral study period but not included in this thesis:

Emilio Chuvieco, Chao Yue, Angelika Heil, Florent Mouillot, Itziar Alonso-Canas, Marc Padilla, José M. Pereira, **Duarte Oom** and Kevin Tansey (2016) A new global burned area product for climate assessment of fire impacts. *Global Ecology and Biogeography*

Bistinas, I., **Oom, D**., Silva, J. & Pereira, J. M.C. (in preparation) A trend analysis of global fire activity using CMG MODIS fire counts.

Benali, A., Mota, B., Carvalhais, N., **Oom, D**., Miller, L. M. & Pereira, J. M.C. (submitted) Bimodal fire regimes unveil the global scale anthropogenic fingerprint.

Brief descriptions of the original contributions

All the papers, but one, were focused on studies at global scale. The exception is Paper IV, which was restricted to Africa. Main research is distributed over Papers I, V and VI and collaborative research are expressed in Papers II, III and IV. All papers used global fire data derived by MODIS sensors (Paper I). Papers II, III and IV are related with the anthropogenic influence on the fire activity. Results of Papers II,III, IV and V contribute to the research performed in Paper VI. Figure 5 summarize the thesis structure displaying relationships between the original contributions.

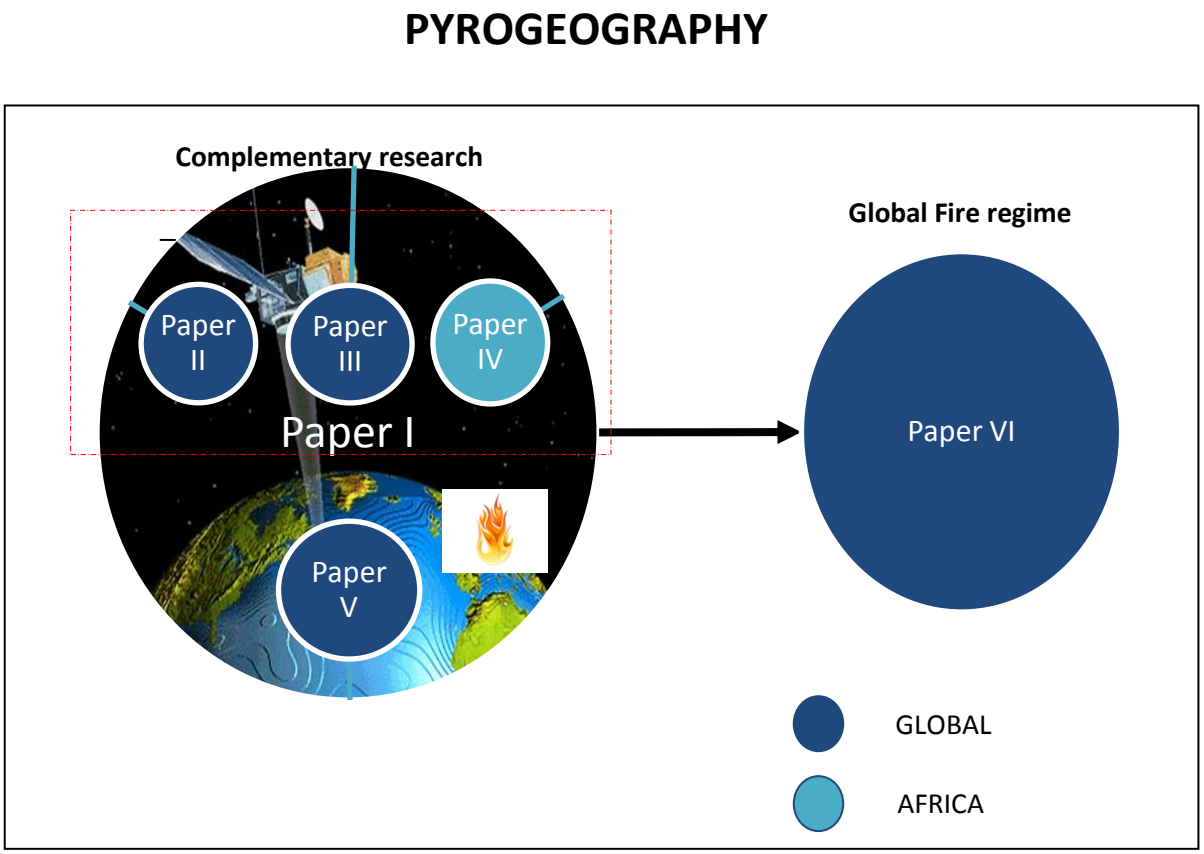

Figure 5 Summary of the structure of the thesis and relationship among papers.

Since previous research (Hawbaker *et al.*, 2008; Hantson *et al.*, 2013; Mota *et al.*, 2006) had revealed limitations on global active fire products, in Paper I the NASA MODIS MCD14ML Collection 5 global active fire dataset, spatially aggregated at 0.5° cell, was screened for false

alarms and non-vegetation fires over the period 2001–2009. Exploratory spatial data analysis (ESDA) of fire autocorrelation patterns was performed with the screened data using the local Moran's Index and the Moran scatterplot. ESDA was designed in this study to help on the identification of relevant covariates, identification of spatial regimes with potentially distinct parameter values, assessing the prevalence and importance of local pockets of spatial non-stationarity that may behave as outliers and other influential observations, and assessing the pertinence of incorporating a spatially lagged independent variable in the specification of spatial regression models. Results highlighted a strong positive autocorrelation between fires at global scale stressing the importance of addressing this data feature in the development of spatial regression models of fire presence and abundance.

Paper II took advantage of the dataset previously acquired in Paper I. This study analyzed time lags (delay or anticipation) between peak fire weather conditions and peak observed fire activity. These delays were interpreted as a consequence of land management and a group of 10 case studies were selected in specific fire regimes location and analyzed to unravel the anthropogenic signature on fire seasonality. A large variety of fire practices associated with land management, deforestation or agriculture activities were highlighted as results of the anthropogenic impact on fire seasonality.

Paper III focused on testing the hypothesis of spatial non-stationarity in the coefficients of the relationship between population density and area burnt, using geographically weighted regression (GWR). This concept affords the opportunity to assess a spatial variability that is not acknowledged in any DGVM, by measuring the magnitude of the relationship between human activities and fire incidence, showing that the inclusion of non-stationarity led to significantly different results from those obtained using global (i.e. spatially stationary) regression techniques.

Paper IV tested the hypothesis that the highly anthropogenic nature of African vegetation burning would lead to weekly cycles in fire activity, modulated by the regionally dominant religion. Croplands are the only major land use type where there is a significant weekly cycle in vegetation burning, with Sunday minimum in Christian regions, and Friday minima in Muslim regions.

Paper V was focused on the need to improve the identification of fire events, and therefore depict better results for fire size distributions, an input variable to Paper VI. In this paper, we developed a novel method to identification of fire events using active fire data. The algorithm encodes the relevant space and time contiguity relationships between the fire patches in a graph structure. An exploratory analysis was performed to evaluate the impact of using time gaps of 2, 8 and 14-days on the number, size and spatial distribution of active fire clusters.

Paper VI was focused on the developing of a new global classification map of *sensu strictu* fire regimes based on the definition proposed by Conedera et al., (2009) using 12 years of MODIS active fire data (Paper I) and integrating outputs derived from Papers II, III, IV and V. A Multiple Correspondence Analysis, and hierarchical clustering was applied to depict, seven fire regimes that can be grouped into three major regimes, corresponding to boreal forests / semi-arid regions, tropical savannas, and croplands / grasslands. The fire regimes classification map was smoothed with a spatial filter parameterized to optimize the trade-off between cluster separation in the principal factorial plane and spatial homogeneity.

The format of the listed contributions, figures and other details may differ among the articles in order to keep consistency with their published format, or the required format of each scientific journal.

I. Exploratory Spatial Data Analysis Of Global Modis Active Fire Data

D.Oom, J.M.C. Pereira

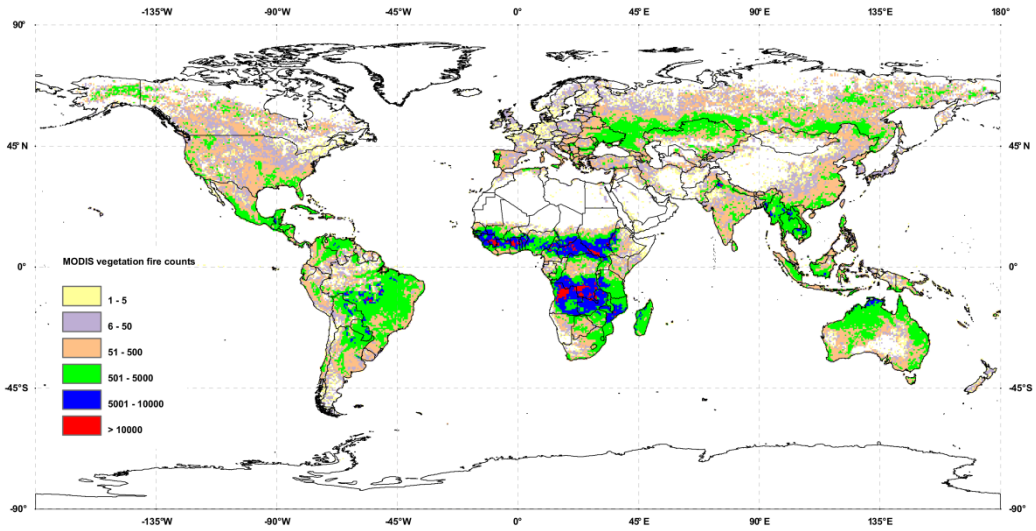

Published in *International Journal of Applied Earth Observation and GeoInformation* in July 2012

International Journal of Applied Earth Observation and Geoinformation 21 (2013) 326–340

Contents lists available at SciVerse ScienceDirect

International Journal of Applied Earth Observation and Geoinformation

journal homepage: www.elsevier.com/locate/jag

Exploratory spatial data analysis of global MODIS active fire data

D. Oom*, J.M.C. Pereira

Forest Research Centre, School of Agriculture, Technical University of Lisbon, Tapada da Ajuda 1349-017 Lisboa, Portugal

ARTICLE INFO

Article history:
Received 13 April 2012
Accepted 27 July 2012

Keywords:
Spatial data analysis
Vegetation fires
Global
MODIS

ABSTRACT

We performed an exploratory spatial data analysis (ESDA) of autocorrelation patterns in the NASA MODIS MCD14ML Collection 5 active fire dataset, for the period 2001–2009, at the global scale. The dataset was screened, resulting in an annual rate of false alarms and non-vegetation fires ranging from a minimum of 3.1% in 2003 to a maximum of 4.4% in 2001. Hot bare soils and gas flares were the major sources of false alarms and non-vegetation fires. The data were aggregated at 0.5° resolution for the global and local spatial autocorrelation Fire counts were found to be positively correlated up to distances of around 200 km, and negatively for larger distances. A value of 0.80 ($p = 0.001$, $\alpha = 0.05$) for Moran's I indicates strong spatial autocorrelation between fires at global scale, with 60% of all cells displaying significant positive or negative spatial correlation. Different types of spatial autocorrelation were mapped and regression diagnostics allowed for the identification of spatial outlier cells, with fire counts much higher or lower than expected, considering their spatial context.

© 2012 Elsevier B.V. All rights reserved.

1. Introduction

Vegetation fires occur worldwide, at different times of the year and inject large amounts of trace gases and particles into the atmosphere, having important environmental and climatic impact at global, regional and local scales. A reliable classification and characterization of the fire geography and seasonality at global scale that includes inter-annual variations is very important, not only to reduce uncertainties in estimates of emissions from biomass burning, but also to elucidate relationships between large scale climatic phenomena and fire occurrence and distribution at global scale. The use of satellite remote sensing allows for the collection of global, consistent fire information (Csiszar et al., 2005; Dwyer et al., 2000).

During the last decades several global fire analyses used different sensors and algorithms. Dwyer et al. (2000) and Stroppiana et al. (2000) analyzed the global spatial and temporal distribution of 12 months of Advanced Very High Resolution Radiometer (AVHRR) data at 1 km spatial resolution. Prins and Menzel (1992) used data from the Geostationary Operations Environmental Satellite (GOES) at 4 km spatial resolution to study fire activity in the western hemisphere. After that, the European Space Agency (ESA) Along Track Scanning Radiometer (ATSR) World Fire Atlas (WFA) (Arino and Rosaz, 1999; Arino et al., 2005), the NASA/Japan Aerospace Exploration Agency (JAXA) Tropical Rainfall Measuring Mission (TRMM) Visible and Infrared Scanner (VIS) (Giglio et al., 2000), and the active fire product from the Moderate Resolution Imaging Spectroradiometer (MODIS) (Justice et al., 2002) were some of the products that provided a good indication of the distribution of the burned area and active fires at different scales and years. These datasets were used to estimate atmospheric emissions of trace gases (Duncan et al., 2003; Schultz, 2002) and burned area (Eva and Lambin, 1998; Kasischke et al., 2003; Pereira, 2003; Pereira et al., 2004). Nevertheless, some of these products have known limitations. The assumption that the WFA contained few commission errors was disproved by Mota et al. (2006) and Oom (2008). They developed a data screening methodology, which led to the removal of about 25% of WFA observations, not corresponding to vegetation fires. NASA is also developing a global active fires dataset starting in 2000, based on the Aqua and Terra sensors (Giglio et al., 2003). Due to the improved specifications of those sensors for fire detection, four daily overpasses and the use of a more sophisticated detection algorithm this data set is expected to provide a more accurate depiction of global fire. However, the product is not error-free. Local and temporal limited validations of the MODIS active fire product were performed by Giglio et al. (2003, 2006), Morisette et al. (2005a, 2005b), Csissar et al. (2005), Schroeder et al. (2008a, 2008b), De Klerk (2008) and Hawbaker et al. (2008). They reported commission errors in the range of 2–3% (Boschetti et al., 2010). Nevertheless, no quantitative assessment of the MODIS global active fire dataset has been performed so far.

Exploratory data analysis (EDA) is of a set of descriptive and graphical statistical tools designed to find patterns in data and suggest hypotheses by imposing as little prior structure as possible

* Corresponding author. Tel.: +351 21 3653387; fax: +351 21 3653338.
E-mail addresses: duarteoom@isa.utl.pt, duarte.oom@gmail.com (D. Oom), jmcpereira@isa.utl.pt (J.M.C. Pereira).

0303-2434/$ – see front matter © 2012 Elsevier B.V. All rights reserved.
http://dx.doi.org/10.1016/j.jag.2012.07.018

(Tukey, 1977). This leads to "potentially explicable patterns" (Good, 1983), which may originate formal hypotheses and theoretical concepts. Objectives of EDA are to suggest hypotheses concerning the causes of observed patterns, to assess assumptions which underlie statistical inference, and to support the choice of correct statistical methods for the problem under analysis. Exploratory spatial data analysis (ESDA) is an extension of EDA to deal with spatial datasets. It involves specific techniques for detecting spatial patterns in data, formulating hypotheses based on the geography of the data, and assessing spatial models (Haining, 1993). A central concept of ESDA is spatial autocorrelation, the propensity for observations in geographical proximity to have similar values. Global spatial autocorrelation quantifies overall clustering of similar values and is tested against a null hypothesis of random location. Rejection of the null is indicative of spatial patterning in the data, providing useful information concerning the process under study. However, tests for global spatial autocorrelation only assess overall clustering and do not inform on the type (correlation between high values or between low values), extent, and location of spatial clusters and outliers (Anselin, 1995). A more detailed exploration of the data is possible with local indicators of spatial autocorrelation (LISA), which allow assessing the significance of local spatial patterns and classifying them into four types of association, distinguishing local clusters (high–high or low–low) or local spatial outliers (high–low or low–high) (Anselin, 1995). A map showing locations with significant Local Moran statistics, classified by type of spatial correlation is referred to as a LISA cluster map. Some studies have applied these techniques to spatial fire data. Pereira et al. (1998) identified spatial autocorrelation patterns in burned areas for Portugal, based on global and local indicators of spatial association. Chou et al. (1993) incorporated fire occurrence neighborhood effects on a spatial regression model for the San Jacinto Mountains, California, after data analysis based on Moran's *I*. Siljander (2009) modeled fire probability in Namibia using logistic regression. Moran's *I* analysis led to the incorporation of an autocovariate explanatory variable, accounting for neighborhood effects on fire incidence. Morisette et al. (2005a) used Moran's *I* to characterize the spatial patterns of active fires detected with high spatial resolution ASTER imagery, within lower resolution MODIS pixels, while validating MODIS active fire maps for southern Africa. In a fire severity assessment based on ASTER data, Coluzzi et al. (2010) used several spatial autocorrelation statistics to measure and analyze dependency among spectral features of areas burned in southern Italy. Finally, a procedure to detect active fires as spatial outliers in MODIS thermal imagery using Moran scatterplot analysis was proposed by Byun et al. (2006).

The aim of the present work is to perform an ESDA of the active fire data from the Moderate Resolution Imaging Spectrometer (MODIS) MCD14ML product (Justice et al., 2002) for the period 2001–2009 and spatially aggregated at 0.5° cell resolution, using the local Moran's *I* and the Moran scatterplot. The analysis may help identify relevant covariates, deal with model specification issues, such as the identification of spatial regimes, with potentially distinct parameter values, assess the prevalence and importance of local pockets of spatial non-stationarity that may behave as outliers and other influential observations, and assess the pertinence of incorporating a spatially lagged independent variable in the specification of spatial regression models, to be developed in a subsequent study

ESDA results are also relevant to assist in model specification for various types of regression modeling approaches, namely generalized additive modeling (Krawchuk et al., 2009), regression trees (Archibald et al., 2009), spatial hierarchical Bayesian modeling (Amaral-Turkman et al., 2010) and geographically weighted regression (Sá et al., 2011). However none of these studies was preceded by an ESDA.

2. Materials and methods

2.1. Data

The dataset consists of 9 years (January 2001–December 2009) of the MCD14ML Collection 5 active fire product (Justice et al., 2002), obtained with data acquired by the Moderate Resolution Imaging Spectroradiometer (MODIS) on board NASA's Earth Observing System (EOS) Terra (since February 24, 2000) and Aqua satellite (since May 4, 2002). MODIS has spectral and radiometric specifications designed for fire observation, with a spatial resolution of 1 km at nadir. Fire detection is accomplished using a contextual algorithm that exploits the strong emission of mid-infrared radiation from fires and is based on brightness temperatures derived from the 4 and 11 μm channels (Giglio et al., 2003), enhancing the sensitivity to smaller, cooler fires and decreasing the occurrence of false alarms. There are some periods with missing data, from June 16th to July 2nd (2001), March 20th to 27th and April 15th (2002). Although our analysis was performed at 0.5° spatial resolution, the decision of not using the Climate Model Grid (CMG) Fire Products (MOD14CMH, MYD14CMH) was due to our interest in screening daily, individual fire observations in the MODIS products.

We used the same ancillary dataset in the screening procedure as Mota et al. (2006), with updated versions: (i) Global Land Cover 2000 (GLC2000) map (Fritz et al., 2003), which is based on SPOT-VEGETATION 1 km satellite imagery for the year 2000; (ii) a 2008 annual global composite of stable nighttime lights (Elvidge et al., 2001) and an independent gas flare mask (2007) from the Version 4 Defense Meteorological Satellite Program (DMSP) Operational Linescan System (OLS) Nighttime lights time series data (http://www.ngdc.noaa.gov/dmsp/index.html); (iii) volcanic activity timing and location data (2001–2009) from the Global Volcanism Program (GVP) (http://www.volcano.si.edu/), Volcano World (http://http://volcano.oregonstate.edu/) and MODVOLC (http://modis.higp.hawaii.edu/). The terminology used by Mota et al. (2006) was also adopted: MODIS observations are the original fire counts, false alarms are observations that do not correspond to fires (hot ground surfaces or calibration errors) and fires are observations associated with combustion process (including vegetation fires and also non-vegetation fires, such as gas flares and volcanic eruptions (Fig. 1)).

2.2. Methodology

2.2.1. Screening procedure

The screening procedure of Mota et al. (2006) and Oom (2008) applied to the MCD14ML Collection 5 product was implemented in two stages (Fig. 1). In the first stage, spatial masks were applied to remove false alarms generated by hot bare ground and nightlights, as well as non-vegetation fires due to gas flares and volcanic activity. In the second screening stage the data were visually inspected and quantitatively analyzed to search for potential erroneous observations missed in the first stage. These inspections were accomplished calculating the difference between daily observation counts and five-day moving averages and, after aggregating to a 0.5° grid cell (fire counts per cell), the application of Local Moran (I_i) spatial index (Anselin, 1995). Based on the findings of Mota et al. (2006), deserts and sparsely vegetated regions were subject to particularly careful analysis, to identify commission errors. Throughout this second stage the observations excluded are considered false alarms, since they not correspond to combustion processes. The two-stage classification of MODIS observations is exhaustive, i.e. it addresses each and every fire count in dataset, but it is not mutually exclusive, i.e., a given observation may be captured by more than one filter. The goal of the screening is remove

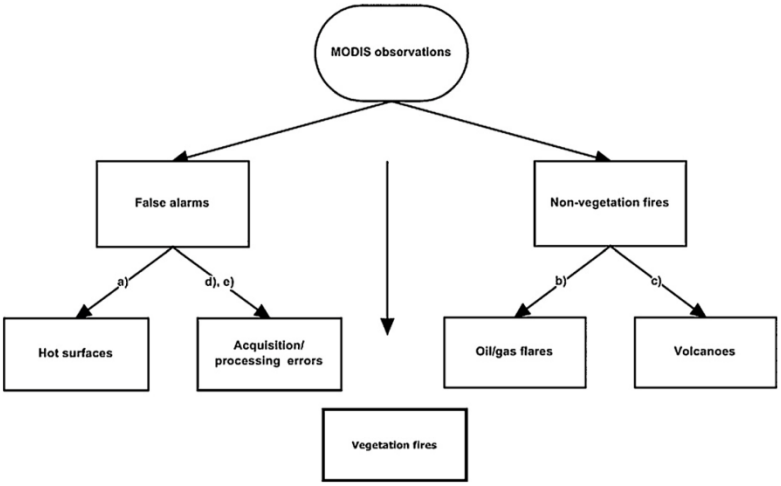

Fig. 1. Hierarchical screening procedure (based on Mota et al., 2006). The parts (a)–(e) are the datasets and index used during the screening procedure. (a) GLC2000, (b) DMSP stable nighttime lights, (c) volcanic activity timing, (d) daily moving average and (e) local Moran index.

non-vegetation fires and false alarms, keeping only vegetation fires in the dataset.

2.2.1.1. First stage screening. The MODIS active fire product (2001–2009) was first screened with the above mentioned combination of ancillary datasets. All the observations falling on GLC2000 classes "bare areas", "natural and artificial water bodies", "snow and ice" and "artificial surfaces and associated areas" were classified as false alarms or non-vegetation fires. Observations (non-vegetation fires) corresponding to gas flares were identified in the gas layer mask based on their circular appearance and lack of coincidence with populated places (Mota et al., 2006). The non-vegetation fires resulting from volcanic activity, were identified through two circular buffers (5 and 10 km radius) plotted around each volcano location, and observations within those buffers were matched against volcanic activity reports. The extent and direction of lava flows were also analyzed. Additionally datasets such as GLC2000 map and Google Earth high resolution images were used to determine whether MODIS observations were generated by volcanic activity, such as pyroclastic eruptions, lava flows, and/or ash plumes, or resulted from actual vegetation fires ignited by volcanic activity. Choice of size of the two buffers was based on analysis of caldera sizes from all the volcanoes. The observations detected in this step were classified as non-vegetation fires.

2.2.1.2. Second stage screening. All the observations that passed the first screening stage were visually screened by identifying very large potentially anomalous, concentrations of observations (in space and/or in time), unlikely to correspond to actual vegetation fires. The difference between daily counts and five-day moving averages was computed to identify atypical temporal clusters in the time-series. This visual/temporal inspection was also performed with exploratory spatial data analysis (ESDA) methods, using local indicators of spatial autocorrelation. Clusters of observations with geometric shapes, as straight lines or arcs were detected and classified as calibration errors (Giglio, 2010). The observations resulting from this screening stage were classified as false alarms. The combination of quantitative, automatic criteria and visual checking complements the first stage screening.

2.2.2. Exploratory spatial data analysis

To quantify spatial heterogeneity at global scale, detect spatial autocorrelation patterns, and identify clusters of similar fire incidence and outliers, an exploratory spatial data analysis (ESDA) of the screened data was performed. The number of fire counts in each 0.5° grid cell was log-transformed ($\log_n$) to reduce the skewness of the original data and improve the performance of ESDA techniques. The new variable was characterized with descriptive statistics and tested for normality with the Kolmogorov–Smirnof test with Lillefors correction. A box and whisker plot was created and the 1.5 Inter-quartile Distance (IQD) rule used to identify distributional outliers. According to this rule, values larger (smaller) than the third (first) quartile + (−)1.5 × IQD were considered outliers (Haining, 1993). To reduce the number of cells to be analyzed and focus on "fire prone cells", an analysis with potentially combustible areas (based on GLC2000 classes with available fuel) and ecoregions of the world (Olson et al., 2001) was performed. The following areas were excluded from further analysis: deserts and small island ecoregions; ecoregions with all grid cells without fire counts or with area smaller than 2500 km^2; all grid cells without fire counts or with less than 10% combustible area. A total of 50 423 half degree cells were kept and used to characterize the spatial pattern of fire at global scale. The global Moran's I statistic measures global (i.e. non-local) spatial autocorrelation and is assessed by testing a null hypothesis of random location, without spatial association (Anselin, 1995; Anselin et al., 2007; Cliff and Ord, 1981). Values of Moran's I larger (smaller) than the expected value $E(I) = -1/(n-1)$, with n as the number of observations, indicate positive-similar (negative-dissimilar) spatial autocorrelation values. However, the global statistic gives a measure of overall clustering and does not reveal the location of clusters or outliers nor the type of spatial correlation that may exist in the data. To overcome these limitations, local indicators of spatial autocorrelation (LISA), such as Local Moran statistic I_i (Anselin, 1995) were used. Anselin (1995) and Anselin et al. (2007) define LISA as an indicator of local spatial patterns and as diagnostics for local instability, i.e. areas where local patterns are not in line with the global indication. Also, as the sum of the I_i for all observations is proportional to the global value of the Moran's I it is possible to decompose Moran's I

into its components, using the Local Moran statistic (I_i), $I_i = (x_i - \mu)\sum W_{ij}(x_j - \mu)$ (Anselin, 1995), where W_{ij} is the element of the spatial weights matrix W corresponding to observation pair (i, j), and represents the component that incorporates "space" (Anselin et al., 2007), denoting the strength of connection between i and j. x_i and x_j are observations for locations i and j, with mean μ. In order to normalize the number of neighbors around a specific location, the spatial weights matrix was row-standardized such that the elements W_{ij} in each row sum to 1. I_i assigns an autocorrelation value to each observation ($\log_n$ fire counts cells). When the data are standardized as $Z_i = (x_i - \mu)/\sigma$, where Z_i is the standardized value of log-transformed fire counts for each cell and σ is the standard deviation, the value of the global Moran's I is equivalent to the slope of a linear regression line of a scatterplot where Z_i is plotted in the x-axis against the mean standardized neighbor value for each location, plotted in the y-axis. This bivariate spatial autocorrelation scatterplot is a graphic tool for detecting local spatial association, also providing a way to categorize the nature of spatial autocorrelation into four types high–high (type 1 – upper right) and low–low (type 3 – lower left) with potential spatial clusters of similar fire frequency, i.e., positive autocorrelation with high or low similar values; high–low (type 2 – lower right) and low–high (type 4 – upper left) with potential spatial clusters of dissimilar values. Positive values of I_i reveal spatial clusters of similar values (either high or low values) and are related with types 1 and 3, while negative values are related with dissimilar values corresponding with types 2 and 4. Thus, the Local Moran statistic in combination with the classification into four types of spatial autocorrelation pattern indicates significant local spatial clusters and facilitates the identification of unusual observations, such as outliers. The significance of Global and Local Moran statistics was evaluated with Monte Carlo randomizations, based on a non-parametric conditional randomization (permutation) approach, where the value x at site i is held fixed and the remaining values are randomly permutated over the other locations in the global dataset (Anselin, 1995). As Local Moran statistics calculated for each grid cell are not independent due overlapping neighborhoods, p-values were corrected with a 0.05 α-level of significance, using the Simes adjustment (Simes, 1986), which is less conservative than the Bonferroni correction.

Three types of regression diagnostics were calculated based on I_i and Moran scatterplot, to detect spatial outliers and analyze their influence on global spatial association: y-discrepancy, leverage and influence measures (Haining, 1994). The first is measured with standardized residuals and detects outliers, observations that are extreme along the dependent variable domain, Y; Leverage (h_i), assessed by the value of the diagonal elements of the hat matrix, is a measure of how far an observation deviates from the mean along the independent variable domain, X. An observation is influential when its exclusion from the dataset determines a large change in the value of the regression coefficients, and can be thought of as combining the effects of the other two diagnostics (Haining, 1994). It is assessed with Cook's distance.

Spatial analysis was performed with Spacestat software vs. 2.0 (Anselin, 1992). The 50 423 standardized, log-transformed fire counts for 2001–2009 were partitioned into four types. The distance range used to define spatial neighborhoods was based on analysis of the correlogram for equal distance bands and was fixed in the 200 km. The neighborhood weighting method used was the inverse distance rank and 999 permutations were employed to build the reference distribution.

Table 1
Annual results of MODIS dataset screening.

Year	Original	Screened	% screened
2001	1 597 241	70 020	4.38
2002	3 349 321	113 672	3.39
2003	4 618 197	141 005	3.05
2004	4 619 040	170 258	3.69
2005	4 670 379	171 415	3.67
2006	4 225 888	160 141	3.79
2007	4 679 841	153 904	3.29
2008	4 369 855	146 789	3.36
2009	4 061 749	134 036	3.30
Mean	4 021 279	1 401 38	3.55

3. Results

3.1. Data screening

The original MODIS dataset has 36 191 511 observations of which 34 930 271 (96.52%) were considered vegetation fires, while 1 261 240 (3.48%) correspond to false alarms or non-vegetation fires. Screening results show an annual percentage of false alarms and non-vegetation fires varying from 3% in 2003 to 4.4% in 2001 (Table 1). Hot bare soils and gas flares are the major sources of false alarms and non-vegetation fires (Table 2).

The years with the most counts were 2007 and 2005, with peaks in August, September and December (Tables 1 and 2). This result is expected because, according to NASA's Goddard Institute for Space Studies (GISS) 2005 and 2007 were two of the hottest years since records began in 1880 (Hansen et al., 2010). The year with fewer counts, excluding 2001 and part of 2002, when one only one sensor was acquiring data, was 2009. Gobron et al. (2010), analyzed a 12-year (1998–2009) time series of Fraction of Absorbed Photosynthetically Active Radiation (FAPAR) and report that 2009 had the strongest negative anomaly for this variable, corresponding to unfavorable conditions for fuel accumulation. Fig. 2 shows the daily time-series of the original MODIS active fire dataset (Fig. 2a), false alarms and non-vegetation fires screened from the original data (Fig. 2b) and the final screened data, containing only vegetation fires (Fig. 2c).

Table 2
Number of observations captured by each filter (observations could be screened by more than one filter).

Year	Landcover				Gas flares	Volcanoes	Calibration errors	Total
	Bare	Water	Artificial	Snow				
2001	23 647	8938	5409	39	32 148	3595	832	74 608
2002	41 641	19 967	8044	17	40 957	7229	0	117 855
2003	42 531	23 878	10 666	40	58 360	7494	0	142 969
2004	60 294	29 391	10 282	16	69 165	6803	705	176 656
2005	57 432	27 147	11 426	164	73 612	7949	0	177 730
2006	55 564	22 758	11 916	42	69 330	6794	0	166 404
2007	48 639	22 485	11 901	102	64 996	7849	0	155 972
2008	42 604	23 679	11 870	64	56 787	6816	6757	148 577
2009	38 430	23 129	10 827	56	52 846	6286	0	131 574
Total	410 782	201 372	92 341	540	518 201	60 815	8294	1 292 345[a]

[a] The total is greater than the number of screened observations due to counting by more than one filter.

The time-series (in particular Fig. 2a and c) shows an increment in fire counts, starting June 2002, justified by the launch of Aqua satellite, while before this date only the MODIS sensor onboard the Terra satellite was acquiring data. The time-series also reveals a seasonal pattern, with a large number of observations during the boreal summer, between July and September, with a peak in August. A secondary peak also occurs between November and February with a maximum in late December and early January. This secondary peak corresponds mainly to savanna fires in northern hemisphere Africa. The year with the most counts is 2007 (in both the original and screened data), with peaks in August–September. The time-series of non-vegetation fires and false alarms (Fig. 2b)

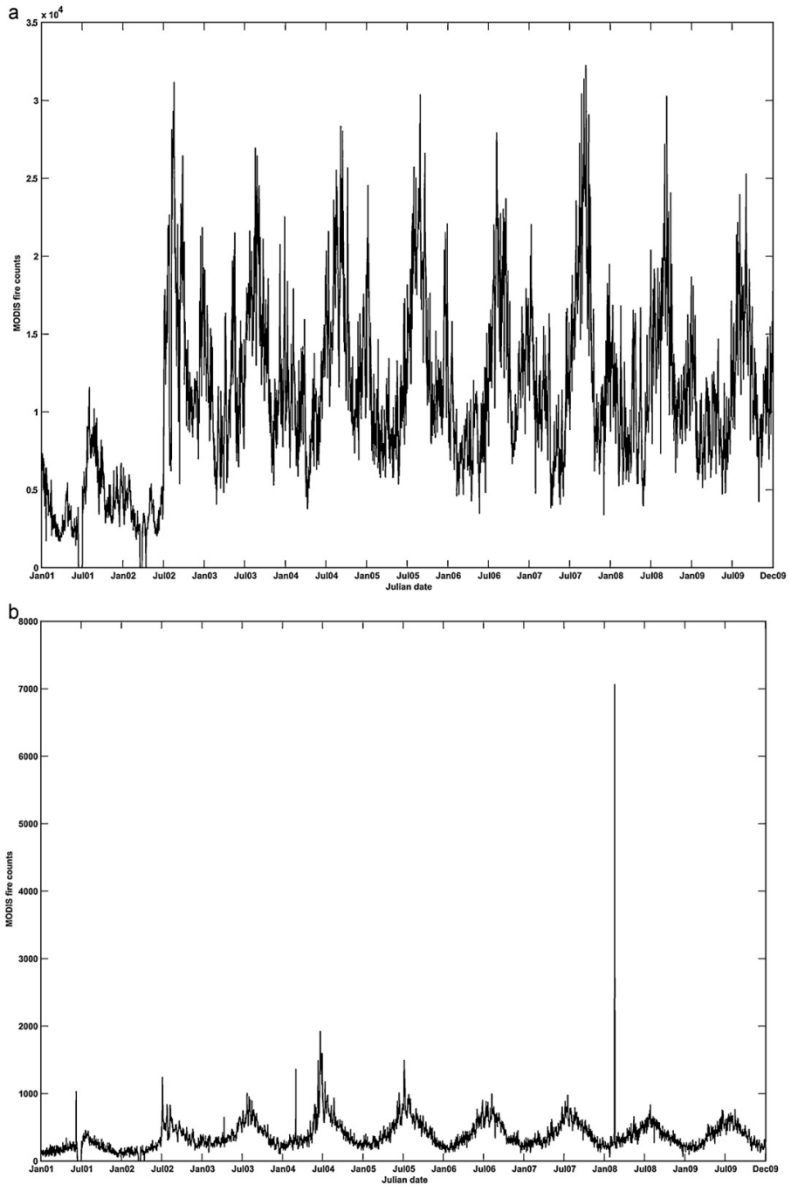

Fig. 2. Daily time-series of (a) original MODIS fire observations, (b) data removed from the original and (c) screened dataset. Only MODIS TERRA data were available from February 2000 to May 2002.

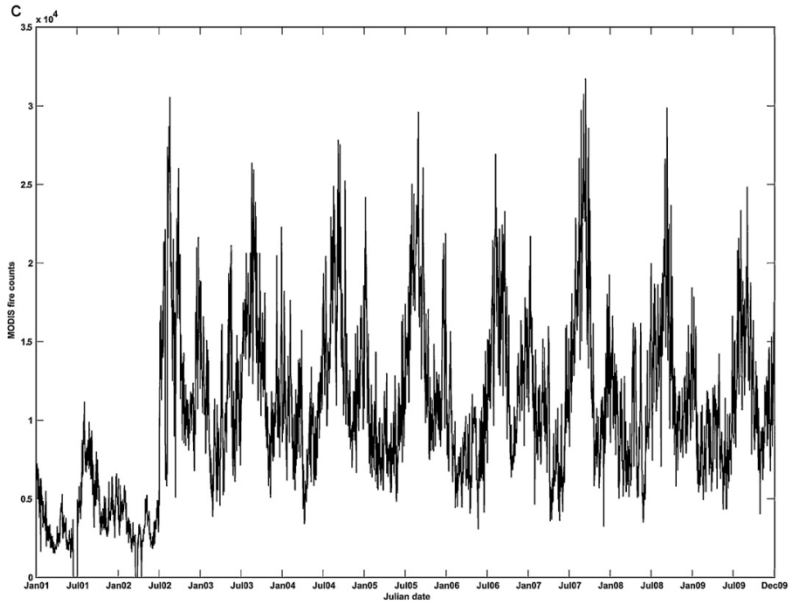

Fig. 2. (*Continued*).

also reveals a seasonal pattern, with a very large spike in February 16, 2008 corresponding to calibration errors. Fig. 3 decomposes the time-series of false alarms and non-vegetation fires into land cover and oil and gas flares filters. Both filters show seasonal patterns with more observations during the boreal summer (note the different scales).

However, while the land cover and oil gas flares time series show a seasonal trend, with more observations during the boreal summer induced by hot land surfaces, the volcanic eruptions time series exhibits a pattern unrelated with climate and with several sporadic spikes, corresponding to large eruptions. The calibration error filter captured three spikes, the largest of which occurred in February 16th, 2008 and corresponds to a cluster of 6757 observations located in northern Russia. The other two spikes are located in Antarctica and northeastern Canada. Fig. 4a–c displays maps of the original MODIS fire data, false alarms and non-vegetation fires, and vegetation fires. Fig. 4a and c is very similar regarding the location of the larger clusters. Fig. 4c displays a geographical fire distribution similar to several previous studies (e.g. Csiszar et al., 2005; Dwyer et al., 2000; Mota et al., 2006), with large clusters located in tropical and sub-tropical zones in the northern and southern hemisphere of Africa, the cerrado savannas of Brazil, savannas and forests in southern Mexico, and tropical savanna in northern Australia. At higher latitudes, Kazakhstan and the northwestern Iberian Peninsula also display high concentration of vegetation fires. The screened observations (Fig. 4b) are mainly concentrated in Kazakhstan and eastern China (landcover filter), Algeria, Libya, Nigeria, Russia and Persian Gulf region (gas flares filter). The land cover filter captured 705 035 observations (55% of all screened observations) with the bare areas class as the most representative, with 410 782 observations (31% of all screened data and 58% of the land cover filtered data).

The gas flares filter, with 518 201 observations removed (40%) and a peak in 2005, shows Iraq (127 499 observations removed), Russia (95 408), Iran (72 575) and Nigeria (40 302) as the countries with the most non-vegetation fires due to oil and gas exploration activities. We analyzed 432 volcanoes which captured 60 815 observations (5% of total screened) for 2001–2009 period, which were not vegetation fires. Volcanoes like Kilauea, in Hawai with 19 985 observations filtered, and African volcanoes like Nyiragongo and Nyamuragira in the Democratic Republic of Congo with a total of 5514 observations, or Erta Ale in Ethiopia with 3989, were those responsible for the larger numbers of observations screened out. Calibration errors were located in Russia, Antarctica and Canada, mainly in 2008. Again, 2005 and 2009 display respectively the largest and smallest number of observations post-screening, for the reasons mentioned above.

3.2. Exploratory spatial data analysis

The 50 423 half degree log-transformed fire counts kept for the period 2001–2009 were used to analyze the spatial structure of fires at global scale. The log-transformation unskewed the data (skewness decreased from 3.690 to −0.022). The Kolmogorov–Smirnof test with Lillefors correction was applied for original fire counts, log-transformed fire counts and log-transformed standardized fire counts and all show that the distributions are non-normal ($p = 0.000$).

The distributional properties of log-transformed fire counts and the geographical distribution of the data classified into quartiles are presented in Table 3 and Fig. 5, respectively. According to the 1.5 IQD rule no distributional outliers were present.

Table 3
Distributional properties of the 50 423 $\log_n$-transformed MODIS fire counts.

Minimum	Maximum	Mean	Std. deviation	Variance
0.000	9.673	3.902	2.840	8.069
Skewness	**Kurtosis**	**1st quartile**	**2nd quartile**	**3rd quartile**
−0.220	−1.245	1.099	4.149	6.267

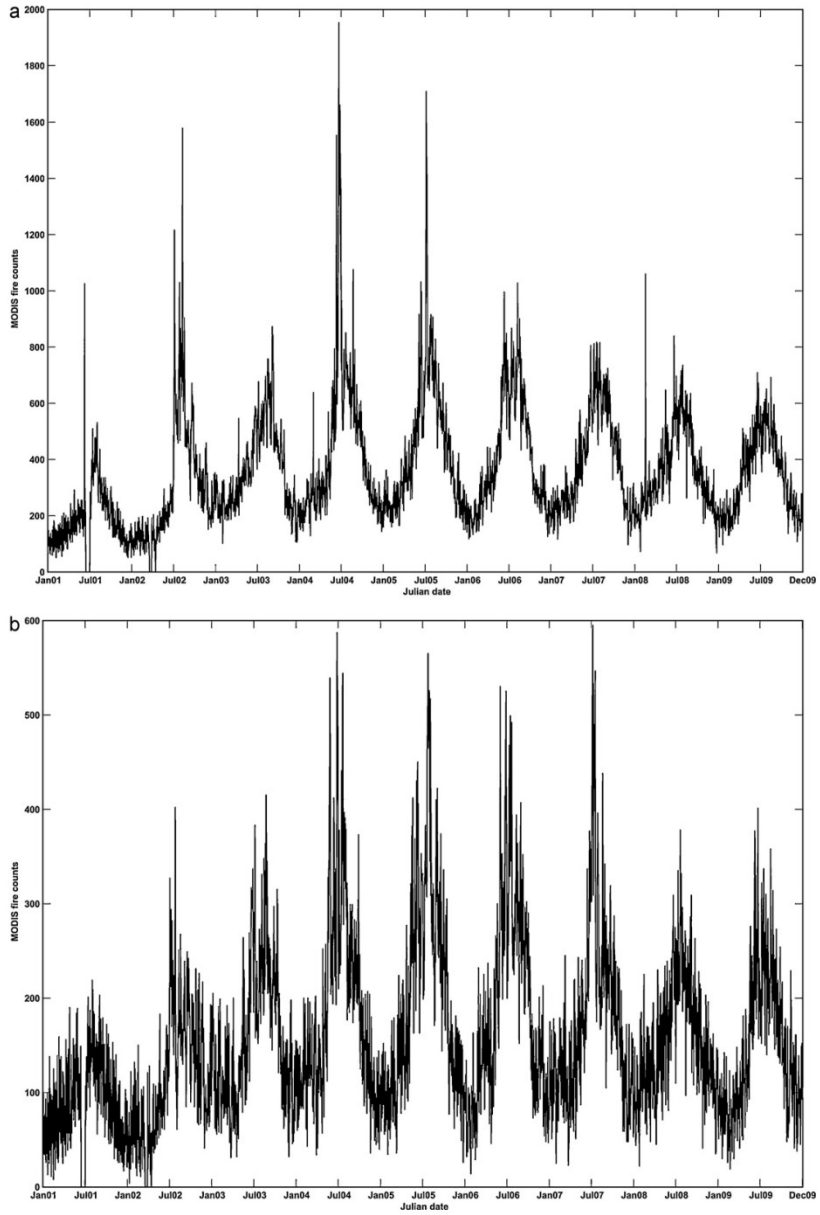

Fig. 3. Daily time-series of original MODIS fire observations removed due each filter: (a) land cover, (b) oil and gas flares. Only MODIS TERRA data were available from February 2000 to May 2002.

3.2.1. Spatial statistics

All calculations were made using standardized log-transformed fire counts. A value of 0.80 ($p = 0.001$) for Global Moran's I was obtained ($\alpha = 0.05$). The expected value for I was −0.00002. Local Moran (I_i) range from −1.82 to 3.90, with a mean of 0.80 (Fig. 6).

Negative values of I_i are located mainly in South America, Canada, Alaska, and Russia. A few cells with negative values are also present in Africa, China, India and Australia. Positive values of Local Moran (I_i) are concentrated in tropical and boreal regions and can be found in all continents. According to the 1.5 IQD rule,

135 I_i spatial outliers were identified, all located in Africa. I_i detected 20 316 cells without significant spatial autocorrelation and 30 107 (60%) spatially autocorrelated cells. From these, 29 269 have a positive sign and 838 a negative sign, indicating correlation of similar and contrasting values, respectively.

3.2.2. Moran scatterplot

The Moran scatterplot (standardized values of the log-transformed fire counts for each cell was plotted against the mean standardized neighbor value for each location) divided the 50 423 cells into four spatial association types (Fig. 7). Out of 30 107 (60%) significantly autocorrelated cells, 14 996 (30%) show spatial clustering of high values (type 1) while 14 273 (28%) display spatial clustering of low values (type 3). 579 cells correspond to type 2 and 259 to type 4. About 20 316 (40%) cells display non-significant autocorrelation ($p > 0.05$). Moran scatterplot regression has a positive slope of 0.80, indicating dominance of positive spatial association and, an r^2 of 0.82.

Fig. 8 displays the geographical distribution of the four types of spatial association.

Regions of positive spatial autocorrelation are colored in gray and yellow (types 1 and 3 respectively) (Fig. 8). Gray regions represents cells of high fire activity, surrounded by similar cells and are located mainly in tropical and subtropical regions, but

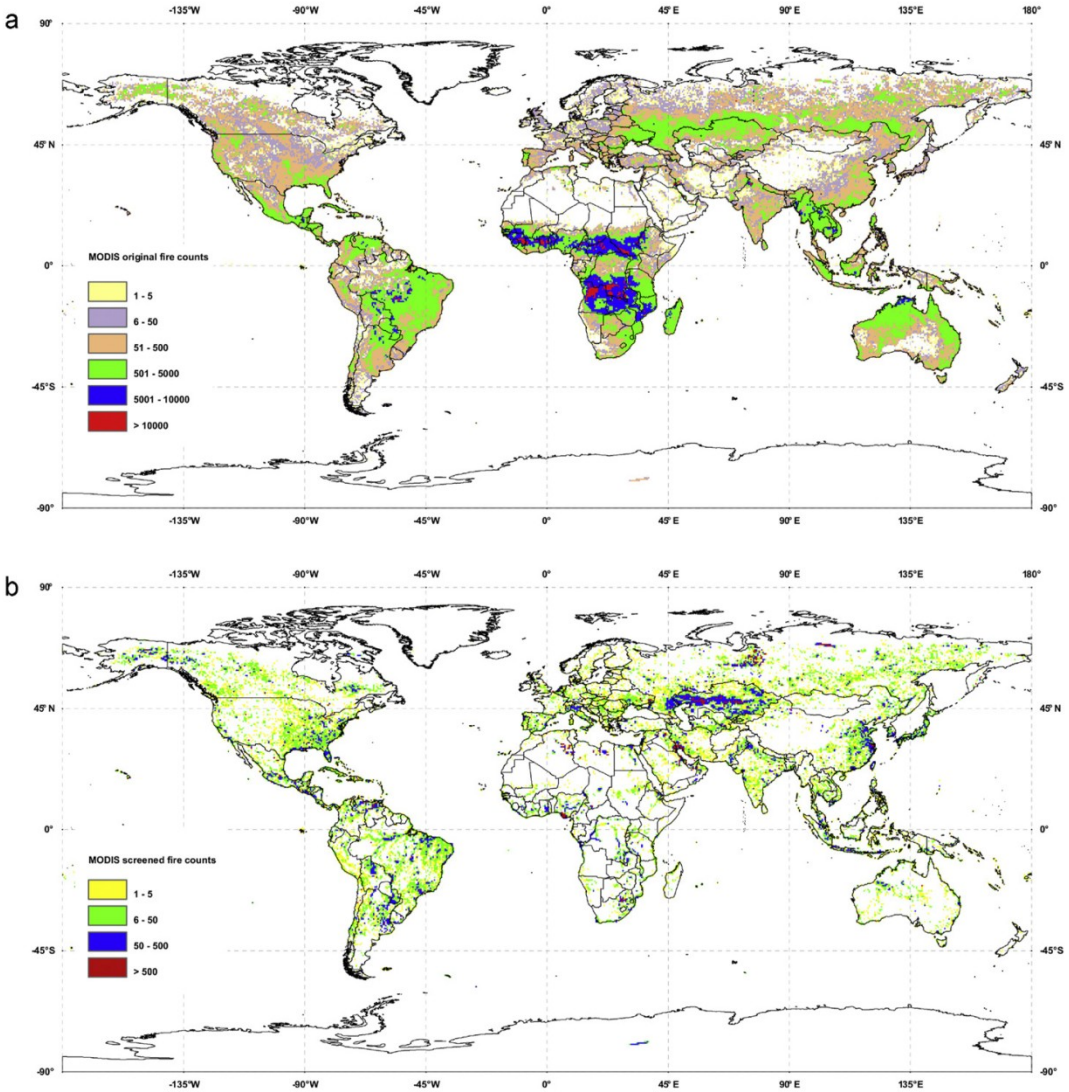

Fig. 4. Global maps (2000–2009) of (a) original MODIS fire counts, (b) removed observations, and (c) vegetation fires data set.

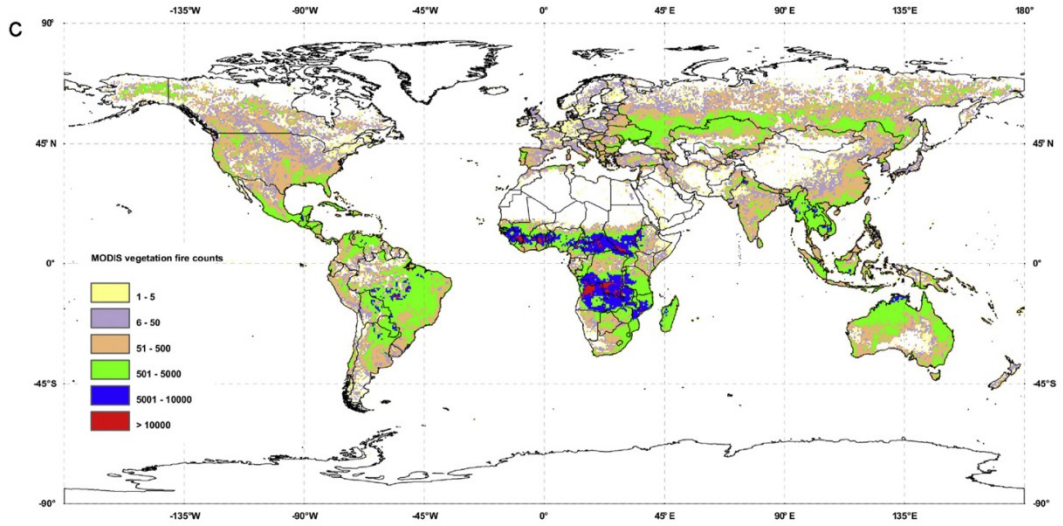

Fig. 4. (*Continued*).

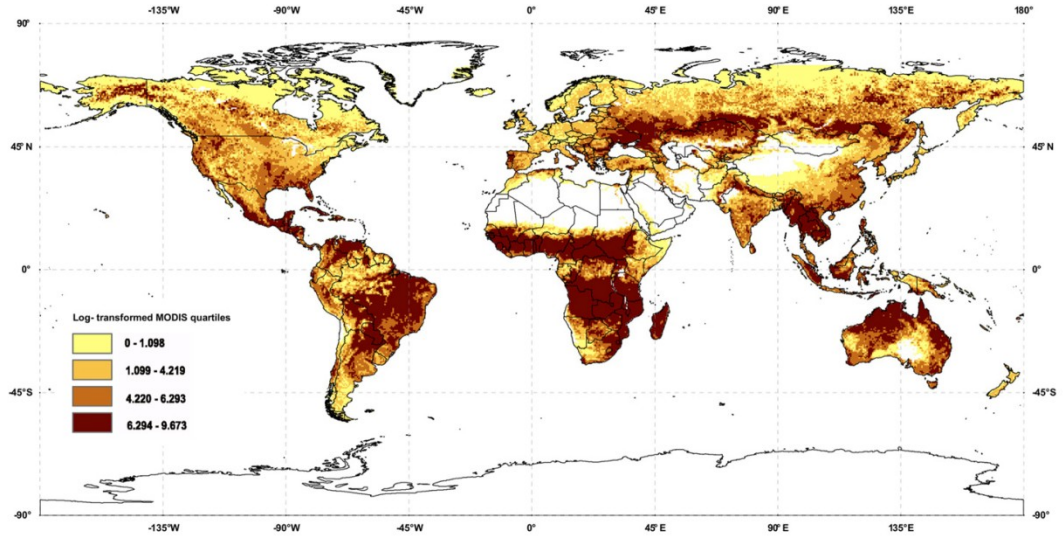

Fig. 5. Log-transformed MODIS fire counts cells quartiles (2001–2009).

also in Alaska, agricultural areas in southeastern USA, and in eastern Europe, extending to northern Kazakhstan. The most positive values are of type 1 (high–high) and are located in tropical zones, such as the sub-Saharan region of northern hemisphere Africa, in the forest savanna-mosaic (Central African Republic and southern Sudan) and in the southern hemisphere tropical woody savannas, especially in Angola miombo woodlands and forest-savanna mosaic. The other positive values of I_i classified as type 3 (low–low), are mainly located in boreal regions, Brazil, Venezuela, and China. The yellow regions represent low fire activity cells located in a low fire activity neighborhood are found mainly in boreal regions, Amazonia, the horn of Africa and Tibet. High–low (type 2) and low–high (type 4) reveal spatial clusters of dissimilar values, i.e. cells with high fire activity in low fire activity neighborhood, and cells with low fire activity in a high fire activity neighborhood. The former are mainly located in Canada, Russia and United States, whereas the latter are found mostly in Brazil and Russia (Fig. 8).

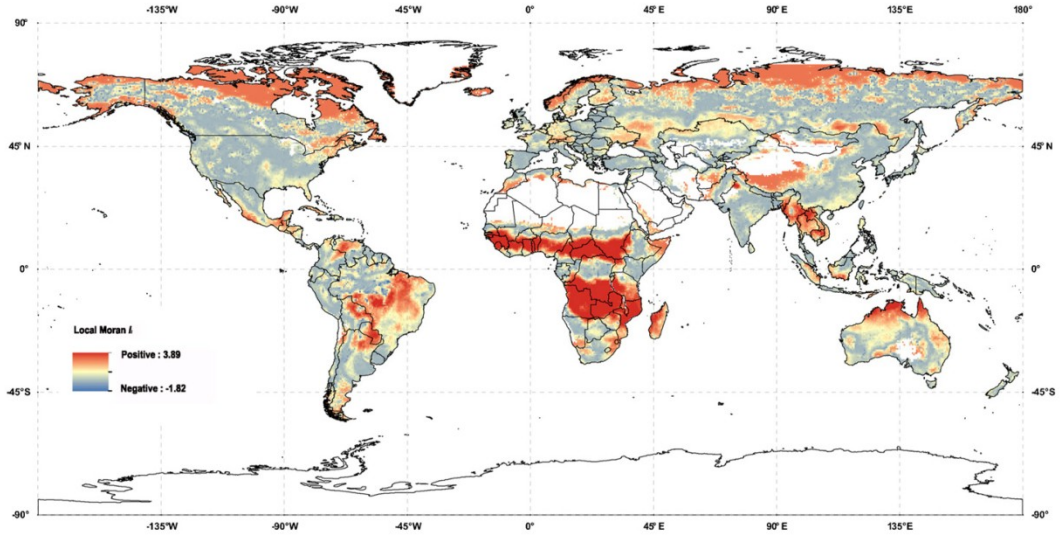

Fig. 6. Geographic distribution of Local Moran, I_i.

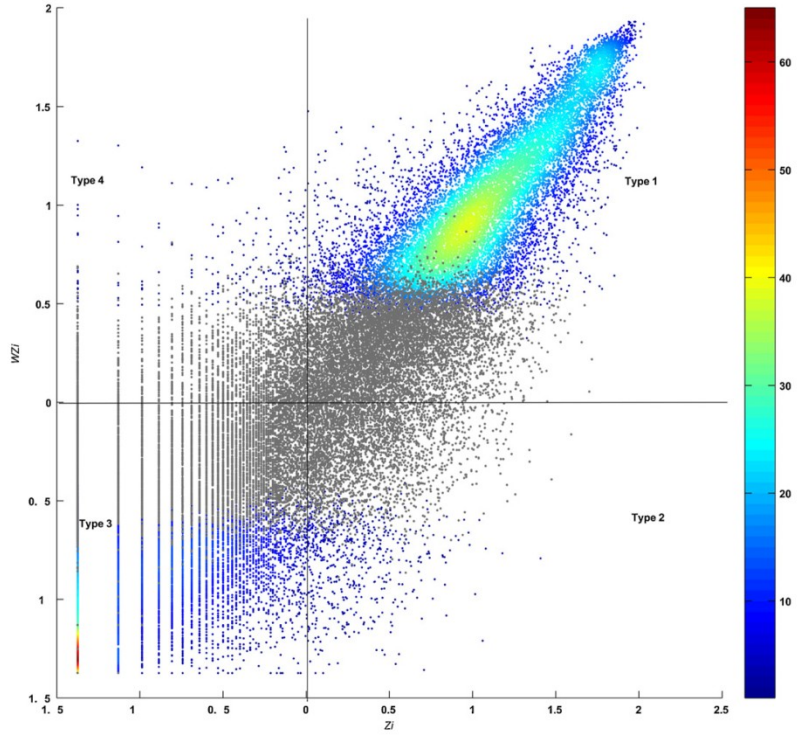

Fig. 7. Moran density scatterplot. Z_i is the standardized value of log-transformed fire counts for each cell and WZ_i is the mean standardized neighborhood value for each cell. Type 1 (high–high, upper right) and type 3 (low–low, lower left) represents potential spatial clusters of similar fire frequency, i.e., positive autocorrelation with high or low similar values respectively; type 2 (high–low, lower right) and type 4 (low–high, upper left) represents potential spatial clusters of dissimilar values. Gray dots are non-significant values.

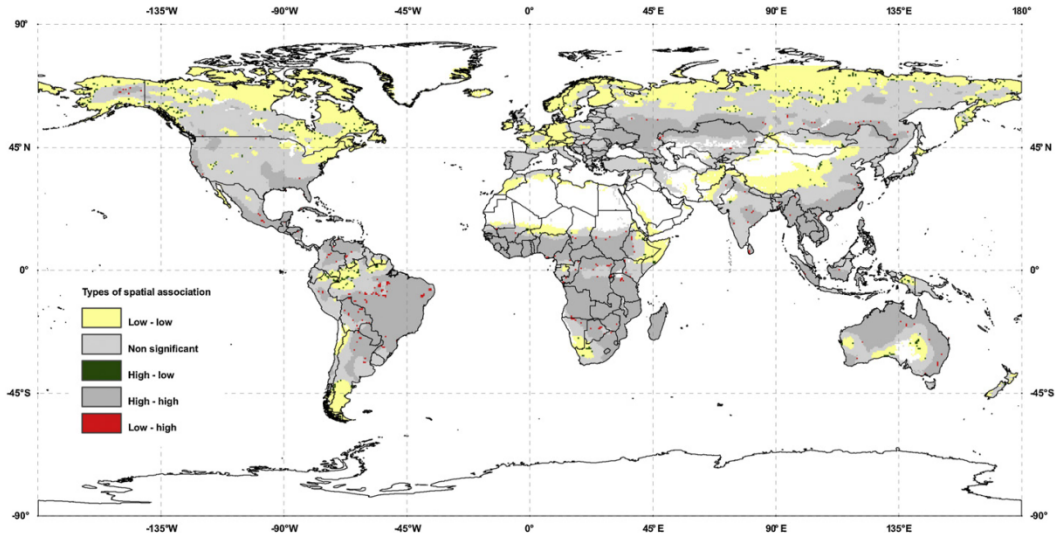

Fig. 8. Geographical distribution of the four types of spatial association, partioned with the Moran scatterplot. The high–low cells are located in Canada, Russia and United States. The low–high cells are mainly located in Brazil, Russia, USA and Canada.

The high–low cell with the most negative I_i value (with 1005 fire counts) is located in Alaska, but that with the most fires is located in Brazil, with 2701 fire counts during the study period. In Russia, the high–low cells with the most fire counts in the period under analysis were located in the Siberian Far East. Brazil is the country with the higher number of low–high cells, with 55, out of a total 259. They are mainly located in protected areas with 34 being located in indigenous areas of the Legal Amazon. The remaining 21 cells occur in four clusters, in the states of Amazonas, Pará, Bahia, and Paraíba. The Russia low–high cells are located near the borders with Kazakhstan, Mongolia and China, where some cells with few fires are surrounded by cells with higher fire activity that are common in those regions.

3.2.3. Regression diagnostics

The ten most extreme observations according to each Moran scatterplot regression diagnostic were analyzed in detail. Fig. 9 displays the spatial distribution of the 30 most extreme observations according to the three types of regression diagnostics (10 for each regression diagnostic): *y*-discrepancy, influence and leverage. Table 4 describes those extreme cells.

Most of these observations are located in the tropical belt, except for three in Alaska. The largest outliers (absolute standardized residuals) are of type 4 (low–high), and type 2 (high–low) and can be found in Brazil, Guatemala, USA (Alaska) and Bolivia. The highest leverage values are of type 1 (high–high) and are located mainly in Africa (Guinea, Sudan and Angola) except for the highest of all, which is located in NW India. The most influential observations, according to Cook's distance, are of type 2 (high–low) for one grid cell in Brazil and one in Alaska, and of type 4 (low–high) for the rest of the cells, located in Brazil, Alaska and Guatemala. Some cells in Brazil, Guatemala, Alaska, Russia and Bangladesh have extreme values, both according to the standardized residuals and Cook's distance diagnostics. For instance, in Brazil the cell with the most extreme residual value is also the most influential one. Due to this identification by more than one diagnostic, the 30 most extreme observations correspond to 22 grid cells, with Brazil (five cells) and Guinea and Angola (four cells each) as the countries with the most extreme values.

4. Discussion

4.1. Data screening

We used a 9-year record of original MCD14ML Collection 5 active fire product, dated from January 2001 through December 2009. The screened fire distribution results are consistent with several global/regional studies, including some performed with data from different sensors. A small percentage of observations (3.5%) were removed from the original dataset, which compares very favorably with the approximately 25% observations found not to be vegetation fires in the ATSR WFA, using a very similar procedure (Mota et al., 2006). The screening procedure highlighted several commission errors caused by a variety of factors, such as hot bare soil surfaces, gas flares, other industrial and urban heat sources, volcanoes, and calibration errors. More than 1 250 000 observations (3.5%) were false alarms or non-vegetation fires, mainly due to hot bare soils. The two-stage screening showed that most false alarms were eliminated with the application of the spatial mask (first stage), while the second stage was much more time consuming identifying anomalies or large clusters concentrated in space and/or time, and unlikely to correspond to actual vegetation fires. All commission errors derived from land cover, gas flares, urban/industrial lights and volcanoes are clustered, either in space, in time, or both, most with a markedly seasonal pattern. As Mota et al. (2006) concluded with ATSR fire data, seasonality in land cover false alarms is mainly induced by hot soil surfaces and, as the observations are captured by more than one filter (not exclusively), the seasonal pattern present in the gas flare observations removed from the dataset results from overlap with those captured with the land cover filter.

4.2. Exploratory spatial data analysis

The Global Moran's *I* statistics provided a good measure of spatial pattern of global fire distribution. A value of $I = 0.80$ revealed

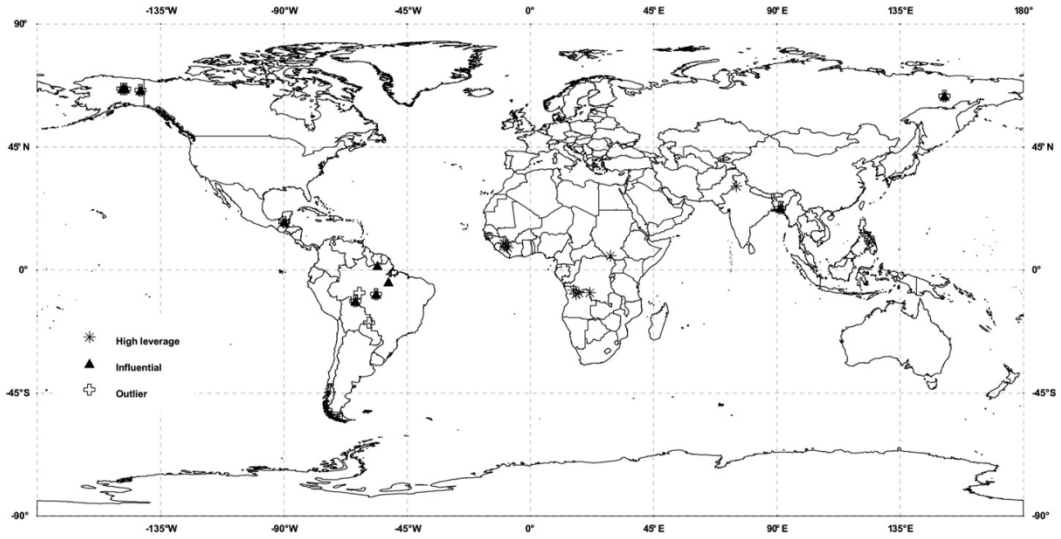

Fig. 9. Geographical distribution of the 10 most extreme observations for each Moran scatterplot regression diagnostic: outliers, high leverage, and influential observations.

strong spatial autocorrelation between fire observations, which was positive at distances up to 200 km. The ESDA detected strong clustering of like values (HH and LL), with the HH clusters primarily located in tropical savannas and temperate agricultural areas, while LL clusters were mostly found in boreal forests. Such strong spatial clustering pattern may indicate the usefulness of developing a regression model with a small number of spatial regimes, to account for likely differences in model parameters in areas associated with these two kinds of cluster. The high spatial autocorrelation values detected, both globally (Moran's *I*), and locally (local Moran's *I*) suggest that it may be worthwhile testing the advantage of developing a spatial lag regression model. Regarding the observations in the LH and HL quadrants of the Moran scatterplot, detailed analysis of the LH cells indicates that it will be appropriate to use an explanatory variable characterizing nature conservation status, at the global scale. The HL cells represent a more difficult problem to model. They typically correspond to large wildfires occurring in areas with fire cycles an order of magnitude longer than the duration of our 9-year dataset, thus representing a temporal sample that is too short to yield stable spatial patterns of fire incidence.

4.3. Regression diagnostics

The spatial distribution of the 30 most extreme observations, according to the Moran scatterplot regression diagnostics is shown in Fig. 9 and Table 4, and discussed below.

4.3.1. Outliers

The largest outlier corresponds to a cell located in the Uru-Eu-Wau-Wau indigenous protected area (11°S, 64°W) in Rondonia, Brazil, an area with around 1 900 000 ha, which was created to protect valuable ecosystems and to preserve a region that represents the transition between Cerrado and Amazonia forests (IBAMA, 2005). The second largest outlier occurs in the Maya Biosphere Reserve, Guatemala (18°N, 90°W), located in the border between Guatemala and Mexico (18°N, 90°W), in a region with three contiguous UNESCO biosphere reserves: the Maya Biosphere Reserve in Guatemala, Calakmul and Montes Azules Biosphere Reserves in southern Mexico. According to the UNESCO Man and Biosphere Programme (MAB), in this Mexican region (more than 3 600 000 ha), one of the biggest areas of tropical forest located north of the Amazon, and the northernmost tropical forest in the Western Hemisphere, efforts have been developed to come up with viable alternatives to slash-and-burn farming. Of the other cells, two are located in Brazil. One is in Pará state (9°S, 56°W), and belongs to a four-cell cluster located at Serra do Cachimbo, in a forest region between two protected areas, located in a military training camp of the Brazilian Air Force. The other cell, located within the Tumucumaque indigenous protected area (2°N, 56°W), was classified as type 2 (high–low) and, from the cells with negative values of I_i, is the one with the most fire observations (2701) during the period of analysis. It coincides with an isolated area of savanna-like vegetation surrounded by moist forests (Tiriyós Savanna), near the border with Surinam. The 2701 fire counts are distributed throughout the entire study period, with a peak in 2004 of around 700 fire observations. Fire, which plays a very important role in the culture of the indigenous population living in the area occurs between September and November, and is used for hunting and pasture renewal (Barbosa and Campos, 2011; Rodrigues et al., 2007). The Bolivia cell (19°S, 59°W) is located in southeastern Bolivia on the borders with Brazil and Paraguay, within in the Otuquis National Park. This protected area is part of one of the largest flood-prone areas in the world – the Pantanal. Although a few agricultural fires may occur within the park, in the surrounding area fire is widely used to clear land for agriculture and ranching, determining the classification of this cell as low–high cell.

Therefore, fire count spatial outlier analysis highlighted the substantial reduction in fire activity in several Amazon protected areas, by contrast with their surroundings, in agreement with Nepstad et al. (2006) suggesting effectiveness of these areas in restricting the use of fire.

The Alaska (USA) cells classified as low–high (66°N, 142°W; 66°N, 148°W; 66°N, 149°W) were adjacent to a group of type 1 (high–high) cells in central-eastern part of the state, where most fire activity occurred in 2004, the worst fire year on record in Alaska (Shulski, 2005). These cells are within Yukon Flats National Wildlife

Table 4
Extreme observations derived from the diagnostic regression. HH – high/high; HL – high/low; LL – low/low; LH – low/high.

Location				Diagnostic regression			Moran scatterplot				Spatial outlier	Observations
ID	Country	Lat., long. (°)	Zone	Outlier	Leverage	Influential	Type 1 (HH)	Type 2 (HL)	Type 3 (LL)	Type 4 (LH)	1.5 IQD rule	
1	Brazil	11S, 64W	Uru-Eu-Wau-Wau	X		X				X		Indigenous protected area[a]
2		9S, 56W	Serra do Cachimbo	X		X				X		Military zone
3		2N, 56W	Tumucumaque	X		X		X				Indigenous protected area[b]
4		4S, 52W	Trincheira Bacajá			X				X		Indigenous protected area[c]
5		5S, 52W				X				X		
6	Guatemala	18N, 90W	Guatemala-Mexico border	X		X				X		UNESCO reserve[d]
7	USA	66N, 142W	Yukon Flats National Wildlife refuge (YFNWR)	X		X				X		Protected area[e]
8		66N, 148W		X		X				X		
9		66N, 149W		X		X				X		
10		61N, 143W	Wrangler St. Elias Nat. Park	X		X		X				2009 Chakina fire[f]
11		63N, 147W	Valdez/Copper River area forestry	X				X				2004 Alphabet Hills fire[g]
12	Bolivia	19S, 59W	Otuquis National Park	X						X		Protected area[h]
13	India	31N, 75W	Punjab		X		X					Agricultural fires[i]
14	Guinea	10N, 10W	Guinea Highlands		X		X				X	Savanna/grassland fires
15		10N, 9W			X		X				X	
16		9N, 9W			X		X				X	
17		8N, 8W			X		X				X	
18	Angola	7S, 16E	Malanje, Lunda and Cuanza provinces		X		X				X	
19		8S, 18E			X		X				X	
20		8S, 22E			X		X				X	
21		9S, 17E			X		X				X	
22	Sudan	5N, 17E	Southwest		X		X				X	

[a] http://pib.socioambiental.org/caracterizacao.php?uf=UF&id_arp=3891.
[b] Rodrigues et al. (2007) and Barbosa and Campos (2011).
[c] http://pib.socioambiental.org/caracterizacao.php?id_arp=3609.
[d] http://www.unesco.org/mab.
[e] Drury and Grissom (2008) and Natcher (2004).
[f] AICC (2009).
[g] Hrobak (2006).
[h] http://www.fcc.org.bo/web/.
[i] Le Page et al. (2010) and Sharma et al. (2010).

Refuge (YFNWR). This is one of the most fire-prone landscapes in Alaska, where fire is allowed as a natural process, under specific environmental conditions depending on values to protect (Natcher, 2004). According to the YFNWR Fire Management Plan summary, the levels defined as critical and full management include zones like villages, native land and with highly valued resources. These zones receive high priority for fire suppression. The cells are in the central part of the refuge where the main villages are located, so fire activity in these cells probably reflects the different levels of intervention used at YFNWR.

The other Alaska cells (61°N, 143°W; 63°N, 147°W) were classified as type 2 (high–low). The first is the high–low cell with the most negative I_i value, and is located within the Wrangell St. Elias National. It corresponds to the Chakina fire of 2009, which burned ca. 23 000 ha. According to the Alaska Interagency Coordination Center (AICC), 2009 was one of the driest and warmest summers on record in southeastern Alaska and had one of the worst wildfire seasons in 50 years. The second cell contains 369 active fires, all observed in 2004 during the Alphabet Hills fire, which lasted for 13 days, burned around 15 000 ha and was part of the Bureau of Land Management (BLM)/Alaska Fire Service (AFS) fuels reduction program to reduced fire danger around communities in the Copper River basin (Hrobak, 2006).

There, outlier analysis highlighted the location of large fires that occurred during the study period. Since this period is very short relatively to the fire cycle of boreal forests, exceptional events stand out clearly.

So, with the exception for the Tumucumaque and Chakina fire events, most of the outliers correspond to protected areas where fire is suppressed and regulated. In fact, wildfires are a major concern in protected area management (Mulongoy and Chape, 2004). Regions like Yukon flats adopted fire managements policies that suppress and exclude fires especially in native owned lands, but around them a "let burn" strategy is the widely adopted (Natcher, 2004).

4.3.2. Leverage

The most extreme values according to the leverage diagnostic were all classified as type 1 (high–high) and are located in Africa (Guinea, Angola and Sudan) with the exception of one cell in Punjab (NW India) near the border with Pakistan. The India cell (31°N, 75°W) contains the second highest number of active fires (of the 30 extreme observations), with 14 066 counts scattered throughout the 9 years, and peaking in 2005. This cell is part of a group of Moran scatterplot high–high cells in Punjab, a region characterized by wheat-rice double crop rotation, where it is common practice

to use of fire for burning agricultural crop residues after the wet season (Le Page et al., 2010; Sharma et al., 2010). All African cells are located in savanna/grassland ecosystems. Five cells are in the northern hemisphere savanna (10°N, 10°W; 10°N, 9°W; 9°N, 9°W; 8°N, 8°W in Guinea and 5°N, 29°E in Sudan) with a large number of fires during the boreal winter (October–March). The Guinea cells are located Guinea Highlands forests. Fires are set intentionally for pasture and farmland clearing. The remaining cells (7°S, 16°E; 8°S, 18°E; 8°S, 22°E; 9°S, 17°E) are located in northern Angola (Malanje, Lunda and Cuanza provinces), the southern part of the Democratic Republic of Congo and in cropland-forest mosaic of Guinea. Fires are set during the dry season (May through September, October), to clear brush, pastures, or old croplands, and also to drive game and livestock.

This diagnostic identifies some of the areas with the highest fire incidence in the world, where fire is regulated for land management purpose

4.3.3. Influence

Cook's distance identifies the cells with the highest influence on the regression coefficients and is the most important regression diagnostic, combining the previous two. The 10 most influential cells are located in the western hemisphere and belong to types 2 (high–low) and 4 (low–high) in the Moran scatterplot. As expected, most were detected by the previous diagnostics, mainly in the absolute standardized residuals (eight out of ten). However two cells (4°S, 52°W; 5°S, 52°W) located in Trincheira Bacajá indigenous protected area (Pará, Brazil), were not included in the 10 extreme values on any the previous diagnostics, but were classified as the 9th and 10th most extreme values according to Cook's distance. These cells (type 4, low–high) coincide with indigenous protected areas in central Pará (Brazil), where restrictions have been imposed on the use of fire. The most influential observation, which was also the largest outlier, is located in the Uru-Eu-Wau-Wau indigenous protected area. These two cells further stress the effectiveness of protected areas in Brazil to contain fire use.

5. Conclusions

The NASA MODIS MCD14ML Collection 5 active fire product for 2001–2009 was screened, prior to performing an ESDA. The global dataset was found to contain 3.5% of observations that are false alarms or non-vegetation fires, and which were eliminated An exploratory spatial data analysis (ESDA) of the screened data revealed strong positive autocorrelation based on global Moran's *I* statistic, stressing the importance of addressing this data feature in the development of spatial regression models of fire presence or abundance Regression scatterplot decomposition of the global Moran's *I*, analysis of its residuals, and local Moran's *I* analysis allowed for the identification and mapping spatial non-stationarity, suggesting heterogeneity in fire–environment relationship across space. Analysis of regression diagnostics highlighted areas with very intensive fire use associated with land management practices, very large fires standing out in regions with long fire cycle, and substantially reduced fire activity in areas with special conservation status.

Acknowledgments

This study was funded by a Ph.D. grant to Duarte Oom (SFRH/BD/47452/2008) from the Foundation for Science and Technology, Ministry for Science and Technology, Portugal. We would like to gratefully acknowledge Minnie Wong (University of Maryland, USA) for providing the MODIS fire dataset, and Alfredo Pereira (INPE, Sao Paulo, Brazil) for help in the interpretation of results.

References

AICC, 2009. Alaska Fire Season 2009, Wildland fire summary and statistics annual report. Alaska Interagency Coordination Center, Predictive Services Center.
Amaral-Turkman, M., Turkman, K., Le Page, Y., Pereira, J.M.C., 2010. Hierarchical space–time models for fire ignition and percentage of land burned by wildfires. Environmental and Ecological Statistics, 1–17.
Anselin, L., 1992. SpaceStat Tutorial: A Workbook for Using SpaceStat in the Analysis of Spatial Data, *Technical Software Series* **S-92-1**. National Center for Geographic Information and Analysis (NCGIA), University of California, Santa Barbara.
Anselin, L., 1995. Local indicators of spatial association – Lisa. Geographical Analysis 27 (2), 93–115.
Anselin, L., Sridharan, S., Gholston, S., 2007. Using exploratory spatial data analysis to leverage social indicator databases: the discovery of interesting patterns. Social Indicators Research 82 (2), 287–309.
Archibald, S., Roy, D.P., van Wilgen, B.W., Scholes, R.J., 2009. What limits fire? An examination of drivers of burnt area in Southern Africa. Global Change Biology 15 (3), 613–630.
Arino, O., Plummer, S., Defrenne, D., 2005. Fire disturbance: the ten years time series of the ATSR World Fire Atlas. In: Lacoste, H. (Ed.), Proceedings of the MERIS (A)ATSR Workshop. September 26–30, ESRIN, Frascati.
Arino, O., Rosaz, J., 1999. 1997 and 1998 world ATSR fire atlas using ERS-2 ATSR-2 data. In: Neuenschwander, L.F., Ryan, K.C., Golberg, G.E. (Eds.), Proceedings of the Joint Fire Science Conference. June 15–17, University of Idaho and the International Association of Wildland Fire, Boise, pp. 177–182.
Barbosa, R.I., Campos, C., 2011. Detection and geographical distribution of clearing areas in the savannas ('lavrado') of Roraima using Google Earth web tool. Journal of Geography and Regional Planning 4 (3), 122–136.
Boschetti, L., Roy, D.P., Justice, C.O., Giglio, L., 2010. Global assessment of the temporal reporting accuracy and precision of the MODIS burned area product. International Journal of Wildland Fire 19 (6), 705–709.
Byun, Y.G., Huh, Y., Yu, K., Kim, Y.I., 2006. Revision of Moran scatterplot approach for more effective forest fire detections. In: World Scientific and Engineering Academy and Society (WSEAS) (Ed.), Proceedings of the 5th WSEAS International Conference on Applied Computer Science. April 16–18, Hangzhou, pp. 951–955.
Chou, Y.H., Minnich, R.A., Chase, R.A., 1993. Mapping probability of fire occurrence in San-Jacinto Mountains, California, USA. Environmental Management 17 (1), 129–140.
Cliff, A.D., Ord, J.K., 1981. Spatial Processes: Models & Applications. Pion, London.
Coluzzi, R., Masini, N., Lanorte, A., Lasaponara, R., 2010. On the estimation of fire severity using satellite ASTER data and spatial autocorrelation statistics. Computational Science and Its Applications-ICCSA 6016, 361–373.
Csiszar, I., Denis, L., Giglio, L., Justice, C.O., Hewson, J., 2005. Global fire activity from two years of MODIS data. International Journal of Wildland Fire 14 (2), 117–130.
De Klerk, H., 2008. A pragmatic assessment of the usefulness of the MODIS (Terra and Aqua) 1-km active fire (MOD14A2 and MYD14A2) products for mapping fires in the fynbos biome. International Journal of Wildland Fire 17 (2), 166–178.
Drury, S., Grissom, P., 2008. Fire history and fire management implications in the Yukon Flats National Wildlife Refuge, interior Alaska. Forest Ecology and Mangement 256, 304–312.
Duncan, B.N., Martin, R.V., Staudt, A.C., Yevich, R., Logan, J.A., 2003. Interannual and seasonal variability of biomass burning emissions constrained by satellite observations. Journal of Geophysical Research 108 (D2), 4100.
Dwyer, E., Pinnock, S., Gregoire, J.M., Pereira, J.M.C., 2000. Global spatial and temporal distribution of vegetation fire as determined from satellite observations. International Journal of Remote Sensing 21 (6–7), 1289–1302.
Elvidge, C.D., Imhoff, M.L., Baugh, K.E., Hobson, V.R., Nelson, I., Safran, J., Dietz, J.B., Tuttle, B.T., 2001. Night-time lights of the world: 1994–1995. ISPRS Journal of Photogrammetry and Remote Sensing 56 (2), 81–99.
Eva, H., Lambin, E.F., 1998. Burnt area mapping in Central Africa using ATSR data. International Journal of Remote Sensing 19 (18), 3473–3497.
Fritz, S., Bartholomé, E., et al., 2003. Harmonisation, Mosaicking and Production of the Global Land Cover 2000 Database (Beta Version). European Commission, Joint Research Centre, EUR 20849 EN.
Giglio, L., 2010. MODIS Collection 4 Active Fire Product User's Guide Version 2.4. Science Systems and Applications, Inc.
Giglio, L., Csiszar, I., Justice, C.O., 2006. Global distribution and seasonality of active fires as observed with the Terra and Aqua Moderate Resolution Imaging Spectroradiometer (MODIS) sensors. Journal of Geophysical Research 111, 1–12.
Giglio, L., Descloitres, J., Justice, C.O., Kaufman, Y.J., 2003. An enhanced contextual fire detection algorithm for MODIS. Remote Sensing of Environment 87 (2–3), 273–282.
Giglio, L., Kendall, J.D., Tucker, C.J., 2000. Remote sensing of fires with the TRMM VIRS. International Journal of Remote Sensing 21 (1), 203–207.
Gobron, N., Belward, A., Pinty, B., Knorr, W., 2010. Monitoring biosphere vegetation 1998–2009. Geophysical Research Letters, 37.
Good, I.J., 1983. Good Thinking: The Foundation of Probability and Its Applications. University of Minnesota Press, Minneapolis.
Haining, R.P., 1993. Spatial Data Analysis in the Social and Environmental Sciences. Cambridge University Press, Cambridge, England/New York.
Haining, R., 1994. Diagnostics for regression modeling in spatial econometrics. Journal of Regional Science 34 (3), 325–341.
Hansen, J., Ruedy, R., Sato, M., Lo, K., 2010. Global surface temperature change. Reviews of Geophysics, 48.

Hawbaker, T.J., Radeloff, V.C., Syphard, A.D., Zhu, Z.L., Stewart, S.I., 2008. Detection rates of the MODIS active fire product in the United States. Remote Sensing of Environment 112 (5), 2656–2664.
Hrobak, J.L., 2006. Alphabet Hills Prescribed Fire (AA30) 2 Year Post-burn Field Monitoring Report. FRAMES Resource Cataloging System (RCS).
IBAMA, 2005. Plano de prevenção aos incêndios florestais Parque Nacional Pacaaás Novos. Ministério do Meio Ambiente, Instituto Brasileiro do Meio Ambiente e Recursos Naturais Renováveis, Campo Novo de Rondônia, Brazil, www.ibama.gov.br/phocadownload/category/44-p?download=2349.pdf (accessed 05.07.10).
Justice, C., Giglio, L., Korontzi, S., Owens, J., Morisette, J., Roy, D., Descloitres, J., Alleaume, S., Petitcolin, F., Kaufman, Y., 2002. The MODIS fire products. Remote Sensing of Environment 83 (1–2), 244–262.
Kasischke, E.S., Hewson, J.H., Stocks, B., van der Werf, G., Randerson, J., 2003. The use of ATSR active fire counts for estimating relative patterns of biomass burning – a study from the boreal forest region. Geophysical Research Letters 30 (18).
Krawchuk, M.A., Moritz, M.A., Parisien, M.A., Van Dorn, J., Hayhoe, K., 2009. Global pyrogeography: the current and future distribution of wildfire. PLoS One 4 (4).
Le Page, Y., Oom, D., Silva, J., Jönsson, P., Pereira, J., 2010. Seasonality of vegetation fires as modified by human action: observing the deviation from eco climatic fire regimes. Global Ecology and Biogeography 19 (4), 575–588.
Morisette, J.T., Giglio, L., Csiszar, I., Justice, C.O., 2005a. Validation of the MODIS active fire product over Southern Africa with ASTER data. International Journal of Remote Sensing 26 (19), 4239–4264.
Morisette, J.T., Giglio, L., Csiszar, I., Setzer, A., Schroeder, W., Morton, D., Justice, C.O., 2005b. Validation of MODIS active fire detection products derived from two algorithms. Earth Interactions, 9.
Mota, B.W., Pereira, J.M.C., Oom, D., Vasconcelos, M.J.P., Schultz, M., 2006. Screening the ESA ATSR-2 World Fire Atlas (1997–2002). Atmospheric Chemistry and Physics 6, 1409–1424.
Mulongoy, J.K., Chape, S., 2004. Protected Areas and biodiversity: An Overview of Key Issues. CBD Secretariat/UNEP – WCMC, Montreal, Canada/Cambridge, UK.
Natcher, D.C., 2004. Implications of fire policy on native land use in the Yukon Flats, Alaska. Human Ecology 32 (4), 421–441.
Nepstad, D., Schwartzman, S., et al., 2006. Inhibition of Amazon deforestation and fire by parks and indigenous lands. Conservation Biology 20, 65–73.
Olson, D.M., Dinerstein, E., et al., 2001. Terrestrial ecoregions of the worlds: a new map of life on Earth. Bioscience 51, 933–938.
Oom, D., 2008. Classificação global de fogos de vegetação com base em padrões espaciais, temporais, e de uso/coberto do solo para o período entre 1996 e 2006. MSc Dissertation. Technical University of Lisbon.
Pereira, J.M.C., 2003. Remote sensing of burned areas in tropical savannas. International Journal of Wildland Fire 12 (3–4), 259–270.
Pereira, J.M.C., Carreiras, J.M.B., Perestrello de Vasconcelos, M.J., 1998. Exploratory data analysis of the spatial distribution of wildfires in Portugal, 1980–1989. Geographical Systems 5, 355–390.
Pereira, J.M.C., Mota, B., Privette, J.L., Caylor, K.K., Silva, J.M.N., Sa, A.C.L., Ni-Meister, W., 2004. A simulation analysis of the detectability of understory burns in miombo woodlands. Remote Sensing of Environment 93 (3), 296–310.
Prins, E.M., Menzel, W., 1992. Geostationary satellite detection of biomass burning in South America. International Journal of Remote Sensing 13 (15), 2783–2799.
Rodrigues, C.A.G., Hott, M.C., Miranda, E.E., Oshiro, O.T., 2007. Análise da savana e queimadas no Parque Indígena de Tumucumaque (PA) através de imagens de satélite Landsat. In: INPE (Ed.), Anais XIII Simpósio Brasileiro de Sensoriamento Remoto. Florianópolis, Brazil, pp. 4195–4202.
Sá, A.C.L., Pereira, J.M.C., Charlton, M.E., Mota, B., Barbosa, P.M., Stewart Fotheringham, A., 2011. The pyrogeography of sub-Saharan Africa: a study of the spatial non-stationarity of fire–environment relationships using GWR. Journal of Geographical Systems 13 (3), 227–248.
Schroeder, W., Prins, E., Giglio, L., Csiszar, I., Schmidt, C., Morisette, J., Morton, D., 2008a. Validation of GOES and MODIS active fire detection products using ASTER and ETM plus data. Remote Sensing of Environment 112 (5), 2711–2726.
Schroeder, W., Ruminski, M., Csiszar, I., Giglio, L., Prins, E., Schmidt, C., Morisette, J., 2008b. Validation analyses of an operational fire monitoring product: the hazard mapping system. International Journal of Remote Sensing 29 (20), 6059–6066.
Schultz, M.G., 2002. On the use of ATSR fire count data to estimate the seasonal and interannual variability of vegetation fire emissions. Atmospheric Chemistry and Physics 2, 387–395.
Sharma, A.R., Kharol, S.K., Badarinath, K.V.S., Singh, D., 2010. Impact of agriculture crop residue burning on atmospheric aerosol loading – a study over Punjab State, India. Annales Geophysicae 28 (2), 367–379.
Shulski, M., 2005. Alaska's exceptional 2004 fire season. In: Sixth Symposium on Fire and Forest Meteorology, Cabmore, AB, Canada.
Siljander, M., 2009. Predictive fire occurrence modelling to improve burned area estimation at a regional scale: a case study in East Caprivi, Namibia. International Journal of Applied Earth Observation and Geoinformation 11 (6), 380–393.
Simes, R.J., 1986. An improved Bonferroni procedure for multiple tests of significance. Biometrika 73 (3), 751–754.
Stroppiana, D., Pinnock, S., Gregoire, J.M., 2000. The global fire product: daily fire occurrence from April 1992 to December 1993 derived from NOAA AVHRR data. International Journal of Remote Sensing 21 (6–7), 1279–1288.
Tukey, J.W., 1977. Exploratory Data Analysis. Addison-Wesley, Reading, MA.

II. Seasonality Of Vegetation Fires As Modified By Human Action: Observing The Deviation From Eco-Climatic Fire Regimes

Y. Le Page, **D.Oom**, J.M.N. Silva, P.Jönsson, J.M.C. Pereira

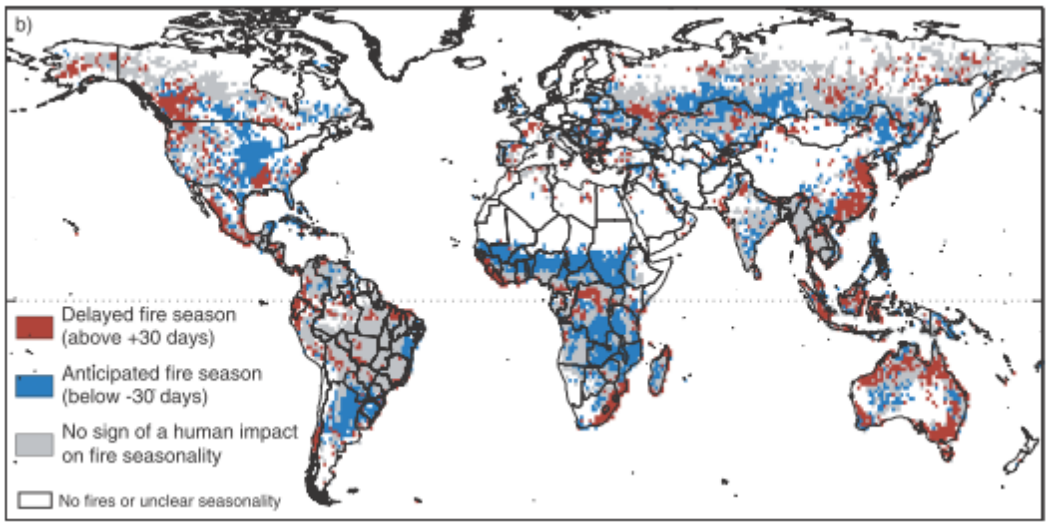

Published in *Global Ecology and Biogeography* in 2010

Global Ecology and Biogeography, (Global Ecol. Biogeogr.) (2010)

A Journal of Macroecology
Global Ecology and Biogeography

RESEARCH PAPER

Seasonality of vegetation fires as modified by human action: observing the deviation from eco-climatic fire regimes

Yannick Le Page[1]*, Duarte Oom[2], João M. N. Silva[2], Per Jönsson[3] and José M. C. Pereira[1]

[1]*Department of Forestry, School of Agronomy, Technical University of Lisbon, Tapada da Ajuda, 1349-017 Lisbon, Portugal,* [2]*Global Development Unit, Tropical Research Institute, 1300-344 Lisbon, Portugal,* [3]*Nature, Environment, Society, Malmö University, SE-205 06 Malmö, Sweden*

*Correspondence: Yannick Le Page, Instituto Superior de Agronomia, Departamento de Engenharia Florestal, Tapada da Ajuda, 1349-017 Lisboa, Portugal.
E-mail: lepagey@isa.utl.pt

ABSTRACT

Aim In any region affected, fires exhibit a strong seasonal cycle driven by the dynamic of fuel moisture and ignition sources throughout the year. In this paper we investigate the global patterns of fire seasonality, which we relate to climatic, anthropogenic, land-cover and land-use variables.

Location Global, with detailed analyses from single 1° × 1° grid cells.

Methods We use a fire risk index, the Chandler burning index (CBI), as an indicator of the 'natural', eco-climatic fire seasonality, across all types of ecosystems. A simple metric, the middle of the fire season, is computed from both gridded CBI data and satellite-derived fire detections. We then interpret the difference between the eco-climatic and observed metrics as an indicator of the human footprint on fire seasonality.

Results Deforestation, shifting cultivation, cropland production or tropical savanna fires are associated with specific timings due to land-use practices, sometimes largely decoupled from the CBI dynamics. Detailed time series from relevant locations provide comprehensive information about these practices and how they are adapted to eco-climatic conditions.

Main conclusions We find a great influence of anthropogenic activities on global patterns of fire seasonality. The specificity of the main fire practices and their easy identification from global observation is a potential tool to support land-use monitoring efforts. Our results should also prove valuable in the development of a methodological approach for improving the representation of anthropogenic fire practices in dynamic global vegetation models.

Keywords
Anthropogenic fires, anticipated/delayed fire season, Chandler burning index, dry season, fire drivers, fire season.

INTRODUCTION

The occurrence of vegetation fires is characterized by a strong annual cycle. The fundamental aspect of this cycle is the alternation of a fire-free season and a fire occurrence season, which is mostly controlled by climate (Dwyer *et al.*, 2000; Giglio *et al.*, 2006a). Broadly, most of the temperate and boreal Northern Hemisphere regions are affected by fires from May to September, when dry conditions are predominant. In the tropics, the movement of the Inter-Tropical Convergence Zone with its associated rains induces a fire season from November to March north of the equator, and from June to October in the southern hemisphere tropical savannas and forests. Further south in the temperate and Mediterranean-like regions of Australia, Africa and South America, fires mostly burn from October to March.

On intra-seasonal time-scales, the distribution of fire activity depends on the evolution of the factors controlling fire ignition, fire spread and fire extinction. The interaction between climate and ecosystems governs the dynamic of fuel moisture (Nelson, 2001; Cheney & Sullivan, 2009). Fine vegetation or dead fuels

© 2010 Blackwell Publishing Ltd

DOI: 10.1111/j.1466-8238.2010.00525.x
www.blackwellpublishing.com/geb

desiccate rapidly after the dry season starts, and are thus predisposed to early season fires, as is the case in grasslands and savannas. Live and wooded vegetation has a slower moisture dynamic, and fire sensitivity may be reached only late in the dry season, as in tropical forests. Early, middle and late season fires have different ecological impacts. Because the vegetation gets drier over the course of the dry season, late season fires tend to spread fast and with high intensity, and may be difficult to control and suppress until reaching a landscape fire break. On the contrary, early fires tend to be easily controlled since the vegetation is greener, and because night temperatures may reach dew point, disrupting the dead fuel desiccation dynamic. The difference between early and late season fires is also to be taken into account when quantifying atmospheric impacts. Carbon monoxide, methane and nitrous oxides are mostly produced during the oxygen-deficient smouldering phase (incomplete combustion), which is favoured during early season fires due to the high moisture content. Conversely, carbon dioxide is mostly emitted during the flaming phase (oxidation combustion), which prevails during late season fires (Hoffa *et al.*, 1999; Russell-smith *et al.*, 2009).

Besides the eco-climatic tendency towards early or late season fires, human pyrogenic behaviour also influences fire seasonality. Fires are used for many purposes related to land-use practices, with preferential timings. Agricultural burnings are applied world-wide for soil fertilization (pre-seeding fires), to prepare fields for harvest work (e.g. sugar cane pre-harvest fires) and to dispose of crop residues (post-harvest fires) (Yevich & Logan, 2003; Korontzi *et al.*, 2006). At large-scale tropical forest conversion sites (Morton *et al.*, 2008) and in most shifting cultivation systems (Thrupp *et al.*, 1997) the area to be deforested is cut at the end of the wet season, and fires are set repeatedly late in the dry season to maximize fuel consumption. Eco-climatic fire regimes are thus altered, and depicting this signal is a potential tool for identifying fire practices associated with specific land-use types. In this paper, the terms 'anticipated' and 'delayed' refer to changes in the fire season resulting from these practices, in parallel with 'early' and 'late', which refer to the dynamic of fuel moisture.

Fire seasonality is an essential feature to consider when integrating fires into dynamic global vegetation models. Fire modules were initially developed with a strong emphasis on vegetation and climate variables to estimate natural fire return intervals and vegetation disturbances (Thonicke *et al.*, 2001; Arora & Boer, 2005). In these models, the anthropogenic component is either absent or simply accounted for by constant fire ignition probabilities. Explicit modelling of human ignition potential has been explored in the Iberian Peninsula using population density as its determinant (Venevsky *et al.*, 2002), but without considering fire practices and their specific agenda. However, a proper representation of large-scale ecological (Bond *et al.*, 2005; Haberl *et al.*, 2007; Morton *et al.*, 2008) and atmospheric (van der Werf *et al.*, 2006) impacts of fires requires a realistic assessment of their timing and incidence. This will be especially important for the models evolving toward an 'anthropogenized' framework (Bondeau *et al.*, 2007).

The first objective of this study is to quantify the anthropogenic influence on fire seasonality. We base our investigation on the use of a simple parameter: the timing of the middle of the fire season. Our approach consists of assessing the eco-climatic seasonality with a fire danger metric, the Chandler burning index (CBI), which accounts for vegetation moisture dynamics (Chandler *et al.*, 1983). The difference between the middle of the CBI and fire seasons is interpreted as being largely of anthropogenic origin. Our second objective is to uncover the reasons for such disparities. At a global scale, spatial patterns of the anthropogenic influence are explored with information on human pyrogenic behaviour and land use. Locally, we discuss a selection of ten case studies representative of relevant fire regimes, with detailed time series and additional support from the literature.

DATA AND METHODS

Our analyses compare the seasonality of the CBI, based on temperature and relative humidity, with the seasonality of observed fires. Precipitation and lightning data are also used as a support to interpret the results, but are not involved in the computations. All the datasets were interpolated or aggregated to a final resolution of 1° × 1° spatially and 8 days temporally. The time series span from July 2002 to June 2007.

Fires

We used fire data from the Moderate Resolution Imaging Spectroradiometer (MODIS)-derived 8-day Climate Modeling Grid (CMG) Collection 5 product (Giglio *et al.*, 2006a). This dataset contains active fire detections on a global scale, with a spatial resolution of 0.5° × 0.5°, from both the TERRA and AQUA satellites. To keep consistent time series, we limited our study to the overlap between both satellites, and with complete 12-month periods only, from July 2002 to June 2007.

Active fires are considered inferior to burned area for many applications, and both products provide different representations of fire regimes (Roy *et al.*, 2008). In our case, active fires have the advantage of accounting for major practices that are not well detected with burned area algorithms. In the case of large-scale deforestation, for example, a substantial amount of biomass is piled prior to being ignited, resulting in a spectral signature too small to be detected optically (Roy *et al.*, 2008). On the other hand, active fires are not a measure of the size of fires but have been shown to be a useful estimator for coarse-resolution applications in most ecosystems (van der Werf *et al.*, 2006; Giglio *et al.*, 2006b). Large fires are detected several times by active fire observation, when the flaming front spans an area larger than the sensor resolution (in our case, 1 km), and when a fire burns longer than the overpass interval (with TERRA and AQUA combined, any location is observed at least four times a day).

Eco-climatic fire susceptibility

Although climate is the major determinant of the seasonal cycle of fire susceptibility, the structure and composition of the veg-

etation also have a significant influence. Soil water retention capacity, rooting depth, canopy density and fuel size determine the capacity of an ecosystem to maintain humidity when the climate gets drier (Nelson, 2001; Cheney & Sullivan, 2009). As the most illustrative comparison, tropical grasslands dry out rapidly after the end of the wet season, while rainforests under similar climate conditions may sustain a fire only late in the dry season (Uhl & Kauffman, 1990).

The CBI is an index of fire susceptibility based on temperature and relative humidity, originally designed for application at a monthly time-scale (Chandler *et al.*, 1983). Although primarily climatic, the CBI integrates a basic representation of the above-mentioned role of the vegetation. Indeed, the moisture-buffering capacity of an ecosystem interacts with relative humidity through water exchanges between the soil–fuel–vegetation layer and the atmosphere (Nelson, 2001; Cheney & Sullivan, 2009). Relative humidity is the main variable of most soil moisture indices (Sharples *et al.*, 2009).

The CBI has been applied to study fire weather in the United States (McCutchan & Main, 1989) and globally (Roads *et al.*, 2008). It is computed as

$$\mathrm{CBI} = \frac{[(110 - 1.373 \times RH) - 0.54(10.20 - T)] \times 124 \times 10^{(-0.0142 \times RH)}}{60} \quad (1)$$

where RH is the relative humidity and T the temperature. Both variables were obtained at a subdaily time step from the National Centers for Environmental Prediction (NCEP) Reanalysis dataset (NOAA/OAR/ESRL PSD, http://www.cdc.noaa.gov), at a native resolution of 2.5 × 2.5°. RH and T are classified as B variables, of intermediate reliability, since both the model and available observations influence their computation during data assimilation (Kalnay *et al.*, 1996).

Preliminary assessments of the CBI revealed an inconsistent behaviour over boreal regions during winter, when low RH induces increased CBI values, while T is negative and the ground is covered by snow. The index was thus modified to be minimum when T is negative, by forcing the RH to 100%.

Precipitation

We used the 1° × 1° daily precipitation dataset (GPCP-1DD) from the Global Precipitation Climatology Project (GPCP; Huffman *et al.*, 2001), which merges satellite and gauge data to produce daily estimates from October 1996 to the present. Validation work revealed important errors in the daily estimates, which rapidly decrease with temporal and/or spatial aggregation (Huffman *et al.*, 2001).

Lightning flashes

For natural sources of fire ignition, we used lightning flash detections produced by the NASA Lightning Imaging Sensor (LIS)/Optical Transient Detector (OTD) Science Team, available from the Global Hydrology Resource Center (Christian *et al.*, 2003; Mach *et al.*, 2007). This dataset contains both inter-cloud and cloud-to-ground flashes, as detected over April 1995 to March 2000 by the OTD, and over January 1998 to December 2005 by the LIS. Since global coverage over our study period was not available as a time series, we used the 0.5° High Resolution Annual Climatology (HRAC) product. Note that the HRAC only represents the average likelihood of lightning ignitions over a typical year, while inter-annual variability is known to be important (Chronis *et al.*, 2008).

The TIMESAT program

TIMESAT was initially developed to extract seasonal parameters from normalized difference vegetation index (NDVI) time series (Jönsson & Eklundh, 2004). It processes data of any temporal resolution in three steps. The pre-filtering step aims at removing outliers within a single time series and at eliminating time series with unclear seasonality. The adaptation step consists of generating smooth time series of the pre-filtered data. Finally, a set of seasonal parameters is extracted (Fig. 1).

We adapted TIMESAT to process non-continuous time series, as is the case with fire data (many consecutive 8-day periods with no fire detection). Further, we carefully selected the user-adjustable processing parameters. The pre-filtering options did not prove adjustable enough, and we developed our own post-filtering rules instead. These rules test for adequate fire activity and seasonality. Most importantly, fire seasons with a peak fire activity below 10 detections over an 8-day period were discarded, along with a few cases of unrealistic time series or computations (e.g. a fire season spanning more than 10 months). For the adaptation step, we used the Savitzky–Golay three-step adaptive filtering, which clearly out-performed the two fitting alternatives of the software. The seasonal parameters were then extracted, imposing a single fire season per year. The procedure for the CBI variables was very similar but for the post-processing step, which we made less restrictive given the clearer seasonality and generally trouble-free processing in TIMESAT.

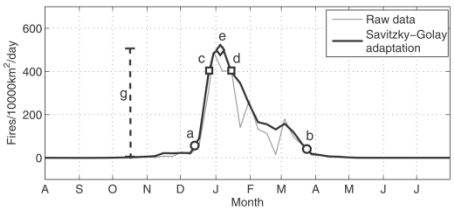

Figure 1 Fire season parameter extraction with the TIMESAT software, over a grid cell in Africa: (a, b) start and end of the fire season, positioned where the fitted function reaches 10% of the amplitude (g); (c, d) positions at which the fitted function reaches 80% of the amplitude; (e) middle of the fire season, centred between (c) and (d).

Averaged seasonality and case studies

Over the 5-year time series, we obtained a maximum of four values (or dates) per grid cell for the middle of the fire season (MFseas) and middle of the CBI season (MCBIseas) metrics (1 year is always left unprocessed by the program and additional years may be filtered out during the post-processing step). For each grid cell, the seasons with one of the two metrics undefined (i.e. not computed or filtered out) are discarded. This ensured we did not compare the fires and CBI from different seasons, which could be misleading in regions of significant inter-annual variability in fire seasonality. The mean MFseas or MCBIseas was then computed as the date minimizing its cumulated distance (in days) to the set of one to four middle season dates, as direct averaging of dates is meaningless (day 1 in January and 365 in December would average to early July). A global view of the relationship between the fire and CBI seasons was then simply achieved by mapping the time gap between their respective middle dates (MFseas minus CBIseas). Note, however, that the results inferred in ecosystems with irregular fire seasons are specific to the 5 years considered and do not assess the long-term seasonality. This is especially the case of boreal forests (stochastic ignitions by lightning) and of ecosystems under the strong influence of low-frequency climate modes (e.g. the El Niño–Southern Oscillation in tropical forests of South America and South East Asia).

To further depict the role of the CBI, precipitation, lightning and anthropogenic activities, we also extracted time series and seasonal parameters of 10 grid cells selected as representative of the most relevant fire regimes.

RESULTS

The global distribution of the MCBIseas reveals large-scale latitudinal patterns (Fig. 2). Temperate and boreal regions of the Northern Hemisphere have a CBI dry season over May to September, the period of maximum incoming solar radiation. The opposite is observed in the Southern Hemisphere temperate regions, with a dry season spanning from October to March. In the tropics and subtropics, which receive a rather constant amount of solar radiation all year round, the timing of the dry season is driven by the position of the tropical rain belt, associated with the Inter-Tropical Convergence Zone. Two opposite fire timings are observed, roughly separated by the equator, with a dry season from November to March in the Northern Hemisphere tropics, and from June to September in the Southern Hemisphere tropics.

The global distribution of the MFseas (Fig. 3) is very similar to that obtained by Dwyer *et al.* (2000) over 1992–93, with a different dataset. As expected, the MFseas patterns are partially related to the MCBIseas, with a clear latitudinal gradient. However, the relative time gap between the MFseas and the MCBIseas (Fig. 4a) reveals significant dissimilarities. Regions of anticipated and delayed fire season (Fig. 4b) appear to be spatially related to the distribution of broad land-cover and land-use types (Fig. 5) and to climate classes (Peel *et al.*, 2007). Major agricultural regions generally display little synchrony in CBI and fire seasonality, with both anticipated (North America, around the Corn Belt) and delayed (eastern China, southern Australia) fire seasons. The transition from arid to tropical ecosystems is clearly apparent, especially in Africa where grass and savanna ecosystems are associated with anticipated fires, while a slightly delayed fire season is found in the most equatorial regions covered by evergreen rainforests. In boreal forests, the fire season is very variable, which seems to be a natural variability as spatial patterns are not related to static eco-climatic or anthropogenic factors. Fire suppression activities, which greatly alter fire frequency in northern America, Europe and Australia, do not have clear impacts on our results. There has been little investigation on this issue, but although the shape of the fire season may be modified due to intra-annual changes in fire suppression efforts or efficiency, we are doubtful of any substantial shifts of the timing of the MFseas itself, as was reported in one case study (Keeley *et al.*, 1999). Unexpected patterns are also identified in south-western Canadian forests, for example, with a delayed MFseas around October to December, at the beginning of winter.

The wide range of interactions between climate, vegetation and anthropogenic activities suggested by these results are explored with 10 case studies, the locations of which are indicated in Fig. 4(a). Their respective time series of active fires, CBI and precipitation (Fig. 6a–k) are detailed and analysed in the Discussion. The annual cycle in lightning activity is also illustrated, but provides little support since significant natural ignitions are generally observed during extreme lightning events, which are not depicted in the averaged climatology.

DISCUSSION

Permanent agriculture fires

Most regions dominated by permanent agriculture display an important positive or negative time gap between the MFseas and MCBIseas, according to the role fire plays in the crop management cycle. Lightning ignitions are likely to be marginal.

In northern America, the large agricultural region extending from Alberta (Canada) to Missouri and Oklahoma (United States of America, USA), has a MFseas around late March to early June, some 50–150 days before the MCBIseas. A variety of crops are found along this whole region, including corn, spring wheat, sunflower, soybean and canola (US 2002 Census Publications from the United States Department of Agriculture (USDA); Canada 2006 Census of Agriculture from Statistics Canada). These burnings are related to field clearing practices and to the harvest of winter, spring and durum wheat (J. McCarty, pers. comm.). In the Corn Belt, dominated by a corn–soybean rotation system, a short crop (October to April) of winter wheat is commonly grown every third to fifth year, to increase nutrients in the soil. Those crops are harvested and burned early (April–May) before the next planting of corn or soybean (J. McCarty, personal communication). Note the gradual change of the MFseas, from early April in the south to

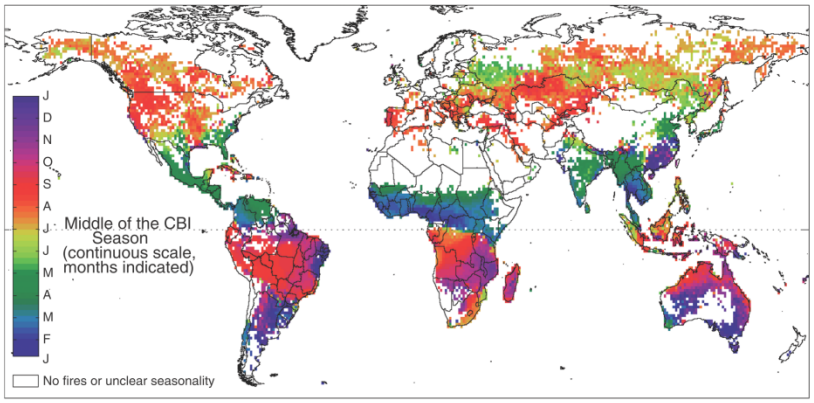

Figure 2 Middle of the Chandler burning index (CBI) dry season (MCBIseas), computed from National Centers for Environmental Prediction (NCEP) relative humidity and temperature data.

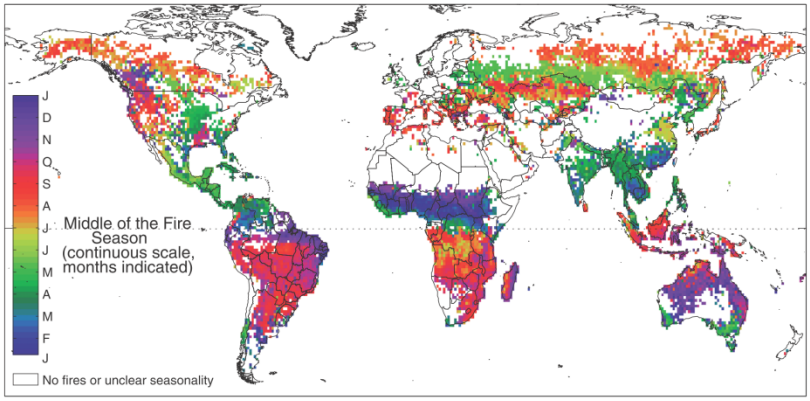

Figure 3 Middle of the fire season (MFseas), computed from Moderate Resolution Imaging Spectroradiometer (MODIS) Collection 5 active fire data.

late May in the northernmost grid cells, suggesting a slightly delayed crop calendar in the north due to a longer winter. The case study reveals a very short fire season, when the CBI just starts increasing in early spring (Fig. 6a). Fire activity is rather low and irregular, with years of very little activity.

Ukraine, Russia and Kazakhstan are among the main world agricultural regions (Leff *et al.*, 2004), where the use of fire is very common and significant at a global scale (Korontzi *et al.*, 2006). Contrasting MFseas are found in the region, one around March and the second around August (Fig. 4). Inspection of the time series from various grid cells (not shown) indicates a bimodal fire season, the dominant peak being retained by TIMESAT given the constraint of a single fire season per year. In between these two peaks, fire activity is almost non-existent. The first fire peak in March is related to crop preparation before the planting of summer crops (mainly barley, sunflower, sugar beet and oats). The second peak occurs immediately after winter crops are harvested, suggesting the burning of crop residues.

In China, most of the wheat and rice crops are concentrated in the eastern part of the country (Leff *et al.*, 2004). Although residues have been reported to be mostly used as biofuels (Yevich & Logan, 2003), recent studies pointed to significant burning in the field (e.g. Cao *et al.*, 2008). The MFseas occurs around early June, some 50 to more than 100 days after the MCBIseas (Fig. 4a), and the fire season is very short, from late May to early June, while the rest of the year is fire-free. Although the CBI seasonality is not very obvious, the precipitation time series clearly establishes a late fire season, just before heavy

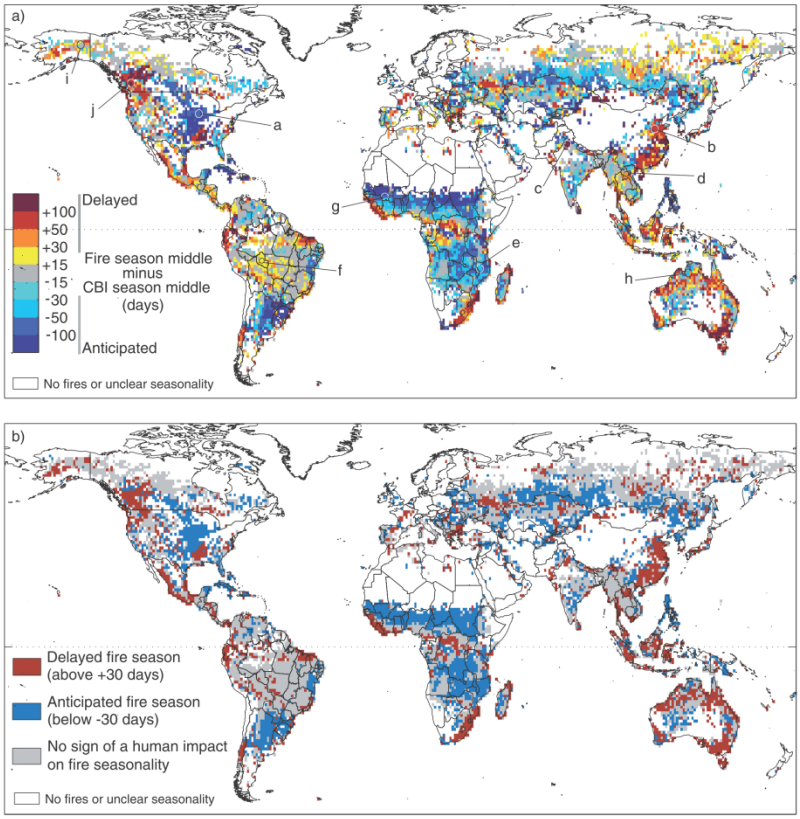

Figure 4 (a) Difference between the middle of the Chandler burning index (CBI) dry season (MCBIseas) and the middle of the fire season (MFseas), and location of the case study grid cells, from a to k (described in Figure 6). (b) Map of early and late fire seasons (threshold at ±30 days of difference between the MFseas and MCBIseas).

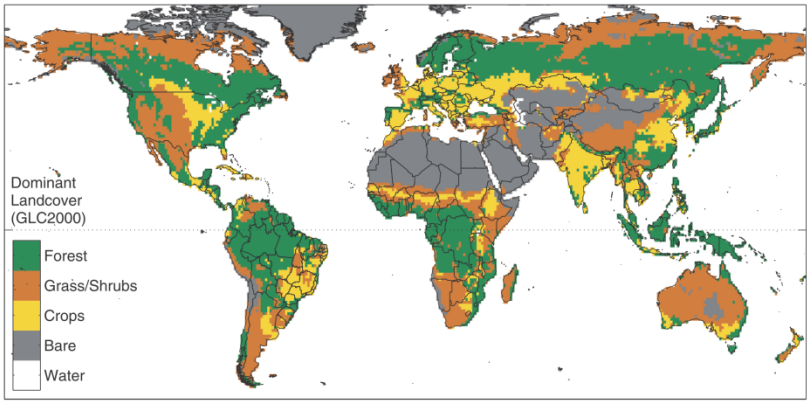

Figure 5 Dominant land cover from the Global Land Cover for the year 2000 (GLC2000, Bartholome & Belward, 2005).

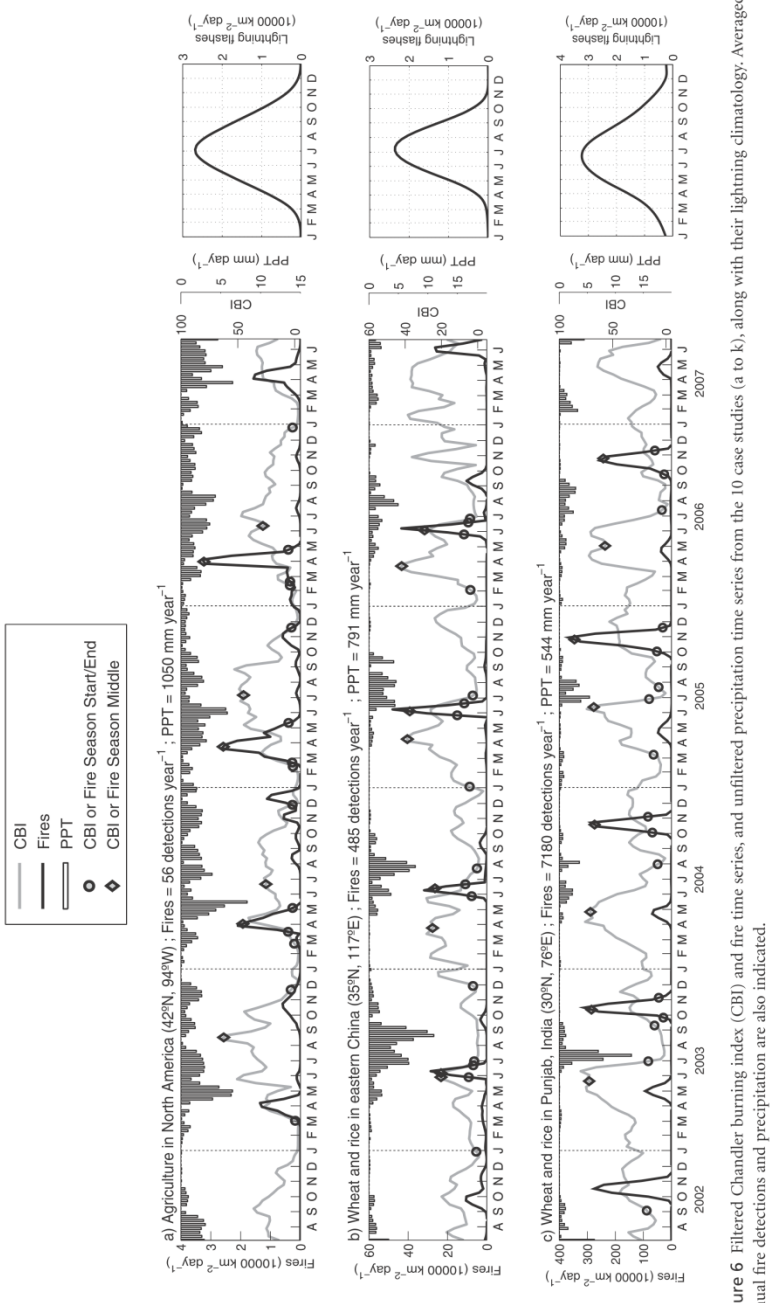

Figure 6 Filtered Chandler burning index (CBI) and fire time series, and unfiltered precipitation time series from the 10 case studies (a to k), along with their lightning climatology. Averaged annual fire detections and precipitation are also indicated.

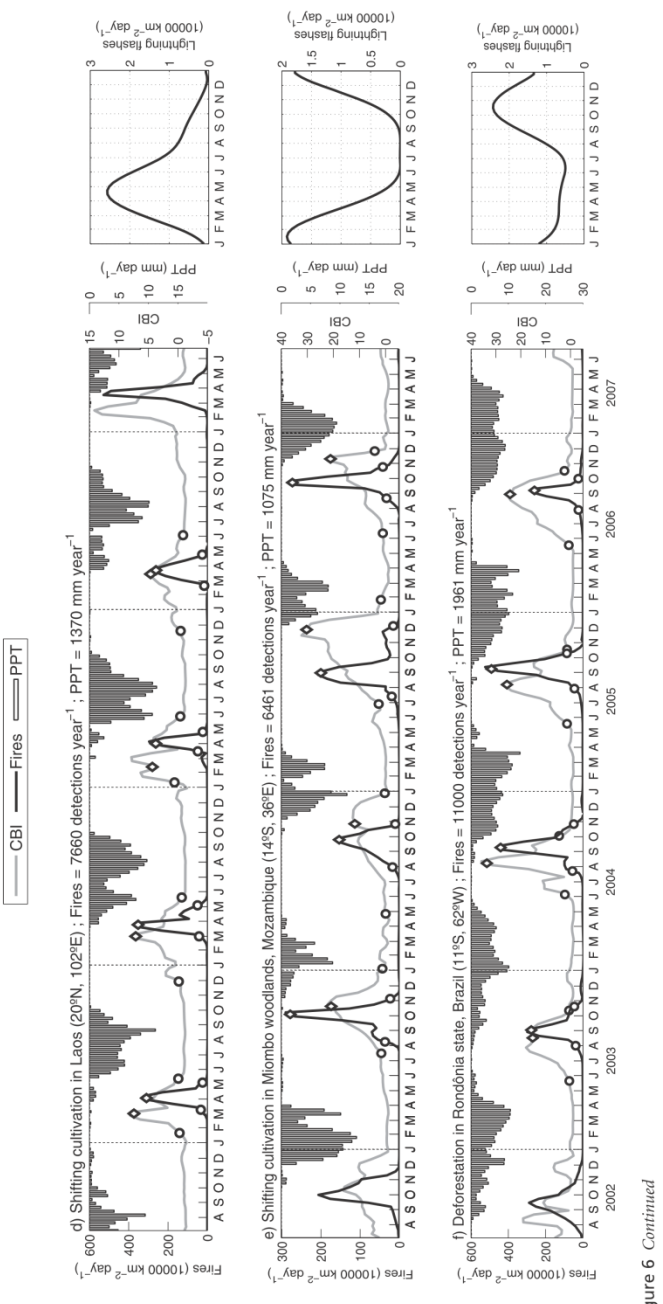

Figure 6 *Continued*

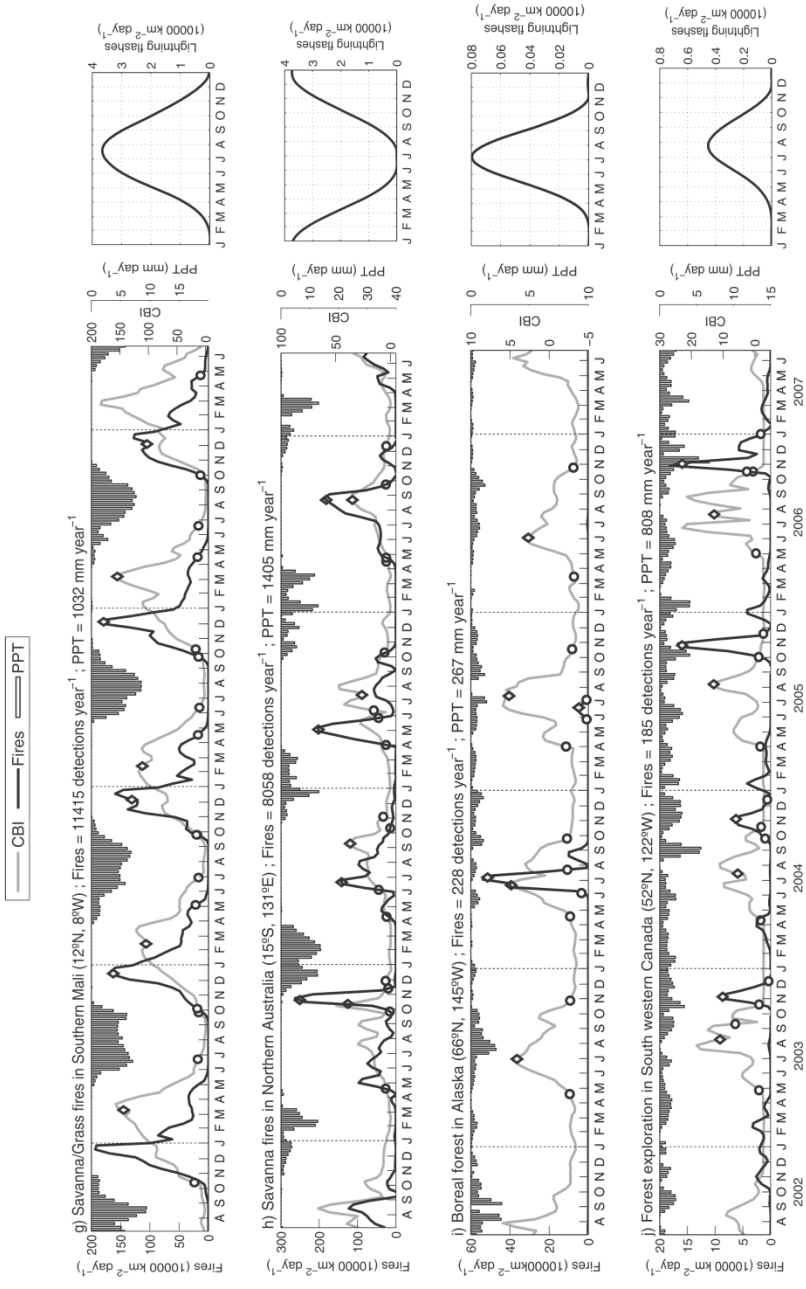

Figure 6 *Continued*

rainfalls set the beginning of the wet season. These findings precisely match the local crop calendar and burning practices reported by Xiao *et al.* (2002): 'By late May, wheat crops ripened and were ready for harvest. Following the harvest of winter wheat, stubble was typically burned and then, within 1–2 weeks, fields were ploughed and flooded'.

In India, the world's second largest producer of rice and wheat, most of the agricultural regions exhibit an anticipated fire season, with a MFseas from February to April. Clearly standing out is the north-western Punjab state, with a short fire season around October, and a very large number of fire detections (Fig. 6c). The CBI and precipitation profiles attest to an anticipated fire season concentrated just after the end of the wet season, contrary to Fig. 4(a) which indicates a delayed fire season (this miscalculation is due to the MFseas of season n being closer to the MCBIseas of season $n - 1$ than to the MCBIseas of season n). Wheat–rice double crop is the dominant crop system in Punjab, and these fires correspond to the burning of rice harvest residues, which is a very common practice (Badarinath *et al.*, 2006). The second peak of lower amplitude in April–May is due to the burning of wheat stubble. Wheat residues are largely used for animal feed, while rice residues are generally not valued and are burned in the field (Badarinath *et al.*, 2006), hence the clear dominance of the October fires, which were again observed in 2008 (NASA, 2008; http://earthobservatory.nasa.gov/NaturalHazards/view.php?id=35765).

Shifting cultivation fires

Shifting cultivation is the most complex form of agriculture in the world and is practiced by a majority of small-scale farmers in tropical regions of Africa, Central and South America and Southeast Asia. It is found in diverse ecosystems, from tropical moist forests to dry forests and savannas, grasslands and even seasonal floodplains (Thrupp *et al.*, 1997). Shifting cultivation is defined as an agricultural system that involves an alternation between cropping for a few years on selected and cleared plots and a fallow period, during which the soil fertility is restored (Ruthenberg, 1976). In the most common systems, vegetation is cut, allowed to dry for some time and then burnt, raising the level of nutrients just before the preparation of the soil for planting.

The first case study is located in northern Laos, dominated by deciduous monsoon rain forest, where shifting agriculture is generalized (Seidenberg *et al.*, 2003). The burning occurs mostly in March and April, with a slight delay compared with the CBI, but clearly at the very end of the precipitation-derived dry season (Fig. 6d). This timing maximizes vegetation flammability and avoids the establishment of weeds prior to plantation (Thrupp *et al.*, 1997). It is also observed in shifting agriculture systems of tropical Africa and South America. On the contrary, in south-eastern Africa, namely the south of the Democratic Republic of the Congo, in Zambia, Tanzania and Mozambique, shifting cultivation is associated with an anticipated fire season. These regions correspond to the distribution of Miombo woodlands, tropical woodlands and dry forest formations growing under a strongly seasonal climate (Frost, 1996). As shown from the province of Niassa in Mozambique, the dry season is longer than in tropical forests (Fig. 6e). Late season fires would be damaging because the biomass gets very dry, and burns are thus applied earlier to prevent damaging fires (Chidumayo *et al.*, 1996). However, the MFseas is still located in the second part of the dry season (anticipated late fire season).

Tropical forest conversion fires

Unlike shifting cultivation, forest conversion, usually applied at large scale, is intended to completely clear portions of the forest for the establishment of permanent croplands and pastures. Large areas of tropical forests have been converted over the past decades, and current observations still point at high deforestation rates (Hansen *et al.*, 2008). The classic sequence of forest conversion is similar to shifting cultivation, i.e. the vegetation is cut after the wet season and burned at the end of the dry season. For the most active deforestation sites, the vegetation is repeatedly piled and burned, causing a fire activity among the highest world-wide (Morton *et al.*, 2008).

In agreement with these practices, the MFseas over tropical forests of South America, Africa and Southeast Asia is found to be either similar to the CBIseas or delayed up to 100 days (Fig. 4). Smaller tropical forest patches are also depicted, e.g. in Madagascar with a clear transition from an anticipated fire season in the western grasslands and shrublands, to a delayed fire season in the eastern tropical forest. The case study was selected in the Brazilian state of Rondônia, under active deforestation. Its fire season peaks in August/September, the last months of a dry season that normally starts in May (Fig. 6g).

In the case of both shifting cultivation and conversion fires in tropical forests, a delayed fire season may rather be the sign of the forcing of a fire season. Indeed, the MCBIseas has little meaning for fire seasonality as eco-climatic conditions rarely allow the natural occurrence of fires. The observed delays could thus indicate that the CBI has a faster dynamics than the curing of recently cut coarse vegetation.

Fires in highly seasonal wet–dry climates of Africa and Australia

Large regions of Africa (Barbosa *et al.*, 1999) and northern Australia (Dyer *et al.*, 2001) are highly affected by fires, due to a very seasonal climate ideal for successive vegetation growth and drying and high ignition probability from widespread and diversified fire practices.

The sub-Saharan region of Northern Hemisphere Africa is affected by fires during the boreal winter (October to March), with a MFseas ahead of the MCBIseas by 30 days in the south to up to 180 days (6 months) in the regions closest to the desert. The case study located in southern Mali (Fig. 6g) illustrates the three burning phases reported by Laris (2002) based on interviews with the local population and field observations. Very early in the dry season (November), fires are lit in the short

annual grass growing on gravel soils, which is unpalatable and dries out very rapidly due to little soil water retention capacity. These fires are set preventively to avoid damaging fires later in the season and are easily controlled, since other types of adjacent vegetation (perennial grass, savannas) are too moist to burn, thus acting as fire barriers (P. Laris, pers. comm.). In a second phase, fires are mostly set in fallow lands in late December, after the harvest, to avoid crop damage. Again, fire spread is usually limited by earlier burns and other landscape discontinuities. These two phases are very well reproduced by the data, with a peak in November and another in late December almost every year (not always apparent in the filtered time series). Finally, late season fire activity is associated with crop preparation and with the occurrence of a few but large uncontrolled fires which spread to the wooded savannas, especially in areas not sufficiently fragmented with earlier burns.

In northern Australia, fire is used as a tool to manage pasture and savanna landscapes (Dyer *et al.*, 2001). Traditional burning by Aboriginal people is also associated with various practices, from land clearing and grass regrowth stimulation to spiritual obligations. The case study is located south of Darwin, in the Northern Territory (Fig. 6h), dominated by eucalypt woodlands with a grass ground layer where as much as 50–70% of the landscape may burn annually (Dyer *et al.*, 2001). It indicates an extended dry season, from April to October, with a changeable regime of early and/or late season fires. This variability suggests the reduction of fire management practices, attributed in Northern Australia to the loss of manpower and to the abandonment of traditional fire use in Aboriginal lands (Dyer *et al.*, 2001). At Kakadu National Park, around 200 km north-east of location h, anticipated preventive burns are applied to limit the occurrence of late season wildfires. Consequently, fire seasons are more regular, and clearly display the signature of an anthropogenic anticipation (Fig. 4 and Russell-Smith *et al.*, 1997).

Boreal forest fires

Boreal forests contain a significant part of the world's biomass and very large stocks of both above- and below-ground carbon (Kasischke, 2000). Fire plays a crucial role in shaping the vegetation (Bond-lamberty *et al.*, 2007) and in driving the carbon balance of these forests (Harden *et al.*, 2000). Very large areas of forest can be burned during a single fire event, spreading freely over several days or weeks in regions with a low human footprint, with no or little fire-fighting facilities. These remote boreal fires are probably the most representative of the 'wildfire' concept, as spread is unlikely to be stopped by human intervention and ignition is often caused by lightning strikes (Ivanova & Ivanov, 2005; DeWilde & Chapin, 2006).

In the eastern Alaska case study, the CBI is at minimum from November to April, and rapidly increases with positive temperatures and snow melt (Fig. 6i). The driest conditions are observed from June to August, a period when the occurrence of thunderstorms is a potential source of lightning ignitions. Over the 5 years of the time series, significant fire activity only occurred in 2004, suggesting natural fire regimes with sporadic ignitions. In Alaska 2004 is the worst fire year on record (Annual report on the climate of 2004, National Climatic Data Center). Over a few days in mid-June, around 15,000 lightning strikes ignited numerous fires, which burned through July and August (NASA, 2005; http://visibleearth.nasa.gov/view_rec.php?id=7009).

A surprising pattern is observed over the managed forests of south-western Canada, with a MFseas estimated from October to December (Fig. 3), long after the most favourable eco-climatic conditions (Fig. 4). Winter is establishing at this time of the year, with the first snowfalls, hence there is a low risk of fire. However, the case study (Fig. 6j) indicates that this delayed fire activity happens every year, and is mostly limited to October and November, discarding the hypotheses of gas flares or other types of false detections. Two sources related to forest exploration activities have been identified for these fires (B. Hawkes, pers. comm.): (1) dry forest restoration burnings, mostly prescribed in the spring but also in autumn, until October to November, before the first snowfalls; and (2) pile burning after logging, usually after the first snowfalls.

Limitations

The main limitation of this study arises from the spatial aggregation of active fires, as land cover and land use can be very heterogeneous in a single 1° × 1° grid cell. For example, the aggregation of anticipated season agricultural fires with adjacent delayed forest fires in the same grid cell may lead to a time series that does not depict any of the two fire regimes. At the time of writing this paper, raw active fire data from MODIS are being made available to the scientific community. Overlapped with a land-cover map and other sources of land-use data, this type of analysis may provide comprehensive information about the seasonality of single fire types (i.e. agricultural fires, deforestation fires, etc.).

This study also bears the generalization of one particular methodology at a global scale. We use the CBI as a global estimator of fire sensitivity, which is dependent on a complex system of interactions (Bachelet *et al.*, 2001; Meyn *et al.*, 2007). Relative humidity and temperature have a constant weight in the CBI equation (equation 1), which may hide an ecosystem-specific response or the involvement of other variables, for example the accumulation of ground litter throughout the dry season (Dyer *et al.*, 2001). In addition, the native resolution of NCEP data (2.5° × 2.5°) implies that relevant spatial patterns are not accounted for at 1° × 1°, including the CBI variability due to regional changes (2.5° approximates 300 km at the equator) in the interaction between climate and vegetation (see Data and Methods).

CONCLUSION

This study reveals a great diversity of fire season regimes, each consistently associated with the regional climate, vegetation, land use and anthropogenic environment. We demonstrate a prevalent anthropogenic influence, while climatic control is loosened. In agricultural regions, climate only acts as a con-

straint to set the date of the beginning and end of the fire potential window and the fire season clearly bears the signature of human practices. A deeper exploration has the potential to uncover specific associations of fire and land use, to identify dominant crop productions or to infer information about the location and progress of shifting cultivation and permanent deforestation practices.

The coupling of a fire module to a dynamic global vegetation model entails extensive work if the impacts of anthropogenic fires are to be properly modelled. We suggest that timing fire ignitions on eco-climatic conditions only, as done in most models, is not appropriate. We propose that three broad types of anthropogenic fires should be considered as the most relevant for development, not only to improve fire seasonality but also to account for changes in fire frequency and the ensuing emissions: (1) agricultural fires, for which a model has to include major crop types along with their productivity and management to assess the timing of fires and the amount of biomass burnt. Regarding crop management, the harvest and planting dates, and the crop-specific fire use (pre-seeding, pre-harvesting or post-harvesting) are the key practices to be considered. Several models have already been implemented with agro-ecosystem modules (De noblet-ducoudré *et al.*, 2003; Bondeau *et al.*, 2007; Stehfest *et al.*, 2007), and should provide good support for evaluating strategies to integrate fire use; (2) tropical deforestation fires, given their widespread use and considerable impact on the vegetation (Cochrane & Schulze, 1999) and carbon balance (Nepstad *et al.*, 1999) of an ecosystem rarely affected under natural conditions; and (3) fire practices in tropical savannas of Africa and Australia, where fire regimes are greatly altered by human activities, resulting in the highest fire frequency world-wide, which climate-driven fire models cannot reproduce (Thonicke *et al.*, 2001), and in a strongly biased seasonality. Accounting for these major fire practices should in turn benefit the vegetation scheme itself by analogy to the natural feedbacks of fires on ecosystem dynamics (Bond *et al.*, 2005), and improve the computation of atmospheric emissions.

ACKNOWLEDGEMENTS

This study was funded by the Marie Curie Research Training Network GREENCYCLES, contract number MRTN-CT-2004 (http://www.greencycles.org/greencycles1). We are very grateful to Jessica McCarty, Paul Laris and Brad Hawkes for their help in the interpretation of the case studies, and to the reviewers for their contributions to improving the manuscript.

REFERENCES

Arora, V.K. & Boer, G.J. (2005) Fire as an interactive component of dynamic vegetation models. *Journal of Geophysical Research-Biogeosciences*, **110**, G02008.

Bachelet, D., Lenihan, J., Daly, C., Neilson, R.P., Ojima, D.S. & Parton, W.J. (2001) *MC1: a dynamic vegetation model for estimating the distribution of vegetation and associated ecosystem fluxes of carbon, nutrients, and water*. Pacific Northwest Research Station, General Technical Report PNW-GTR-508.USDA Forest Service, Washington, DC.

Badarinath, K.V.S., Chand, T.R.K. & Prasad, V.K. (2006) Agriculture crop residue burning in the Indo-Gangetic plains – a study using IRS-P6 AWiFS satellite data. *Current Science*, **91**, 1085–1089.

Barbosa, P.M., Grégoire, J.M. & Pereira, J.M.C. (1999) An algorithm for extracting burned areas from time series of AVHRR GAC data applied at a continental scale. *Remote Sensing of Environment*, **69**, 253–263.

Bartholome, E. & Belward, A.S. (2005) GLC2000: a new approach to global land cover mapping from Earth observation data. *International Journal of Remote Sensing*, **26**, 1959–1977.

Bond, W.J., Woodward, F.I. & Midgley, G.F. (2005) The global distribution of ecosystems in a world without fire. *New Phytologist*, **165**, 525–537.

Bondeau, A., Smith, P.C., Zaehle, S., Schaphoff, S., Lucht, W., Cramer, W. & Gerten, D. (2007) Modelling the role of agriculture for the 20th century global terrestrial carbon balance. *Global Change Biology*, **13**, 679–706.

Bond-Lamberty, B., Peckham, S.D., Ahl, D.E. & Gower, S.T. (2007) Fire as the dominant driver of central Canadian boreal forest carbon balance. *Nature*, **450**, 89–92.

Cao, G.L., Zhang, X.Y., Wang, Y.Q. & Zheng, F.C. (2008) Estimation of emissions from field burning of crop straw in China. *Chinese Science Bulletin*, **53**, 784–790.

Chandler, C., Cheney, P., Thomas, P., Trabaud, L. & Williams, D. (1983) *Fire in forestry Vol. 1: forest fire behavior and effects*. John Wiley and Sons, New York.

Cheney, P. & Sullivan, A. (2009) *Grassfires: fuel, weather and fire behaviour*. CSIRO Publishing, Collingwood, Australia.

Chidumayo, E., Gambiza, J. & Grundy, I. (1996) Managing miombo woodlands. *The miombo in transition: woodlands and welfare in Africa* (ed. by B. Campbell), pp. 175–193. Center for International Forestry Research, Bogor, Indonesia.

Christian, H.J., Blakeslee, R.J., Boccippio, D.J., Boeck, W.L., Buechler, D.E., Driscoll, K.T., Goodman, S.J., Hall, J.M., Koshak, W.J., Mach, D.M. & Stewart, M.F. (2003) Global frequency and distribution of lightning as observed from space by the Optical Transient Detector. *Journal of Geophysical Research-Atmospheres*, **108**, 4005. doi:10.1029/2002JD002347.

Chronis, T.G., Goodman, S.J., Cecil, D., Buechler, D., Robertson, F.J., Pittman, J. & Blakeslee, R. (2008) Global lightning activity from the ENSO perspective. *Geophysical Research Letters*, **35**, L19804.

Cochrane, M.A. & Schulze, M.D. (1999) Fire as a recurrent event in tropical forests of the eastern Amazon: effects on forest structure, biomass, and species composition. *Biotropica*, **31**, 2–16.

DeWilde, L. & Chapin, F.S. (2006) Human impacts on the fire regime of interior Alaska: interactions among fuels, ignition sources, and fire suppression. *Ecosystems*, **9**, 1342–1353.

Dwyer, E., Pereira, J.M.C., Grégoire, J.M. & Dacamara, C.C. (2000) Characterization of the spatio-temporal patterns of

global fire activity using satellite imagery for the period April 1992 to March 1993. *Journal of Biogeography*, **27**, 57–69.

Dyer, R., Jacklyn, P., Partridge, I., Russell-Smith, J. & Williams, D. (2001) *Savanna burning: understanding and using fire in Northern Australia*. Tropical Savannas CRC, Darwin, NT.

Frost, P. (1996) The ecology of miombo woodlands. *The miombo in transition: woodlands and welfare in Africa* (ed. by B. Campbell), pp. 11–57. Center for International Forestry Research, Bogor, Indonesia.

Giglio, L., Csiszar, I. & Justice, C.O. (2006a) Global distribution and seasonality of active fires as observed with the Terra and Aqua Moderate Resolution Imaging Spectroradiometer (MODIS) sensors. *Journal of Geophysical Research-Biogeosciences*, **111**, G02016.

Giglio, L., Van Der Werf, G.R., Randerson, J.T., Collatz, G.J. & Kasibhatla, P. (2006b) Global estimation of burned area using MODIS active fire observations. *Atmospheric Chemistry and Physics*, **6**, 957–974.

Haberl, H., Erb, K.H., Krausmann, F., Gaube, V., Bondeau, A., Plutzar, C., Gingrich, S., Lucht, W. & Fischer-Kowalski, M. (2007) Quantifying and mapping the human appropriation of net primary production in earth's terrestrial ecosystems. *Proceedings of the National Academy of Sciences USA*, **104**, 12942–12947.

Hansen, M.C., Stehman, S.V., Potapov, P.V., Loveland, T.R., Townshend, J.R.G., Defries, R.S., Pittman, K.W., Arunarwati, B., Stolle, F., Steininger, M.K., Carroll, M. & Dimiceli, C. (2008) Humid tropical forest clearing from 2000 to 2005 quantified by using multitemporal and multiresolution remotely sensed data. *Proceedings of the National Academy of Sciences USA*, **105**, 9439–9444.

Harden, J.W., Trumbore, S.E., Stocks, B.J., Hirsch, A., Gower, S.T., O'Neill, K.P. & Kasischke, E.S. (2000) The role of fire in the boreal carbon budget. *Global Change Biology*, **6**, 174–184.

Hoffa, E.A., Ward, D.E., Hao, W.M., Susott, R.A. & Wakimoto, R.H. (1999) Seasonality of carbon emissions from biomass burning in a Zambian savanna. *Journal of Geophysical Research-Atmospheres*, **104**, 13841–13853.

Huffman, G.J., Adler, R.F., Morrissey, M.M., Bolvin, D.T., Curtis, S., Joyce, R., McGavock, B. & Susskind, J. (2001) Global precipitation at one-degree daily resolution from multisatellite observations. *Journal of Hydrometeorology*, **2**, 36–50.

Ivanova, G.A. & Ivanov, V.A. (2005) Fire regimes in Siberian forests. *International Forest Fire News*, 67–69.

Jönsson, P. & Eklundh, L. (2004) TIMESAT – a program for analyzing time-series of satellite sensor data. *Computers and Geosciences*, **30**, 833–845.

Kalnay, E., Kanamitsu, M., Kistler, R. *et al.* (1996) The NCEP/NCAR 40-year reanalysis project. *Bulletin of the American Meteorological Society*, **77**, 437–471.

Kasischke, E.S. (2000) Boreal ecosystems in the global carbon cycle. *Fire, climate change and carbon cycling in the boreal forest* (ed. by E.S. Kasischke and B.J. Stocks), pp. 19–30. Springer-Verlag, New York.

Keeley, J.E., Fotheringham, C.J. & Morais, M. (1999) Reexamining fire suppression impacts on brushland fire regimes. *Science*, **284**, 1829–1832.

Korontzi, S., McCarty, J., Loboda, T., Kumar, S. & Justice, C. (2006) Global distribution of agricultural fires in croplands from 3 years of Moderate Resolution Imaging Spectroradiometer (MODIS) data. *Global Biogeochemical Cycles*, **20**, G–2021.

Laris, P. (2002) Burning the seasonal mosaic: preventative burning strategies in the wooded savanna of southern Mali. *Human Ecology*, **30**, 155–186.

Leff, B., Ramankutty, N. & Foley, J.A. (2004) Geographic distribution of major crops across the world. *Global Biogeochemical Cycles*, **18**, GB1009.

McCutchan, M.H. & Main, W.A. (1989) The relationship between mean monthly fire potential indices and monthly fire severity. *Proceedings of the 10th Conference on Fire and Forest Meteorology* (ed. by D.C. MacIver, H. Auld and R. Whitewood), pp. 430–435. Forestry Canada, Ottawa, Ontario, Canada.

Mach, D.M., Christian, H.J., Blakeslee, R.J., Boccippio, D.J., Goodman, S.J. & Boeck, W.L. (2007) Performance assessment of the optical transient detector and lightning imaging sensor. *Journal of Geophysical Research-Atmospheres*, **112**, D09210.

Meyn, A., White, P.S., Buhk, C. & Jentsch, A. (2007) Environmental drivers of large, infrequent wildfires: the emerging conceptual model. *Progress in Physical Geography*, **31**, 287–312.

Morton, D.C., Defries, R.S., Randerson, J.T., Giglio, L., Schroeder, W. & Van Der Werf, G.R. (2008) Agricultural intensification increases deforestation fire activity in. Amazonia. *Global Change Biology*, **14**, 2262–2275.

National Aeronautics and Space Administration (NASA) (2005) *Visible earth catalog*. Available at: http://visibleearth.nasa.gov/view_rec.php?id=7009 (accessed 16 January 2010).

National Aeronautics and Space Administration (NASA) (2008) *Visible earth catalog*. Available at: http://earthobservatory.nasa.gov/NaturalHazards/view.php?id=35765 (accessed 16 January 2010).

Nelson, R.M. (2001) Water relations of forest fuels. *Forest fires: behavior and ecological effects* (ed. by E.A. Johnson and K. Miyanishi), pp. 79–149. Academic Press, San Diego, CA.

Nepstad, D.C., Verissimo, A., Alencar, A., Nobre, C., Lima, E., Lefebvre, P., Schlesinger, P., Potter, C., Moutinho, P., Mendoza, E., Cochrane, M. & Brooks, V. (1999) Large-scale impoverishment of Amazonian forests by logging and fire. *Nature*, **398**, 505–508.

de Noblet-Ducoudré, N., Gervois, S., Ciais, P., Viovy, N., Brisson, N., Seguin, B. & Perrier, A. (2003) Coupling the soil–vegetation–atmosphere transfer scheme ORCHIDEE to the agronomy model STICS to study the influence of croplands on the European carbon and water budgets. *Agronomie*, **24**, 397–407.

Peel, M.C., Finlayson, B.L. & McMahon, T.A. (2007) Updated world map of the Köppen–Geiger climate classification. *Hydrology and Earth System Sciences*, **11**, 1633–1644.

Roads, J.P., Tripp, P., Juang, H., Wang, J., Chen, S. & Fujioka, F. (2008) ECPC/NCEP March 2008 seasonal fire danger forecasts. *Experimental Long-Lead Forecasts Bulletin*, **17**, 7 pp.

Roy, D.P., Boschetti, L., Justice, C.O. & Ju, J. (2008) The collection 5 MODIS burned area product – global evaluation by comparison with the MODIS active fire product. *Remote Sensing of Environment*, **112**, 3690–3707.

Russell-Smith, J., Ryan, P.G. & Durieu, R. (1997) A LANDSAT MSS-derived fire history of Kakadu National Park, Monsoonal Northern Australial, 1980–94: seasonal extent, frequency and patchiness. *Journal of Applied Ecology*, **34**, 748–766.

Russell-Smith, J., Murphy, B.P., Meyer, C.P., Cook, G.D., Maier, S., Edwards, A.C., Schatz, J. & Brocklehurst, P. (2009) Improving estimates of savanna burning emissions for greenhouse accounting in northern Australia: limitations, challenges, applications. *International Journal of Wildland Fire*, **18**, 1–18.

Ruthenberg, H. (1976) *Farming systems in the tropics*. Clarendon Press, Oxford.

Seidenberg, C., Mertz, O. & Kias, M.B. (2003) Fallow, labour and livelihood in shifting cultivation: implications for deforestation in northern Lao PDR. *Danish Journal of Geography*, **103**, 71–80.

Sharples, J.J., McRae, R.H.D., Weber, R.O. & Gill, A.M. (2009) A simple index for assessing fuel moisture content. *Environmental Modelling and Software*, **24**, 637–646.

Stehfest, E., Heistermann, M., Priess, J.A., Ojima, D.S. & Alcamo, J. (2007) Simulation of global crop production with the ecosystem model DayCent. *Ecological Modelling*, **209**, 203–219.

Thonicke, K., Venevsky, S., Sitch, S. & Cramer, W. (2001) The role of fire disturbance for global vegetation dynamics: coupling fire into a dynamic global vegetation model. *Global Ecology and Biogeography*, **10**, 661–677.

Thrupp, L.A., Hecht, S. & Browder, J. (1997) *The diversity and dynamics of shifting cultivation: myths, realities, and policy implications*. World Resources Institute, Washington, DC.

Uhl, C. & Kauffman, J.B. (1990) Deforestation, fire susceptibility, and potential tree responses to fire in the eastern Amazon. *Ecology*, **71**, 437–449.

Venevsky, S., Thonicke, K., Sitch, S. & Cramer, W. (2002) Simulating fire regimes in human-dominated ecosystems: Iberian Peninsula case study. *Global Change Biology*, **8**, 984–998.

van der Werf, G.R., Randerson, J.T., Giglio, L., Collatz, G.J., Kasibhatla, P.S. & Arellano, A.F. (2006) Interannual variability in global biomass burning emissions from 1997–2004. *Atmospheric Chemistry and Physics*, **6**, 3423–3441.

Xiao, X., Boles, S., Frolking, S., Salas, W., Moore, B., Li, C., He, L. & Zhao, R. (2002) Observation of flooding and rice transplanting of paddy rice fields at the site to landscape scales in China using VEGETATION sensor data. *International Journal of Remote Sensing*, **23**, 3009–3022.

Yevich, R. & Logan, J.A. (2003) An assessment of biofuel use and burning of agricultural waste in the developing world. *Global Biogeochemical Cycles*, **17**, 1095.

BIOSKETCH

Yannick Le Page is a PhD student at the Department of Forestry of the School of Agronomy of Lisbon (http://www.isa.utl.pt). His research interests centre on the role of climate, human activities and land use/land cover on regional to global patterns of vegetation fires.

Editor: Thomas Gillespie

III. Relationships between human population density and burned area at continental and global scales

Bistinas, I., **Oom, D**., Sá, A. C., Harrison, S. P., Prentice, I. C. & Pereira, J.M.C.

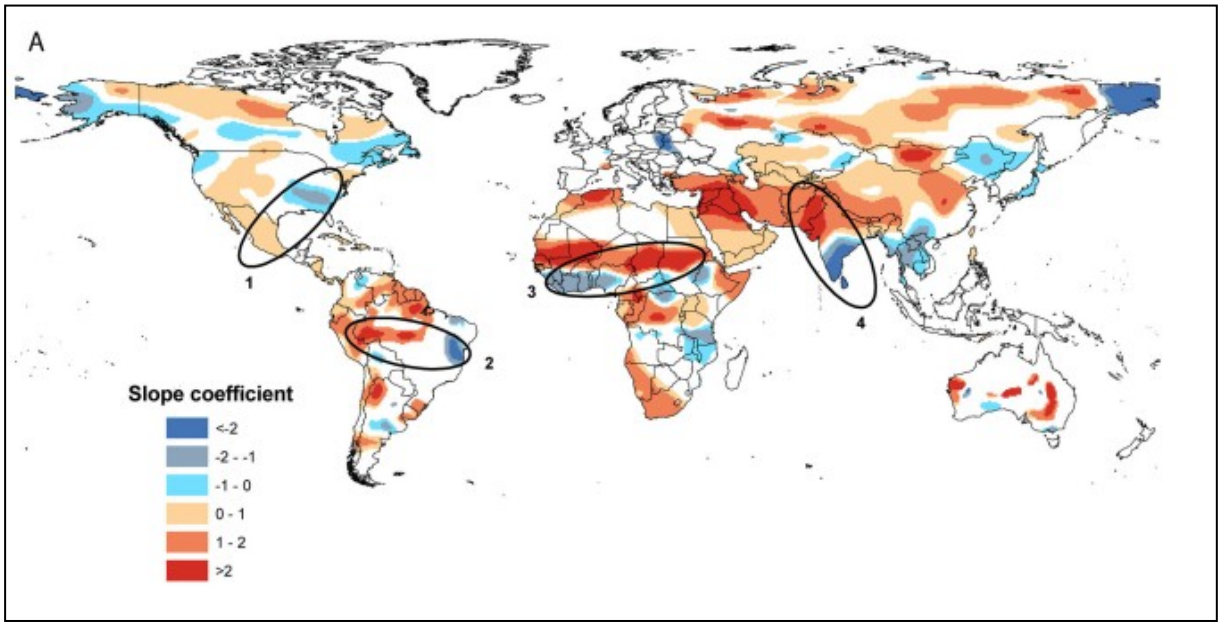

Published in *PloS One* in December 2013

OPEN ACCESS Freely available online

PLOS ONE

Relationships between Human Population Density and Burned Area at Continental and Global Scales

Ioannis Bistinas[1], Duarte Oom[1], Ana C. L. Sá[1], Sandy P. Harrison[2,3], I. Colin Prentice[2,4*], José M. C. Pereira[1]

1 Centro de Estudos Florestais, Instituto Superior de Agronomia, Universidade de Lisboa, Tapada da Ajuda, Lisboa, Portugal, **2** Department of Biological Sciences, Macquarie University, North Ryde, Australia, **3** Geography & Environmental Sciences, School of Human and Environmental Sciences, Reading University, Whiteknights, Reading, United Kingdom, **4** Grantham Institute for Climate Change, and Department of Life Sciences, Imperial College, Silwood Park Campus, Ascot, United Kingdom

Abstract

We explore the large spatial variation in the relationship between population density and burned area, using continental-scale Geographically Weighted Regression (GWR) based on 13 years of satellite-derived burned area maps from the global fire emissions database (GFED) and the human population density from the gridded population of the world (GPW 2005). Significant relationships are observed over 51.5% of the global land area, and the area affected varies from continent to continent: population density has a significant impact on fire over most of Asia and Africa but is important in explaining fire over < 22% of Europe and Australia. Increasing population density is associated with both increased and decreased in fire. The nature of the relationship depends on land-use: increasing population density is associated with increased burned are in rangelands but with decreased burned area in croplands. Overall, the relationship between population density and burned area is non-monotonic: burned area initially increases with population density and then decreases when population density exceeds a threshold. These thresholds vary regionally. Our study contributes to improved understanding of how human activities relate to burned area, and should contribute to a better estimate of atmospheric emissions from biomass burning.

Citation: Bistinas I, Oom D, Sá ACL, Harrison SP, Prentice IC, et al. (2013) Relationships between Human Population Density and Burned Area at Continental and Global Scales. PLoS ONE 8(12): e81188. doi:10.1371/journal.pone.0081188

Editor: Bin Jiang, University of Gävle, Sweden

Received February 25, 2013; **Accepted** October 11, 2013; **Published** December 16, 2013

Copyright: © 2013 Bistinas et al. This is an open-access article distributed under the terms of the Creative Commons Attribution License, which permits unrestricted use, distribution, and reproduction in any medium, provided the original author and source are credited.

Funding: This study was funded by the Marie Curie Research Training Network GREENCYCLES, contract number MRTN-CT-2004 (www.greencycles.org). The funders had no role in study design, data collection and analysis, decision to publish, or preparation of the manuscript.

Competing interests: The authors have declared that no competing interests exist.

* E-mail: i.bistinas@gmail.com

Introduction

Fire is a natural process that has played a key role in the maintenance of natural ecosystems for millions of years, and regulates plant and animal population dynamics [1-3]. However, fire is also a tool used by people to transform the natural environment [4-6]. Humans are the dominant influence over most of the land surface today [7]. Prior to the industrial revolution only ca 5 % of the ice free land surface was used for agriculture and settlement. However, between 1700 and 2000 AD, the terrestrial biosphere transitioned from being mostly wild to mostly anthropogenic, passing the 50% threshold early in the 20th century [8]. This transformation makes it important to consider human influence on modern fire regimes [9].

Guyette et al. (2002) [9] identified four ways in which human influence the amount of land burnt (or the burned area fraction): anthropogenic ignitions, fuel production, fuel fragmentation and cultural behaviour. All these factors are linked to population density. Many regional studies show a single-peaked relationship between human population and fire extent and/or numbers of fires, with intermediate populations at the peak of this parabola, after which different land use activities and land cover types attenuate fire frequency and reduces burnt area fraction [10-13].

The objective of this study is to investigate the influence of population density on burnt area by exploring its spatial variability using Geographically Weighted Regression, and try to detect existence of critical thresholds in population density for fire behaviour using quantile regression. We then interpret the findings in the light of differences in major land use management classes.

Data and Methods

Data

Satellite-derived burned area maps covering 13 years (1997-2009) are available from the Global Fire Emissions Database version 3 (GFED3: [14]) at 0.5° cell resolution for the

whole globe (Fig. 1a), available at: http://www.globalfiredata.org/. This spatial resolution can reveal first-order global and continental-scale patterns in burnt area [15]. Giglio et al. (2010) [14] demonstrated that the GFED v3 data used in this study has improved accuracy over version 2 in Canada and the USA. Since active fire detection can capture mush smaller events (sub-pixel) than burned area products, GFED may indeed better represent area burned in small fires than products that do not rely on active fire data. For 0.5° spatial resolution burned area, GFED v3 uses either VIRS or ATSR world fire atlas fire counts [14]. The input data for a GWR are the centroids of the 0.5° cells. Cells that intersect water bodies, ice and artificial surfaces are considered to be non-combustible areas and were removed using a mask from the Global Land Cover 2000 database [16]. The global combustible area extent was calculated from the area of each cell using a latitude correction. The annual mean burned area (km^2) for the 13 years of observations was used as the response variable. Population density (persons per square kilometre: p/km^2) was obtained from the Gridded Population of the World version 3 [17] at 0.5° spatial resolution (Fig. 1b) available at: http://sedac.ciesin.columbia.edu/data/collection/gpw-v3, and is used as the predictor variable. As both burned area and population density are highly skewed toward small values, we applied a decimal logarithmic transformation to both variables.

To support the interpretation of our analyses of the human influence on burned area, we use the anthropogenic biomes (Anthromes) of the world [18] available at: http://ecotope.org/anthromes/v1/guide/. This dataset classifies terrestrial biomes based on the level of human influence, estimated as a function of population density, land use and land cover. The 21 anthromes are grouped into 6 major anthrome types in the original publication (Table 1; Figure 1c) and we use these major types here to simplify interpretation of the GWR results.

Statistical Analyses

We initially computed the global linear relationship between burned area and population density using Ordinary Least Squares (OLS). The global OLS regression model assumes that the studied relationship is stationary, i.e. the estimated parameters do not vary spatially. To test the hypothesis that the relationship varies spatially, we use Geographically Weighted Regression (GWR). GWR estimates local parameter values as in (Eq. 1) [19,20].

$$y=\beta_o(\mu,\nu)+\sum_{j=1}^{p}\beta_j(\mu,\nu)X_j+\varepsilon \quad (1)$$

Where (μ,ν) is the coordinate location and j is the number of the explanatory variables of the X matrix, β is a matrix with the regression coefficients and ε is a random error whose distribution is $N(0, \sigma^2 I)$ [20].

We initially ran the GWR at 0.5° spatial resolution, which is the original resolution of both the burned area and population data sets, but also the resolution used by several Dynamic Global Vegetation Models (DGVM). Other than such pragmatic criteria, the choice of an appropriate level of spatial aggregation for analyses of spatial relationships is essentially arbitrary [21]. The basic assumption of the GWR is that observations closer to a target point have more impact on the modelled relationship at that point than more distant observations. A distance decay function centered on each observation is used for this purpose, and this makes it important to choose an appropriate level of aggregation. The GWR procedure includes a step that assesses whether the selected scale is appropriate. However, to assess the sensitivity of the spatial relationship between population density and burned area to the choice of spatial resolution, we used Africa as a test case and re-ran the analyses for this continent using 0.25° and 1.0° cells. The distance-decay depends on the bandwidth of the spatial kernel used, which is the radius or the number of observations around each point [19]. Here, we used a continental space scale, defining the continents according to political borders (M. Charlton, personal communication). We used an adaptive Gaussian kernel, whose bandwidth varies according to the density of the data, an approach usually adopted when there is no prior knowledge of the studied relationship [19]. The optimal bandwidth for each continent was determined by minimizing the Akaike information criterion (AIC) [22,23]. Due to the different extent of land of each continent and the minimization of the AIC coefficient for the highest adjusted R^2, the bandwidth varies, but remains proportional at 5.1% of the total observations in all cases. The use of the AIC ensures that we use the appropriate level of spatial aggregation for each continent. The analysis is performed with GWR version 3.0. (see 20).

A Monte Carlo permutation test is used to test the significance of the spatial variability of local coefficient estimates. We only map the statistically significant values of the GWR output parameters (slope coefficients and intercept), as determined by a t-test. As multiple hypotheses tests are used, an alpha correction is employed to reduce type I errors [23]. The parameter coefficients were tested for significance according to the family-wise error rate ξ_m by choosing

$$a=\frac{\xi_o}{1+p_e-\frac{p_e}{np}} \quad (2)$$

where p_e is the effective number of parameters, n is the total number of observations and p is the number of parameters in each model [23,24].

The relationship between population density and burned area is expected to be non-linear and non-monotonic. To examine whether there are abrupt changes in the nature of the relationship switches, we fit a linear "broken stick" version of quantile regression [25-28], using the package "quantreg" in R (http://cran.r-project.org/web/packages/quantreg/index.html). This technique makes no prior assumption of abruptness [29]. Since there could be more than a single slope in rate of change because of interactions between factors [30], we consider the 50th and 90th burned area percentiles, to explore the impact of human activities on area burnt.

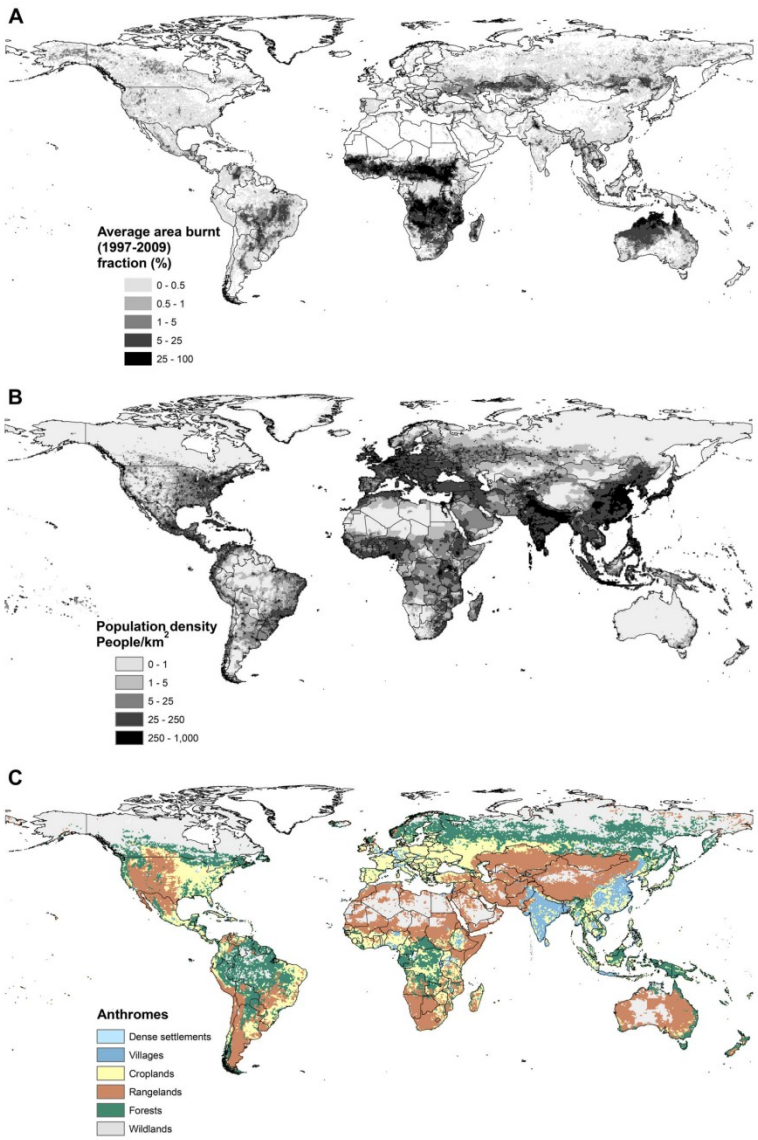

Figure 1. Input data sets. Average mean annual burned area (showed in cell area fraction instead of km^2 in order to help the interpretation), based on data from the Global Fire Emissions Database version 3 (GFED3: Giglio et al., 2010) for the period 1997-2009; (B) Population density (persons per square kilometre: p/km^2) from the Gridded Population of the World version 3 (Ciesin, 2005); and (C) The anthropogenic biomes (anthromes) of the world, mapped as the six major anthrome types (see Table 1) defined by Ellis and Ramankutty (2008).

doi: 10.1371/journal.pone.0081188.g001

Table 2. Percentage of statistically significant values per continent, AIC coefficients and adjusted R^2 for the OLS and the GWR model.

Continent	Number of observations	% significant slopes	% positive slopes	AIC (OLS)	AIC (GWR)	Adjusted R^2 (OLS)	Adjusted R^2 (GWR)
Africa	10647	61.3	75.5	52871.22	39362.11	0.27	0.80
Asia	23799	65.7	78.3	115337.97	101721.13	0.04	0.46
N. America	17192	42.9	55.1	76372.24	67573.16	0.24	0.55
S. America	6551	46.8	81.8	31317.89	26493.67	0.07	0.56
Europe	6899	21.44	68	32402.14	27009.41	0.11	0.60
Australia	3038	20.51	76.4	14508.43	11947.93	0.001	0.58

doi: 10.1371/journal.pone.0081188.t002

Table 1. Anthromes and major anthrome types defined by Ellis and Ramankutty (2008).

Anthrome	Major anthrome type
Urban	Dense Settlement
Dense settlements	Dense Settlement
Rice villages	Villages
Irrigated villages	Villages
Cropped and pastoral villages	Villages
Pastoral villages	Villages
Rainfed villages	Villages
Rainfed mosaic villages	Villages
Residential irrigated cropland	Croplands
Residential rainfed mosaic cropland	Croplands
Populated irrigated cropland	Croplands
Populated rainfed cropland	Croplands
Remote croplands	Croplands
Residential rangelands	Rangelands
Populated rangelands	Rangelands
Remote rangelands	Rangelands
Populated forest	Forest
Remote forest	Forest
Wild forest	Wildlands
Sparse trees	Wildlands
Barren	Wildlands

doi: 10.1371/journal.pone.0081188.t001

Results

OLS versus GWR comparison

The relationship between log-transformed population density and burned area estimated using OLS is poor, with R^2 values varying from 0.001 (Australia) to a maximum of 0.27 (Africa). The relation between the log-transformed population density and burned area using the GWR models at 0.5° resolution is significant for all continents; the proportion of variability in burned area explained varies from 46% (Asia) to 80% (Africa). Thus, GWR performs much better than OLS for every continent. The GWR models also have lower AIC coefficients than OLS model and much higher adjusted R^2 values (Table 2), showing that the local model (GWR) is a significant improvement on the global (OLS) model for all continents.

The GWR analysis shows that there is no significant relationship between population density and burned area over 48.5% of the total area of the globe. A significant relationship between population density and burned area is found for ca 66% of the total area of Asia, ca 61% of Africa, ca 47% of South America and 43% of North America. Less than 22% of Europe and Australia are characterised by a significant relationship between burned area and population density.

Spatial patterns

The relationship between population density and burned area is non-stationary and shows patterns that differ both in sign and magnitude (Figure 2a). The relationship can be positive or negative, where positive relationships indicate that human activities increase burned area and negative relationships indicate that human activities have negative influence on fire. The magnitudes of the slope coefficients are different in different continents, so we focus on the sign in regions showing significant relationships between population density and burned area. The intercept can be an estimate of the area burnt when population density is small (1 p/km^2), although absolute values are influenced by the slope coefficient. However, for regions displaying similar slopes, the intercept can be interpreted as a measure of the fire-proneness of the landscape, where positive intercepts indicate that the region is fire-prone and negative intercepts indicate that the region is less likely to burn.

Africa

On average over the period 1997-2009, 69% of the global area burned is in Africa. This is comparable to Tansey et al.'s (2004) [31] estimate that Africa accounted for 64% of the total area burned in 2000. The relationship between population density and burned area is statistically significant over nearly 61% of the continental area, with positive relationships in the Maghreb, the Sahel, the Horn of Africa, central Africa, and south-western Africa (Figure 2a) and negative relationships in the Sudanian savannah region and parts of eastern Africa (Figure 2a). Over most of these areas, the slope coefficients are >1 (or < -1), indicating that the impact of people becomes progressively larger at higher population densities. Regions with positive relationships between burned area and population density generally occur in rangelands (Figure 1c), while the areas with negative relationships have a higher incidence in

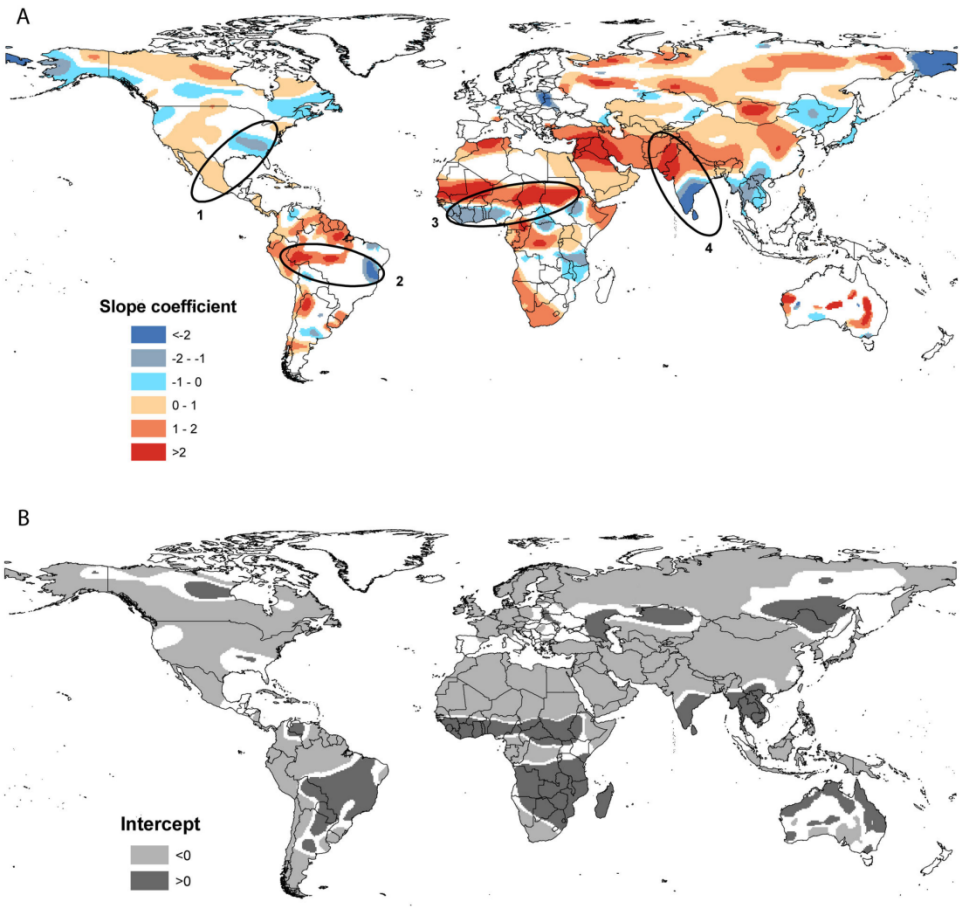

Figure 2. Output parameters and local R^2. The upper panel (A) shows results from the GWR analysis, showing the nature of the relationship between population density and burned area for those regions where the relationship is significant at the 95% level (red shows a positive relationship, blue shows a negative relationship). The slope coefficient classes are defined separately for each continent; (B) Mapped patterns in the sign and magnitude of the statistically significant intercept values from the GWR analysis of population density and burned area. Dark grey shows positive intercept values, where the area burned is large even at negligible population density (i.e. where the landscape is naturally fire-prone), while light grey shows negative intercept values where climatic or vegetation factors do not favour fire; (C) Showing the significant patterns for both intercept and slopes according to the sign of the relationship, thus the four combinations show both out being positive (red), positive slopes and negative intercept (green), negative slopes and positive intercept (yellow) and both being negative (blue) ;(D) Mapped patterns of the local R^2 for the regions where the relationship between population density and burned area is statistically significant.

doi: 10.1371/journal.pone.0081188.g002

areas of croplands and villages, and in forests. Absence of fire (because of lack of fuel) explains the absence of significant relationships in the Sahara, but the absence of any significant relationship associated with the high burned area (Figure 1a) in the Angola-Congo-Zambia region is perhaps more surprising (Figure 2a), given the general view that Miombo woodlands are

highly susceptible to anthropogenic fires (e.g. 32) and has been identified as one of the highest fire incidence in the world [15]. Population density in this region is rather low (5-15 people per km^2) and shows little spatial variability. This could partly explain the lack of a significant relationship between burned area and population. However, the region is characterised by a mosaic of open, fire-prone savannah vegetation and it is likely that both the high incidence and variability of fire is mainly determined by variability in climate and vegetation.

About 40.1% of the regions showing a significant relationship between burned area and population density have positive values for the intercept (Figure 2b), most particularly the Sudanian savannah region and parts of eastern Africa, where the relationship between fire and population density is inverse (Figure 2a). The positive intercept values indicate that these regions are naturally fire-prone, and help to explain why increasing population density should lead to lower area burnt. In contrast, the regions with negative intercepts can be interpreted suggesting that low fuel loads would normally limit fire and human modification of the vegetation cover is responsible for the relatively high levels of fire in these regions. This is consistent with the finding that burned area increases strongly (values > 1) with population density, because landscape modification will also increase with population density.

Asia

Asia is the continent with the largest area (over 49 million km^2) and the highest percentage (66%) of statistically significant slope values (Table 2). There are three regions that show a positive effect of population. The first extends from Turkey and Saudi Arabia through Iran and across to Afghanistan, Pakistan and northern India, the second is the rangelands of Mongolia and northern China, and the third occurs in the boreal parklands of Russia. Whereas the slope coefficients of the first two regions are always >1 (Figure 2a), a large part of the Russian parklands has slope coefficients <1, showing that the largest effects on fire occur for small population increments. Regions with significant negative slope coefficients occur in southern India, Southeast Asia and southern China, north-eastern China and Chukotka (north-eastern Siberia). As in the case of Africa, the regions showing positive relationships between burned area and population density tend to be predominantly characterised by rangelands. Regions characterised by villages and croplands, rangelands with extremely high population densities (e.g. in northern India and Pakistan, where populations densities are >250 p/km^2) and forested areas tend to show positive relationships between burned area and population density.

About 14% of the area of the total significant intercept values are positive (Figure 2b). Positive intercepts occur in southern India, Southeast Asia and north-eastern China – all areas where the relationship between burned area and population density is negative (i.e. an increase in population leads to suppression of fire). Areas with negative intercept values in the region stretching from Turkey through northern India to Mongolia show positive relationships between burned area and population density. The relationship in the boreal parklands is more complex, since although areas with positive slope coefficients mostly have negative intercept values, there are some limited areas with positive slope coefficients. However, the R^2 values (Figure 2d) in these regions are low (< 0.25), and the difference in the signals may not be robust. A different relationship occurs in Chukotka (and indeed in parts of Alaska), where negative relationships between burned area and population density are characterised by negative intercepts. Thus, in this not particularly fire-prone tundra region, increasing population density can significantly reduce fire incidence.

North America

The relationship between population density and burned area is statistically significant for over 43% of the area of North America (Table 2a). Positive relationships are found in the semi-arid (and mostly rangeland areas) of northern Mexico and the Great Basin, and in the boreal parkland regions of Canada and north-eastern Alaska. Negative relationships are found in the forested and cropped landscapes of south-eastern U.S.A (Alabama, Georgia, South Carolina), the forested regions of the Pacific Northwest and southern Alaska, and the boreal forest zone of central and eastern Canada (Figure 2a). Across virtually all of North America, slope coefficients are between 1 and -1, a feature that is consistent with the high technological levels of agriculture and contrasts strongly with regions of more traditional agricultural practices, such as Africa.

Only 4.1% of the regions showing statistically significant intercept have positive values. Positive intercept values (Figure 2b) are found in the south-eastern U.S.A., where the relationship between burned area and population density is negative, and in the boreal parklands of northern Canada where the slope of the relationship is positive. Areas with negative intercepts are characteristic of the southern boreal forest in eastern Canada and southern Alaska, and the semi-arid rangelands of the Great Basin and northern Mexico. The relationship between slope and intercept in the rangeland areas (positive slope coefficients, negative intercepts) is consistent with what is observed in semi-arid rangelands in other parts of the world; the relationship in the southern boreal forests (negative slopes, negative intercepts) is distinctive.

South America

The relationship between population density and burned area is statistically significant for 47% of the area of South America (Table 2). The relationship is positive around the margins of Amazonia, and in northern Argentina (Figure 2a). Negative relationships are found in the Bahia state in Brazil and, somewhat anomalously, in the rangeland area of central Argentina. The areas characterised by negative relationships between burned area and population density have positive intercepts (Figure 2b), i.e. these are fire-prone areas where increasing population leads to a reduction in fire. Most of the regions where the relationship between burned area and population density is positive are characterised by negative intercept values. However, in some parts of the so-called “arc of deforestation” on the southern side of the Amazon forest the positive relationship between fire and population density is associated with positive intercept values (Figure 2b), indicating

Table 3. Summary statistics of the GWR analysis for Africa, comparing the results obtained using 0.25°, 0.5° and 1.0° grid cell resolutions.

Continent	Number of observations	% significant slopes	% positiveslopes	AIC (OLS)	AIC (GWR)	Adjusted R^2 (OLS)	Adjusted R^2 (GWR)
Africa (0.25)	40864	67.7	65.5	189463.45	138841.26	0.21	0.77
Africa (0.5)	10647	61.3	75.5	52871.22	39362.11	0.27	0.80
Africa (1)	2557	52.4	97.8	12261.02	8188.66	0.36	0.87

doi: 10.1371/journal.pone.0081188.t003

fire-prone landscapes where human activity is increasing the amount of burning.

Europe and Australia

The relationship between population density and area burned is significant in < 22% of Europe and Australia (Table 2). In Europe, the only areas showing statistically significant negative relationships are in Poland, Ukraine and Belarus. However, intercept values in this region are positive, indicating some level of landscape susceptibility to fire. This feature most likely reflects a pattern dominated by the forested landscapes of e.g. the Carpathians, where natural forest fire regimes are suppressed with increasing population. Positive relationships between population density and burned area are found in some forested parts of north-western Russia; the intercept values are negative.

There are no significant relationships between area burned and population density in the savannah and rangeland areas of northern and western Australia characterised by the highest incidence of fire in the continent (Figure 1a). Areas showing a positive relationship between burned area and population density are in the rangelands of the Murray-Darling basin, on the northern margin of the Lake Eyre basin and to the south of the Hamersley Range in Western Australia. These regions are all associated with positive intercept values. Small areas showing a negative relationship between burned area and population density occur on rangelands of the Nullarbor Plain and in the densely-settled region (Figure 2a) around Melbourne in southern Victoria. The Nullarbor is characterised by negative intercept values (Figure 2b), presumably because of the very low vegetation cover and hence fuel loads in this region. In contrast, the area around Melbourne is characterised by positive intercept values – this is a fire-prone area where human activities work to suppress fire.

Sensitivity to spatial resolution

As expected, the GWR is sensitive to the choice of spatial resolution (Table 3). The extent of the area with significant relationships decreases with spatial resolution, from 68% at 0.25° resolution to 52% at 1° resolution. Changing resolution does not affect the conclusion that most of the relationships between burned area and population density are positive, but the proportion of positive values increases with increasing resolution, reaching an unrealistically high value of 98% at 1° resolution. This presumably reflects the increasing homogenisation of grid cell values of burnt area and/or population density with increasing resolution. The geographical patterns of significant values, and positive and negative relationships, are not impacted by the change from 0.25° resolution to 0.5° resolution, although areas showing negative relationships between population density and burned area have virtually disappeared in the analyses at 1° resolution. These sensitivity tests suggest that the overall conclusions of our GWR analysis would not be affected by running at finer than 0.5° resolution, but clearly information is likely to be lost in analyses at coarser resolution.

Impact of land-use on the relationship between burned area and population density

Both positive and negative relationships between burned area and population density are found in every type of anthrome (Figure 3). Wild lands represent a significant proportion of the regions where there is a significant correlation between burned area and population density, but nevertheless the proportion showing positive or negative correlations is about the same (29% of the total area showing positive, 31% showing negative correlations). However, croplands and rangelands are not equally represented in the two classes of relationship: 37% of the area where there is a negative relationship between burned area and population density is cropland and only 10% is rangelands. Conversely, rangelands account for nearly 40% of the area where there is a positive relationship between burned area and population density, while croplands account for only 11% of these regions.

Quantile regression analysis

Although regions may show an overall positive or negative relationship between burned area and population density, the nature and strength of the relationship is not necessarily constant at different levels of population [33]. We examine whether there are critical thresholds in population density at which the relationship between population density and the burned area extent changes using quantile regression, focusing on four different regions in Africa, Asia and the Americas (Figure 2a). Each region is characterised by close bipolar patterns, thus displaying areas with both strongly positive and strongly negative slope coefficients (Figure 2a).

In Asia, the relationship between population density and burned area is monotonic (Figure 4, case 4): as population density increases the impact on fire, whether positive or negative, increases. This is true for regions with moderate levels (50%) and at higher levels of burned area. In Africa and South America, the relationship between population density and burned area is non-monotonic: burnt area increases up to

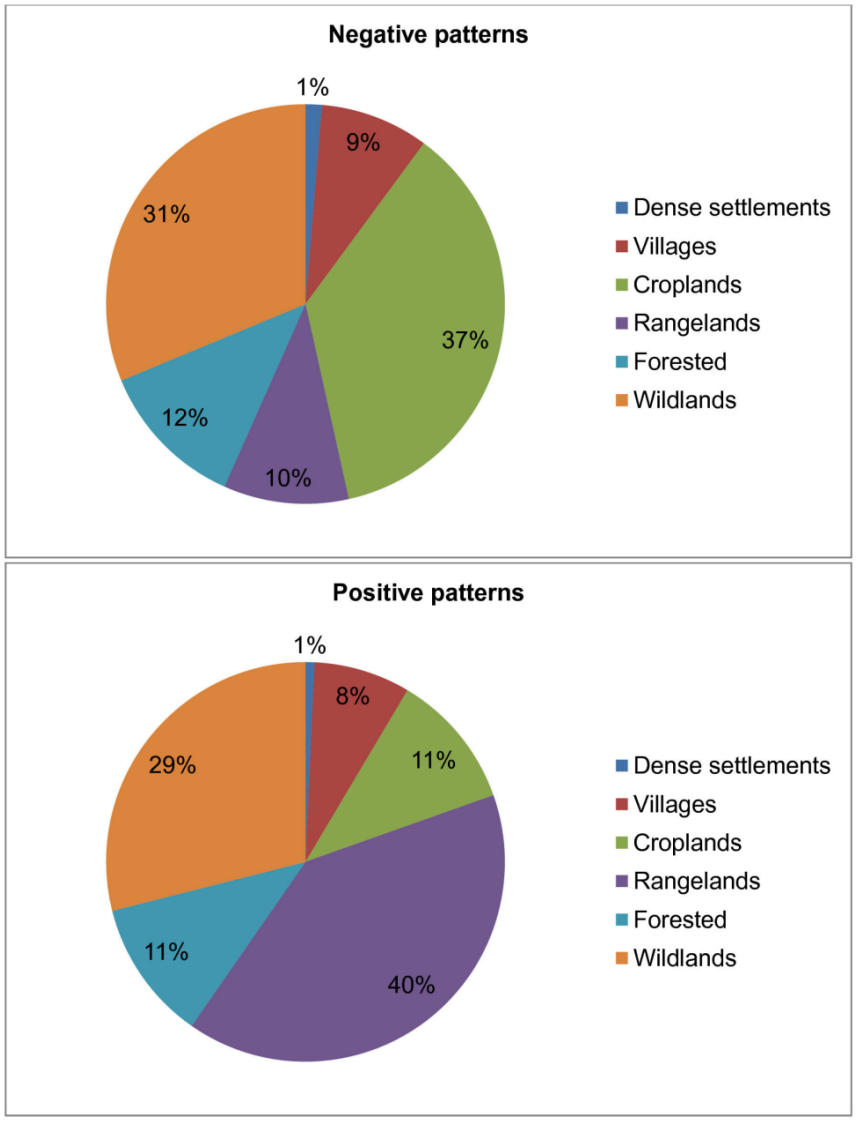

Figure 3. Proportion of Anthromes showing negative and positive relationship. Pie-charts showing the relative proportion of the total area showing (A) positive and (B) negative significant relationships between burned area and population density, classified according to the six major anthrome types defined by Ellis and Ramankutty (2008).

doi: 10.1371/journal.pone.0081188.g003

a given threshold, reaches a peak and then declines (Figure 4, cases 2-3). In both regions, the change point in the nature of the relationship occurs at about 7 p/km^2 in both regions with moderate and high levels of fire. The impact of changes in population density on burned area becomes negligible at population densities greater than ca 10 p/km^2 in both regions. The relationship between burned area and population density in North America is also non-monotonic (Figure 4, case 1). In regions with only moderate levels of fire (as shown by the 50% quantile regression), the relationship is similar to that observed in South America and Africa: increasing population density leads to increasing impact on burned area up population densities of 7 p/km^2 and then becomes negative and the slope becomes more gentle at population densities of > 12 p/km^2. However, in regions with higher levels of fire (as shown by the 90% regressions), the negative relationship at population densities > 7 p/km^2 is reversed and becomes positive at population levels > 30 p/km^2.

Discussion and Conclusions

This study quantifies the spatial variability in the relationship between human activities (as measure by population density) and fire (as measured by burned area). There is no statistically significant relationship between burned area and population density over more than 50% of the global land area. The univariate relationship between population density and area burnt is relatively unimportant in Australia and Europe: in the case of Australia this supports the idea of a strong climate control on fire regimes, while in Europe the lack of relationship most likely reflects the closely managed nature of the landscape. At a sub-continental scale, there are regions where population density has little or no impact on burned area. In Kazakhstan, for example, variability in burning shows no relationship with population density despite the fact that this is one of the biggest agricultural areas in the world [34] and the country that contributes with highest amount of area burnt in dry land ecosystems in central Asia [35]. A similar situation pertains in the Miombo woodlands region of Angola-Congo-Zambia, where variability in burned area is unrelated to population density. The absence of a relationship between population density and burned area over much of the globe does not imply that human activities have no influence on fire regimes. Several studies have shown, for example, that humans can alter the timing [36] or the number of fires [13,37]. However, since it is burned area (rather than timing or number) that is most important for the carbon cycle and pyrogenic emissions, the lack of a strong relationship between human activities and burned area over much of the globe, including areas characterised by high levels of burning, is noteworthy.

In areas where there is a statistically significant relationship, this relationship is positive (i.e. burned area increases with population density) over 73.3% of the global land area. However, there are substantial parts of the world, where the relationship between burned area and population density is negative (i.e. increasingly human activity leads to fire attenuation). The relative proportion of the land area showing positive/negative relationships varies from continent to continent. There has been considerable focus on the positive relationship between human activities and burned area, through using fire to clear land and as part of the agricultural regime [34,38]. The impact of landscape fragmentation on reducing fire in agricultural area has also been documented [16,39,40].

About 30% of the regions where a significant relationship between population density and burned area are classified as wild lands, but the relative proportion of wild lands in the areas showing positive or negative relationships between fire and human activity is approximately the same. This is not the case for all anthromes. Rangelands are over-represented in the regions showing positive relationships between fire and population, while croplands are over-represented in the regions showing negative relationships between fire and population. The distribution of rangelands is to some extent a reflection of climate controls, with most rangeland areas occurring in semi-arid regions and croplands occurring in more well-watered regions, nevertheless these tendencies suggest that land-use practices can have a significant impact of fire regimes.

The GWR analysis shows that, in general, regions which display a negative relationship between burned area and population density generally have positive intercept values, and vice versa. In other words, in regions where climate and/or vegetation create conditions where fires are likely (i.e. fire prone landscapes), people tend to supress fire whereas in regions that are less fire-prone because of e.g. lack of fuel, people tend to increase the area burned. However, there are regions where there is both a positive relationship between population and burned area and the intercept is also positive. One of these regions is the arc of deforestation on the southern border of Amazonia, suggesting that deforestation is exploiting a landscape that is already susceptible to the impact of fire. This is not a new suggestion; Le Page et al. (2010) [41] pointed out that this region experiences three to five months of low precipitation which facilitates extended periods of burning.

In most regions of the world, the nature of the relationship between population density and burned area is non-monotonic: increasing human activity (as measured by population density) initially lead to an increase in burned area but this peaks at intermediate levels of population density and then declines. The critical value in three of the case studies regions examine here is around 7 p/km^2 and above values of 12 p/km^2 there is no further impact of population density changes on fire. Our results for Africa support previous findings [13,42] that suggest that fire extent in this region displays a non-monotonic relationship with anthropogenic variables. However, in areas of North America characterised by high fire, there is a second threshold at ca > 30 p/km^2 where increasing population density leads to increasing burned area. The situation in Asia seems anomalous in that increasing population density always leads to an increased impact in burned area.

The GWR approach allows an appropriate spatial scale of comparison to be selected continent by continent through the choice of bandwidth combined with use of the AIC. Fotheringham et al. (2002) [20] showed that the GWR approach was more robust to the choice of spatial resolution than models that do not take spatial non-stationarity into

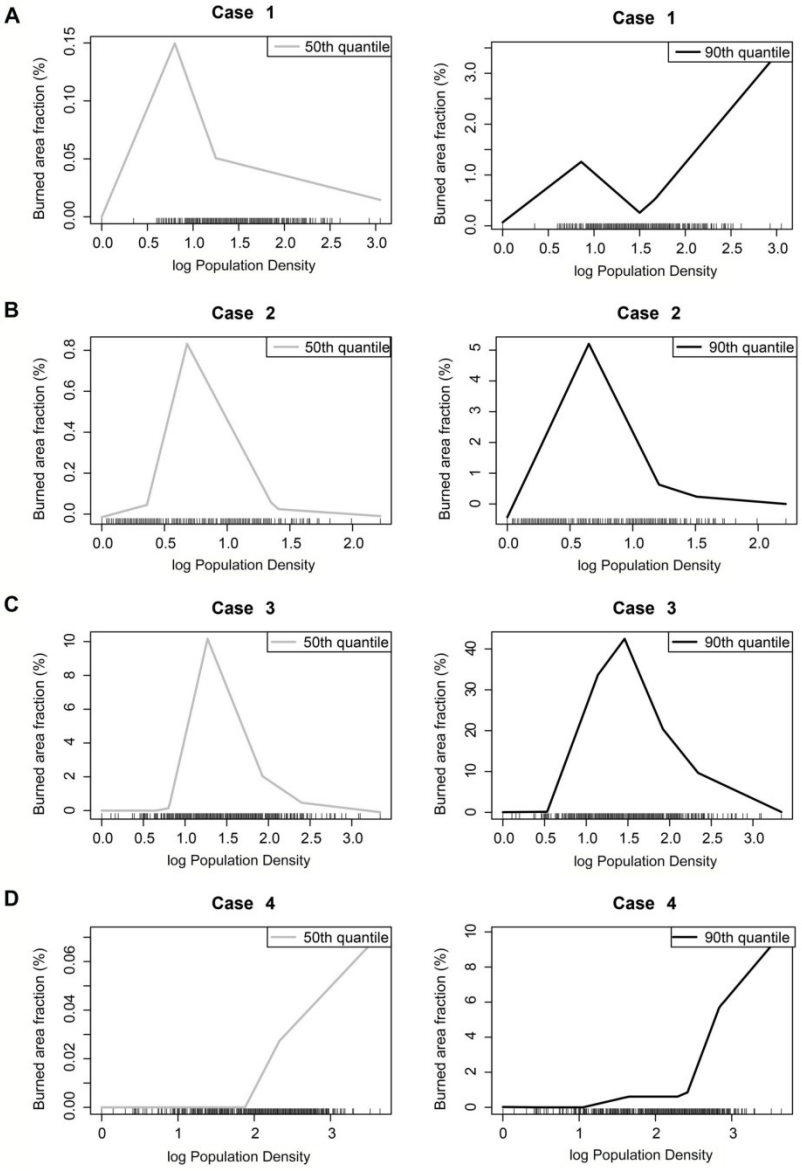

Figure 4. The relationship between burned area and population density at different levels of burned area (50 and 90%) for the 4 case studies. (A) Case 1 in North America. (B) Case 2 in South America. (C) Case 3 in Africa. (D) Case 4 in Asia.

doi: 10.1371/journal.pone.0081188.g004

account. Nevertheless, we examined the impact of the choice of spatial resolution using Africa as a test case. The use of a higher resolution than our baseline of 0.5° produces no change in the geographic patterns of regions showing significant positive or negative relationships between population density and burnt area, although the percentage of grid cells showing positive values declines slightly (and the percentage showing negative values correspondingly increases). The overall impact of increasing the resolution is slight, and this suggests that our regional findings are robust. Most other studies of the controls on burnt area have used coarser spatial resolutions (e.g. 12,43). Our sensitivity analyses show that decreasing the resolution has a larger impact on the geographic patterns, and particularly on the recognition of areas where the relationship between population density and burnt area is negative. This suggests that these earlier studies may miss important aspects of the relationship between population density and burnt area because of their choice of spatial scale. The selection of spatial scale is can affect the conclusions about the nature of spatial relationships, making it important to use a technique (such as the AIC optimization) that allows this choice to be made objectively.

Understanding the complexity of the relationships between people and fire is important in a modelling context. Fire-enabled dynamic vegetation models can be used to predict the consequences of projected changes in climate on fire regimes (see e.g. 44-46). However, those models that explicitly include anthropogenic fire generally focus on human impacts on ignitions and furthermore employ either a universal population density value as a threshold for anthropogenic fire ignitions [47], or single-peaked global function of population density [48]. Other fire-enabled DGVMs (e.g. LPX: [49]) ignore anthropogenic ignitions, although they allow for human suppression of fire in agricultural areas. No extant model incorporates spatially varying relationships between burned area and population density that are dependent on vegetation types, land-use and cultural practices – which our analyses show a non-negligible influence on regional fire regimes. However, this study has not exhausted the analyses necessary to arrive at a complete understanding of the biogeography of fire.

Author Contributions

Conceived and designed the experiments: IB DO ACLS JMCP. Performed the experiments: IB DO. Analyzed the data: IB DO ACLS SPH ICP JMCP. Contributed reagents/materials/analysis tools: IB DO ACLS JMCP. Wrote the manuscript: IB DO ACLS SPH ICP JMCP.

References

1. Bond WJ, Wilgen B (1996) Fire and plants. Chapman and Hall. London. UK.
2. Johnson E (1996) Fire and Vegetation Dynamics: Studies from the North American Boreal Forest. Cambridge University Press. Cambridge.
3. Pyne SJ, Andrews PL, Laven RD (1996) Introduction to wildland fire. New York, John Wiley and Sons. p.769.
4. Pyne SJ (2009) The human geography of fire: a research agenda. Progress in Human Geography. 33(4): 443–446. doi: 10.1177/0309132508101598.
5. Flannigan MD, Stocks BJ, Wotton BM (2000) Climate Change and Forest Fires. 1–9. Sci Total Environ 262(3): 221-229. doi:10.1016/S0048-9697(00)00524-6. PubMed: 11087028.
6. IPCC (2007) Climate Change 2007: The Physical Science Basis. Contribution of Working Group I to the Fourth Assessment Report of the Intergovernmental Panel on Climate Change [S SolomonD QinM ManningZ ChenM Marquis. Cambridge University Press, Cambridge, UK and New York, NY, USA.
7. Sanderson EW, Jaiteh M, Levy MA, Redford KH, Wannebo AV et al. (2002) The Human Footprint and the Last of the Wild. BioScience, 52(10): 891-904.
8. Ellis EC, Goldewijk K, Siebert S, Lightman D, Ramankutty N (2010) Anthropogenic transformation of the biomes, 1700 to 2000. Global Ecology and Biogeography 19(5). doi:10.1111/j.1466-8238.2010.00540.x.
9. Guyette RP, Muzika RM, Dey DC (2002) Dynamics of an anthropogenic fire regime. Ecosystems 5: 472-486. doi:10.1007/s10021-002-0115-7.
10. Barbosa PM, Stroppiana D, Gregoire J-M, Pereira JMC (1999a) An assessment of vegetation fire in Africa (1981–1991): burned areas, burned biomass, and atmospheric emissions. Glob Biogeochem Cycles 13(4): 933–950. doi:10.1029/1999GB900042.
11. Syphard AD, Radeloff VC, Keeley JE, Hawbaker TJ, Clayton MK et al. (2007) Human influence on California fire regimes. Ecol Appl 17(5): 1388–1402. doi:10.1890/06-1128.1. PubMed: 17708216.
12. Aldersley A, Murray SJ, Cornell SE (2011) Global and regional analysis of climate and human drivers of wildfire. Sci Total Environ 409(18): 3472–3481. doi:10.1016/j.scitotenv.2011.05.032. PubMed: 21689843.
13. Archibald S, Roy DP, vanWilgen BW, Sholes RJ (2009) What limits fire? An examination of drivers of burnt area in Southern Africa. Glob Change Biol 15(3): 613–630. doi:10.1111/j.1365-2486.2008.01754.x.
14. Giglio L, Randerson JT, van der Werf GR, Kahsibhatla PS, Collatz GJ et al. (2010) Assessing variability and long term trends in burned area by merging multiple satellite fire products. Biogeosciences 7: 1171–1186. doi:10.5194/bg-7-1171-2010.
15. Oom D, Pereira JMC (2013) Exploratory spatial data analysis of global MODIS active fire data. International Journal of Applied Earth Observation and Geoinformation 21: 326–340. doi:10.1016/j.jag.2012.07.018.
16. Bartholomè E, Belward AS (2005) A new approach to global land cover mapping from Earth observation data. International Journal of Remote Sensing 26(9): 1959–1977. doi:10.1080/01431160412331291297.
17. Center for International Earth Science Information Network (CIESIN), Columbia University, Centro Internacional de Agricultura Tropical (CIAT) (2005) Gridded population of the World version 3 (GPWv3): population density grids. Socioeconomic Data and Applications Center (SEDAC), Columbia University, Palisades.
18. Ellis EC, Ramankutty N (2008) Putting people in the map: anthropogenic biomes of the world. Frontiers in Ecology and the Environment 6(8): 439–447. doi:10.1890/070062.
19. Brunsdon CA, Fotheringham AS, Charlton ME (1998) Geographically weighted regression–modelling spatial non-stationarity. Stat 47(3): 431–443.
20. Fotheringham S, Brunsdon C, Charlton M (2002) Geographically Weighted Regression: the analysis of spatially varying relationships. John Wiley & Sons, UK.
21. Openshaw S, Taylor PJ (1981) The modifiable areal unit problem. in: Quantitative geography: a British View, (eds) N. Wrigley and R.J. Bennett, (Routledge and Kegan Paul: London), p. 60-70
22. Akaike H (1981) Likelihood of a model and information criteria. J Econ 16(1): 3–14. doi:10.1016/0304-4076(81)90071-3.
23. Byrne G, Charlton M, Fotheringham S (2009) Multiple dependent hypothesis tests in geographically weighted regression. In: BG LeesSW Laffan. 10th International conference on geocomputation. UNSW, Sydney November-December
24. Brunsdon C, Charlton M (2011) An assessment of the effectiveness of multiple hypothesis testing for geographical anomaly detection. Environment and Planning B: Planning and Design 38(2): 216 - 230. doi:10.1068/b36093.
25. Toms JD, Lesperance ML (2003) Piecewise Regression: A tool for identifying ecological thresholds. Ecology 84(8): 2034-2041. doi: 10.1890/02-0472.

26. Koenker R, Basset G (1978) Regression Quantiles. Econometrica 46(1): 33-50. doi:10.2307/1913643.
27. Koenker R (2005) Quantile Regression. Cambridge University Press. Cambridge. UK.
28. Sankaran M, Hanan NP, Scholes RJ, Ratnam J, Augustine DJ et al. (2005) Determinants of woody cover in African savannas. Nature 438(7069): 846–849. doi:10.1038/nature04070. PubMed: 16341012.
29. Chiu GS (2003) Bent cable Regression for Assesing Abruptness of Change. PhD Thesis, University of British Columbia: Canada.
30. Cade SB, Noon BR (2003) A gentle introduction to quantile regression for ecologists. Front Ecol Environment 1(8): 412-420. Available online at: doi:10.1890/1540-9295(2003)001[0412:AGITQR]2.0.CO;2
31. Tansey K, Gregoire J-M, Stroppiana D, Sousa A, Silva J, et al. (2004) Vegetation burning in the year 2000: global burned area estimates from SPOT VEGETATION data. J Geophys Res 109: D14S03 DOI 10.1029/2003JD003598.
32. Ryan CM, Williams M (2011) How does fire intensity and frequency affect miombo woodland tree populations and biomass? Ecol Appl 21: 48-60. doi:10.1890/09-1489.1. PubMed: 21516887.
33. Archibald S, Staver AC, Levin SA (2012) Evolution of human-driven fire regimes in Africa. Proc Natl Acad Sci U S A 109(3): 847-852. doi: 10.1073/pnas.1118648109. PubMed: 22184249.
34. Leff B, Ramankutty N, Folley JA (2004) Geographic distribution of major crops across the world. Global Biogeochemical Cycles 18.
35. Loboda TV, Giglio L, Boschetti L, Justice CO (2012) Regional fire monitoring characterization using global NASA MODIS fire products in dry lands of Central Asia. Front. Earth Sci. 6(2): 196-205. doi:10.1007/s11707-012-0313-3.
36. Page Le Y, Oom D, Silva JMN, Jonsson P, Pereira JMC (2009) Seasonality of vegetation fires as modified by human action: Observing the deviation from eco-climatic fire regimes. Global Ecology and Biogeography 19: 575-588.
37. Gralewicz NJ, Nelson TA, Wulder MA (2011) Spatial and temporal patterns of wildfire ignitions in Canada from 1980 to 2006. International Journal of Wildland Fire 21(3): 230-242.
38. Silva JMN, Carreiras JMB, Rosa I, Pereira JMC (2011) Greenhouse gas emissions from shifting cultivation in the tropics, including uncertainty and sensitivity analysis. Journal of Geophysical Research, 116(D20) DOI 10.1029/2011JD016056.
39. Laris P (2002) Burning the seasonal mosaic: Preventive burning strategies in the wooded savanna of southern Mali. Human Ecology 30: 155-186. doi:10.1023/A:1015685529180.
40. Marlon JR, Bartlein PJ, Carcaillet C, Gavin DG, Harrison SP et al. (2008) Climate and human influences on global biomass burning over the past two millennia. Nature Geoscience, 1(10): 697–702. doi: 10.1038/ngeo313.
41. Page Le Y, van der Werf GR, Morton DC, Pereira JMC (2010) Modelling fire-driven deforestation potential in Amazonia under current and projected climate conditions. Journal of Geophysical Research 115: 11
42. Sá ACL, Pereira JMC, Charlton ME, Mota B, Barbosa PM et al. (2010) The pyrogeography of sub-Saharan Africa: a study of the spatial non-stationarity of fire–environment relationships using GWR. Journal of Geographical Systems 13(3): 227–248. doi:10.1007/s10109-010-0123-7.
43. Krawchuk MA, Moritz MA, Parisien M-A, Van Dorn J, Hayhoe K (2009) Global Pyrogeography: the Current and Future Distribution of Wildfire. PLOS ONE 4(4): e5102. doi:10.1371/journal.pone.0005102. PubMed: 19352494.
44. Scholze M, Knorr W, Arnell NW, Prentice IC (2006) A climate change risk analysis for world ecosystems. Proc of the Natl Acad of Sciences of the USA 103: 13116–13120. doi:10.1073/pnas.0601816103. PubMed: 16924112.
45. Lenihan J, Bachelet D, Neilson R, Drapek R (2008) Response of vegetation distribution, ecosystem productivity, and fire to climate change scenarios for California. Clim Change 87: 215–230. doi: 10.1007/s10584-007-9362-0.
46. Harrison SP, Marlon J, Bartlein PJ (2010) Fire in the Earth System. Changing Climates, Earth Systems and Society. International Year of Planet Earth 2010, Climate Change Theme, 21-48.
47. Venevsky S, Thonicke K, Sitch S, Cramer W (2002) Simulating fire regimes in human-dominated ecosystems: Iberian Peninsula case study. Global Change Biology 8(10): 984–998. doi:10.1046/j.1365-2486.2002.00528.x.
48. Thonicke K, Spessa A, Prentice IC, Harrison SP, Dong L et al. (2010) The influence of vegetation, fire spread and fire behavior on biomass burning and trace gas emissions: results from a process-based model. Biogeosciences 7(6): 1991–2011. doi:10.5194/bg-7-1991-2010.
49. Prentice IC, Kelley DI, Foster PN, Friendlingstein P, Harrison SP et al. (2011) Modeling fire and the terrestrial carbon balance. Global Biogeochemical Cycles 25. doi:10.1029/2010GB003906.

IV. Religious Affiliation Modulates Weekly Cycles of Cropland Burning in Sub-Saharan Africa

Pereira, J. M. C., **Oom, D**., Pereira, P., Turkman, A. A. & Turkman, K. F.

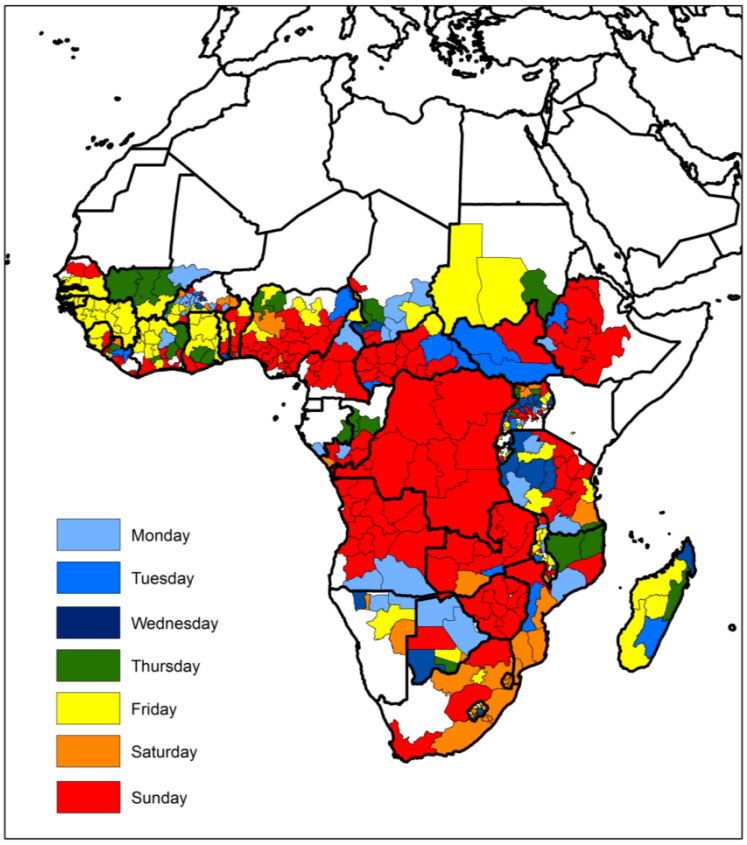

Published in *PloS One* in September 2015

PLOS | ONE

RESEARCH ARTICLE

Religious Affiliation Modulates Weekly Cycles of Cropland Burning in Sub-Saharan Africa

José M. C. Pereira[1]*, Duarte Oom[1], Paula Pereira[2], Antónia A. Turkman[3], K. Feridun Turkman[3]

1 Centro de Estudos Florestais, Instituto Superior de Agronomia, Universidade de Lisboa, Lisbon, Portugal, **2** Escola Superior de Tecnologia de Setúbal, Instituto Politécnico de Setúbal, Setúbal, Portugal, **3** Centro de Estatística e Aplicações, Faculdade de Ciências da Universidade de Lisboa, Lisbon, Portugal

* jmocpereira@gmail.com

CrossMark
click for updates

OPEN ACCESS

Citation: Pereira JMC, Oom D, Pereira P, Turkman AA, Turkman KF (2015) Religious Affiliation Modulates Weekly Cycles of Cropland Burning in Sub-Saharan Africa. PLoS ONE 10(9): e0139189. doi:10.1371/journal.pone.0139189

Editor: Philip Anglewicz, Tulane University School of Public Health, UNITED STATES

Received: October 14, 2014

Accepted: September 10, 2015

Published: September 29, 2015

Copyright: © 2015 Pereira et al. This is an open access article distributed under the terms of the Creative Commons Attribution License, which permits unrestricted use, distribution, and reproduction in any medium, provided the original author and source are credited.

Data Availability Statement: Anthromes data are publicly available from http://ecotope.org/anthromes/data/. The screened MODIS active fires data are publicly available at http://www.isa.utl.pt/cef/pub/modisactivefires-screend Global Administrative Areas data are publicly available at http://www.gadm.org/. Data from the 2010 World Religion database were kindly provided by the Gordon-Conwell Theological Seminary, Boston. Data source: Todd M. Johnson and Brian J. Grim, eds. World Religion Database (Leiden/Boston: Brill, accessed November, 2012). Researchers interested in obtaining the WRD data should contact info@globalchristianity.org

Abstract

Vegetation burning is a common land management practice in Africa, where fire is used for hunting, livestock husbandry, pest control, food gathering, cropland fertilization, and wildfire prevention. Given such strong anthropogenic control of fire, we tested the hypotheses that fire activity displays weekly cycles, and that the week day with the fewest fires depends on regionally predominant religious affiliation. We also analyzed the effect of land use (anthrome) on weekly fire cycle significance. Fire density (fire counts.km^{-2}) observed per week day in each region was modeled using a negative binomial regression model, with fire counts as response variable, region area as offset and a structured random effect to account for spatial dependence. Anthrome (settled, cropland, natural, rangeland), religion (Christian, Muslim, mixed) week day, and their 2-way and 3-way interactions were used as independent variables. Models were also built separately for each anthrome, relating regional fire density with week day and religious affiliation. Analysis revealed a significant interaction between religion and week day, i.e. regions with different religious affiliation (Christian, Muslim) display distinct weekly cycles of burning. However, the religion vs. week day interaction only is significant for croplands, i.e. fire activity in African croplands is significantly lower on Sunday in Christian regions and on Friday in Muslim regions. Magnitude of fire activity does not differ significantly among week days in rangelands and in natural areas, where fire use is under less strict control than in croplands. These findings can contribute towards improved specification of ignition patterns in regional/global vegetation fire models, and may lead to more accurate meteorological and chemical weather forecasting.

Introduction

Vegetation burning displays spatial and temporal patterns at various scales [1,2,3] affected by the seasonal occurrence of dry periods and thunderstorms, and by sporadic heat waves and droughts [4,5]. Land management practices, which often rely on fire, also influence those patterns, timing its use according to crop calendars and ecoclimatic constraints [6]. African vegetation fires are mostly anthropogenic, used for hunting, livestock husbandry, pest control,

Funding: Funding for this research was provided by Fundação para a Ciência e a Tecnologia (http://www.fct.pt/) research projects PEst-OE/AGR/UI0239/2014 (JMCP and DO), PEst-OE/MAT/UI0006/2014 (KFT, AT and PP), PTDC/MAT/118335/2010 (KFT, AT, PP and JMCP) and doctoral grant SFRH/BD/4752/2008 (DO). The funders had no role in study design, data collection and analysis, decision to publish, or preparation of the manuscript.

Competing Interests: The authors have declared that no competing interests exist.

facilitating food gathering, managing agricultural plot fertility, and for reducing the risk of large, uncontrolled fires [7]. Although the annual and daily dynamics of African biomass burning have been analyzed [8], the occurrence of intermediate scale temporal patterns is undocumented. Biomass burning, a large source of greenhouse gases and aerosols, constitutes a major factor controlling the inter-annual variability of atmospheric composition [9], and has been analysed at time scales ranging from a million years [10], to millennia [11], centuries [12], years [13], and days [8]. Patterns found in these studies were interpreted as a function both of climate dynamics and human activity. Regular cycles in vegetation burning are found at annual scale, mostly in seasonally dry areas, and at the daily scale as a consequence of underlying cycles in meteorological variables and land management practices. Weekly cycles were detected in aerosols and cloud droplet number concentration in several studies, and models confirm that the difference in emissions between week days and weekends generates this cycle. Since there is no natural forcing with a seven-day period, weekly cycles provide evidence of an anthropogenic fingerprint [14]. A weekly cycle of aerosol optical depth (AOD), observed in the United States (U.S.) and in Central Europe, is stronger in urban sites than in rural sites. A reversed AOD weekly cycle occurs in the Middle East and India, with lower AODs on Thursday and Friday, the weekend for Middle Eastern cultures. Therefore, cultural practices and the industrial activity schedule of this region are consistent with the observed AOD weekend effect [15]. Chemical weather forecasting models use meteorological and emissions information as input to simulate transport, chemistry, and deposition processes to predict short-term variability of air quality. Good performance of a chemical weather forecast model requires accurate representation of the temporal distribution of natural and anthropogenic emissions. However, some atmospheric chemistry modelling studies have assumed that, contrary to emissions from industry and transportation, biomass burning does not display weekly cycles [14,16]. Considering that vegetation burning in Africa is mostly anthropogenic and used as a land management tool [4,7,17], we tested the hypotheses that there is a day of the week with lower fire activity, and that this day depends on the regionally predominant religious affiliation: Sunday on predominantly Christian areas, and Friday on predominantly Muslim areas. We also tested the effect of regionally dominant land use on significance of the weekly fire activity minima, which is expected to depend on land management intensity. Our analysis is restricted to the two major religions in sub-Saharan Africa, which account for 62.9% (Christians) and 30.2% (Muslims) of the total population, and are the only ones that prescribe a weekly day of rest [18, 19]. African traditional religions are followed by 3.3% of sub-Saharan Africans, while Hindus and Buddhists jointly represent less than 0.3% of the population, 0.2% have other religious affiliations, including Judaism, and 3.2% are not religiously affiliated [20]. Muslims are concentrated in northern hemisphere sub-Saharan Africa, in a belt extending from the southern part of Sudan, in the east, to Senegal and Sierra Leone in the west, while the southern hemisphere is very predominantly Christian, with the exception of the east coast from northern Mozambique to Somalia. Additional information on the geography of religion in Africa, as classified for the purposes of our analysis, is provided in Materials and Methods.

Materials and Methods

Religious affiliation, land use, and fire activity spatial data

The geographical basis for our analysis is the Global Administrative Areas (GADM, version 2, Jan 2012, http://www.gadm.org/) first level divisions for Africa, which contains a total of 554 units and is the spatial support for the religious affiliation data (Fig 1A) of the 2010 World Religion Database [21]. Land use / land cover data (Fig 1B) are from the Anthropogenic Biomes of the World (Anthromes) dataset [22], at 5′ (ca. 9 km) spatial resolution and dated from the year

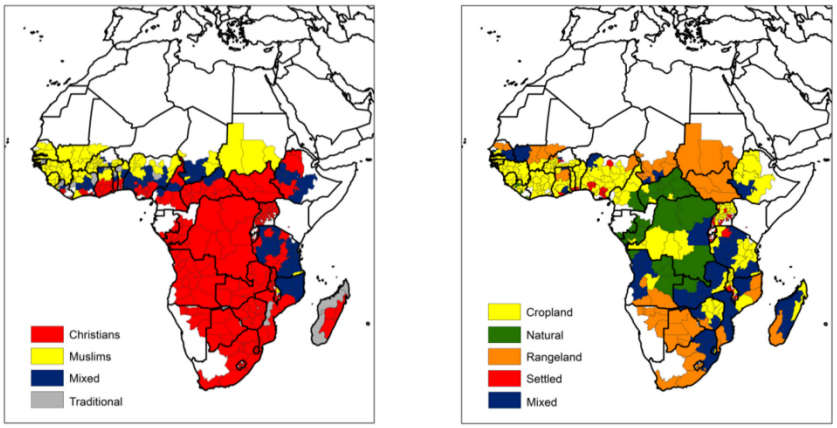

Fig 1. Regional geography of religion and land use in Africa. a) Classification of predominant religious affiliation; b) Classification of predominant anthrome.

doi:10.1371/journal.pone.0139189.g001

2000. Anthrome data incorporate information on population density, land cover and land use and map global patterns of sustained direct human interaction with ecosystems [23]. Given the strongly anthropogenic character of vegetation burning in Africa they were considered particularly suited for our analysis and preferred over biophysical variables such as vegetation type or land cover. The alternative of using annual land cover data (e.g. the MODIS MCD12Q1 product) would suffer from the interannual classification inconsistencies reported by [24]. The relative stability of spatial patterns depicted by the Anthromes dataset justifies its use to analyze active fire counts from the period 2003–2011.

Daily fire activity was quantified with data from the NASA MODIS MCD14ML Collection 5 active fire product [25] for the period 2003–2011 (TERRA and AQUA sensors) at 1km spatial resolution, after screening for false alarms and non-vegetation fires according to the procedures detailed in [26]. Fig 2 shows regional fire count densities per week day (Fig 3A–3G) and total density.

Religious affiliation and land use classification

The screened MODIS active fires dataset contains a total of 22,749,687 observations. One hundred and sixty one GADM regions with less than 0.1 km^{-2} active fire counts accumulated over the nine-year study period were excluded from analysis. An additional nineteen regions where the sum of Christian and Muslim believers falls below 50% of the total population were also removed from analysis, since a weekly day of rest is specific of the Abrahamic monotheisms [18, 19], while in such regions most of the population follows African traditional religions. Two more regions were excluded due to lack of data on religious affiliation, resulting in a total of 372 spatial units analyzed. Wherever Christians (Muslims) represent over 75% of the sum of Christian + Muslim believers, the region was considered Christian (Muslim). When neither religion accounted for at least 75% of the population, the region was labelled mixed Christian-

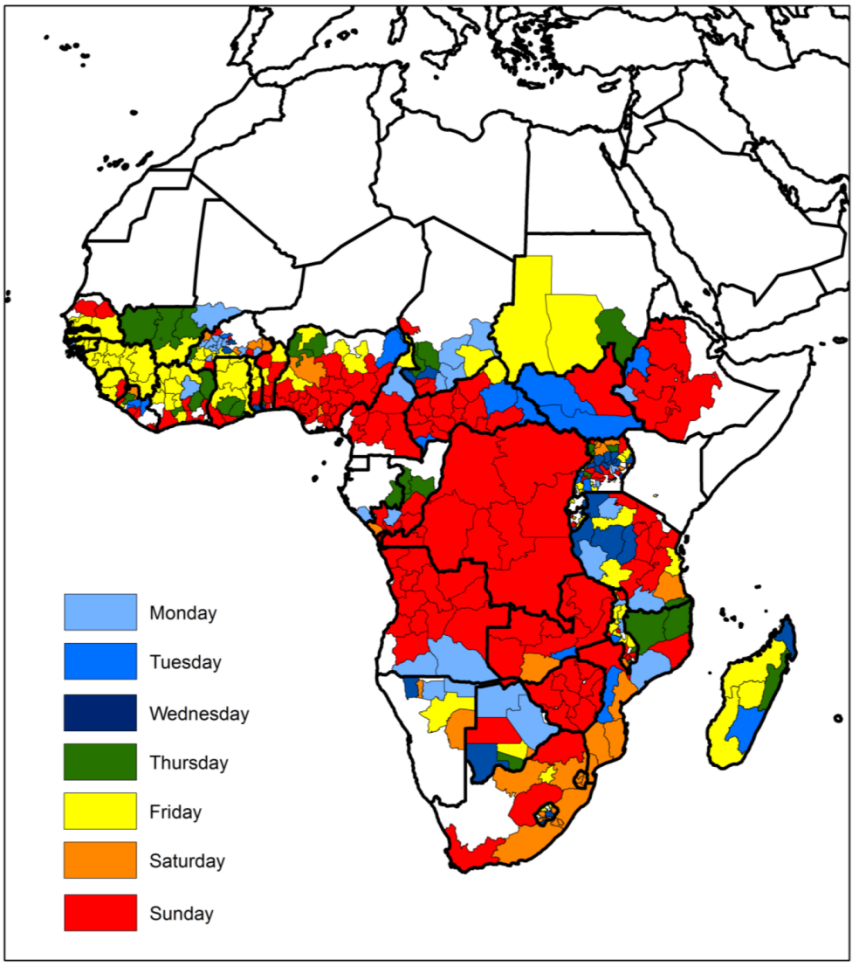

Fig 2. Week day with the fewest fire counts.

doi:10.1371/journal.pone.0139189.g002

Muslim (Fig 1A). Classification of each region in terms of dominant land use relied on the highest level Anthromes legend [22] with aggregation of the Dense Settlement and Villages classes into a single class (Settled) and the Forest class and Wildland class into a single Natural class. Cropland and Rangeland classes were not altered. The percent area in each region covered by each of the four new classes was calculated and wherever a single class represented at least 50% of the area, the region was labelled as belonging to that class. If no single class exceeded the 50% area threshold, the region was considered as having Mixed land use (Fig 1B). Religious affiliation and Anthrome classification thresholds were selected with the aim of

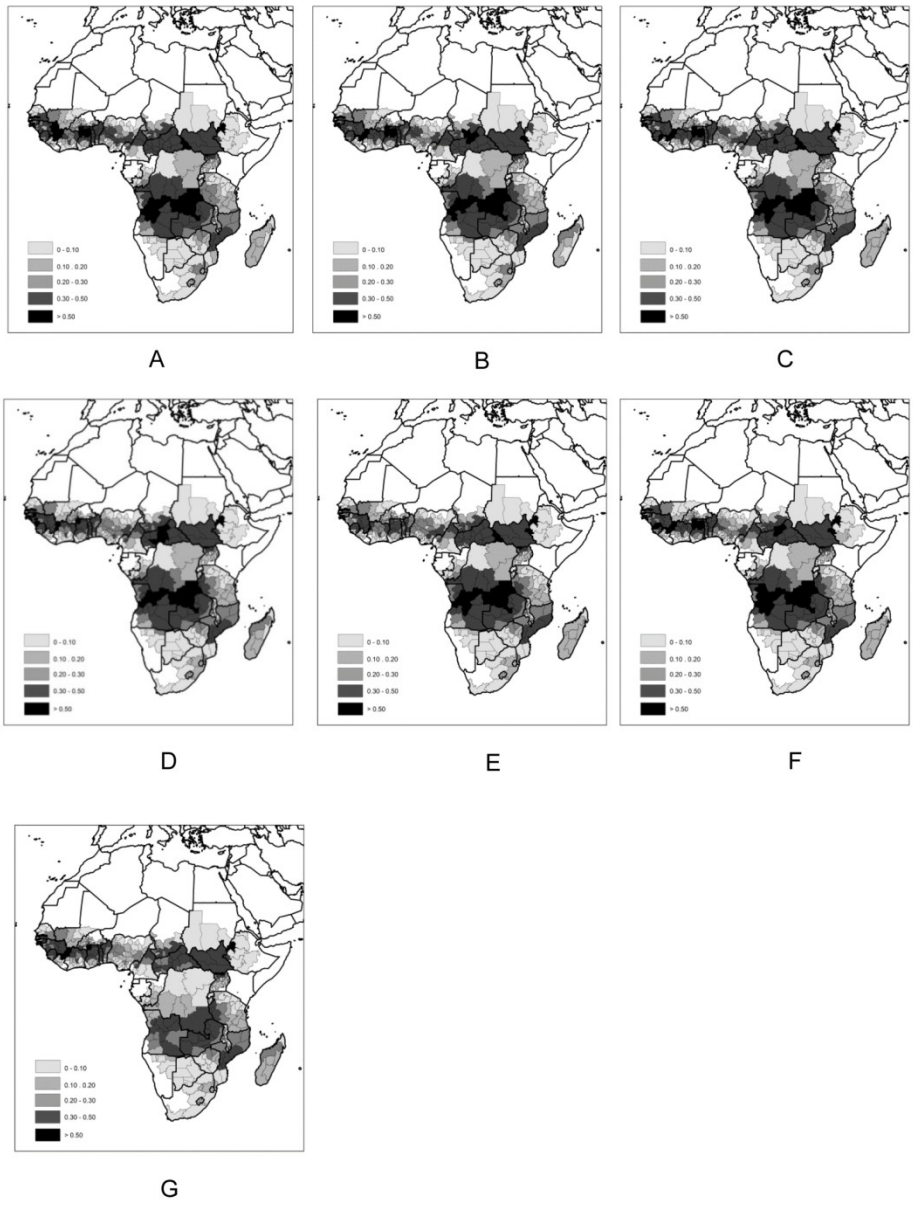

Fig 3. Mean MODIS active fire regional density (fires.km^{-2}), 2003–2011. a) Monday; b) Tuesday; c) Wednesday; d) Thursday; e) Friday; f) Saturday; g) Sunday.

doi:10.1371/journal.pone.0139189.g003

Table 1. Number of regions by dominant religion and dominant anthrome.

	Religion			
Anthrome	**Christian**	**Muslim**	**Mixed**	**Total**
Cropland	69	47	48	164
Natural	27	0	5	32
Rangeland	30	14	12	56
Settled	48	4	5	57
Mixed	42	7	14	63
Total	216	72	84	372

doi:10.1371/journal.pone.0139189.t001

obtaining clear dominance of a class in each region, while ensuring that the respective mixed classes do not cover an unduly large fraction of the study area. Evidently, this was more easily achieved for the three-class religious affiliation variable than for the five class Anthrome variable. Table 1 shows the number of regions by religion and by anthrome, based on these classification rules. Fifty-eight percent of regions (216/372) were classified as Christian and 19% (72/372) as Muslim. Cropland is the anthrome accounting for the highest percentage of regions (164/372, 44%), while the Natural anthrome accounts for the fewest (32/372, 9%).

According to our thresholds for defining predominant religious affiliation, Muslim regions are mostly located in West Africa, in southeastern Chad and in the southern part of Sudan. Most of southern hemisphere Africa is Christian, with the exception of Tanzania and northern Mozambique. Predominantly Christian regions are also found in the southern regions of Ghana, Togo, Benin, Nigeria, and Cameroon, the western part of Central African Republic, South Sudan, and western Ethiopia. Mixed Christian/Muslim regions are located in West Africa, throughout most of Cameroon, in southwestern Chad, the eastern part of Central African Republic and part of Ethiopia, and also in most of Tanzania and northern Mozambique. African traditional religions are dominant in a few regions of West Africa, and in western Madagascar (Fig 1A). Aggregated Anthromes data show that croplands predominate in West Africa, Ethiopia, Uganda, Rwanda, and Burundi, and in parts of the Democratic Republic of Congo, Zimbabwe, and Tanzania. Natural areas are primarily located in central Africa, from the Central African Republic and Cameroon, down to eastern Angola and western Zambia. Rangelands occupy arid areas in the Sahel, and in southern Angola, Namibia, Botswana, and South Africa. Settled regions are concentrated in West Africa, and in the Great Lakes region. Finally, regions of Mixed land use, according to our definition, predominate in southern hemisphere Africa, namely in parts of Angola, Tanzania, Zambia, Mozambique, Madagascar, and South Africa (Fig 1B). Classification of regional fire counts by week day minimum reveals that most of Africa displays a weekly minimum of fire activity on Sunday, especially evident in the southern half of Nigeria, large parts of Cameroon, the Central African Republic, western Ethiopia, the Democratic Republic of Congo, Angola, Zambia, and Zimbabwe. Friday weekly fire minima are primarily found in West Africa, in the southern part of Sudan, and in western Madagascar (Fig 2).

Statistical modelling

The fire density observed in each region (Fig 3A–3G) was modeled using a negative binomial model [27] with fire counts as response variable, region area as offset and a structured random effect, in the form of a ICAR model [28], to account for spatial dependence. Anthrome, religion and week day, together with their two-way and three-way interactions were used as independent variables. A Bayesian methodology was used to fit these spatial generalized linear model

using R-INLA [29]) and the respective package (www.r-inla.org). The best model was chosen using the deviance information criterion (DIC) [30]. For each region $i = 1, \ldots, 372$ characterized by anthrome $A = 1, \ldots, 5$ and religion $R = 1,2,3$, the full model assumes that the total number of fires per year in each week day $W = 1, \ldots, 7$ (Y_{iW}) are conditionally independent observations following the full negative binomial model,

$$P(Y_{iW} = y) = \frac{\Gamma(y+\theta)}{\Gamma(\theta)y!}\left(\frac{\mu_{iW}}{\mu_{iW}+\theta}\right)^{y}\left(\frac{\theta}{\mu_{iW}+\theta}\right)^{\theta} \quad \text{(Eq 1)}$$

with shape parameter θ and mean μ_{iW} such that:

$$\ln(\mu_{iW}) = \ln(area_i) + \alpha_0 + \alpha_{1A} + \alpha_{2R} + \alpha_{3W} + \alpha_{1RW} + \alpha_{2RA} + \alpha_{3WA} + \alpha_{RWA} + z_i \quad \text{(Eq 2)}$$

where α is a vector of parameters accounting for the intercept, (α_0) the effect of the three main factors anthrome (α_{1A}), religion (α_{2R}), and week day (α_{3W}), together with the corresponding two-way (α_{1RW}, α_{2RA}, α_{3WA}) and three-way (α_{RWA}) interactions. The area of the region enters in the linear predictor as an offset, $\ln(\text{area}_i)$. The term z_i is the structured spatial random effect for region i, defined by the ICAR model.

To prevent confounding due to association of the anthrome variable both with fire density and religion, the hypothesis of a significant interaction between religion and week day was tested for each of the negative binomial regression models built separately for the different anthromes, taking spatial dependence into account. Again under a Bayesian framework, DIC values of the models were compared with and without the interaction term, and the model with the lowest DIC was selected.

We analyzed specific pairwise contrasts of interest, namely between Sunday and every other week day in Christian regions, and between Friday and every other week day in Muslim regions. The following hypotheses were tested:

$$H_0 : \mu_{Christian:7} - \mu_{Christian:i} = 0, \qquad \text{for i} = 1,2,3,4,5,6;$$

$$H_0 : \mu_{Muslim:5} - \mu_{Muslim:i} = 0, \qquad \text{for i} = 1,2,3,4,6,7;$$

$$H_0 : \mu_{Christian:7} - \mu_{Muslim:5} = 0;$$

$$H_0 : \mu_{Christian:7} - \mu_{Mixed:7} = 0;$$

$$H_0 : \mu_{Muslim:5} - \mu_{Mixed:5} = 0;$$

where 1 = Monday, 2 = Tuesday, 3 = Wednesday, 4 = Thursday, 5 = Friday, 6 = Saturday, and 7 = Sunday. All testing was performed under a Bayesian methodology, by computing, for each of the respective contrasts, the posterior contour probability of zero. The contour probability equals one minus the content of the highest posterior density (HPD) interval just covering zero [31], and is the probability that the posterior density function of the contrast is less than or equal to the posterior density function of the contrast at zero. This probability can be interpreted as a p-value in checking the posterior support of specific values of interest, an approach motivated by well-known analogies between Bayesian and classical inference concepts [32]. To account for multiple comparisons, adjusted values for these probabilities were calculated using the Benjamini-Hochberg method [33]. In addition 95% credible intervals were calculated and displayed.

Results

Statistical models relating regional annual fire counts and regional area with week day of occurrence (nine annual replicates, 2003–2011), religious affiliation, and anthrome, and taking spatial dependence into account, were fit to the data (Table 2). The best model selected using DIC contained the two-way interactions between week day and land use, and between religion and land use, and the spatial random effect in the form of a ICAR model, revealing the existence of a significant interaction between religion and week day, i.e. regions with different religious affiliation (Christian, Muslim, and mixed) display distinct weekly cycles of vegetation burning (Fig 4A). The anthrome variable is strongly associated with religious affiliation and with fire density, acting as a confounding factor in the model. To address this problem, statistical models relating fire density in each region with week day of occurrence, religious affiliation, and the corresponding interaction term were built separately for each anthrome, taking into account spatial dependence. The best model in each anthrome was chosen using DIC. Only for the croplands anthrome (which accounts for 31.2% of the total number of active fires used in the study) did the best model contain the interaction between weekday and religion (Table 3 and Fig 4B).

To test the hypotheses that the weekly fire counts minima occur on Sunday (Friday) in Christian (Muslim) regions, we analyzed the pairwise contrasts Sunday *versus* every other week day in Christian regions, and Friday *versus* every other week day in Muslim regions. We also tested contrasts between fire counts on Sunday in Christian areas *versus* Friday in Muslim areas; on Sunday in Christian areas *versus* on Sunday in mixed religion areas; on Friday in Muslim areas *versus* on Friday in mixed areas (Table 4). The contrast analysis showed that, as hypothesized, there are significantly fewer fires on Sunday than on any other week day in Christian regions and on Friday than on any other week day in Muslim regions.

Discussion

Previous research based on remotely sensed data revealed different aspects of the anthropogenic nature of African vegetation burning. The very low interannual variability and strong annual periodicity of African fire activity, combined with the presence of a diurnal cycle were

Table 2. Deviance Information Criterion (DIC) scores for all negative binomial models fitted. The best model (lowest DIC, bold) includes all single variables, the two-way interactions between religion and week day, between religion and anthrome, and the spatial term.

MODEL	DIC
R + W + A + R:W + R:A + W:A + R:W:A + ICAR	285 977.17
R + W + A + R:W + R:A + W:A + R:W:A	313 319.00
R + W + A + R:W + R:A + W:A + ICAR	285 936.84
R + W + A + R:W + R:A + W:A	313 252.28
R + W + A + R:W + R:A + ICAR	**285 928.25**
R + W + A + R:W + R:A	313 212.31
R + W + A + R:W + W:A + ICAR	285 938.44
R + W + A + R:W + W:A	313 827.29
R + W + A + R:W + ICAR	285 929.88
R + W + A + R:W	313 787.56
R + W + A + ICAR	285 955.56
R + W + A	313 793.07

R–Religion; W–Week day; A–Anthrome; ICAR–Intrinsic conditional autoregressive term.

doi:10.1371/journal.pone.0139189.t002

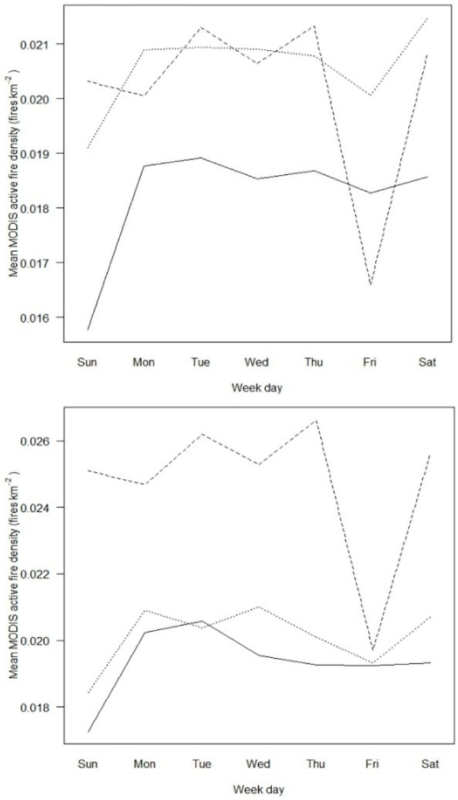

Fig 4. Mean MODIS active fire density (fires.km^{-2}) per week day. a) All anthromes; b) Croplands. Solid line: Christian regions; Large dashed line: Muslim regions; Fine dashed line: mixed Christian-Muslim regions.

doi:10.1371/journal.pone.0139189.g004

considered as evidence of markedly anthropogenic fire, caused by large-scale burning for land management purposes [34]. Anticipation of the fire season relatively to the dry season for periods of over one month throughout most of Africa was shown by [6], and interpreted as due to preventative break-up of fuel continuity at the landscape scale to avoid large, damaging fires, later in the season [7]. Statistical significance of the weekly cycle of fire activity in croplands, as opposed to the other anthromes, is understandable, considering that cropland fires typically are closely managed, small and low intensity. Less strictly controlled burning in natural areas and rangelands means that fires may be more intense [34], larger, and last longer than in agricultural areas [7,17]. Therefore, rangeland and forest fires observed by satellite on Friday (Sunday) in Muslim (Christian) regions are more likely to have been set in previous work days than the smaller, carefully controlled burns in fragmented agricultural landscapes, potentially reducing the difference between fire counts on holidays and week days. A study of preventative landscape burning in Mali [35] found that cropland fires were very well contained, with only a

Table 3. Negative binomial model Deviance Information Criterion (DIC) for each anthrome. Best models are shown in bold.

MODEL	DIC
CROPLAND	
R + W + R:W + ICAR	**128 354.10**
R + W + R:W	138 164.47
R + W + ICAR	128 374.22
R + W	138 166.24
RANGELAND	
R + W + R:W + ICAR	47 328.74
R + W + R:W	51 057.93
R + W + ICAR	**47 308.52**
R + W	51 035.93
SETTLED	
R + W + R:W + ICAR	29 799.93
R + W + R:W	32 597.90
R + W + ICAR	**29 784.36**
R + W	32 571.26
MIXED	
R + W + R:W + ICAR	52 781.57
R + W + R:W	58 049.01
R + W + ICAR	**52 780.20**
R + W	62 391.97
NATURAL	
R + W + R:W + ICAR	29 684.53
R + W + R:W	32 991.69
R + W + ICAR	**29 677.66**
R + W	32 981.13

doi:10.1371/journal.pone.0139189.t003

small number of farmers interviewed reporting that fires lit to prepare fields for agriculture had burned into the lands adjacent to their plots. Also in Mali, the occurrence of few, large fires in the northern pastoral areas of the Sahel, is opposed to a pattern of many small fires in agricultural south [7]. The same study refers smaller burns in croplands than in slash-and-burn farming in forest areas of Madagascar, while in southern Mozambique fires set to clear agricultural fields are smaller than those used to manage pastures [36].

Identification of a previously undetected weekly cycle in cropland burning further highlights the extent to which African fire is anthropogenic, and provides evidence that religion, although an essentially symbolic cultural system, has material impacts on the land surface that can be observed from space. Detailed geographical analysis of weekly cycles of fire activity will further elucidate the global geography and magnitude of anthropogenic vegetation burning, and may inform specification of the ignition component of fire modules incorporated in dynamic global vegetation models. Our detection of weekly cycles in vegetation burning contradicts the assumption of [14, 16] and lends support to the use of operational chemical weather forecasting models that rely on daily fire remote sensing data to estimate biomass burning emissions [37], which have important climatic effects [38,39] and impacts on public health [40]. Since biomass burning aerosols are strong absorbers of sunlight, they may also alter the thermodynamic structure of the atmosphere and contribute towards observed large scale weekly cycles in meteorological variables [41].

Table 4. Cropland anthrome estimated pairwise contrasts between Sunday (Friday) and every other week day in Christian (Muslim) regions, and between Sunday and Friday. The contrasts refer to the best cropland anthrome model shown in Table 3 (R + W + R:W + ICAR).

			95% credible interval			
Contrast	mean	s.d.	Lower	upper	p-value*	BH p-value**
Chr:Sun-Chr:Mon	-0.2113	0.0339	-0.2779	-0.1448	0.00000	0.00000
Chr:Sun-Chr:Tue	-0.2025	0.0338	-0.2689	-0.1361	0.00000	0.00000
Chr:Sun-Chr:Wed	-0.1204	0.0338	-0.1868	-0.0540	0.00036	0.00004
Chr:Sun-Chr:Thu	-0.1321	0.0339	-0.1986	-0.0657	0.00000	0.00000
Chr:Sun-Chr:Fri	-0.0996	0.0338	-0.1661	-0.0333	0.00319	0.00342
Chr:Sun-Chr:Sat	-0.1458	0.0339	-0.2123	-0.0794	0.00000	0.00000
Mus:Fri-Mus:Mon	-0.1807	0.0408	-0.2608	-0.1007	0.00000	0.00000
Mus:Fri-Mus:Tue	-0.2243	0.0408	-0.3044	-0.1444	0.00000	0.00000
Mus:Fri-Mus:Wed	-0.1985	0.0408	-0.2785	-0.1185	0.00000	0.00000
Mus:Fri-Mus:Thu	-0.2410	0.0408	-0.3211	-0.1610	0.00000	0.00000
Mus:Fri-Mus:Sat	-0.2104	0.0408	-0.2904	-0.1304	0.00000	0.00000
Mus:Fri-Mus:Sun	-0.1832	0.0408	-0.2632	-0.1032	0.00000	0.00000
Chr:Sun-Mus:Fri	0.5169	0.0906	0.3395	0.6951	0.00000	0.00000
Chr:Sun-Mix:Sun	0.6674	0.1374	0.4012	0.9403	0.00000	0.00000
Mus:Fri-Mix:Fri	0.0985	0.1718	-0.2362	0.4382	0.57856	0.57856

Chr: Christian; Mus: Muslim; Mon: Monday; Tue: Tuesday; Wed: Wednesday; Thu: Thursday; Fri: Friday; Sat: Saturday; Sun: Sunday.

* Probability that the posterior density function of the contrast is less than or equal to the posterior density function of the contrast at zero.

** Benjamini-Hochberg adjusted p-value.

doi:10.1371/journal.pone.0139189.t004

Acknowledgments

Regional religious affiliation data for Africa were kindly provided by the Gordon-Conwell Theological Seminary, Boston. Funding for this research was provided by Fundação para a Ciência e a Tecnologia (http://www.fct.pt/) research projects PEst-OE/AGR/UI0239/2014 (JMCP and DO), PEst-OE/MAT/UI0006/2014 (KFT, AT and PP), PTDC/MAT/118335/2010 (KFT, AT, PP and JMCP) and doctoral grant SFRH/BD/4752/2008 (DO).

Author Contributions

Conceived and designed the experiments: JMCP AAT KFT. Performed the experiments: AAT PP DO KFT. Analyzed the data: DO PP AAT. Contributed reagents/materials/analysis tools: JMCP DO. Wrote the paper: JMCP AAT KFT.

References

1. Dwyer E, Pereira JMC, DaCamara CC, Grégoire J-M. Characterization of the spatio-temporal patterns of global fire activity using satellite imagery for the period April 1992 to March 1993. J Biogeogr, 1999; 27 (1), 57–69.
2. Balzter H, Gerard FF, George CT, Rowland CS, Jupp TE, McCallum I, et al. Impact of the Arctic Oscillation pattern on interannual forest fire variability in Central Siberia. Geophys Res Lett, 2005; 32 (14) L14709, doi: 10.1029/2005GL022526
3. Archibald S, Roy DP, van Wilgen BW, Scholes RJ. What limits fire? An examination of drivers of burnt area in Southern Africa. Glob Chang Biol, 2009; 15: 613–630, doi: 10.1111/j.1365-2486.2008.01754.x
4. Bond WJ. Fire. In: Cowling RM, Richardson DM, and Pierce SM, editors. Vegetation of Southern Africa. Cambridge UK: Cambridge University Press; 1997, pp. 421–446.
5. Wooster MJ, Perry GLW, Zoumas A. Fire, drought and El Niño relationships on Borneo (Southeast Asia) in the pre-MODIS era (1980–2000). Biogeosciences, 2012; 9, 317–340, doi: 10.5194/bg-9-317-2012

6. Le Page Y, Oom D, Silva JMN, Jönsson P, Pereira JMC. Seasonality of vegetation fires as modified by human action: observing the deviation from eco-climatic fire regimes. Glob Ecol Biogeogr, 2010; 19 (4), 575–588. doi: 10.1111/j.1466-8238.2010.00525.x
7. Kull C, Laris P. Fire ecology and fire politics in Mali and Madagascar. In: Cochrane MA, editor. Tropical Fire Ecology: Climate Change, Land Use and Ecosystem Dynamics. Heidelberg: Springer-Praxis; 2009, pp. 171–226.
8. Roberts G, Wooster MJ, Lagoudakis E. Annual and diurnal African biomass burning temporal dynamics. Biogeosciences, 2009; 6, 849–866.
9. Schultz MG, Heil A, Hoelzemann JJ, Spessa A, Thonicke K, Goldammer JG, et al. Global wildland fire emissions from 1960 to 2000. Global Biogeochem Cycles, 2008; 22 (2) GB2002, doi: 10.1029/2007GB003031
10. Bird MI, Cali JA. A million-year record of fire in sub-Saharan Africa. Nature, 1998; 394: 767–769 doi: 10.1038/29507
11. Marlon JR, Bartlein PJ, Carcaillet C, Gavin DG, Harrison SP, Higuera PE, et al. Climate and human influences on global biomass burning over the past two millennia. Nat Geosci, 2008; 1, 697–702 doi: 10.1038/ngeo313
12. Lamarque J-F, Bond TC, Eyring V, Granier C, Heil A, Klimont Z, et al. Historical (1850–2000) gridded anthropogenic and biomass burning emissions of reactive gases and aerosols: methodology and application. Atmos Chem Phys, 2010; 10, 7017–7039, doi: 10.5194/acp-10-7017-2010
13. Le Page Y, Pereira JMC, Trigo R, da Camara C, Oom D, Mota B. Global fire activity patterns (1996–2006) and climatic influence: an analysis using the World Fire Atlas. Atmos Chem Phys, 2008; 8, 1911–1924.
14. Quaas JO, Boucher O, Jones A, Weedon GP, Kieser J, Joos H. Exploiting the weekly cycle as observed over Europe to analyse aerosol indirect effects in two climate models. Atmos Chem Phys, 2009; 9, 8493–8501.
15. Xia X, Eck TF, Holben BN, Goloub P, Chen H. Analysis of the weekly cycle of aerosol optical depth using AERONET and MODIS data. J Geophys Res Atmos, 2008; 113 D14, 27, doi: 10.1029/2007JD009604
16. Beirle S, Platt U, Wenig M, Wagner T. Weekly cycle of NO2 by GOME measurements: a signature of anthropogenic sources. Atmos Chem Phys, 2003; 3: 2225–2232.
17. Archibald S, Scholes RJ, Roy DP, Roberts G, Boschetti L. Southern African fire regimes as revealed by remote sensing. Int J Wildland Fire, 19: 861–878.
18. Goitein SD (1959) The origin and nature of the Muslim Friday worship. The Muslim World, 2010; 49 (3), 183–195.
19. Ringwald CD. A Day Apart: How Jews, Christians, and Muslims Find Faith, Freedom and Joy on the Sabbath. New York: Oxford University Press; 2007.
20. Hackett C, Grim B, Stonawski M, Skirbekk V, Potančoková M. The Global Religious Landscape. Pew Research Center's Forum on Religion & Public Life. Washington D.C., 2012.
21. Johnson TM, Grim BJ, eds. World Religion Database. Boston University Institute on Religion, Culture and World Affairs (CURA), Gordon-Conwell Theological Seminary. Brill Publishers, Leiden/Boston, 2012.
22. Ellis EC, Goldewijk KK, Siebert S, Lightman D, Ramankutty N. Anthropogenic transformation of the biomes, 1700 to 2000. Glob Ecol Biogeogr, 2010; 19 (5), 589–606.
23. Ellis EC, Ramankutty N. Putting people in the map: anthropogenic biomes of the world. Front Ecol Environ, 2008; 6: 439–447 doi: 10.1890/070062
24. Friedl MA, Sulla-Menashe D, Tan B, Schneider A, Ramankutty N, Sibley A, et al. MODIS Collection 5 global land cover: Algorithm refinements and characterization of new datasets. Remote Sensing of Environment, 2010; 114 (1): 168–182.
25. Justice C, Giglio L, Korontzi S, Owens J, Morisette JT, Roy D, et al. The MODIS fire products. Remote Sens Environ, 2002; 83 (1–2), 244–262.
26. Oom D, Pereira JMC. Exploratory spatial data analysis of global MODIS active fire data. Int J Appl Earth Obs, 2013; 21, 326–340.
27. Hilbe JM. Negative Binomial Regression, 2nd ed. Cambridge, UK: Cambridge,: University Press, 2011.
28. Banerjee S, Carlin BP, Gelfand AE. Hierarchical Modeling and Analysis for Spatial Data, 2nd. ed. Boca Raton, FL: CRC Press, 2014.
29. Rue H, Martino S, Chopin N. Approximate Bayesian inference for latent Gaussian models using integrated nested Laplace approximations (with discussion). J R Stat Soc B, 2009; 71(2):319–392,.

30. Spiegelhalter DJ, Best NG, Carlin BP, Van Der Linde A. Bayesian measures of model complexity and fit. J R Stat Soc B, 2002; 64, 4: 583–639.
31. Held L. Simultaneous posterior probability statements from Monte Carlo output. J. Comput Graph Statist, 2004; 13, 20–35.
32. Box GEP, Tiao GC. Bayesian Inference in Statistical Analysis, Reading, MA: Addison-Wiley; 1973.
33. Benjamini Y, Hochberg Y. Controling the false discovery rate: a practical and powerful approach to multiple testing. J R Stat Soc Series B Stat Methodol, 1995; 57: 289–300.
34. Giglio L, Csiszar I, Justice CO. Global distribution and seasonality of active fires as observed with the Terra and Aqua Moderate Resolution Imaging Spectroradiometer (MODIS) sensors. J Geophys Res Biogeosci, 2006; 111 (G2) G02016, doi: 10.1029/2005JG000142
35. Laris P. Burning the seasonal mosaic: Preventative burning strategies in the wooded savanna of southern Mali. Hum Ecol, 2002; 30 (2), 155–186.
36. Shafer LJ. Indigenous fire use to manage savanna landscapes in southern Mozambique. Fire Ecol, 2010; 6 (2), 43–59. doi: 10.4996/fireecology.0602043
37. Kaiser JW, Heil A, Andreae MO, Benedetti A, Chubarova N, Jones L, et al. Biomass burning emissions estimated with a global fire assimilation system based on observed fire radiative power. Biogeosciences, 2012; 9, 527–554, doi: 10.5194/bg-9-527-2012
38. Crutzen PJ, Andreae MO. Biomass burning in the tropics: impact on atmospheric chemistry and biogeochemical cycles. Science, 1990; 250 (4988), 1669–1678 doi: 10.1126/science.250.4988.1669 PMID: 17734705
39. Penner JE, Dickinson RE, O'Neill CA. Effects of aerosol from biomass burning on the global radiation budget. Science, 1992; 256 (5062), 1432–1434 doi: 10.1126/science.256.5062.1432 PMID: 17791612
40. Johnston FH, Henderson SB, Chen Y, Randerson JT, Marlier M, DeFries RS, et al. Estimated global mortality attributable to smoke from landscape fires. Environ Health Perspect, 2012; 120 (5), 695–701. doi: 10.1289/ehp.1104422 PMID: 22456494
41. Sanchez-Lorenzo A, Laux P, Franssen H-J, Calbó J, Vogl S, Georgoulias AK, et al. Assessing large-scale weekly cycles in meteorological variables: a review. Atmos Chem Phys, 2012; 12, 5755–5771 doi: 10.5194/acp-12-5755-2012

V. Highlighting biome-specific sensitivity of fire size distributions to time-gap parameter using a new algorithm for fire event individuation

Duarte Oom, Pedro C. Silva, Ioannis Bistinas, and José M. C. Pereira

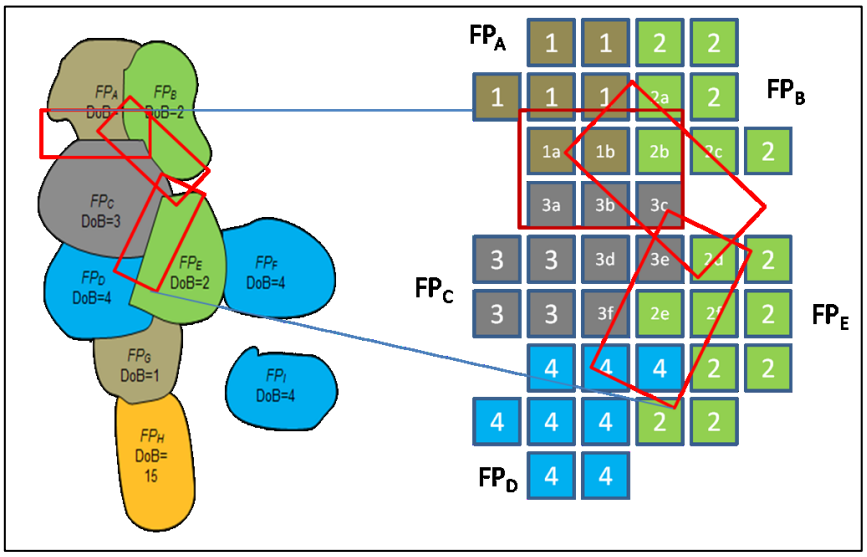

Paper to be submitted to Remote Sensing

remote sensing

MDPI

Article

Highlighting Biome-specific Sensitivity of Fire Size Distributions to Time-gap Parameter Using a new Algorithm for Fire Event Individuation

Duarte Oom [1,*], Pedro C. Silva[1] , Ioannis Bistinas[2] and José M.C. Pereira[1]

[1] Centro de Estudos Florestais, Instituto Superior de Agronomia, Universidade de Lisboa, Tapada da Ajuda, 1349-017 Lisboa, Lisbon, Portugal; pcsilva@isa.utl.pt (PCS); jmocpereira@gmail.com (JMCP)

[2] Department of Meteorology, University of Reading, RG6 66BX, Reading,UK; i.bistinas@gmail.com (IB)

* Correspondence: duarte.oom@gmail.com; Tel.: +351-2136-53484

Academic Editor: date

Received: date; Accepted: date; Published: date

Abstract: Detailed spatial-temporal characterization of individual fire dynamics using remote sensing data is important to understand fire-environment relationships, to support landscape-scale fire risk management, and to obtain improved statistics on fire size distributions over broad areas. Individuation of events to quantify fire size distributions has been performed with the flood-fill algorithm. A key parameter of such algorithms is the time-gap used to cluster spatially adjacent fire-affected pixels and declare them as belonging to the same event. Choice of a time-gap to define a fire event entails several assumptions affecting the degree of clustering/fragmentation of the individual events. We evaluate the impact of different time-gaps on the number, size and spatial distribution of active fire clusters, using a new algorithm.. The information produced by this algorithm includes number, size, and ignition date of potential-fire events (*PFE*). The algorithm was tested at global scale using active fire observations from the Moderate Resolution Imaging Spectroradiometer (MODIS). *PFE* size distributions were characterized with the Gini coefficient, and the impact of changing time-gap values was analyzed on a 0.5° cell grid. As expected, number of *PFE* decreased and mean size increased with the time-gap value. The largest sensitivity of fire size distributions to time-gap was observed in African tropical savannas and, to a lesser extent, in South America, Southeast Asia, and eastern Siberia. Sensitivity of fire individuation, and thus Gini coefficient values, to time-gap demonstrate the difficulty of individuating fire events in tropical savannas, where coalescence of flame fronts with distinct ignition locations and dates is very common, and fire size distributions strongly depend on algorithm parameterization.

Keywords: fire event, algorithm, *time-gap*, fire size distribution, active fire, MODIS, Gini coefficient

1. Introduction

Statistical descriptors of fire size distributions (FSD) are often used in the characterization of vegetation fire regimes [1-3]. Information on FSDs is applied in landscape fire management, for planning and evaluating prevention and suppression efforts [4,5], to understand fire impacts on vegetation dynamics [6,7], and to diagnose climate and/or land use changes [8].

Global, daily burned area and active fire data, at spatial resolutions of 500m and 1km respectively, have been available for the last 15 years, from the NASA MODIS Terra and Aqua instruments [9], and an active fire dataset of comparable length was produced by the European Space Agency Along-Track Scanning Radiometers [10]. Availability of such data provides the opportunity to

characterize fire size distributions in a systematic and consistent way at global scale. However, this is not a trivial task because it requires the ability to identify individual fire events, by patching together or splitting apart the snapshots of fire spatial/temporal dynamics afforded by satellite imagery. This is particularly problematic in regions with extensive burning and fast spreading fires, such as tropical savannas, where formation of the "seasonal burning mosaic" [11] entails extensive coalescence of flame fronts with distinct ignition sources. Individuating fire events may be difficult too in regions affected by persistent cloud cover, like boreal forests.

Accurate identification of a "fire event", described as a burning event with a single ignition location and contiguous spread in space and time [12], has been deemed critical to assess fire behavior and environmental impacts [13]. Various authors have sought to resolve the complex process of identifying individual fire events with the intent of accurately quantifying fire size distribution patterns. Pixel aggregation algorithms based on flood-fill techniques were used in past studies in an attempt to identify individual fire events [1,7,14,15]. These algorithms, initially proposed by [16] to detect individual fire events from MODIS burned area patches (MCD45A1), use a roving window to detect a fire-affected pixel, identify its date of burning and, in a recursive way, search for the date of burning of all spatially adjacent fire pixels to check whether they burned within some specified temporal threshold of their neighbors' burning dates. If these two rules are met (spatial adjacency and temporal proximity), pixels are assumed to belong to the same fire event. This process will continue until one of the rules is not fulfilled [16]. In a different approach, [12] reconstructed the spread of large fires in northern Eurasia using MODIS active fire detections. Their algorithm starts with the earliest date of burning (point of ignition) and searches for all active fires occurring before a given temporal threshold and falling within a 2.5 km radius from the seed pixel. Once both criteria are met the pixel is assigned to the new fire event and excluded from further consideration [12]. A fire event is considered complete when no new unassigned fire pixels fall within the temporal and spatial bounds of the fire pixels already assigned to a given event. A critical aspect of both algorithms is the selection of the time-gap used to cluster contiguous burned pixels and declare them as belonging to the same fire event [7]. The choice of a temporal threshold to define a fire event entails several assumptions affecting the degree of clustering/fragmentation of the individualized fire events [1]. Short time-gaps will yield a large number of small fires, while longer time-spans will promote higher spatial aggregation, resulting in a smaller number of larger events. Different time-gaps have been used in previous studies: [16] and [14] tested an 8-day time-gap in southern Africa. At the global scale, [1] used a 2-day time-gap and [7,15] used a 14-day time-gap to produce global fire size distributions. The 14-day time-gap used by [7,15] was justified with the purpose of overcoming the artificial increase in the number of fires that occurred with shorter time-gaps in areas with temporary cloud cover, or due to smoke obscuration of the land surface.

Here, we propose to evaluate the impact of using three different time-gaps of 2, 8 and 14-days, on the number, size and spatial distribution of active fire (hereafter *AF*) clusters. To accomplish this, we developed an alternative algorithm to the flood-algorithm in order to identify individual active fire clusters using MODIS satellite fire data. The algorithm relies on encoding in a graph structure the relevant space-time contiguity relationships among patches of active fires with the same date of burning (hereafter *DoB*), which we call fire patch units (*FP*). A standard graph technique is then used to decompose the set of *FP* into disjoint spatially connected clusters with consistent fire-path histories, which we designated as potential-fire events (*PFE*). The newly developed algorithm is employed to perform a global scale assessment of the sensitivity of the Gini coefficient as a measure of fire size inequality to a range of settings of the time-gap parameter. Results are provided for 6 case studies and in the form of a 0.5° grid map, and assessed using the global Anthromes map of [17] and the global biomes map of [18].

2. Materials and Methods

2.1. Fire data

Active fire data used for this study were taken from the MODerate Resolution Imaging Spectroradiometer (MODIS) MCD14ML Collection 5 daily Active Fire Product [19] for the year of 2003. This dataset reports the location and timing of active fires at native resolution (1 km at nadir) for both MODIS satellites: Terra and, since May 4th 2002, Aqua. MODIS active fire were screened for false alarms and non-vegetation fires according to the procedures described in [20], and aggregated into a final grid of 31066 0.5° spatial resolution cells.

2.2. PFE individuation algorithm

A new four-step algorithm to individuate *PFE* was developed, including the following steps:

i) **Fire patch identification**: The algorithm assumes that adjacent *AF* with the same *DoB* belong to the same *PFE*. We designate as fire patch (*FP*) a spatially connected region formed by *AFs* with the same *DoB* that cannot be enlarged with new *AF*. *FP* are the basic units upon which *PFE* are built. To identify the set of fire patches, we consider a graph whose set of vertices are the set of *AF* such that two *AF* are connected by an edge, if they are adjacent and have the same *DoB*. In this framework each *FP* correspond to a connected component of this graph, i.e., to a maximal set of vertices such that any pair of vertices can be connected to each other by a path within the connected component.

Figure 1 shows a conceptual example, created to facilitate explanation of the algorithm, depicting a collection of fire events. In this example, nine *FP* are depicted, each one with its respective *DoB*. Each *FP*, identified with a unique ID (ranging from FP_A to FP_I), corresponds to a maximal connected region formed by *AF* pixels with the same *DoB*. *FP* with the same *DoB* are depicted in Figure 1a with the same color. An illustration of *FP* as spatially connected groups of pixels (*AF*) of the same color is shown in Figure 1b.

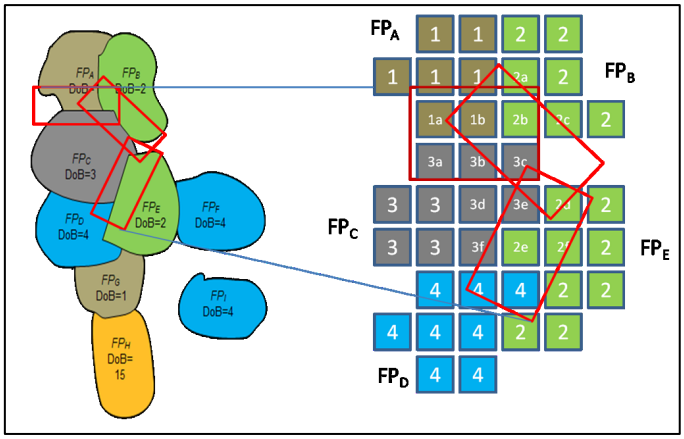

(**a**) (**b**)

Figure 1. (a) Simulated example of a group of nine Fire Patches (*FP*). *FP* depicted by the same colour have the same *DoB*: FP_A and FP_G have *DoB* 1 (light brown); FP_B and FP_E have *DoB* 2 (green); FP_C has *DoB* 3 (grey); FP_D, FP_F and FP_I have *DoB* 4 (blue) and FP_H has *DoB* 15 (orange); **(b)** red rectangles highlight the simulated *AF* located at the border between FP_C and FP_A, FP_B and FP_E. The number in each box correspond to the *DoB* of each *FP*. *AF* located at the border were additionally identified by a letter.

ii) ***FP* contiguity relationships encoding**: the relevant spatial-temporal contiguity relationships among *FP* are encoded in a weighted directed graph structure as follows: the vertices of the directed graph (digraph) is the set of *FP* such that two *FP* are connected by a weighted directed edge, starting at the *FP* with the earlier *DoB*, if the following two conditions hold: 1) the *FP* are spatially adjacent and 2) the date difference between the corresponding *DoB* lies within the time-gap considered. The edge weight between the two *FP* is defined as the contact number between the *FP*, i.e., as the number of pairs of adjacent pixels, with one pixel in each one of the *FP*. A *FP* for which no other adjacent *FP* exists with an earlier *DoB* such that the *DoB* difference lie within the time-gap considered, is designated a point of ignition (hereafter *PoI*). Thus, a *PoI* correspond in the digraph to a source vertex, i.e., to a vertex at which no directed edge terminates.

Figure 2 depicts the digraph encoding the spatial-temporal contiguity relationships among the *FP* of example in Figure 1, assuming a time-gap of 2 days. The digraph contains 4 *FP* corresponding to *PoI* (marked using oversized letter IDs).

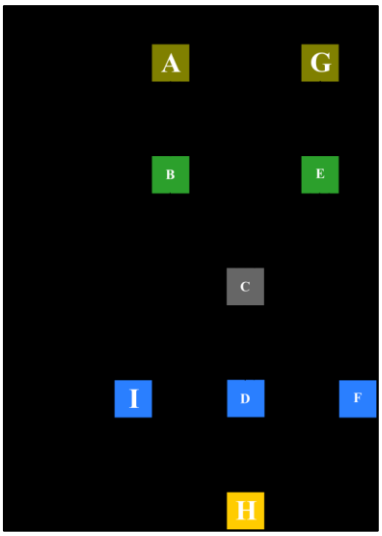

Figure 2. (a) Weighted digraph structure encoding the space-time contiguity relationships (edges) connecting the nine Fire Patches (*FP*) (vertices) referred in Figure 1 for a 2-day time-gap. For each Fire patch (*FP)* the corresponding date of burning (*DoB*) is also shown. The digraph contains the 4 *PoI* (displayed with oversized letter IDs): FP_A, FP_G, FP_I and FP_H. Edge weighs (contact numbers) for the connections FP_A - FP_C, FP_B - FP_C and FP_E - FP_C, are also displayed.

The edge weights five, three, and six depicted on the directed edges connecting FP_A to FP_C, FP_B to FP_C and FP_E to FP_C, respectively, correspond to contact numbers between these pairs of *FP* (Table 1).

Table 1. Contact number between Fire Patches (*FP*) FP_C and FP_A, FP_B and FP_E. Each X symbol represents the existence of a pair of spatially adjacent *AFs*, lying in distinct *FP*. Numbers with lower caps labels refer to the *AF* depicted in Figure 1.

		FP_C					
		3a	3b	3c	3d	3e	3f
FP_A	1a	X	X				
	1b	X	X	X			
		3a	3b	3c	3d	3e	3f
FP_B	2b		X	X			
	2c			X			
		3a	3b	3c	3d	3e	3f
FP_E	2d			X		X	
	2e				X	X	X
	2f						X

iii) ***Causal relations configuration***: to each *FP* that is not a *PoI* we assign a unique spatially adjacent *FP* with an earlier *DoB*, such that the *DoB* difference lies within the time-gap considered. This assignment identifies the adjacent *FP* from which the fire has propagated. Causal relations are randomly chosen in such a way that pairwise *FP* connecting large fire perimeter segments are more likely to be aggregated. More precisely, the probability that a causal relation between two *FP* is chosen is proportional to the weight of the directed edge connecting the *FP*, i.e., proportional to the contact number between *FP*. In Figure 2, FP_C can be connected by a causal relation to FP_A, FP_B or FP_E, with probability of success 5/14, 3/14 and 3/7 respectively. We call the set of all causal relations the causal relations configuration, which we represent in the digraph by dashed arrows (Figure 3a). The causal relations configuration determines the fire-path histories in the following sense: each *FP* that is not a *PoI* can be traced back to a unique *PoI* by a sequence of causal relations with monotonically decreasing *DoB*, such that date differences between consecutive *FP* lie within the time-gap. For instance, according to the causal relation configuration depicted in Figure 3a, the FP_D can be traced back to its *PoI*, FP_G by the sequence of causal relations *FP*: FP_D -->FP_C -->FP_E --> FP_G. Using the causal relations configuration we modify the original digraph encoding the spatial-temporal contiguity relationships by adding the directed edges corresponding to the causal relations and by suppressing the directed edges connecting *FP* with no causal relation between them. The modified digraph derived from the causal relations configuration of Figure 3a is shown in Figure 3b.

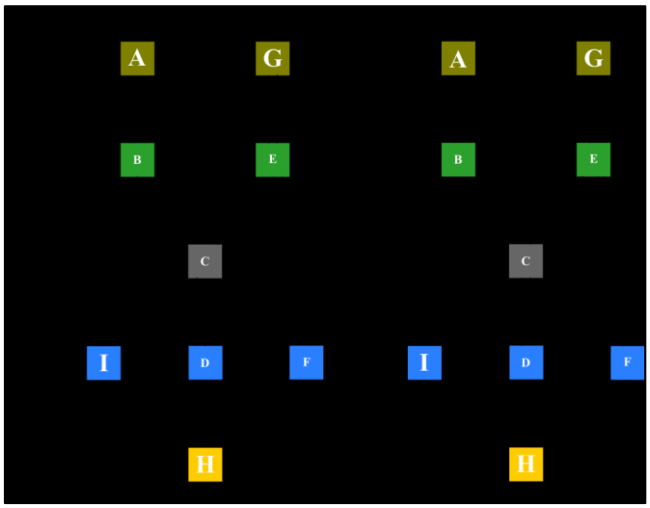

(**a**) (**b**)

Figure 3. Digraph structure encoding the space-time contiguity relationships (edges) connecting the 9 Fire Patches (*FP)* (vertices) referred in Figure 1 for a 2-day time-gap threshold. **(a)** A possible causal relations configuration and **(b)** modified graph containing only the directed edges connecting *FP* when a causal relation (dashed arrows) is present. Causal relations are displayed as dashed arrows. For each *FP* the corresponding date of burning (*DoB*) is also shown.

iv) **Decomposition into *PFE***: the set of *FP* was partitioned into disjoint components consisting of spatially connected unions of *FP*, with a single *PoI* per component, according to the chosen causal relations configuration. Each one of these components is the union of all fire-path histories starting at its (unique) *PoI* and corresponds to a unique *PFE*. By construction, the number of *PFE* is equal to the number of *PoI*, and therefore independent of the causal relations configuration (depending only on the digraph structure encoding the spatial-temporal relationships). Mathematically, the partition into *PFE* can be easily achieved by decomposing the modified digraph encoding the spatial-temporal relationships into strongly connected components, i.e., into maximal sub-graphs for which any pair of vertices in the sub-graph can be connected in both directions by directed paths. This decomposition is unique and can be efficiently obtained using Tarjan's algorithm [21], which has, in the worst case, linear time-complexity with respect to the input dimension (number of vertices plus number of edges). In particular, the decomposition is scalable and thus can be applied to large data sets. Returning to the previous example, the causal relations configuration of Figure 3 led to the decomposition into four *PFE* shown in Figure 4, where each *PFE* is depicted using a different colour, along with the corresponding fire-path histories (black arrows).

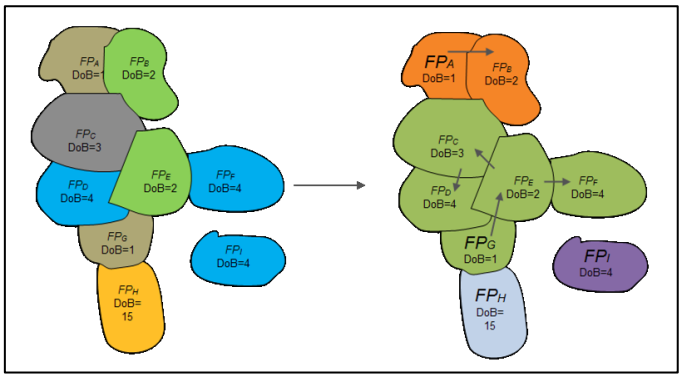

(**a**) (**b**)

Figure 4. (a) Original Fire Patches (*PF*) and **(b)** possible 4 potential-fire events (*PFE*) derived from the algorithm implementation. The black arrows display a possible fire path history based on the algorithm assumptions: spatial adjacency and temporal contiguity. Points of ignition (*PoI*) for this configuration are FP_A (Day of burning (*DoB*): 1); FP_G (*DoB*:1); FP_I (*DoB*: 4) and FP_H (*DoB*:15).

2.3. Sensitivity of fire size distributions to the time-gap parameter

Total number of fire events and fire size distribution were analyzed for each 0.5° cell using MODIS active fire data for 2003 and different time-gaps. The fire size distribution was characterized using the Gini coefficient [22] as a measure of size inequality, assessing the extent to which burned area is dominated by a small number of large events or, conversely, if it results from a larger number of fires with similar sizes. Time-gaps of 2, 8, and 14 days were used to cluster individual active fires into *PFE* and evaluate impacts on size distribution. The spatial distribution of Gini coefficient values was interpreted with the aid of the Anthropogenic Biomes of the World dataset (Anthromes) [17] and the global biomes map of [18]. The Anthrome dataset, which represents global patterns of anthropogenic transformation of terrestrial biomes integrating information on population density, land cover and land use, was resampled to a 0.5° grid cell and reclassified into 6 major classes (Dense Settlements, Villages, Croplands, Rangelands, Forest and Wildland). For a description of the classes see [17] and [18]. To assess the spatial distribution of *PFE* and the Gini coefficient values with the land use/land cover data, six case studies (grid cells) corresponding to six different Anthromes classes were analyzed.

3. Results

3.1. Sensitivity of fire size distributions to the time-gap parameter

A total of 4477192 fire observations were included in the analysis. Three different time-gaps used in the algorithm led to different *PFE* number and size distributions (Table 2).

Table 2. Time-gap sensitivity analysis for 2, 8, and 14-days and the corresponding number of potential-fire events (*PFE*) for 2003. Values for each fire size class and time-gap are in percent (%).

Time-gap (days)	Number of *PFE*	Fire size classes (km)					
		1	1 - 5	5 - 10	10 - 20	20 - 50	> 50
2	2101171	65.86	31.09	2.27	0.60	0.16	0.02
8	1900092	62.15	33.50	3.24	0.86	0.22	0.03
14	1764628	59.48	34.98	4.10	1.13	0.27	0.04

As expected, a time-gap increase led to a decrease in the total number of *PFE* identified and to a smaller proportion of single fire pixel (Table 2). Increasing the time-gap also increased the proportion of *PFE* in the larger fire size classes. Figures 5 and 6 respectively map the differences in the number of *PFE* and Gini coefficient values obtained using 2- and 14-day time-gaps. In Figure 5, 16112 out of 31066 half degree cells (51.86%) show no difference in the number of *PFE*. There are 122744 unchanged *PFE*, with a mean size of 1.7 km². Areas with a stable number of *PFE* occurred mainly in agricultural regions, characterized by small, short duration fires, with similar Gini coefficient values for both time-gaps (Figure 6). The cell with the largest difference in the number of *PFE* was located in north-western India (Punjab, Haryana and Uttar Pradesh districts), where 774 (mean size of 1.5 km²) and 401 (mean 2.5 km²) *PFE* were identified with the 2- and 14-day time-gap parameter values, respectively. This area is responsible for two thirds of grain production in India, and has one of the highest fire densities in the world [20] due to extensive straw burning [23]. Large differences in number of *PFE* as a function of time-gap parameter are also found in both African hemispheres, with a high incidence in the Miombo savanna woodlands [24], characterized by a high fire size inequality [25], and also in Brazil and south-eastern Asia. Figure 6 shows 15881 cells (51%) with positive values, meaning that the use of the 14-day time-gap led to increased fire size

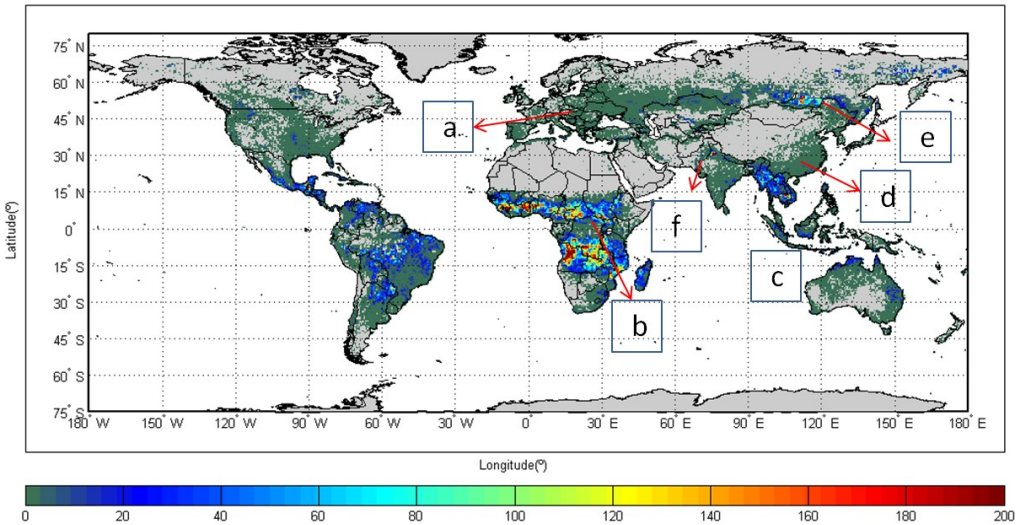

Figure 5. Potential-fire events (*PFE*) number difference for 2-day and 14-day time-gaps for each 0.5° cell in 2003. Cells with no change in the *PFE* number are represented in dark green. Boxes with letters (a-f) are the location of case study cells.(a) Ukraine; (b) Sudan; (c) Cambodia; (d) China; (e) Russia and (f) India.

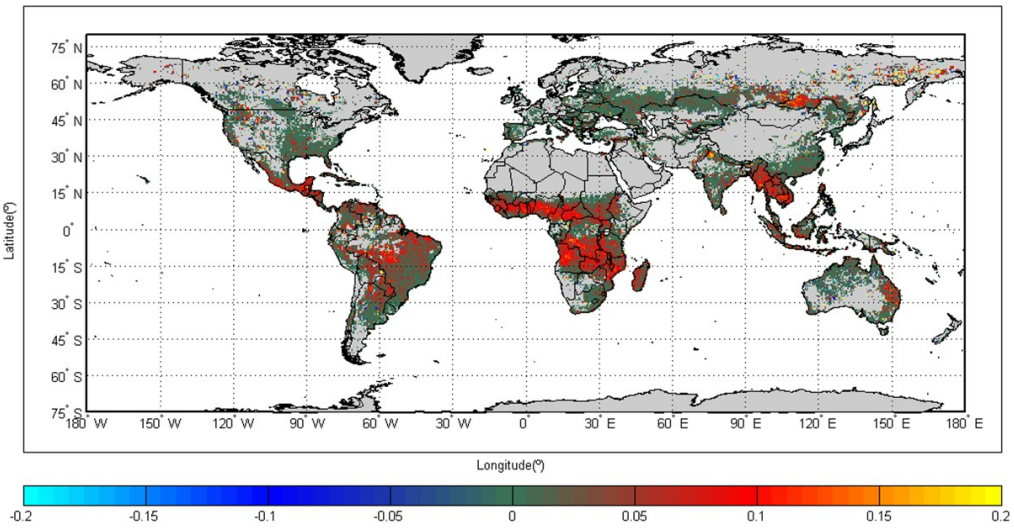

Figure 6. Gini coefficient values difference for 14-day and 2-day time-gaps for each 0.5° cell in 2003. The differences are reported cell by cell. Cells with no change in the potential-fire events (*PFE*) number are represented in dark green.

inequality. The largest positive Gini coefficient difference (0.6752) was observed in a cell located in the eastern Siberian steppe. This cell recorded group of 5 individual *PFE*, with a mean size of 3.12 km² when the 2-day time-gap was used, and only two *PFE* (1km² and 16 km²) with the 14-day time-gap. The corresponding Gini coefficient values were 0.1582 and 0.8333 for the 2 and 14-day time-gaps, respectively. With sparse population and vast, uninterrupted expanses of grasslands, this region tends to have most of its burned area concentrated in a small number of very large events. Gini coefficients positive differences were also found in other semi-arid to arid dry lands of Central Asia, namely along the border between Mongolia and northern Kazakhstan. Woodland savannas in both African hemispheres, southeastern USA, the *Llanos* savannas of Colombia and Venezuela, the "arc of deforestation" in Brazil, the *Chaco* of Paraguay, eastern Australia, and insular south-east Asia also show positive Gini differences. A large patch with a high number of *PFE* is also east of Lake Baikal, in the Amur River basin steppe, a sparsely inhabited area characterized by fire regimes dominated by wildfires in semi-arid to arid grasslands and shrublands. In the summer of 2003, this region recorded a large number of wildfires [26]. Negative values of the difference between using 14-day and 2-day time-gaps, occurred in 9% of all cells (2836), scattered all over the globe. Most of these negative values correspond to rearrangements of fire size inequality towards a more balanced distribution with the 14-day time-gap, which occurs, for instance, with the largest negative Gini value observed in eastern Siberian steppe. In this case two *PFE* exhibit different arrangements according to the time-gap used. With a 2-day time-gap, fire sizes of 1 km² and 15 km² were individuated, resulting in a value of Gini coefficient of 0.8235. With the 14-day time-gap, a new arrangement led to a more balanced fire size distribution with 7 km² and 9 km² and a value to which corresponded a Gini coefficient value of 0.08. Places exhibiting no significant differences between both time-gaps (12349 cells, 40%) are mainly located in areas of intense land use management and high population density, dominated by small fire sizes. They are found over a very broad area spreading along the 5 continents: south-eastern/eastern of Mississippi river (USA), south-eastern Brazil, Peru, the Pampas of Uruguay and northern Argentina, large areas over eastern Europe, Kazakhstan, India, and eastern/south-eastern China.

To interpret the impact on fire size distribution, Gini coefficient was calculated for each time-gap (Figure 7) and its spatial distribution was analyzed with six Anthromes classes derived from [17] (Figure 8) and 13 biomes derived from [18] (Figure 9).

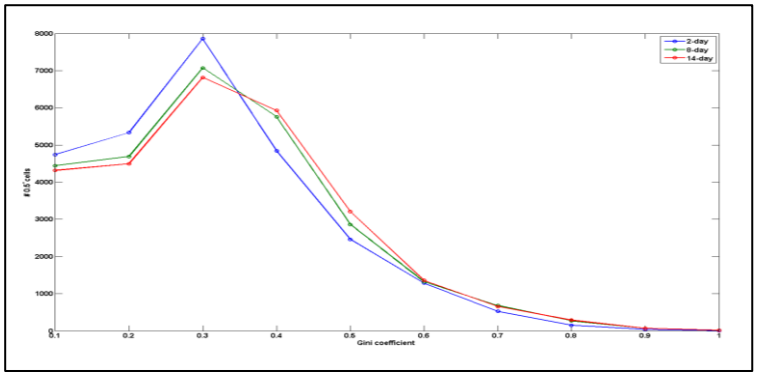

Figure 7. Gini coefficient global frequency distributions for time-gaps 2- ,8- and 14-days.

Although all three distributions peak in frequency at a Gini value of 0.3, the distribution for 2-day time-gap displays higher frequencies for lower Gini values, indicating a more balanced distribution of *PFE* by size class than those obtained with 8- and 14-day time-gaps, which tend to concentrate fire activity into a smaller number of larger events. Differences between the latter two distributions are of smaller magnitude.

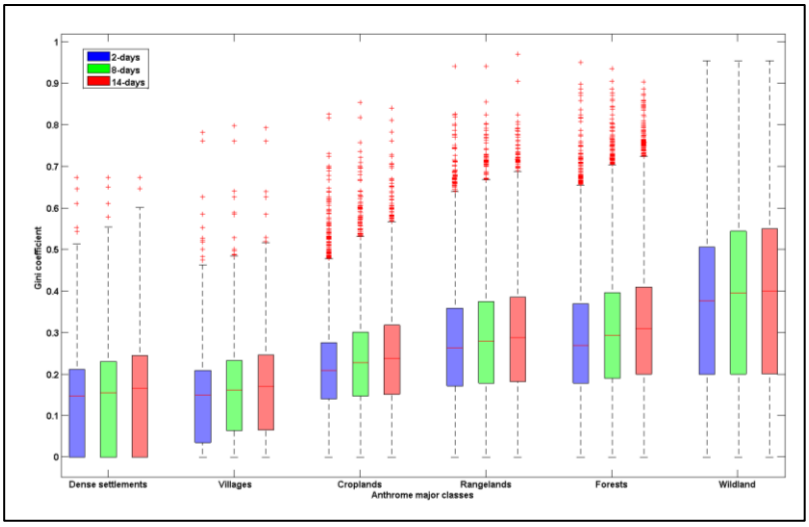

Figure 8. Gini coefficient values for the 6 major Anthrome classes using 2- ,8- and 14-day time-gaps.

Gini coefficient values increase from densely settled and managed landscapes to sparsely populated, unmanaged areas, reflecting the shift from balanced distributions with many small fires, to distributions dominated by a small number of very large fires. No major differences between Anthromes in sensitivity to the time-gap parameter are apparent, although the 75th percentile seem to be slightly more sensitive than the 25th percentile in most Anthromes. For each Anthrome class, one 0.5 °cell was selected (Figure 5) and the total number of *PFE* and Gini coefficient vales were calculated for the 3 different time-gaps (Table 3).

Table 3. Total number of potential-fire events (*PFE*) for each case study using three different time-gaps. Gini coefficients values in parenthesis.

Case study	Country	Anthrome class	Time-gap (days)		
			2	8	14
a)	Ukraine	Cropland	46 (0.21)	44 (0.21)	44 (0.21)
b)	Sudan	Rangeland	470 (0.35)	423 (0.37)	409 (0.39)
c)	Cambodja	Forests	472 (0.25)	397 (0.32)	319 (0.38)
d)	China	Villages	32 (0.15)	31 (0.16)	31 (0.16)
e)	Russia	Wildland	129 (0.7)	56 (0.71)	56 (0.71)
f)	India (Punjab district)	Dense settlements	774 (0.26)	480 (0.42)	401 (0.44)

Table 3 shows that cells classified as Villages (d) and Croplands (a) have the lowest number of *PFE* and the lowest difference between the difference time-gaps. The highest number recorded for the three time-gaps belongs to Punjab district in India (f), with the biggest difference in the number of *PFE* occurring between 2- and 14-day time-gaps. As already mentioned, the 14-day time-gap yields considerably higher pixel aggregation than the 2- or 8-day time-gaps.

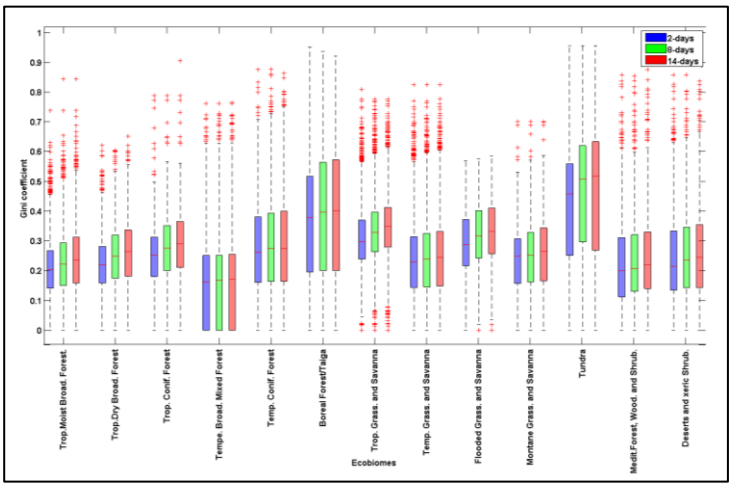

Figure 9. Gini coefficient values for 13 biomes, using 2-, 8-, and 14-day time-gaps.

A biome based analysis [18], picks up a pattern not discernible with the Anthromes data: Gini coefficient sensitivity to time-gap is relatively higher in tropical biomes, such as Tropical Dry Broadleaf Forest, Tropical Grasslands and Savannas, and Flooded Grasslands and Savannas (most of which are located in the tropics) than in temperate of boreal biomes, with the lowest sensitivities occurring in Temperate Broadleaf Mixed Forests and in Temperate Conifer Forests.

3.2. Performance of the PFE individuation algorithm

As an example of algorithm performance, Figures 10 show in detail the consequences of using different time-gaps (2- and 14-day) in a case study located in Sudan (Figure 10a, b), exploring the behaviour in this type of fire regime. Figure 10b, based on a 14-day time-gap, exhibits a clearly more aggregated pattern with fewer *PFE* than the 2-day time-gap case of Figure 10a. For this cell, the number of *PFE* was respectively 470 and 409 for 2- and 14-day time-gaps (Table 2).

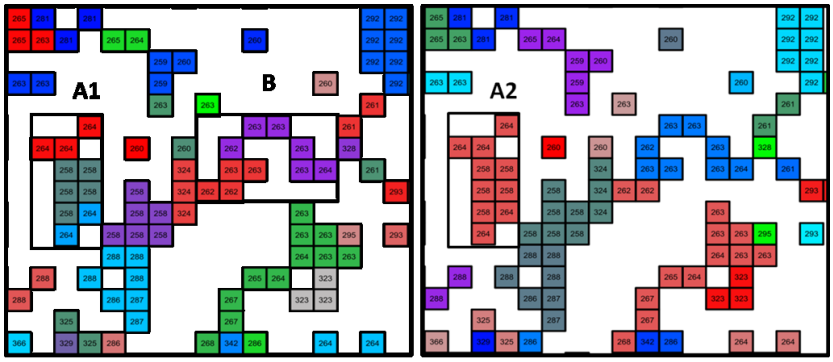

(**a**) (**b**)

Figure 10. Region of a Sudan 0.5° cell (8ºN, 27ºE), using **(a)** 2-day and **(b)** 14-day time-gaps. Colored small squares are MODIS 1km² active fire pixels for 2003. Each color is allocated to one pseudo-fire event (*PFE*). Number in boxes correspond to the date of burning (*DoB*,1-365) for 2003. Box A1, A2 and B are described in the text and detailed in Figures 11 and 12.

We analyzed in detail the decomposition into *PFE* for boxes A1 and A2 in the Sudan region (Figure 11a and 11b respectively), to investigate if differences in the number of *PFE* emerge between the two time-gaps (A1:2-day; A2:14-day). Figure 11 depicts several *AF* pixels aggregated into three *FP*. The common *DoB* differences among these three *FP* (six days) is above and below the 2-(Figure 11a) and 14-day time-gap (Figure 11b), respectively. As a consequence, in the former case no temporal contiguity relationships exist, yielding three different *PFE*. In the latter case, with the time-gap considered FP_B and FP_D are linked to FP_A by causal relations (dashed arrows) and only one *PFE* is obtained. No other causal relations configuration exist in this case.

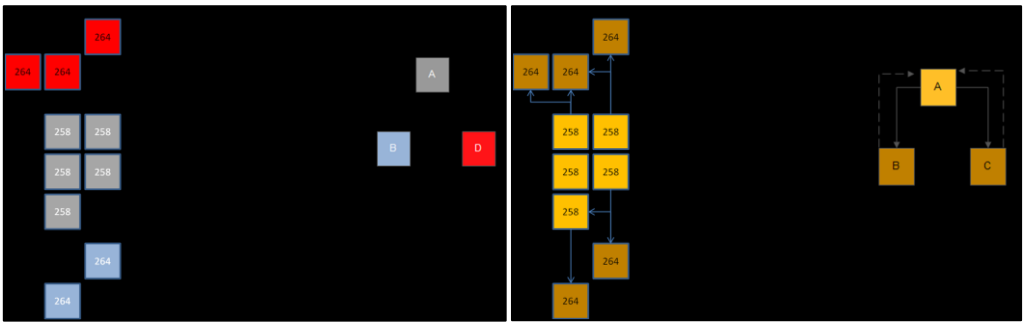

(**a**) (**b**)

Figure 11. (a) Detail of A1 with 2-day time-gap and **(b)** A2 with 14-day time-gap boxes mentioned in Figure 10. On the left side of the figures, each square represents a MODIS active fire (*AF*) with the number inside related to the date of burning (*DoB*). These *AF* are aggregated into Fire Patches (FP_A, FP_B and FP_C) and their spatial-temporal contiguity relationships are encoded in the corresponding digraph structure shown on right side of the figures.

Box B of Figure 12 displays two distinct decompositions into *PFE* using a 2-day time-gap, induced by different choices of the causal relations configurations (although the number of *PFE* remains the same in both cases). In Figure 12a the algorithm chose the causal relation from *FPB* to *FPA*, leading to the decomposition into two *PFE*: union of FP_A and FP_B (*PFE* starting in *DoB* 262 and ending in *DoB* 263) and union of FP_C, FP_D and FP_E (*PFE* starting at *DoB* 262 and ending in *DoB* 264). In Figure 12b the algorithm opted for the causal relation from FP_B to FP_C leading to different decomposition into the two *PFE*, the isolated FP_A (*PFE* with the unique *DoB*-262) and the union of FP_B, FP_C, FP_D and FP_E (*PFE* starting at *DoB* 262 and spreading in two directions, one ending at *DoB* 263 and the other at *DoB* 264). Note that since the blue *PFE* have ignition date 262, the other *FP* with *DoB* 262 could not be included because that would cause non-adjacent ignition points to occur in the same *PFE*, contradicting a model assumption.

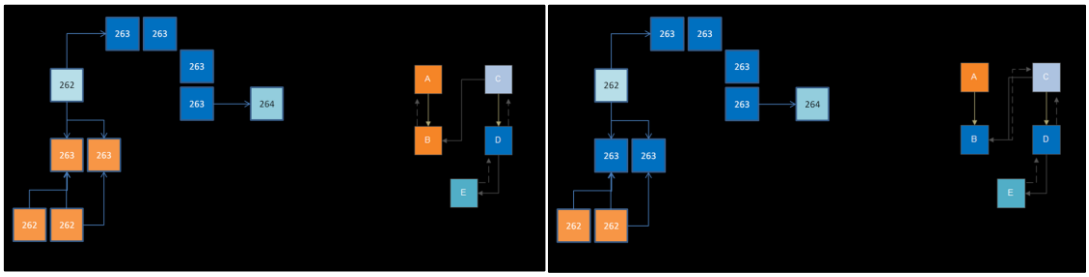

(**a**) (**b**)

Figure 12. Detail of the box B depicted from Figure 10a with two distinct decomposition into two new potential-fire events (*PFE*) using 2-day time-gap showing the corresponding digraph structure:**(a)** choosing the causal relationship between Fire patches (*FP*) FP_B to FP_A and **(b)** choosing the causal relationship FP_B to FP_C. Colored small squares are MODIS 1km² active fire pixels for 2003. Each similar color is allocated to one *PFE* (orange and blue). Number in boxes correspond to the date of burning (*DoB*,1-365).

Thus, in spite of the fact that adjacent *FP* lie within the time-gap considered, the set of *FP* is broken up into *PFE* to preserve consistent fire histories, which helps keeping the number of *PFE* and their sizes limited, even when larger time-gap thresholds are considered.

4. Discussion

Selection of a single value of the time-gap parameter for global studies [1,7,14], not accounting for fire regimes specificities, such as the formation of a "seasonal mosaic" of fire-affected areas [11,27], and the occurrence of consecutive days of missing land surface observation due to clouds or smoke, may lead to artefactual results in fire individuation and, consequently, in fire size distributions. Short time-gap values may break up fires and artificially increase the number of events in regions affected by persistent cloud cover, like boreal forests, while longer time-spans may promote excessive spatial aggregation, resulting in a smaller number of larger events. In tropical savannas, where a large fraction of the landscape burns every season as a result of many independent ignitions, individuation of fire events and the resulting fire size distributions critically depend on the time-gap parameter value. Detailed analysis of individual grid cells showed that the relatively high Gini coefficient sensitivity to the time-gap parameter observed in many tropical regions is due to very high ignition densities, which lead to extensive coalescence of neighboring (in space and time) fire events. Evidently, higher time gap parameter values will increase the extent of coalescence, reducing the number and increasing the size of potential-fire events, and yielding higher Gini coefficient values. Our results show that in regions where only a small fraction of the landscape burns in a given season, and thus coalescence of fires with distinct ignitions is minimal, *PFE* size distributions are robust with respect to time-gap parameter values.

The algorithm proposed in this study to individuate fire events, although tested with active fire data, is meant as an alternative to the flood-fill algorithm previously used in most studies with burned area data [1,7,15,16]. Starting from a seed (*AF*), the flood-fill algorithm assigns each unclassified *AF* that can be spatially connected to the seed, building a path of classified *AFs*, such that consecutive *AF* have *DoB* within the time-gap considered. This time-gap restriction *per se* does not ensure consistency of *DoB* required to reconstruct the fire path-histories in each fire event. Our approach has been designed to overcome this limitation, by conveniently translating the individuation problem to a standard graph technique, according to a set of pre-defined causal relations. Contrary to the flood-fill approach, with our algorithm aggregation in the same event of adjacent *AF* with *DoB* differences within the time-gap considered, only occurs if no inconsistent fire-path histories arise. In this way, aggregation of *AF* in the same fire event is often self-limited by the fire dynamics, even when adjacent *FP* with *DoB* within the time-gap considered can be found. This situation is illustrated in Figure 13. In a), the fire event consisting of all *AFs* (in orange) verifies the spatial and temporal restrictions of the flood-fill-algorithm and could be generated by it. With our algorithm, the case shown in Figure 13 a) would not occur, otherwise non-adjacent *AFs* with the same *DoB* would be aggregated in the same fire event, yielding two causal relations assigned to the same *FP*. Thus, the algorithm necessarily decomposes the set of *AF* into two fire events, as shown in Figure 13 b (blue and orange).

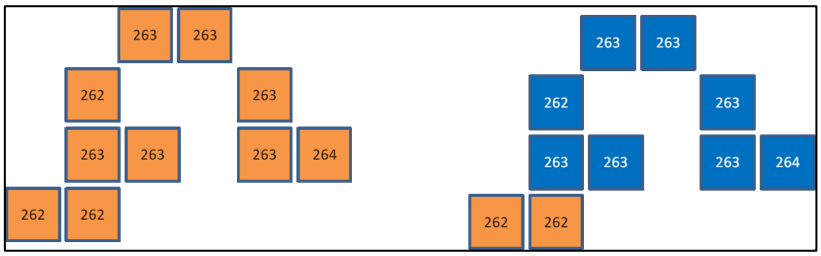

Figure 13. Detail of the example shown in box B depicted from Figure 10a with **(a)** flood-fill algorithm and **(b)** the algorithm proposed in this study to individuate potential-fire events (*PFE*) using 2-day time-gap. Colored small squares are MODIS 1km² active fire pixels. Each similar color is allocated to one *PFE* (orange and blue). Numbers in boxes are the date of burning (*DoB*,1-365).

We believe that the assumptions incorporated in the algorithm for individuating fire events are reasonable representations of the real process of the spatial dynamics of fire ignition and spread, as observed with thermal infrared satellite remote sensing with daily temporal resolution and 1 km spatial resolution. We chose values for the time-gap parameter matching those used in previous studies, to ensure comparability of results. Further algorithm improvements may be achievable by fine tuning the rules defining the causal relations to allow for coalescence of fire events (multiple ignition points in the same fire event), or to account for *DoB* differences. It is however beyond the scope of this work to perform a thorough comparison of algorithm output values against independent observations. That would be a difficult task, anyway, because data on the location of flame fronts at various moments throughout the duration of fire events are not widely available from ground-based measurements. At this stage, evaluation of model outputs can only be performed qualitatively and at a very aggregate level, by expert evaluation of size distributions of potential-fire events generated by the algorithm. Detailed illustrations of algorithm performance are meant to expose its internal logic and the consequences of its underlying assumptions, not to establish its external validity.

5. Conclusions

Given the different types of fire regimes that occur across different biomes, and the limitations of current Earth observation satellites in terms of spatial and temporal resolution, results of algorithms purporting to individuate fire events must be considered with great care, acknowledging the extent to which they may be produce artefactual results. We performed a global study, using a novel algorithm, to assess the effect of different time-gap parameter values for individuating fire events, as well as to evaluate their impact on the size distribution and spatial patterns of active fire clusters. Fire size distributions show little sensitivity to the time-gap parameter in cropland areas, where individual fire events tend to be small and annual percent burned area is not very large. African savannas are particularly sensitive to the time-gap parameter due to the large number of fires and, extensive area burned, which yield a complex spatio-temporal fire mosaic and abundant coalescence of fire fronts with distinct origins. In boreal regions, due to persistent cloud cover, which may prevent observation of the land surface for a few consecutive days, setting a short time-gap may split large, long duration fire events. The next step in algorithm development ought to be the elimination of a fixed, global time-gap parameter, and replacing it with an active fire aggregation stopping rule representing a compromise between fire event size and *DoB* homogeneity, operating at the level of the individual fire event. Such an improvement will automate contextualization of the time-gap parameter choice, and will allow the validation of resulting fire size distributions against actual fire atlas data.

Acknowledgments: This study was funded by a Ph.D. grant to Duarte Oom (SFRH/BD/47452/2008) from the Foundation for Science and Technology, Ministry for Science and Technology, Portugal.

Author Contributions: D.O., J.M.C.P, I.B and P.S. conceived and designed the study; P.S, D.O developed the code algorithm; D.O., P.S. and J.M.C.P. analyzed the data; D.O., P.S., and J.M.C.P wrote the paper. All the authors reviewed the manuscript.

Conflicts of Interest: The authors declare no conflict of interest

Abbreviations

The following abbreviations are used in this manuscript:

PFE: Pseudo-fire event
MODIS: Moderate Resolution Imaging Spectroradiometer
FSD: Fire size distributions
AF: Active fire
DoB: Date of Burning
FP: Fire Patch Unit
PoI: Point of ignition

References

1. Archibald, S.; Lehmann, C.E.; Gómez-Dans, J.L.; Bradstock, R.A. Defining pyromes and global syndromes of fire regimes. *Proceedings of the National Academy of Sciences* **2013**, *110*, 6442-6447.

2. Kasischke, E.S.; Turetsky, M.R. Recent changes in the fire regime across the north american boreal regional:Spatial and temporal patterns of burning across canada and alaska. *Geophysical Research Letters* **2006**, *33*.

3. van Wagtendonk, J.; Lutz, J. Fire regime attributes of wildland fires in yosemite national park, USA. Fire ecol. 3, 34-52. 2007.

4. Cui, W.; Perera, A.H. What do we know about forest fire size distribution, and why is this knowledge useful for forest management? *International Journal of Wildland Fire* **2008**, *17*, 234-244.

5. Haire, S.L.; McGarigal, K.; Miller, C. Wilderness shapes contemporary fire size distributions across landscapes of the western united states. *Ecosphere* **2013**, *4*, art15.

6. Barclay, H.J.; Li, C.; Hawkes, B.; Benson, L. Effects of fire size and frequency and habitat heterogeneity on forest age distribution. *ecological modelling* **2006**, *197*, 207-220.

7. Hantson, S.; Pueyo, S.; Chuvieco, E. Global fire size distribution is driven by human impact and climate. *Global Ecology and Biogeography* **2014**, *24*, 77-86.

8. Pausas, J.G.; Fernández-Muñoz, S. Fire regime changes in the western mediterranean basin: From fuel-limited to drought-driven fire regime. *Climatic change* **2012**, *110*, 215-226.

9. Justice, C.; Giglio, L.; Korontzi, S.; Owens, J.; Morisette, J.; Roy, D.; Descloitres, J.; Alleaume, S.; Petitcolin, F.; Kaufman, Y. The modis fire products. *Remote Sensing of Environment* **2002**, *83*, 244-262.

10. Arino, O.; Rosaz, J. In *1997 and 1998 world atsr fire atlas using ers-2 atsr-2 data*, Proc. Joint Fire Sci. Conf, 1999; Boise, ID: pp 177-182.

11. Laris, P. Burning the seasonal mosaic: Preventative burning strategies in the wooded savanna of southern mali. *Human Ecology* **2002**, *30*, 155-186.

12. Loboda, T.; Csiszar, I. Reconstruction of fire spread within wildland fire events in northern eurasia from the modis active fire product. *Global and Planetary Change* **2007**, *56*, 258-273.

13. Ichoku, C.; Kaufman, Y.; Giglio, L.; Li, Z.; Fraser, R.; Jin, J.-Z.; Park, W. Comparative analysis of daytime fire detection algorithms using avhrr data for the 1995 fire season in canada: Perspective for modis. *International Journal of Remote Sensing* **2003**, *24*, 1669-1690.

14. Archibald, S.; Scholes, R.; Roy, D.; Roberts, G.; Boschetti, L. Southern african fire regimes as revealed by remote sensing. *International Journal of Wildland Fire* **2010**, *19*, 861-878.

15. Hantson, S.; Lasslop, G.; Kloster, S.; Chuvieco, E. Anthropogenic effects on global mean fire size. *International Journal of Wildland Fire* **2015**, *24*, 589-596.

16. Archibald, S.; Roy, D. In *Identifying individual fires from satellite-derived burned area data*, Geoscience and Remote Sensing Symposium, 2009 IEEE International, IGARSS 2009, 2009; IEEE: pp III-160-III-163.

17. Ellis, E.C.; Klein Goldewijk, K.; Siebert, S.; Lightman, D.; Ramankutty, N. Anthropogenic transformation of the biomes, 1700 to 2000. *Global Ecology and Biogeography* **2010**, *19*, 589-606.

18. Olson, D.M.; Dinerstein, E.; Wikramanayake, E.D.; Burgess, N.D.; Powell, G.V.; Underwood, E.C.; D'amico, J.A.; Itoua, I.; Strand, H.E.; Morrison, J.C. Terrestrial ecoregions of the world: A new map of life on earth a new global map of terrestrial ecoregions provides an innovative tool for conserving biodiversity. *BioScience* **2001**, *51*, 933-938.

19. Giglio, L.; Descloitres, J.; Justice, C.O.; Kaufman, Y.J. An enhanced contextual fire detection algorithm for modis. *Remote Sensing of Environment* **2003**, *87*, 273-282.

20. Oom, D.; Pereira, J. Exploratory spatial data analysis of global modis active fire data. *International Journal of Applied Earth Observation and Geoinformation* **2013**, *21*, 326-340.

21. Tarjan, R. Depth-first search and linear graph algorithms. *SIAM journal on computing* **1972**, *1*, 146-160.

22. Gini, C. Variability and mutability, contribution to the study of statistical distribution and relaitons. *Studi Economico-Giuricici della R* **1912**.

23. Sharma, A.R.; Kharol, S.K.; Badarinath, K.; Singh, D. In *Impact of agriculture crop residue burning on atmospheric aerosol loading- a study over punjab state, india*, Annales geophysicae: atmospheres, hydrospheres and space sciences, 2010; p 367.

24. Tarimo, B.; Dick, Ã.y.B.; Gobakken, T.; Totland, Ã.r. Spatial distribution of temporal dynamics in anthropogenic fires in miombo savanna woodlands of tanzania. *Carbon balance and management* **2015**, *10*, 1-15.

25. Archibald, S.; Staver, A.C.; Levin, S.A. Evolution of human-driven fire regimes in africa. *Proceedings of the National Academy of Sciences* **2012**, *109*, 847-852.

26. Lee, K.H.; Kim, J.E.; Kim, Y.J.; Kim, J.; von Hoyningen-Huene, W. Impact of the smoke aerosol from russian forest fires on the atmospheric environment over korea during may 2003. *Atmospheric Environment* **2005**, *39*, 85-99.

27. Laris, P.S. Spatiotemporal problems with detecting and mapping mosaic fire regimes with coarse-resolution satellite data in savanna environments. *Remote Sensing of Environment* **2005**, *99*, 412-424.

28. Hawbaker, T.J.; Radeloff, V.C.; Syphard, A.D.; Zhu, Z.; Stewart, S.I. Detection rates of the modis active fire product in the united states. *Remote Sensing of Environment* **2008**, *112*, 2656-2664.

© 2016 by the authors; licensee MDPI, Basel, Switzerland. This article is an open access article distributed under the terms and conditions of the Creative Commons by Attribution (CC-BY)

VI. Global mapping of sensu strictu pyrogeographic regimes using MODIS active fire data

Duarte Oom, Pedro C. Silva, Ioannis Bistinas, Akli Benali and José M. C. Pereira

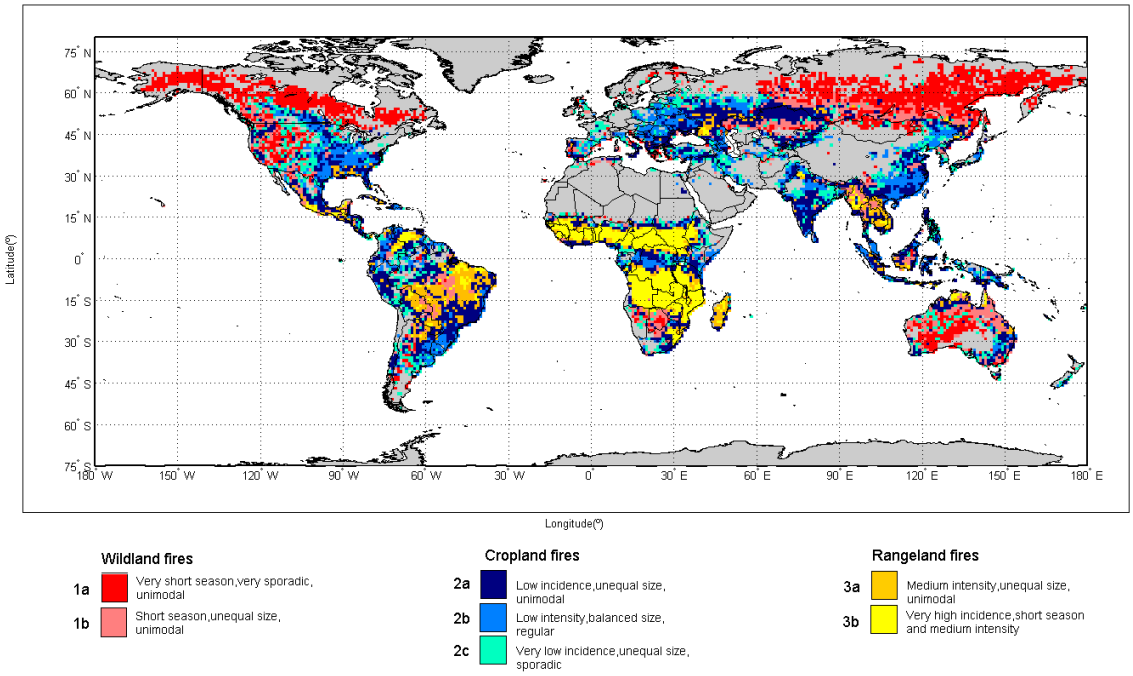

Submitted to *Remote Sensing of Environment*

Global mapping of *sensu strictu* pyrogeographic regimes using MODIS active fire data

Duarte Oom[1] *, Pedro C. Silva[1], Ioannis Bistinas[2], Akli Benali[1], and José M. C. Pereira[1]

[1]*Centro de Estudos Florestais, Instituto Superior de Agronomia, Universidade de Lisboa, Tapada da Ajuda, 1349-017, Lisbon, Portugal,*

[2] *Department of Meteorology, University of Reading, Earley Gate, RG6 6BB, Reading,UK*

***corresponding author**

ABSTRACT

A new global classification map of *sensu strictu* fire regimes was developed using 11 years of MODIS active fire data (MCD14ML) encoded in a set of six fire regime variables (Incidence, Size Inequality, Season Length, Regularity, Seasonality and Intensity), discretized into 22 modalities. Multiple Correspondence Analysis (MCA) and hierarchical clustering were used to identify groups of observations with similar fire regime characteristics. Seven regimes were identified and grouped into three fire macro-regimes: i) *Wildland fires* in boreal forests / semi-arid regions characterized by intense fires with, low fire incidence, unequal fire size distribution, and very short unimodal fire seasons, ii) *Cropland fires* in croplands / grasslands with small, low intensity and regular fires in long fire seasons and iii) *Rangeland fires* in tropical savannas characterized by a high fire incidence, low intensity fires, and regular unimodal fire seasons. Fire Incidence, Regularity, and Season Length contributed the most for the fire regime classification, while Intensity and Seasonality contributed the least. The resulting fire regimes classification map was smoothed with a spatial filter to

optimize the trade-off between cluster separation in the principal coordinates plot and spatial homogeneity. Fire regimes labels were developed using a rigorous procedure based on modality impurity. The new global fire regimes map improves upon previous research by expanding the global land area classified, incorporating new fire regime variables, deriving a two-level fire regime classification, and developing an objective, quantitative procedure for creating fire regime labels with a variable number of fire regimes descriptors. The proposed fire regimes classification is highly interpretable in terms of ecoclimatic and landuse drivers.

Keywords

Global fire regimes, pyrogeography, MODIS active fires, fire descriptors, Multiple Correspondence Analysis, hierarchical clustering

1. INTRODUCTION

Fire is a natural ecological phenomenon, necessary to maintain ecosystem dynamics, productivity, and biodiversity. It is also a ubiquitous land management tool used in croplands, rangelands, and forests throughout the world. On the other hand, wildfires annually affect millions of hectares of forests, woodlands and other vegetation, leading to loss of lives and enormous economic losses in terms of resources destroyed and suppression costs (Bond *et al.*, 2005). Characterizing and mapping fire regimes entails defining a key set of fire descriptors that may be organized in different ways according to user needs (Conedera *et al.*, 2009). The concept of fire regime may refer to different time scales (decades to millennia) and different geographical extents (ecosystem to global). *Sensu strictu* definitions of fire regime concentrate on describing specific characteristics of fires as an ecological factor, including, when, where and which fire types occur (Krebs *et al.*, 2010). Creating a global map of pyrogeographic units defined by patterns of coherent relations between key fire regime descriptors is useful for identifying how climate, topography, vegetation, and land use can influence fire regimes (Morgan *et al.*, 2001).

Goldammer *et al.* (1993) presented one of the earliest attempts at large-scale of fire regimes classification and mapping, having identified seven regimes for tropical and sub-tropical regions. Dwyer *et al.* (2000), based on 12 months of daily global Advanced Very High Resolution Radiometer (AVHRR) active fire data create a five classes global map of major pyrogeographical units using principal component analysis (PCA) and an unsupervised clustering algorithm.. More recently, Chuvieco *et al.* (2008) used six years of daily Moderate Resolution Imaging Spectroradiometer (MODIS) active fire data and cross-tabulation of three discretized ordinal variables to map eight major pyrogeographical classes. Archibald *et al.* (2013) performed principal components analysis and Bayesian clustering to map five global

"pyromes", using burned area data from the Global Fire Emissions Database (GFED) and a set of five fire descriptors. Fire frequency, intensity, fire return interval or fire seasonality were some of the fire regime descriptors used to describe each fire regime in the studies aforementioned, regardless of their relevance.

Here, we revisit the topic using a novel approach, and develop a global map of *sensu strictu* fire regimes using 11 years of MODIS active fire data, almost twice the length of the period previously analyzed by Chuvieco *et al.* (2008). We also expect that reliance on active fire data will improve detection and characterization of anthropogenic fire regimes, in comparison with the analysis of Archibald *et al.* (2013), who used a burned area product, inherently less capable of sensing the small fires that are typical of fire use as a land management tool. We introduce new fire regime descriptors, a previously unused dimensionality reduction technique capable of handling quantitative and qualitative variables, and incorporate spatial context in a cluster analysis to improve interpretability of the fire spatial patterns. Additionally, we propose a formal and rigorous approach to identify the set of key modalities pertinent to characterize and label each fire regime, accounting for their relevance.

2. MATERIAL AND METHODS

Daily MODIS active fire data were used to create a spatial database of variables considered appropriate to develop a *sensu strictu* (Krebs *et al.*, 2010) characterization of global fire regimes. A four stages methodology was applied to the spatial database of variables: i) a variable discretization procedure; ii) a Multiple Correspondence Analysis (MCA) (Greenacre, 1984) to analyse the structure and strength of relations between variables, reducing the dataset dimensionality; iii) a hierarchical ascending classification to identify a

nested structure groups of observations with similar fire regime characteristics; finally a iv) a spatial 3x3 moving window filter applied to the global map of fire regimes to improve its level of spatial homogeneity, accounting for the trade-off between degrading cluster quality in the space of the MCA variables, and improving the spatial coherence and readability of the geographical map. Figure 1 illustrates the data analysis flow.

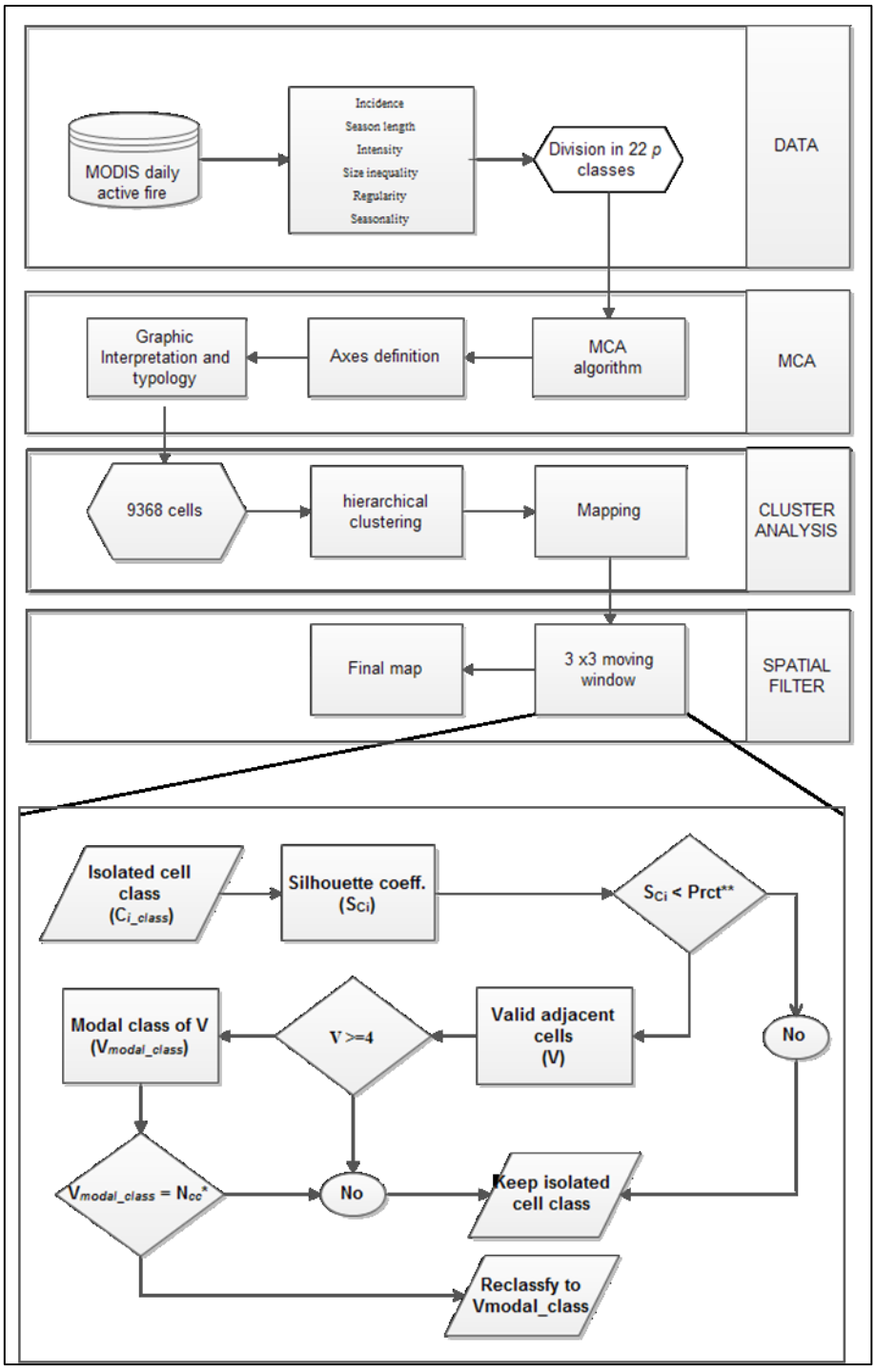

Fig. 1. Flowchart describing the four stages (data encoding procedure, MCA, cluster analysis and spatial filter) of the classification algorithm and spatial filter in detail. Ncc* stands for neighboring cluster class and Prct** for percentile.

2.1. Fire data

We used daily active fire data from the MODIS fire Product (MCD14ML) (Giglio *et al.*, 2006) spanning the period March 1st 2001 to February 28th 2012. This dataset reports the location and timing of active fires at native resolution (1 km at nadir) for both MODIS satellites: Terra and, since May 4th 2002, Aqua. MODIS active fire was screened for false alarms and non-vegetation fires according to the procedures described in Oom & Pereira (2013) and aggregated to 1º spatial resolution. Using satellite active fire data enhance the detection of small fires compared with burned area products (Randerson *et al.*, 2012) providing a better representation of spatial and temporal patterns of fire activity, especially in croplands and rangelands where other fire data could not be so effective.

2.2. Fire regime descriptors

We developed fire regime descriptors to quantify *where* (spatial) and *when* (temporal) fires occur, and *which* characteristics they display using the core definition of fire regime (*sensu strictu*) proposed by Krebs *et al*. (2010). Six fire regime descriptors variables (Incidence, Size Inequality, Season Length, Regularity, Seasonality and Intensity) were developed (respective maps are displayed in Figure 2a-f:

Spatial descriptors

1) **Incidence** (counts grid cell^{-1}), defined as the total number of screened MODIS active fire counts for the entire study period, is a basic metric of fire activity (Dwyer *et al.*, 2000; Csiszar

et al., 2005; Chuvieco *et al.*, 2008; Krawchuk *et al.*, 2009). A cosine square root correction was performed to ensure equal area weighting. Only cells with more than 10 fire counts over the 11 years analyzed were considered (Figure 2a).

2) Size Inequality (*adim*). Was calculated using the Gini coefficient (Gini, 1912). It is a measure of inequality, assessing the extent to which area affected by fire is dominated by a small number of large events or, conversely, it results from a larger number of fires with similar sizes. Individual active fires were clustered into pseudo-fire events using a spatio-temporal flooding algorithm (Archibald & Roy, 2009; Hantson *et al.*, 2014; 2015). The number and size of pseudo-fire events identified depends critically on the temporal threshold used (Hantson *et al.*, 2014). Shorter time spans would yield a larger number of small fires, while a longer time span would result in a smaller number of larger events. Therefore, the Gini coefficient value at each cell should decrease with the temporal threshold. The Gini coefficient takes the minimum value of 0 when all pseudo-fire events have the same size, and the maximum of 1 when all measurements but one have a value of 0. Several authors tested different temporal thresholds to calculate fire size distributions and identify "fire events", namely 2 (Archibald *et al.*, 2013), 4- (Loboda & Csiszar, 2007), 8- (Archibald & Roy, 2009; Archibald *et al.*, 2010) and 14-day thresholds (Hantson *et al.*, 2014; 2015). We performed a sensitivity analysis using thresholds of 2 8 and 14- days and chose a 2-day threshold and a 3x3km neighborhood to cluster individual 1km active fires into fire patches, or *pseudo*-fire events. Lacking an objective criterion to choose a global temporal threshold, we used 2 days as a compromise between the risks of unduly aggregating individual events in areas with many small, neighboring fires, and unduly splitting individual events in regions with very large, long-lasting fires. This coefficient allows the comparison of spatial patterns between different fire regimes. Spatial-temporal aggregation of active fire observations is stopped at

the edges of each 1º cell, such that no pseudo-fire event extends across a cell edge. The final Gini coefficient value assigned to each cell is an average of 11 annual values (Figure 2b).

Temporal descriptors

3) **Season Length** (months), derived from seasonality metrics calculated from 10-day active fires composite time series for each grid cell and year. TIMESAT 2.3 (Jõnsson & Eklundh, 2004) was used to estimate fire season start, peak, and end dates. Initially developed to smooth and extract seasonal parameters from normalized difference vegetation index (NDVI) time series (Jõnsson & Eklundh, 2004), TIMESAT was adapted to process interrupted time series such as those of fire activity, which ceases during the local rainy season (Le Page *et al.,* 2010). To generate smooth time series of the original 10-day active fires composite time series, a local polynomial function was implemented as an adaptive three-step Savitzky-Golay filter. The season start was defined as the date when the cumulative fire counts reach 5% of the total annual counts, and the end date at 95% cumulative fire counts. The peak fire date corresponds the maximum value, in fire counts, of the fitted function. Season length was calculated as the difference between the end and the start of the fire season for each year and cell, and rounded off to months. An average of 11 annual values were calculated for each cell (Figure 2c).

4) **Regularity** (adim), was calculated as the interannual coefficient of variation of fire incidence. The term was based in disturbance and temporal dynamics studies in White *et al,* (1999). Giglio *et al*. (2006) developed a similar measure with 12- month lagged autocorrelation of 5-year of monthly MODIS fire data, to assess interannual variability and periodicity of fire activity at global scale. Low values of the coefficient of variation indicate

regular fire occurrence, and high values represent high interannual variability, or sporadic fire occurrence pattern (Figure 2d).

5) **Seasonality** (adim) distinguishes between one and two fire seasons per year (Benali *et al.,* unpublished results). The active fire data were composited to 16-day time periods. The temporal behavior of the active fire time series were modeled using circular probability distributions (Fischer, 1995). The number of fitted von Mises distributions varied from one to two, corresponding to uni and bimodal distributions, respectively. The model was optimized and evaluated using the Nash-Sutcliffe model efficiency index (MEF) (Nash & Suttclife, 1973), by comparing observed and estimated normalized fire frequencies. Only cells with model efficiency higher than 0.6 were classified as bimodal/unimodal, while the remaining were classified as "Other" (Figure 2e).

Fire characteristics

6) **Intensity** (MW pixel $^{-1}$), was measured as the mean annual value of the Fire Radiative Power (FRP) distribution 90th percentile (Kaufman *et al.*, 1998). It quantifies the rate of energy release by the vegetation combustion process. FRP is a proxy for the aerosol emission rate (Ichoku & Kaufman, 2005) and for fireline intensity (Smith & Wooster, 2005), quantifying fire intensity at the time of observation (Wooster & Zhang, 2004). The FRP distribution is highly skewed towards low values, with a heavy tail of high values. Since very intense fires are not observed in all land cover types (Wooster & Zhang, 2004), a high FRP quantile is effective to discriminate between fire regimes (Figure 2f).

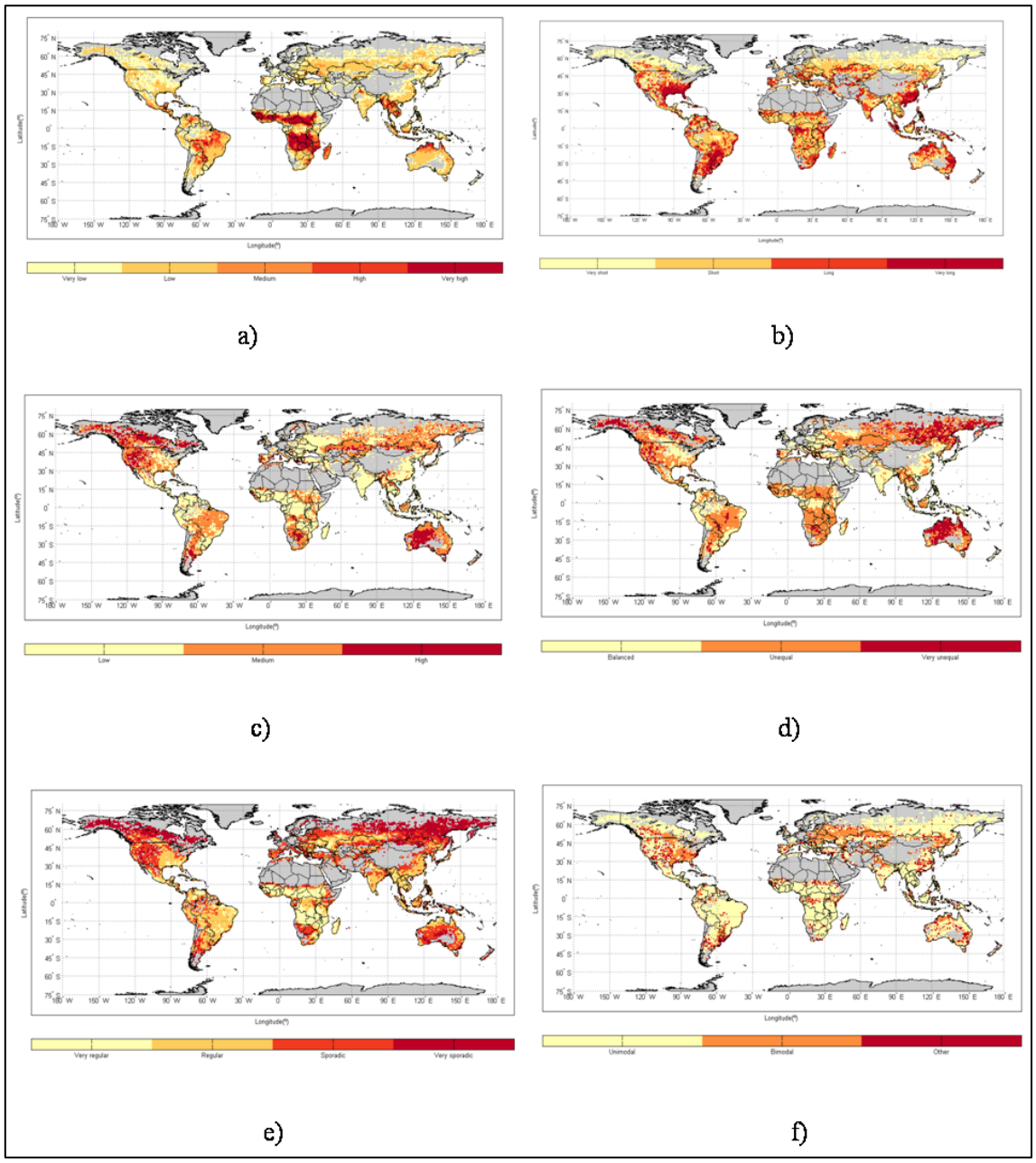

Fig.2. Fire regime descriptors variables maps at 1º spatial resolution (a) Incidence, (b) Season length , (c) Intensity, (d) Size inequality, (e) Regularity and (f) Seasonality.

2.3. Variable encoding procedure

Only 1º cells with information available for all variables were analyzed, totaling 9368 cells. MCA requires nominal or ordinal-level data, and thus the six variables were discretized into classes, or modalities (Table 1). The choice of the number of classes and respective

thresholds for each variable was based on exploratory analysis, literature review and expert knowledge.

Table 1 Modality ordinal/nominal labels, units and discretization thresholds in parenthesis.

		Modalities				
Variable	**Unit**	1	2	3	4	5
Incidence	counts pixel $^{-1}$	Very low (40-500)	Low (501-5000)	Medium (5001-10000)	High (10001-20000)	Very high (> 20000)
Season Length	months	Very short (< 3)	Short (3-6)	Long (6-9)	Very long (> 9)	
Intensity	mW pixel $^{-1}$	Low (13-100)	Medium (100-200)	High (> 200)		
Size Inequality	adim	Balanced (0-0.25)	Unequal (0.25-0.5)	Very unequal (> 0.5)		
Regularity	adim	Very regular (0.2-0.5)	Regular (0.5-1.0)	Sporadic (1.0-2.0)	Very sporadic (> 2.0)	
Seasonality	adim	Unimodal (MEF* > 0.6)	Bimodal (MEF > 0.6)	Other (MEF < 0.6)		

* See 2.2

2.4. Multiple correspondence analysis

Correspondence analysis (CA) is a generalized PCA designed for qualitative data analysis. MCA is an extension of CA for analyzing patterns of relationships of several categorical dependent variables (Benzécri, 1982). Unlike PCA, MCA is capable of dealing with categorical variables and to represent both data and variables as points in the same low-dimensional Euclidean space (Abdi & Valentin, 2007), providing interpretable visual schemes of their relationships. MCA can be applied to analyze observations described by multi-level nominal or ordinal variables, and/or quantitative variables through their division into bins. Each bin of each variable is coded as a binary variable, yielding a Disjunctive Matrix (DM).

Our original data matrix of 9368 (n) individuals by 6 (q) variables was coded to a DM with the same number of individuals as the original data matrix, but with the six variables split into a total of 22 modalities (p), according to the variable discretization scheme displayed in Table 1.

The *eigenvalues* (inertia, λ) and absolute contributions (C^a) were calculated as a measure of variance, and as an indicator of the weight of each variable and each modality to global inertia, respectively. Allocation of variables to axes depends on their nature: for ordinal variables, the sum of C^a of all modalities should be greater than $100/q$; when the variables are nominal the sum of C^a of the modalities should be greater than $100/p$ (Abdi & Valentin, 2007). Adjusted inertia (λ^{adj}) was calculated for all axes with *eigenvalues* greater than $1/q$ (Abdi & Valentin, 2007), following Greenacre (1984). The resulting number of axes is determined by the difference between the number of modalities and the number of variables included in the analysis (Benzécri, 1982).

2.5. Cluster analysis in the space of the MCA variables

A preliminary classification was obtained by applying an ascending hierarchical clustering to the cloud of individuals projected onto the first principal components of MCA, using Ward's variance criterion with the standard Euclidean distance. Ward's method, shares the objective function with PCA, and is regarded as the natural hierarchical clustering method to be applied in conjunction with CA (Cadoret *et al.*, 2011). The optimal number of clusters was estimated from the minimum value of Davies-Boudin index (DB) (Davies & Bouldin, 1979), accounting for the dendrogram produced by the clustering algorithm.

2.6. Smoothing the fire regimes global map - spatial filter

The clustering algorithm tries to minimize the intra-cluster variance accounting only for pairwise dissimilarities between projected points in the principal coordinates plot, disregarding spatial information, such as contiguity relations between cell locations. Therefore, unless data exhibits a high degree of spatial autocorrelation, the resulting geographical map of fire regimes is likely to become quite fragmented. To improve its spatial coherence and interpretability, the map was filtered with a 3x3 moving window to reclassify cells that may be misplaced in their clusters. Only isolated cells, i.e., cells that are only representative of their class in the 3x3 window were considered for reclassification. An isolated cell was reclassified, to the class of its neighboring cluster, i.e., to the class of the cluster with lowest average dissimilarity with respect to the cell (in the space of MCA axes), if three conditions were fulfilled: i) the isolated cell should have at least 4 valid adjacent cells (cells with a specific class), ii) the modal class of the neighboring valid cells should be the same of the neighboring cluster class; and iii) the isolated cell silhouette coefficient (ranging from -1 to 1) should be lower than a specific threshold (Rousseeuw, 1987). High cells silhouette coefficients were considered well classified, whereas low cells silhouette coefficients lied at cluster boundaries and may be misclassified.

We tested the smoothing filter with silhouette coefficient percentiles ranging from the 0^{th} (no reclassification) to the 95^{th} percentiles and opted for the percentile yielding the best trade-off between the two conflicting goals: to maximize cluster separation in the principal coordinates plot and to maximize spatial homogeneity in the fire regimes map. This was accomplished by analyzing the joint behavior of two indexes: i) overall discriminate separability index ($oDSI$) (Cerdeira *et al.*, 2012) and the ii) aggregation index (AI_L) (Hong *et al.*, 2000). The former assesses the separation between clusters and relies on the choice of the interiority measure of a point within a cloud of points, whereas the latter applies to raster data and assesses the degree of aggregation of patches, also known as landscape texture. We

applied $oDSI$ with Tukey's half-space depth (Tukey, 1975), a robust centrality measure that generalizes the quantile concept to multivariate data. The AI_L was computed averaging class specific aggregation indexes AI_i, (which rely on the number of edges that are shared by adjacent cells of class *i*), by the proportions of area occupied by each class in the fire regimes map.

2.7. Fire regime labeling

Each cluster was considered to represent a fire regime and was labeled based upon the modalities projected onto the principal coordinates plot. Only the better classified points in each cluster, corresponding to the fourth quartile silhouette coefficients values were used to label the clusters. For each cluster, all modalities associated to the better classified points were cross-tabulated and an ordinal impurity index (Piccarreta, 2001) was calculated for each variable. Only combinations representing 90% of all points in each cluster were considered. The most represented modality of variables with impurity values below 0.30 were retained to label fire regimes and the less impure were used to designate each fire regime. The combo 90% with the 0.30 impurity threshold turn out to be a good choice yielding fire regimes described by a set of a key characteristics.

3. RESULTS

3.1. Multiple correspondence analysis

The MCA projected the original data onto 16 axes with high variance explained in the first two axes (both representing 93.77 % of total inertia). Table S1 summarizes the MCA statistics for each axis. Regularity, Season Length, and Size Inequality ordinal variables are associated with the 1^{st} axis where the sum of absolute contributions of their modalities (0.3048, 0.2593 and 01866, respectively) is greater than the inverse of the number of variables (i.e. 0.1667; see Table S2). The ordinal variable Intensity has a sum of absolute contributions smaller than 0.1667 but the 1^{st} axis contributes seven times more for the total inertia than the 2^{nd} axis. Incidence and Seasonality are allocated to the 2^{nd} axis. The former contributes with the largest fraction of total inertia of any variable to any of the two axes (35%), while the latter nominal variable Seasonality contributes with the smallest fraction with only 6 and 12% of the total inertia to 1^{st} and 2^{nd} axes, respectively. This is also shown in Figure 3a with the Seasonality as the shortest of all vectors. The principal coordinates plot of the modalities in the first two axes (Figure 3b), illustrates the predominant contribution of Incidence to the 2^{nd} axis and the arch effect associated to the 1^{st} axis that emerges for modalities of the variables Regularity, Season Length, Size Inequality, and Intensity as a consequence of their arrangement along a gradient (Benzécri, 1982) .

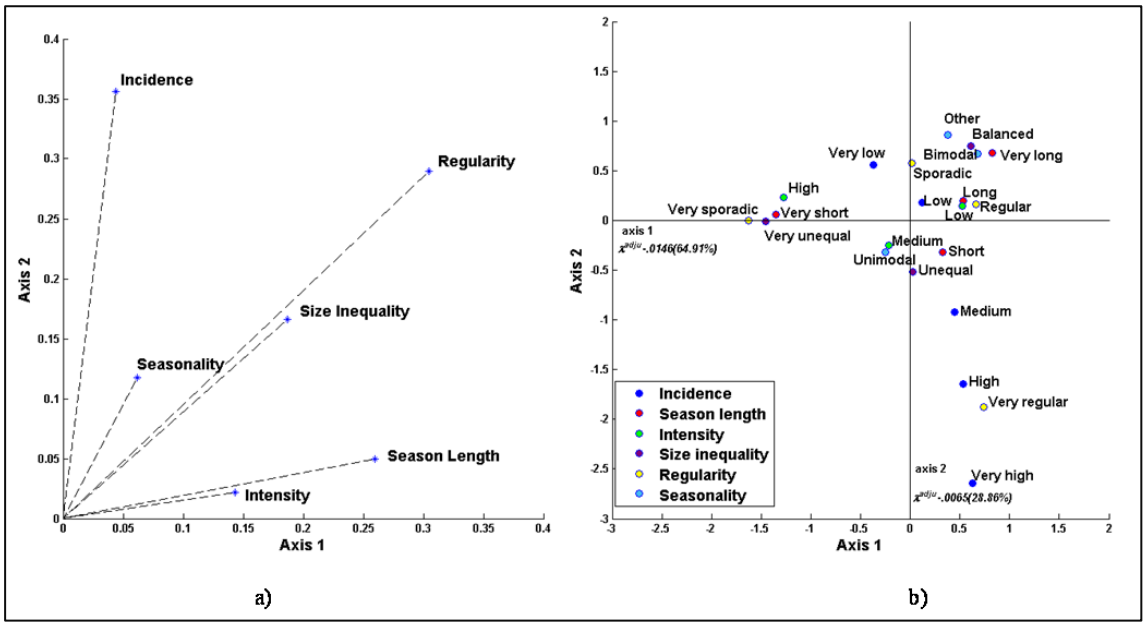

Fig. 3. (a) MCA results in the principal coordinates plot: a)Fire regime variables plotted as a function of their absolute contributions and (b) modality profiles in main two axes (adjusted inertias (λ^{adj}) and percentages of inertia are shown on the respective axes).

Along the 1st axis, Season Length displays its modalities in an opposite way to all other variables associated with the same axis, with low modalities on the negative side and high modalities on the positive side of the axis. *Unimodal* Seasonality lies close to the origin of the principal coordinates axes, while *bimodal* Seasonality displays higher contributions along both axes, i.e. it is more useful to discriminate fire regimes. *Low* fire Incidence, *sporadic* burning, *medium* Intensity, and *unequal* fire Size all plot close to the origin, implying modalities with a small contribution towards fire regime distinction.

3.2. Cluster analysis in the MCA variable space

The clustering algorithm applied to the cloud of 9368 cells projected onto the principal coordinates plot yielded the dendrogram depicted in Figure 4a. The cells correspond to 622 distinct combinations of modalities with a single modality per variable, i.e., to 622 distinct

points in the principal coordinates plot (grey points in Figure 4b). As a consequence, only the final 621 aggregation steps had non-zero merging costs. An optimal number of 7 clusters was estimated and are displayed in Figure 4b by their convex envelope boundaries. The 7 clusters can be organized into three macro-clusters (fire macro-regimes) with high pairwise dissimilarity levels, grouping clusters 1a and 1b (the most dissimilar), clusters 2a, 2b and 2c and clusters 3a and 3b, as shown in the dendrogram of Figure 4a. These macro-clusters are located in separated regions in the principal coordinates plot and nearby to distinct sets of modalities, inducing three macro-fire regimes with very distinctive characteristics.

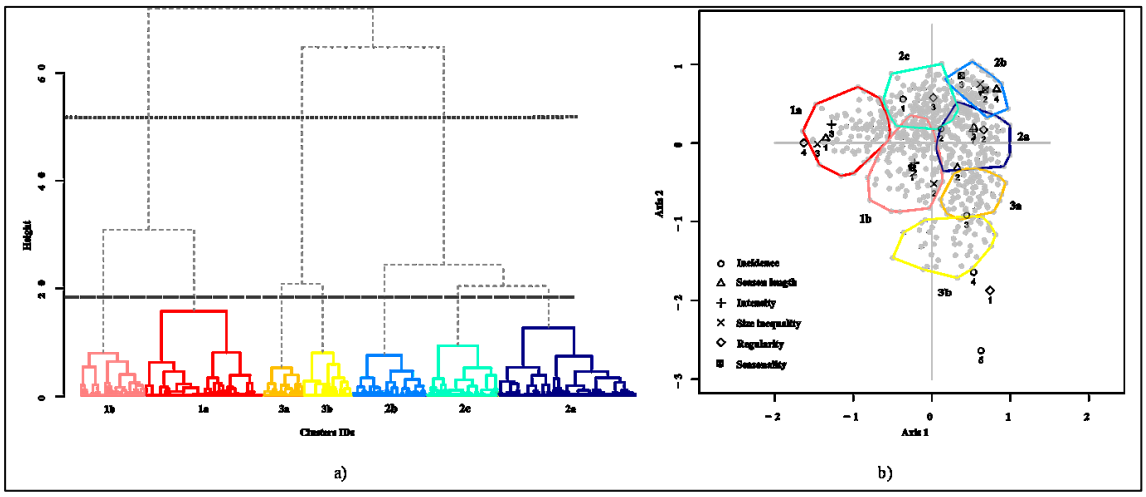

Fig. 4. Preliminary classification in the MCA variables space - a) Dendrogram produced by the hierarchical clustering method applied onto the first principal components of MCA. The vertical axis correspond to merging costs defined by Ward's method. The cutoff represented by the horizontal dashed line yielded the 7 clusters depicted using distinct colors (numbered from 1 to 7). The cutoff represented by the horizontal dotted line, rearranged these clusters into the 3 macro-clusters, containing clusters 1 and 2, clusters 3, 4 and 5 and clusters 6 and 7; b) Principal coordinates plot of the 9368 individuals (grey) and 22 modalities profiles. The convex sets are the convex envelopes of the clusters defined by the partition of the projected points into 7 classes. Smaller numbers close to the modalities refer to the modality numbers shown in Table 1.

3.3. Smoothing the fire regimes global map - spatial filter

The 65^{th} percentile threshold was identified as the best trade-off between the levels of spatial aggregation (AI_L) of the fire regime map and the cluster separability ($oDSI$) in the principal coordinates plot (Figure 5).

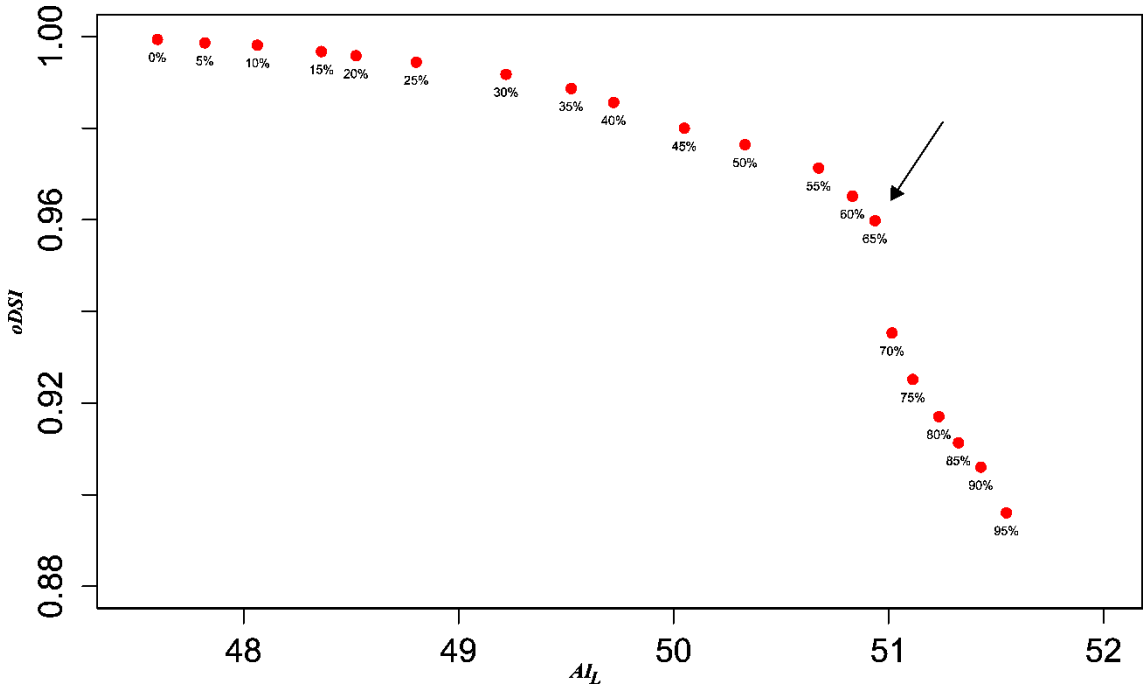

Fig. 5. Overall discriminate separability index (***oDSI***) and aggregation index ($\boldsymbol{AI_L}$) scores in 5% increments.The point indicated by the arrow (65^{th} percentile) was determined by the "elbow criterion" and improved the $\boldsymbol{AI_L}$ score from 47.6. to 50.9. Percentile values above this point do not substantially improve geographical aggregation and cause a large increase in cluster overlap.

For this threshold, AI_L substantially improved while $oDSI$ only marginally degraded. Out of a total of 9368 cells, 254 isolated cells with silhouette coefficients below percentile 65^{th}, and with at least 4 valid neighbors, were reclassified.. Table 2 displays spatial statistics on the global fire regimes map before and after reclassification by the 65^{th} percentile-smoothing filter. Fire regimes 1b and 2c accounts for more than 50% of the reclassified cells, while cluster 3b remains almost unchanged. All class specific aggregation indexes improved after reclassification by the spatial filter.

Table 2 Fire regime specific statistics for the fire regime map before and after (**bold**) reclassification by the 65th percentile smoothing filter: number of patches, number of cells, number of reclassified cells, % of occupied area, and cluster aggregation indexes values $\boldsymbol{AI_i}$. All values rounded to one decimal place.

Fire regime	Patches #	Cells #	Reclassified cells #	Area (%)	AI_i (%)
1a	184/**169**	2001/**2015**	14	15.5/**15.5**	61.9/**63.8**
1b	325/**252**	1107/**1086**	65	11.5/**11.4**	33.7/**39.0**
2a	320/**270**	2321/**2372**	40	26.8/**27.4**	47,9/**51.4**
2b	264/**224**	1239/**1235**	34	13.8/**13.8**	42,2/**45.3**
2c	430/**348**	1212/**1191**	69	13.1/12.8	26,6/**31.3**
3a	163/**135**	658/**640**	28	8.3/**8.1**	39,6/**43.0**
3b	50/**46**	830/**829**	4	11.0/**11.0**	79.5/**80.1**
Total	1736/**1444**	9368/**9368**	254	100/**100**	47.6/**50.9**

3.4. Fire regime labeling and map

The global maps displaying the seven fire regimes organized into three fire macro-regimes are shown in Figure 6. The modalities of the fire descriptors associated to each fire regime and used to its designation are displayed in bold and in grey shaded respectively in Table 3. Only the modalities with impurity values below 0.3 corresponding to 90% of all possible combinations were considered to designate fire regimes. Fire regimes 1a, 2a, 2b and 3b are described by all variables (one modality per variable) while fire regimes 2c is described by only three variables. Additional statistics are shown in Table S3.

Table 3 Fire regime characterization using modalities (bold) with low impurity index value (< 0.3). Modalities chosen to designate fire regimes are grey shaded. Values reported are for the ordinal impurity index for all variables except for the nominal variable Seasonality, which are from the Gini impurity index.

Fire regime	Incidence	Season length	Intensity	Size Inequality	Regularity	Seasonality
1a	**V.low** (0.2222)	**V.short** 0	**Medium/High** (0.2222)	**V.unequal** (0.2222)	**V.sporadic** 0	**Unimodal** 0
1b	**Low** (0.2469)	**Short** (0.16)	Medium 0.32	**Unequal** (0.16)	Sporadic 0.32	**Unimodal** *0*
2a	**Low** 0	**Short** (0.2469)	**Low** (0.2469)	**Unequal** (0.16)	**Regular** 0	**Bimodal** (0.2469)
2b	**V.low** (0.2469)	**Long** (0.2469)	**Low** 0	**Balanced** 0	**Regular** (0.2222)	**Bimodal** (0.2469)
2c	**V.low** (0.1983)	Short/Long 0.6302	Low 0.4587	**Unequal** (0.25)	**Sporadic** (0.2004)	Other 0.3905
3a	High/medium 0.48	Short/Long 0.4	**Medium** (0.24)	**Unequal** 0	**Regular** (0.24)	**Unimodal** 0
3b	**Very High** 0	**Short** 0	**Low/Medium** 0	**Unequal** 0	**V.regular** 0	**Unimodal** 0

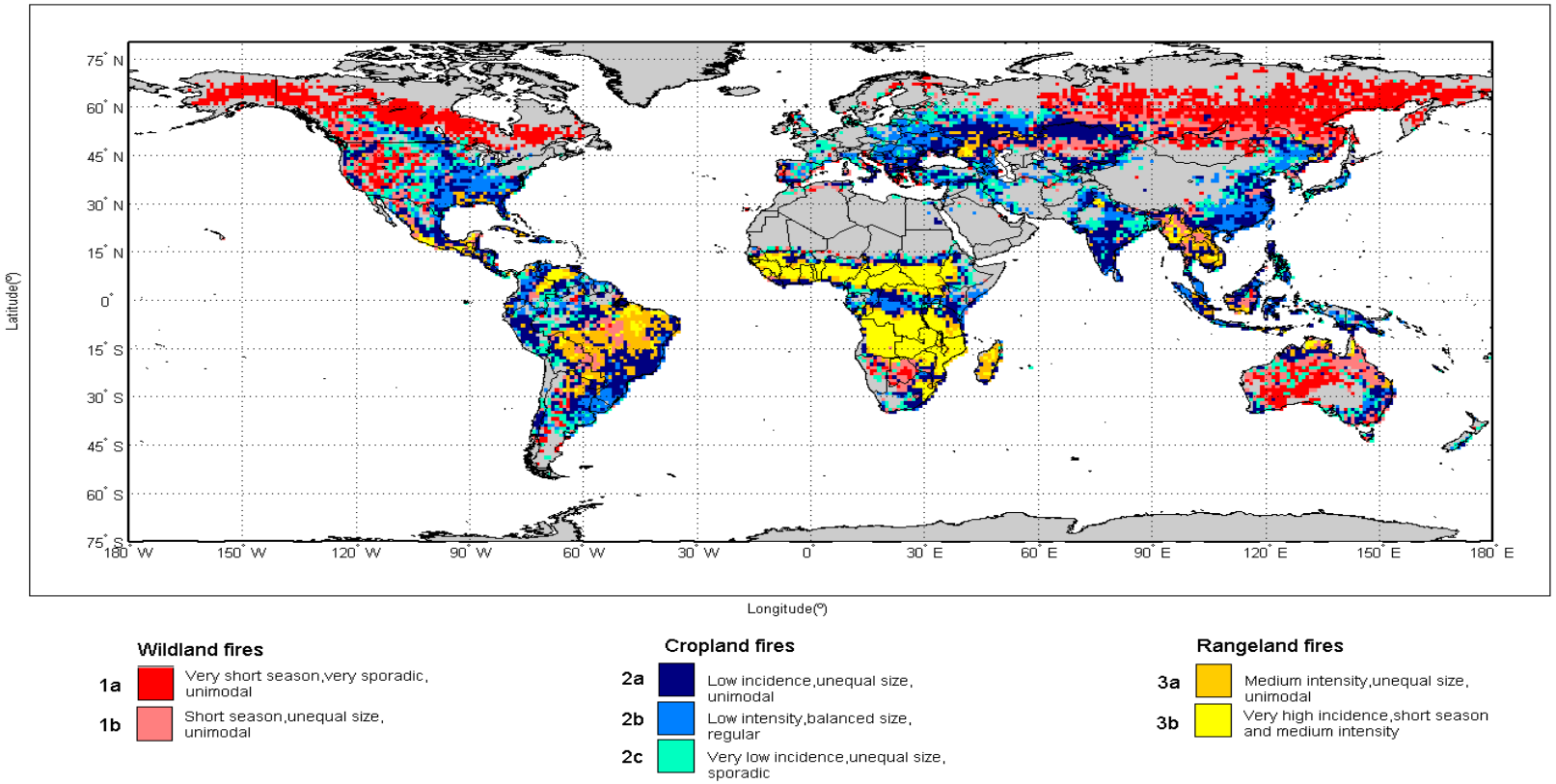

Fig. 6. Global fire regime classification displaying the high level of aggregation in three fire macro-regimes and the designation for the 7 fire regimes. The modalities associated to each fire regime are: *Wildland fires*: 1a) Very low incidence, very short season, medium/high intensity, very unequal size, very sporadic burning, unimodal season; 1b) Low incidence, short season, unequal size, unimodal season; *Cropland fires*: 2a) Low incidence, short season, low intensity, unequal size, regular burning, bimodal; 2b) Very low incidence, long season, low intensity, balanced size, regular burning, bimodal; 2c) Very low incidence, unequal size, sporadic burning; *Rangeland ires*:3a) Medium intensity, unequal size, regular burning, unimodal; 3b) Very high incidence, short season, low /medium intensity, unequal size, very regular burning, unimodal season.

4. DISCUSSION

Seven fire regimes were identified at global scale and aggregated into three fire macro-regimes, grouping fire regimes 1a and 1b, fire regimes 2a, 2b and 2c and fire regimes 3a and 3b (Figure 6). The discussion is structured by fire macro-regime, with further details for each regime. Variable modalities, are italicized. Fire macro-regimes are named on the basis of their geographical correspondence with the Anthromes of Ellis *et al.* (2010), which provide simple, easy to remember designations.

1 - *Wildland fires*

The first fire macro-regime is found mostly in Wildland and remote Rangeland anthromes (Ellis *et al.,* 2010). It is characterized by *low* fire Incidence, *sporadic*/*very sporadic* Regularity, *very short*, *unimodal* seasons, *medium* Intensity fires, and a unequal/*very unequal* fire size distribution. These modalities exhibit a geographical distribution along boreal forests and tropical deserts. Both have low net primary productivity, a small fraction of which is appropriated by humans (Lauk & Erb, 2009), and are similar in terms of *sensu strictu* fire regime attributes; however, constraints on fire incidence and regularity are distinct: the taiga fire regime is drought-driven, while that of tropical deserts is fuel-limited (Pausas & Ribeiro, 2013). The sporadic nature and relatively high intensity of fires in this regime suggest a lower degree of management than that found for the other two fire macro-regimes. Most of the modalities associated with this fire macro-regime are projected onto the negative side of the 1^{st} axis in the principal coordinates plot (Figure 3b) and well separated from the modalities associated to other fire regimes.

Fire regime 1a - Very short season, very sporadic, unimodal

Fire regime 1 is located in taiga boreal forests, at latitudes between 45°and 65ºN. A large patch of this cluster also occurs in central Australian deserts. Similar patterns were found by Chuvieco *et al*. (2008), and in the two boreal pyromes defined by Archibald *et al*. (2013). This fire regime is characterized by *high* interannual variability, with *very short*, *unimodal* fire season, where, total burned area tends to be concentrated in a few large sized and *medium-to-high* Intensity fire events (Table 3). These attributes of boreal fire regimes have been described before, namely the *low* fire Incidence (Gralewicz *et al.*, 2012), and large inter-annual variation (Loboda & Csiszar, 2007), *short* fire seasons (Loboda & Csiszar, 2007; Chuvieco *et al.*, 2008; Giglio *et al.*, 2006), *unequal* fire size distribution (Ivanova & Ivanov, 2005) and *medium to high* fire Intensity (Wooster & Zhang, 2004).

Fire regime 1b - Short season, unequal size, unimodal

Geographically and ecologically close, fire regimes 1a and 1b share low incidences, short seasons, *unequal* fire size distributions and a single annual fire (*unimodal*) season. Despite the modalities associated to this fire regime are not so extreme as 1a (small contributions to the inertia conveyed by both axes), this fire regime forms coherent patches mainly over the dry-lands of Central Asia in the Brazilian *cerrado* savanna, the semi-arid Kalahari *Acacia-Baikiaea* woodland savannas, and in pastoral tussock grasslands and semi-arid savannas of Queensland, Australia (Figure 6). This fire regime occurs in regions where fire frequency is fuel-limited (Andela & Van Der Werf, 2014) and dependent on soil moisture and previous year rainfall (Hudak *et al.*, 2004). Andela & Van der Werf (2014) and Archibald *et al.* (2010) identified regimes dominated by large and intense fires in the dry savannas of Namibia and Botswana. In the dry lands of Central Asia, namely near the border between

Mongolia and northern Kazakhstan (Loboda *et al.*, 2012) this fire regime is well defined, especially due to the Size Inequality (S2d), Regularity (S2e) and Seasonality (S2f) variables.

2 - Cropland fires

Geographical distribution of the second fire macro-regime corresponds closely with Croplands and Villages anthromes (Ellis *et al.,* 2010). Small, *regular*, *low* intensity fires that burn in *longer* seasons than those of fire macro-regime 1 characterize this group, and are diagnostic traits for the use of fire as a land management tool (Korontzi *et al.*, 2006). These modalities also exhibit a geographical distribution similar to that found by Ramankutty *et al.* (2008) for croplands and pastures, and Korontzi *et al.* (2006) for agricultural fires, revealing that this fire macro-regime tends to occur in areas of high population density (Bistinas *et al.*, 2013) and high net primary productivity, a large fraction of which is appropriated by humans (Lauk & Erb, 2009), leaving small amounts of fuel available to burn. Modalities associated with this macro-fire regime are projected onto the positive side of the 1st axis, opposite to the modalities associated with macro-fire regime 1 (Figure 3b).

Fire regime 2a - Low incidence, unequal size, regular

This regime occurs worldwide and covers the largest area of all regimes. It is located mainly in Eurasia, extending from the eastern Ukraine to southwestern Russia and northern Kazakhstan, India and China. Fire regime 2a is associated with large agricultural regions characterized by having *short* fire seasons, small, *low* intensity fires (Liu *et al.*, 2015) and *regular* burning (Korontzi *et al.*, 2006). Particularly notable is the area stretching from the Caspian Sea to northern Kazakhstan, intertwining fire regimes 1b and 2a. Fire regime 1b stands out because this region is part of the Central Asian steppe, a region with croplands and

pastures, although less intensively managed than the cropland areas of fire regime 2a (Loboda *et al.*, 2012). Also worth mentioning is the Asian rice belt, extending from eastern India to the coastal region of China. In India, the world's second largest producer of rice and wheat, active fires reveal harvest residue burning of cereal crops (Korontzi *et al.*, 2006). In China, agricultural open fires are mainly located in the eastern part of the country, from Russia border to Vietnam, Laos and Myanmar (Huang *et al.*, 2012).

Fire regime 2b - Low intensity, balanced size, regular

Fire regime 2b has close geographical and ecological ties with regime 2a, with which it shares similar modalities for the variables Incidence, Intensity, and Regularity. The specificity of this fire regime lies in its *long*, double peaked fire season (*bimodal*), and a more even fire size distribution than regime 2a (*balanced* Size Inequality). Its global distribution is similar to that of fire regime 2a, with which it is interspersed throughout the US southeast and Midwest, extending north into Canada. This regime's bimodal seasonality is linked to two distinct fire peaks related with cereal crop management as reported in studies such as Korontzi *et al*. (2006) or Benali *et al*. (unpublished results). Chuvieco *et al* (2008) also remarked on the low fire activity and long fire seasons throughout most of the southeastern USA. Regularity of annual burning in this region is described by McCarty *et al*. (2007) and Zhang *et al*. (2014). A patch of this fire regime is located in the Brazil-Uruguay-Argentina border region, probably related to the extensive double crop rotation management of soybeans/ maize, and to cattle ranching (Brannstrom *et al.*, 2008). Large areas are also found in cropland areas where fire is used in a double cropping system in the Balkans region of Eastern Europe (Korontzi *et al*., 2006; Le Page *et al*., 2010) and in southeastern China (Huang *et al.*, 2012).

Fire regime 2c - Very low incidence, unequal size, sporadic

It is the most spatially fragmented regime, confirmed by the lowest value of the AI_L index (31.3%) shown in Table 2. Fire regime 2c is located along the edges of fire regimes 2a and 2b, in areas with low fire activity. The modalities associated with this fire regime have the highest impurity levels of all seven regimes (Table 3) with *very low* Incidence, *unequal* size and *sporadic* Regularity as the only characteristic descriptors. It is found mainly in the prairies of Texas and northern Montana, USA, in areas with a mixture of pastures and intensive production of wheat and sorghum (Leff *et al.*, 2004), where burning is sporadic (Zhang *et al.*, 2014).

3 - *Rangeland fires*

The third fire macro-regime occurs primarily over residential and populated Rangeland anthromes (Ellis et *al.,* 2010). In spite of the high impurity of the Incidence variable in fire regime 3a, *high* Incidence levels characterize this fire macro-regime, which also exhibits *regular*, *low*/*medium* intensity burning, and *unimodal* fire seasons. It is found mainly over the tropical belt savannas, between 30ºS and 15ºN, with the highest fire incidence in the world (Dwyer *et al.*, 2000; Oom & Pereira, 2013). These areas have high net primary productivity, but the fraction appropriated by humans is smaller than in the more intensively managed fire regimes 2a-c, thus leaving substantial amounts of fuel available to burn (Lauk and Erb, 2009). Strong precipitation seasonality further facilitates *regular* burning. Correspondence with Rangeland anthromes and the levels of modalities for the variables that characterize regimes 3a and 3b suggest a fire macro-regime with a fire management level intermediate between those of the Wildland and Cropland fire macro-regimes. Analogously to the fire regimes 2a, 2b and 2c, Figure 4 shows a high similarity between the fire regimes composing this fire macro-regime (4a and 4b), with an aggregation level immediately above

the selected cut-off. Unlike the other fire macro-regimes, the modalities associated with this one are mainly located along the negative part of the 2nd axis (Figure 3b).

Fire regime 3a - Medium intensity, unequal size, unimodal

Its main areas of occurrence are the fire-prone *cerrado* savannas of central Brazil, eastern Bolivia and northeastern Paraguay (Pivello, 2011), Madagascar grasslands (Kull & Laris, 2009), south-east Asia (Langner & Siegert, 2009), and in the tropical savannas of the Northern Territory and Queensland (Oliveira *et al.*, 2013). All of these regions display *high* fire Incidence and *regular* fire activity.

Fire regime 3b - Very high incidence, short season, low/medium intensity

It is the "most pure" of all fire regimes with all its modalities having zero impurity levels (Table 3). It is mainly located in African savannas, the *Llanos* grasslands of Colombia and Venezuela, and the tropical savannas of northern Australia. *Very high* fire Incidence in *short* seasons, *unequal* fire size distribution, and *regular* burning describe this *unimodal* fire regime. In Africa, regime 3b usually is associated with a pronounced wet-dry season rainfall contrast (Barbosa *et al.*, 1999). The high annual regularity of African fire activity (Giglio *et al.*, 2006), combined with the presence of a weekly cycle is evidence of the anthropogenic influence of most African vegetation burning (Pereira *et al.*, 2015). A fire season anticipated relatively to the peak fire weather severity period is common throughout Africa (Le Page *et al.* 2010), with a spatially fragmented regime of small, low intensity fires, created to avoid large, intense fires during the late dry season, especially in Western Africa (Laris, 2005). The area classified with this fire regime in southern hemisphere Africa mostly covers Miombo woodlands, also characterized by high variability of fire sizes (Archibald *et al.*, 2010). *High* Incidence, *unequal* fire size distribution, and low interannual variability are also characteristic

of the *Llanos* savannas of Colombia and Venezuela (Romero-Ruiz *et al.*, 2010) and of the tropical savannas of northern Australia (Oliveira *et al.*, 2013)

Relation with pre-existing global fire regimes maps

While previous studies (Chuvieco *et al.,* 2008; Archibald *et al.,* 2013) classified about 32% of the global land area, on a 0.5° grid, we traded-off spatial resolution for the ability to classify a larger fraction of the globe (55%) at 1° resolution. We used MCA to reduce the dimensionality of a dataset containing five quantitative variables and one qualitative variable, and performed hierarchical clustering on the resulting 2-dimensional principal coordinates plot. This contrasts with the approach of Archibald *et al*. (2013), who only used PCA to identify the relevant clustering variables, and a non-hierarchical Bayesian clustering in a 5-dimensional space of original variables. Computational constraints prevented them from running the cluster analysis on their entire datasets, and ca. 55% of the data were classified with discriminant analysis trained on the 45% clustered data. Our reduced spatial resolution and clustering approach allowed for uniform application of a single methodology to the entire study area. Furthermore, the nested structure of the clustering algorithm defined meaningful fire macro-regimes, highlighting major pyreogeographical patterns. We introduced the number of annual fire seasons (Seasonality variable) as a new, qualitative variable distinguishing between unimodal and bimodal fire seasons, considered a reliable diagnostic of the anthropogenic character of fire activity (Benali *et al*., unpublished observations). Fire size heterogeneity was characterized in a novel way with the Gini index, which relies on the entire distribution of fire size data and not just on a specific percentile value. Our classification procedure takes spatial context into account, by revising the initial hierarchical clustering results with a contextual, rule-based filter. This step was deemed useful since the limited number of years available in the dataset is prone to lead to scattered, single-cell instances of

spurious classification, primarily affecting cells with high uncertainty in the initial classification. In such cases, the expectation of similar behavior between neighboring cells will lead to greater confidence in the revised classification. The filtered global fire regimes map exhibits a higher level of spatial aggregation, improving interpretability of the fire spatial patterns. Unlike previous studies (Archibald *et al.*, 2013; Chuvieco *et al.*, 2008), where all variables were used to describe each fire regime, regardless of their relevance, we used a formal, quantitative approach to identify the key modalities pertinent to characterize each regime, and only those are used to label and designate them. The proposed fire regimes end classified by a numbers of variables, ranging from three to six.

Archibald *et al.* (2013) describe one of their pyromes as "human-modified". With intermediate fire return intervals, and cool, small fires (ICS pyrome), it is related to our Cropland fires macro-regime in terms of defining attributes and geographical coverage. However, we provide a more detailed analysis of anthropogenic burning by distinguishing three Cropland fire regimes, characterized by distinct sets of variables/modalities. Since we also interpret the Rangeland fires macro-regime as essentially anthropogenic, albeit with less intensely managed fires than those of the Cropland fires macro-regime, our analysis considers that human-modified fire regimes prevail over a substantially larger area than that proposed by Archibald *et al.* (2013), in agreement with Lauk & Erb (2009), who reported fractions of human-caused fires ranging from 15% in the Canadian boreal forest, to 51% in the Russian boreal forest, and 98% in tropical rainforests. Our reliance on active fire data may contribute to explain the difference, since those data more effectively capture the small burning events that represent a large part of anthropogenic fire regimes. This interpretation appears to be corroborated by Archibald *et al*. (2013) statement that area burned was hardly detectable in their rare-cool-small (RCS) and intermediate-cool-small (ICS) pyromes.

5. CONCLUSIONS

A new global map of fire regimes is presented which improves upon previous research by expanding the global land area mapped and creating a two-level classification where each fire regime is parsimoniously described only in terms of relevant attributes. Additionally, spatial filtering the original map improved its geographical coherence and interpretability. Our proposed classification of fire regimes is very interpretable in terms of ecoclimatic and landuse drivers, as evidenced by the literature reviewed. The MCA technique of projecting supplementary data points onto the plane of its principal coordinates easily accommodates a more formal exploration of the relationships between the fire regime map and its environmental correlates, including the dimensions of degree of human intervention, primary productivity, and climate. It will allow for expanding the present study to a *sensu latu* fire regime analysis and contribute towards improved understanding of fire regime etiology at the global scale.

6. ACKNOWLEDGEMENTS

This study was funded by a Ph.D. grant to Duarte Oom (SFRH/BD/47452/2008) from the Foundation for Science and Technology, Ministry for Science and Technology, Portugal. ***Author contribution***: D.O., J.M.C.P. and P.S. conceived and designed the study; D.O., P.S., J.M.C.P and I.B. performed the analysis; D.O., P.S. and J.M.C.P. analyzed the data; A.B. developed the Seasonality variable; D.O., P.S., and J.M.C.P wrote the paper. All the authors reviewed the manuscript.

REFERENCES

Abdi, H. & Valentin, D. (2007) Multiple correspondence analysis. *Encyclopedia of measurement and statistics*, 651-657.

Archibald, S. & Roy, D. (2009) Identifying individual fires from satellite-derived burned area data. *Geoscience and Remote Sensing Symposium, 2009 IEEE International, IGARSS 2009*, pp III-160-III-163. IEEE.

Archibald, S., Lehmann, C. E., Gómez-Dans, J. L. & Bradstock, R. A. (2013) Defining pyromes and global syndromes of fire regimes. *Proceedings of the National Academy of Sciences*, **110**, 6442-6447.

Andela, N. & Van Der Werf, G. R. (2014) Recent trends in African fires driven by cropland expansion and El Nino to La Nina transition. *Nature Climate Change*.

Archibald, S., Scholes, R., Roy, D., Roberts, G. & Boschetti, L. (2010) Southern African fire regimes as revealed by remote sensing. *International Journal of Wildland Fire*, **19**, 861-878.

Barbosa, P. M., Stroppiana, D., Grégoire, J.-M. & Cardoso Pereira, J. M. (1999) An assessment of vegetation fire in Africa (1981-1991) Burned areas, burned biomass, and atmospheric emissions. *Global Biogeochemical Cycles*, **13**, 933-950.

Benali, A., Mota, B., Carvalhais, N., Oom, D., Miller, L. M., Campagnolo, M., Pereira, J.M.C. (unpublished results) Bimodal fire regimes unveil the global scale anthropogenic fingerprint.

Benzécri, J. (1982) *Histoire et préhistoire de l'analyse des données*, edn. Dunod.

Bistinas, I., Oom, D., Sá, A. C., Harrison, S. P., Prentice, I. C. & Pereira, J. M. (2013) Relationships between human population density and burned area at continental and global scales. *PloS one*, **8**, e81188.

Bond, W. J., Woodward, F. I. & Midgley, G. F. (2005) The global distribution of ecosystems in a world without fire. *New Phytologist*, **165**, 525-538.

Brannstrom, C., Jepson, W., Filippi, A. M., Redo, D., Xu, Z. & Ganesh, S. (2008) Land change in the Brazilian Savanna (Cerrado), 1986-2002: comparative analysis and implications for land-use policy. *Land Use Policy*, **25**, 579-595.

Cadoret, M., Fournier, G. & Le Poder, F. (2011) EnQuireR: Analyzing questionnaires with R. *Journal of statistical software, VV (II)*, 6.

Cerdeira, J. O., Martins, M. J. O. & Silva, P. C. (2012) A combinatorial approach to assess the separability of clusters. *Journal of Classification*, **29**, 7-22.

Chuvieco, E., Giglio, L. & Justice, C. (2008) Global characterization of fire activity: toward defining fire regimes from Earth observation data. *Global Change Biology*, **14**, 1488-1502.

Conedera, M., Tinner, W., Neff, C., Meurer, M., Dickens, A. F. & Krebs, P. (2009) Reconstructing past fire regimes: methods, applications, and relevance to fire management and conservation. *Quaternary Science Reviews*, **28**, 555-576.

Csiszar, I., Denis, L., Giglio, L., Justice, C. O. & Hewson, J. (2005) Global fire activity from two years of MODIS data. *International Journal of Wildland Fire*, 14, 117-130.

Davies, D. L. & Bouldin, D. W. (1979) A cluster separation measure. *IEEE Transactions on Pattern Analysis and Machine Intelligence*, 224-227.

Dwyer, E., Pereira, J. M., Gregoire, J.-M. & Dacamara, C. C. (2000) Characterization of the spatiol-temporal patterns of global fire activity using satellite imagery for the period April 1992 to March 1993. *Journal of Biogeography*, **27**, 57-69.

Ellis, E. C., Klein Goldewijk, K., Siebert, S., Lightman, D. & Ramankutty, N. (2010) Anthropogenic transformation of the biomes, 1700 to 2000. Global Ecology and Biogeography, 19, 589-606.

Giglio, L., Csiszar, I. & Justice, C. O. (2006) Global distribution and seasonality of active fires as observed with the Terra and Aqua Moderate Resolution Imaging Spectroradiometer (MODIS) sensors. *Journal of Geophysical Research: Biogeosciences (2005-2012)*, **111**.

Gini, C. (1912) Variability and Mutability, Contribution to The Study of Statistical Distribution and Relaitons. *Studi Economico-Giuricici della R*.

Goldammer, J., Crutzen, P. & Goldammer, J. (1993) Historical biogeography of fire: tropical and subtropical. *Fire in the environment: The Ecological, Atmospheric, and Climatic Importance of Vegetation Fires, 1993a*, **297314**.

Gralewicz, N. J., Nelson, T. A. & Wulder, M. A. (2012) Spatial and temporal patterns of wildfire ignitions in Canada from 1980 to 2006. *International Journal of Wildland Fire*, **21**, 230-242.

Greenacre, M. J. (1984) *Theory and applications of correspondence analysis*, edn.

Hantson, S., Lasslop, G., Kloster, S. & Chuvieco, E. (2015) Anthropogenic effects on global mean fire size. *International Journal of Wildland Fire*, 24, 589-596.

Hantson, S., Pueyo, S. & Chuvieco, E. (2014) Global fire size distribution is driven by human impact and climate. *Global Ecology and Biogeography*, 24, 77-86.

Hong, T.-P., Wang, T.-T., Wang, S.-L. & Chien, B.-C. (2000) Learning a coverage set of maximally general fuzzy rules by rough sets. *Expert Systems with Applications*, **19**, 97-103.

Huang, X., Li, M., Li, J. & Song, Y. (2012) A high-resolution emission inventory of crop burning in fields in China based on MODIS Thermal Anomalies/Fire products. *Atmospheric Environment*, **50**, 9-15.

Hudak, A. T., Fairbanks, D. H. & Brockett, B. H. (2004) Trends in fire patterns in a southern African savanna under alternative land use practices. *Agriculture, Ecosystems & Environment*, **101**, 307-325.

Ivanova, G. A. & Ivanov, V. A. (2005) Fire regimes in Siberian forests. *International Forest Fires News (IFFN)*, 67-69.

Korontzi, S., Mccarty, J., Loboda, T., Kumar, S. & Justice, C. (2006) Global distribution of agricultural fires in croplands from 3 years of Moderate Resolution Imaging Spectroradiometer (MODIS) data. *Global Biogeochemical Cycles*, **20**, 1-15.

Krawchuk, M. A., Moritz, M. A., Parisien, M.-A., Van Dorn, J. & Hayhoe, K. (2009) Global pyrogeography: the current and future distribution of wildfire. *PloS one*, 4, e5102.

Krebs, P., Pezzatti, G. B., Mazzoleni, S., Talbot, L. M. & Conedera, M. (2010) Fire regime: history and definition of a key concept in disturbance ecology. *Theory in Biosciences*, **129**, 53-69.

Kull, C. A. & Laris, P. (2009) Fire ecology and fire politics in Mali and Madagascar. *Tropical Fire Ecology*, Climate Change, Land Use, and Ecosystem Dynamics, pp 171-226. Springer.

Langner, A. & Siegert, F. (2009) Spatiotemporal fire occurrence in Borneo over a period of 10 years. *Global Change Biology*, **15**, 48-62.

Lauk, C. & Erb, K.-H. (2009) Biomass consumed in anthropogenic vegetation fires: Global patterns and processes. Ecological Economics, 69, 301-309.

Laris, P. S. (2005) Spatiotemporal problems with detecting and mapping mosaic fire regimes with coarse-resolution satellite data in savanna environments. *Remote Sensing of Environment*, **99**, 412-424.

Le Page, Y., Oom, D., Silva, J., Jönsson, P. & Pereira, J. M. (2010) Seasonality of vegetation fires as modified by human action: observing the deviation from eco-climatic fire regimes. *Global Ecology and Biogeography*, **19**, 575-588.

Leff, B., Ramankutty, N. & Foley, J. A. (2004) Geographic distribution of major crops across the world. *Global Biogeochemical Cycles*, **18**.

Liu, M., Song, Y., Yao, H., Kang, Y., Li, M., Huang, X. & Hu, M. (2015) Estimating emissions from agricultural fires in the North China Plain based on MODIS fire radiative power. *Atmospheric Environment*, **112**, 326-334.

Loboda, T. & Csiszar, I. (2007) Reconstruction of fire spread within wildland fire events in Northern Eurasia from the MODIS active fire product. *Global and Planetary Change*, **56**, 258-273.

Loboda, T. V., Giglio, L., Boschetti, L. & Justice, C. O. (2012) Regional fire monitoring and characterization using global NASA MODIS fire products in dry lands of Central Asia. *Frontiers of Earth Science*, **6**, 196-205.

McCarty, J., Justice, C. & Korontzi, S. (2007) Agricultural burning in the Southeastern United States detected by MODIS. *Remote Sensing of Environment*, **108**, 151-162.

Morgan, P., Hardy, C. C., Swetnam, T. W., Rollins, M. G. & Long, D. G. (2001) Mapping fire regimes across time and space: understanding coarse and fine-scale fire patterns. *International Journal of Wildland Fire*, **10**, 329-342.

Oliveira, S. L., Turkman, M. A. & Pereira, J. M. (2013) An analysis of fire frequency in tropical savannas of northern Australia, using a satellite-based fire atlas. *International Journal of Wildland Fire*, **22**, 479-492.

Oom, D. & Pereira, J. (2013) Exploratory spatial data analysis of global MODIS active fire data. *International Journal of Applied Earth Observation and Geoinformation*, **21**, 326-340.

Pausas, J. G. & Ribeiro, E. (2013) The global fire-productivity relationship. *Global Ecology and Biogeography*, **22**, 728-736.

Pereira, J. M. C., Oom, D., Pereira, P., Turkman, A. A. & Turkman, K. F. (2015) Religious Affiliation Modulates Weekly Cycles of Cropland Burning in Sub-Saharan Africa. *PloS one*, **10**, e0139189.

Piccarreta, R. (2001) A new measure of nomina-ordinal association. *Journal of Applied Statistics*, **28**, 107-120.

Pivello, V. N. R. (2011) The use of fire in the Cerrado and Amazonian rainforests of Brazil: past and present. *Fire Ecology*, **7**, 24-39.

Ramankutty, N., Evan, A. T., Monfreda, C. & Foley, J. A. (2008) Farming the planet: 1. Geographic distribution of global agricultural lands in the year 2000. *Global Biogeochemical Cycles*, **22**.

Randerson, J., Chen, Y., Werf, G., Rogers, B. & Morton, D. (2012) Global burned area and biomass burning emissions from small fires. *Journal of Geophysical Research: Biogeosciences (2005-2012)*, **117**.

Romero-Ruiz, Etter, A., Sarmiento, A. & Tansey, K. (2010) Spatial and temporal variability of fires in relation to ecosystems, land tenure and rainfall in savannas of northern South America. *Global Change Biology*, **16**, 2013-2023.

Rousseeuw, P. J. (1987) Silhouettes: a graphical aid to the interpretation and validation of cluster analysis. *Journal of computational and applied mathematics*, **20**, 53-65.

Tukey, J. W. (1975) Mathematics and the picturing of data. *Proceedings of the International Congress of Mathematicians*, pp 523-531.

White, P. S., Harrod, J., Romme, W. H. & Betancourt, J. (1999) Disturbance and temporal dynamics. *Ecological Stewardship: A common reference for ecosystem management. Oxford, England*, 281-305.

Wooster, M. & Zhang, Y. (2004) Boreal forest fires burn less intensely in Russia than in North America. *Geophysical Research Letters*, **31**.

Zhang, X., Kondragunta, S. & Roy, D. P. (2014) Interannual variation in biomass burning and fire seasonality derived from geostationary satellite data across the contiguous United States from 1995 to 2011. *Journal of Geophysical Research: Biogeosciences*, **119**, 1147-1162.

CHAPTER 3

Conclusions

Research goals

The work undertaken in this thesis led to improved understanding of global pyrogeography, via research on relationships of fire activity with climate patterns, anthropogenic presence, and cultural factors, and culminating in the development of a new global map of fire regimes. Widespread availability of satellite imagery has revolutionized the assessment of geographic patterns of fire activity, and allowed the possibility to test the role of biophysical and social processes as drivers of those patterns. With the premise that wildfire is recognized as an important key Earth system process, and considered a natural process which affects ecosystems and their fire regimes over multiple temporal and spatial scales, the research presented here demonstrated the importance and richness of long, accurate and reliable datasets to elucidate the relationships between people and fire and how they interact to originate global fire regimes.

Paper I demonstrated that, in spite of providing extremely useful data, the global active fire product derived from the Moderate Resolution Imaging Spectroradiometer (MODIS) is not error-free. From the same study, and confirmed in paper VI, it was shown that MODIS active fire data display strong positive autocorrelation at global scale and heterogeneity in fire–environment relationships across space. The role of the anthropogenic factor and how human activity can affect the fire regime in all its aspects was analyzed in Papers II to IV. Development of an improved algorithm for individuating active fire clusters according to spatial and temporal proximity criteria, and sensitivity analysis of algorithm parameter effects on fire size distributions were undertaken in Paper V. The new global map of fire regimes obtained (Paper VI), integrating results from the studies undertaken in this thesis, unveiled groups with very distinctive characteristics.

The global fire regimes map produced exhibits a higher level of spatial aggregation, improving the readability of the fire spatial patterns. This result improves upon previous ones by expanding the global land area classified, incorporating new fire regime variables, deriving a two-level hierarchical classification, and developing an objective, quantitative procedure for

creating legends with a variable number of fire regimes descriptors. The proposed fire regimes classification is highly interpretable in terms of ecoclimatic and landuse drivers.

Outputs

An important output derived from the research work undertaken in this thesis was a valuable global active fire product at 1km spatial resolution spanning from January 2001 to December 2012. The screening of 12 years (2001-2012) of the original NASA MODIS MCD14 ML Collection 5 global active product, resulted in more than 40 millions observations which corresponding to vegetation fires (Oom & Pereira, 2013). This dataset also complements the previous ten years of WFA screened active fire product started by (Mota *et al.*, 2006) and followed by (Oom, 2008). Several studies have already used the data (Pereira *et al.*, 2015a; Bedia *et al.*, 2015)

The data is available free of charge through duarte.oom@gmail.com

Ongoing research and future perspectives

Due the limited time-frame allocated to this thesis, some complementary analysis could not be made, and to date some of them are already subject of ongoing research and others will be further investigated.

In order to complement the characterization of global fire activity in specific topics, global analysis were done using MODIS screened data depicted from Paper I, and are now in a process of submission to a peer-review papers:

- Explore the seasonality patterns through a fire global classification using MODIS screened data derived from Paper I, taking into account the bimodal fire seasons which occupy a significant fraction of the fire-prone land surface.

*Benali, A., Mota, B., Carvalhais, N., **Oom, D**., Miller, L. M. & Pereira, J. M.C. (submitted to Global Ecology and Biogeography) Bimodal fire regimes unveil the global scale anthropogenic fingerprint.*

- Trend analysis on fire activity at grid cell level for the period 2001-2013 to provide direction of active fires trends at global scale and interpret the main patterns in terms of land use change.

*Bistinas, I., **Oom, D**., Silva, J. & Pereira, J. M.C. (in process of submission) A trend analysis of global fire activity using CMG MODIS fire counts.*

Following Paper VI, future research will be focus in extend the *sensu strictu* to *sensu lato* fire regime concept considering a wider fire regime definition, including not only the condition controlling fire (fire weather, fuel flammability) but also the impacts on the ecosystem, human goods or infrastructures, using human related variables (e.g. population density).

Following Paper IV, and using fire data depicted from Paper I, a new study is being performed to the conterminous United States testing if there is a day of the week with lower fire activity, and if that day depends on the regionally predominant religious affiliation.

Following Paper V, new improvements to the fire events identification algorithm is ongoing .

References

Aldersley, A., Murray, S. J. & Cornell, S. E. (2011) Global and regional analysis of climate and human drivers of wildfire. Science of the Total Environment, 409, 3472-3481.

Archibald, S., Lehmann, C. E., Gómez-Dans, J. L. & Bradstock, R. A. (2013) Defining pyromes and global syndromes of fire regimes. Proceedings of the National Academy of Sciences, 110, 6442-6447.

Archibald, S., Roy, D. P., Wilgen, V., Brian, W. & Scholes, R. J. (2008) What limits fire? An examination of drivers of burnt area in Southern Africa. Global Change Biology, 15, 613-630.

Archibald, S., Staver, A. C. & Levin, S. A. (2012) Evolution of human-driven fire regimes in Africa. Proceedings of the National Academy of Sciences, 109, 847-852.

Arino, O., Casadio, S. & Serpe, D. (2012) Global night-time fire season timing and fire count trends using the ATSR instrument series. Remote Sensing of Environment, 116, 226-238.

Arino, O., Plummer, S. & Defrenne, D. (2005) Fire disturbance: the ten years time series of the ATSR World Fire Atlas. ATSR Workshop, pp 26-30.

Arino, O. & Rosaz, J. (1999) 1997 and 1998 world ATSR fire atlas using ERS-2 ATSR-2 data. Proc. Joint Fire Sci. Conf, pp 177-182. Boise, ID.

Barbosa, P. M., Stroppiana, D., Grégoire, J.-M. & Cardoso Pereira, J. M. (1999) An assessment of vegetation fire in Africa (1981-1991): Burned areas, burned biomass, and atmospheric emissions. Global Biogeochemical Cycles, 13, 933-950.

Barrett, K. & Kasischke, E. S. (2013) Controls on variations in MODIS fire radiative power in Alaskan boreal forests: Implications for fire severity conditions. Remote Sensing of Environment, 130, 171-181.

Bedia, J., Herrera, S., Gutiérrez, J. M., Benali, A., Brands, S., Mota, B. & Moreno, J. M. (2015) Global patterns in the sensitivity of burned area to fire-weather: Implications for climate change. Agricultural and Forest Meteorology, 214, 369-379.

Bistinas, I., Oom, D., Sá, A. C., Harrison, S. P., Prentice, I. C. & Pereira, J. M. (2013) Relationships between human population density and burned area at continental and global scales. PloS one, 8, e81188.

Bond, W. J., Woodward, F. I. & Midgley, G. F. (2005) The global distribution of ecosystems in a world without fire. New Phytologist, 165, 525-538.

Boschetti, L., Roy, D. P., Justice, C. O. & Giglio, L. (2010) Global assessment of the temporal reporting accuracy and precision of the MODIS burned area product. International Journal of Wildland Fire, 19, 705-709.

Bowman, D. M., Balch, J., Artaxo, P., Bond, W. J., Cochrane, M. A., D'antonio, C. M., Defries, R., Johnston, F. H., Keeley, J. E. & Krawchuk, M. A. (2011) The human dimension of fire regimes on Earth. Journal of Biogeography, 38, 2223-2236.

Bowman, D. M., Balch, J. K., Artaxo, P., Bond, W. J., Carlson, J. M., Cochrane, M. A., D'antonio, C. M., Defries, R. S., Doyle, J. C. & Harrison, S. P. (2009) Fire in the Earth system. science, 324, 481-484.

Bowman, D. M., O'brien, J. A. & Goldammer, J. G. (2013) Pyrogeography and the global quest for sustainable fire management. Annual Review of Environment and Resources, 38, 57.

Bradstock, R. A. (2010) A biogeographic model of fire regimes in Australia: current and future implications. Global Ecology and Biogeography, 19, 145-158.

Carmona-Moreno, C., Belward, A., Malingreau, J.-P., Hartley, A., Garcia-Alegre, M., Antonovskiy, M., Buchshtaber, V. & Pivovarov, V. (2005) Characterizing interannual variations in global fire calendar using data from Earth observing satellites. Global Change Biology, 11, 1537-1555.

Chuvieco, E. & Congalton, R. G. (1989) Application of remote sensing and geographic information systems to forest fire hazard mapping. Remote Sensing of Environment, 29, 147-159.

Chuvieco, E., Giglio, L. & Justice, C. (2008) Global characterization of fire activity: toward defining fire regimes from Earth observation data. Global Change Biology, 14, 1488-1502.

Conedera, M., Tinner, W., Neff, C., Meurer, M., Dickens, A. F. & Krebs, P. (2009) Reconstructing past fire regimes: methods, applications, and relevance to fire management and conservation. Quaternary Science Reviews, 28, 555-576.

Csiszar, I., Denis, L., Giglio, L., Justice, C. O. & Hewson, J. (2005) Global fire activity from two years of MODIS data. International Journal of Wildland Fire, 14, 117-130.

Csiszar, I., Schroeder, W., Giglio, L., Ellicott, E., Vadrevu, K. P., Justice, C. O. & Wind, B. (2014) Active fires from the Suomi NPP Visible Infrared Imaging Radiometer Suite: Product status and first evaluation results. Journal of Geophysical Research: Atmospheres, 119, 803-816.

Duguy, B., Paula, S., Pausas, J. G., Alloza, J. A., Gimeno, T. & Vallejo, R. V. (2013) Effects of climate and extreme events on wildfire regime and their ecological impacts. Regional Assessment of Climate Change in the Mediterranean, pp 101-134. Springer.

Dwyer, E., Pereira, J. M., Gregoire, J.-M. & Dacamara, C. C. (2000) Characterization of the spatiol-temporal patterns of global fire activity using satellite imagery for the period April 1992 to March 1993. Journal of Biogeography, 27, 57-69.

Elvidge, C. D., Baugh, K. E., Kihn, E. A., Kroehl, H. W., Davis, E. R. & Davis, C. W. (1997) Relation between satellite observed visible-near infrared emissions, population, economic activity and electric power consumption. International Journal of Remote Sensing, 18, 1373-1379.

Eva, H. & Lambin, E. F. (2000) Fires and land-cover change in the tropics: a remote sensing analysis at the landscape scale. Journal of Biogeography, 27, 765-776.

Fao. (2007). Fire management global assessment 2006. FAO, Rome.

Flannigan, M., Cantin, A. S., De Groot, W. J., Wotton, M., Newbery, A. & Gowman, L. M. (2013) Global wildland fire season severity in the 21st century. Forest Ecology and Management, 294, 54-61.

Gcos, W. (2011) Systematic observation requirements for satellite-based products for climate: Supplemental details to the satellite-based component of the "Implementation Plan for the Global Observing System for Climate in Support of the UNFCCC (2010 update)□. GCOS 154.

Giglio, L., Csiszar, I. & Justice, C. O. (2006) Global distribution and seasonality of active fires as observed with the Terra and Aqua Moderate Resolution Imaging Spectroradiometer (MODIS) sensors. Journal of Geophysical Research: Biogeosciences (2005-2012), 111.

Giglio, L., Descloitres, J., Justice, C. O. & Kaufman, Y. J. (2003a) An enhanced contextual fire detection algorithm for MODIS. Remote Sensing of Environment, 87, 273-282.

Giglio, L., Kendall, J. & Mack, R. (2003b) A multi-year active fire dataset for the tropics derived from the TRMM VIRS. International Journal of Remote Sensing, 24, 4505-4525.

Giglio, L., Loboda, T., Roy, D. P., Quayle, B. & Justice, C. O. (2009) An active-fire based burned area mapping algorithm for the MODIS sensor. Remote Sensing of Environment, 113, 408-420.

Gill, A. M. (1975) Fire and the Australian flora: a review. Australian forestry, 38, 4-25.

Goldammer, J., Crutzen, P. & Goldammer, J. (1993) Historical biogeography of fire: tropical and subtropical. Fire in the environment: The Ecological, Atmospheric, and Climatic Importance of Vegetation Fires, 1993a, 297314.

Hantson, S., Lasslop, G., Kloster, S. & Chuvieco, E. (2015) Anthropogenic effects on global mean fire size. International Journal of Wildland Fire, 24, 589-596.

Hantson, S., Padilla, M., Corti, D. & Chuvieco, E. (2013) Strengths and weaknesses of MODIS hotspots to characterize global fire occurrence. Remote Sensing of Environment, 131, 152-159.

Hantson, S., Pueyo, S. & Chuvieco, E. (2014) Global fire size distribution is driven by human impact and climate. Global Ecology and Biogeography, 24, 77-86.

Harrison, S. P., Marlon, J. R. & Bartlein, P. J. (2010) Fire in the Earth system, edn. Springer.

Hawbaker, T. J., Radeloff, V. C., Syphard, A. D., Zhu, Z. & Stewart, S. I. (2008) Detection rates of the MODIS active fire product in the United States. Remote Sensing of Environment, 112, 2656-2664.

Ichoku, C. & Kaufman, Y. J. (2005) A method to derive smoke emission rates from MODIS fire radiative energy measurements. Geoscience and Remote Sensing, IEEE Transactions on, 43, 2636-2649.

Justice, C., Giglio, L., Korontzi, S., Owens, J., Morisette, J., Roy, D., Descloitres, J., Alleaume, S., Petitcolin, F. & Kaufman, Y. (2002) The MODIS fire products. Remote Sensing of Environment, 83, 244-262.

Kaiser, J., Heil, A., Andreae, M., Benedetti, A., Chubarova, N., Jones, L., Morcrette, J.-J., Razinger, M., Schultz, M. & Suttie, M. (2012) Biomass burning emissions estimated with a global fire assimilation system based on observed fire radiative power. Biogeosciences, 9, 527-554.

Kaufman, Y. J., Justice, C. O., Flynn, L. P., Kendall, J. D., Prins, E. M., Giglio, L., Ward, D. E., Menzel, W. P. & Setzer, A. W. (1998) Potential global fire monitoring from EOS-MODIS. Journal of Geophysical Research: Atmospheres, 103, 32215-32238.

Keeley, J. E. (2009) Fire intensity, fire severity and burn severity: a brief review and suggested usage. International Journal of Wildland Fire, 18, 116-126.

Korontzi, S., Mccarty, J., Loboda, T., Kumar, S. & Justice, C. (2006) Global distribution of agricultural fires in croplands from 3 years of Moderate Resolution Imaging Spectroradiometer (MODIS) data. Global Biogeochemical Cycles, 20.

Krawchuk, M. A. & Moritz, M. A. (2011) Constraints on global fire activity vary across a resource gradient. Ecology, 92, 121-132.

Krawchuk, M. A., Moritz, M. A., Parisien, M.-A., Van Dorn, J. & Hayhoe, K. (2009) Global pyrogeography: the current and future distribution of wildfire. PloS one, 4, e5102.

Krebs, P., Pezzatti, G. B., Mazzoleni, S., Talbot, L. M. & Conedera, M. (2010) Fire regime: history and definition of a key concept in disturbance ecology. Theory in Biosciences, 129, 53-69.

Le Page, Y., Oom, D., Silva, J., Jõnsson, P. & Pereira, J. M. (2010) Seasonality of vegetation fires as modified by human action: observing the deviation from eco-climatic fire regimes. Global Ecology and Biogeography, 19, 575-588.

Liu, Z. & Wimberly, M. C. (2015) Direct and indirect effects of climate change on projected future fire regimes in the western United States. Science of the Total Environment, 542, 65-75.

Loboda, T. V., Hoy, E. E., Giglio, L. & Kasischke, E. S. (2011) Mapping burned area in Alaska using MODIS data: a data limitations-driven modification to the regional burned area algorithm. International Journal of Wildland Fire, 20, 487-496.

Marlon, J. R., Bartlein, P. J., Daniau, A.-L., Harrison, S. P., Maezumi, S. Y., Power, M. J., Tinner, W. & Vanniére, B. (2013) Global biomass burning: a synthesis and review of Holocene paleofire records and their controls. Quaternary Science Reviews, 65, 5-25.

Mckenzie, D., Gedalof, Z. E., Peterson, D. L. & Mote, P. (2004) Climatic change, wildfire, and conservation. Conservation Biology, 18, 890-902.

Morgan, P., Hardy, C. C., Swetnam, T. W., Rollins, M. G. & Long, D. G. (2001) Mapping fire regimes across time and space: understanding coarse and fine-scale fire patterns. International Journal of Wildland Fire, 10, 329-342.

Morisette, J. T., Giglio, L., Csiszar, I. & Justice, C. O. (2005) Validation of the MODIS active fire product over Southern Africa with ASTER data. International Journal of Remote Sensing, 26, 4239-4264.

Moritz, M. A., Parisien, M.-A., Batllori, E., Krawchuk, M. A., Van Dorn, J., Ganz, D. J. & Hayhoe, K. (2012) Climate change and disruptions to global fire activity. Ecosphere, 3, art49.

Mota, B., Pereira, J., Oom, D., Vasconcelos, M. & Schultz, M. (2006) Screening the ESA ATSR-2 World Fire Atlas (1997â€“2002). Atmospheric Chemistry and Physics, 6, 1409-1424.

Mouillot, F. & Field, C. B. (2005) Fire history and the global carbon budget: a 1ºx1º fire history reconstruction for the 20th century. Global Change Biology, 11, 398-420.

Murphy, B. P., Bradstock, R. A., Boer, M. M., Carter, J., Cary, G. J., Cochrane, M. A., Fensham, R. J., Russell-Smith, J., Williamson, G. J. & Bowman, D. M. (2012) Fire regimes of Australia: a pyrogeographic model system. Journal of Biogeography, 40, 1048-1058.

Oom, D. & Pereira, J. (2013) Exploratory spatial data analysis of global MODIS active fire data. International Journal of Applied Earth Observation and Geoinformation, 21, 326-340.

Parisien, M.-A. & Moritz, M. A. (2009) Environmental controls on the distribution of wildfire at multiple spatial scales. Ecological Monographs, 79, 127-154.

Pausas, J. G. & Paula, S. (2012) Fuel shapes the fire-climate relationship: evidence from Mediterranean ecosystems. Global Ecology and Biogeography, 21, 1074-1082.

Pechony, O. & Shindell, D. T. (2010) Driving forces of global wildfires over the past millennium and the forthcoming century. Proceedings of the National Academy of Sciences, 107, 19167-19170.

Pereira, J. M., Sá, A. C., Sousa, A. M., Silva, J. M., Santos, T. N. & Carreiras, J. M. (1999) Spectral characterisation and discrimination of burnt areas. Remote sensing of large wildfires, pp 123-138. Springer.

Prins, E. M. & Menzel, W. (1992) Geostationary satellite detection of bio mass burning in South America. International Journal of Remote Sensing, 13, 2783-2799.

Randerson, J., Chen, Y., Werf, G., Rogers, B. & Morton, D. (2012) Global burned area and biomass burning emissions from small fires. Journal of Geophysical Research: Biogeosciences (2005-2012), 117.

Roberts, G., Wooster, M. & Lagoudakis, E. (2009) Annual and diurnal african biomass burning temporal dynamics. Biogeosciences, 6, 849-866.

Roy, D. P., Boschetti, L., Justice, C. O. & Ju, J. (2008) The collection 5 MODIS burned area product-Global evaluation by comparison with the MODIS active fire product. Remote Sensing of Environment, 112, 3690-3707.

Schroeder, W., Oliva, P., Giglio, L. & Csiszar, I. A. (2014) The New VIIRS 375m active fire detection data product: algorithm description and initial assessment. Remote Sensing of Environment, 143, 85-96.

Schroeder, W., Prins, E., Giglio, L., Csiszar, I., Schmidt, C., Morisette, J. & Morton, D. (2008a) Validation of GOES and MODIS active fire detection products using ASTER and ETM+ data. Remote Sensing of Environment, 112, 2711-2726.

Schroeder, W., Ruminski, M., Csiszar, I., Giglio, L., Prins, E., Schmidt, C. & Morisette, J. (2008b) Validation analyses of an operational fire monitoring product: The Hazard Mapping System. International Journal of Remote Sensing, 29, 6059-6066.

Smith, A. M. & Wooster, M. J. (2005) Remote classification of head and backfire types from MODIS fire radiative power and smoke plume observations. International Journal of Wildland Fire, 14, 249-254.

Stroppiana, D., Pinnock, S. & Gregoire, J.-M. (2000) The global fire product: Daily fire occurrence from April 1992 to December 1993 derived from NOAA AVHRR data. International Journal of Remote Sensing, 21, 1279-1288.

Van Der Werf, G. R., Randerson, J. T., Giglio, L., Collatz, G., Mu, M., Kasibhatla, P. S., Morton, D. C., Defries, R., Jin, Y. V. & Van Leeuwen, T. T. (2010) Global fire emissions and the contribution of deforestation, savanna, forest, agricultural, and peat fires (1997-2009). Atmospheric Chemistry and Physics, 10, 11707-11735.

Westerling, A. L., Turner, M. G., Smithwick, E. A., Romme, W. H. & Ryan, M. G. (2011) Continued warming could transform Greater Yellowstone fire regimes by mid-21st century. Proceedings of the National Academy of Sciences, 108, 13165-13170.

Whitlock, C., Higuera, P. E., Mcwethy, D. B. & Briles, C. E. (2010) Paleoecological perspectives on fire ecology: revisiting the fire-regime concept. The Open Ecology Journal, 3, 6-23.

Wooster, M. & Zhang, Y. (2004) Boreal forest fires burn less intensely in Russia than in North America. Geophysical Research Letters, 31.